Thin Film Nanocomposite Membranes Using Cellulose Nanocrystals for Water Treatment

By

Fatemeh Abedi

A thesis submitted in partial fulfillment of the requirements for the Doctorate in Philosophy degree in Chemical Engineering

Department of Chemical and Biological Engineering, Faculty of Engineering

University of Ottawa, Ottawa, Canada

Abstract

Access to clean water is one of the world's greatest concerns. Because 97% of global water resources are seawater, desalination via reverse osmosis (RO) membrane process has become a vital technology to obtain drinkable water. At the same time, the discharge of industrial waste effluents containing heavy metal ions to the available water resources (seawater and brackish water) without adequate pre-treatment is a major cause of water pollution. Heavy metal rejection using nanofiltration (NF) membrane process is a recognized water treatment methodology. Thin-film nanocomposite (TFN) membranes have shown vast performance enhancement using both RO and NF processes. However, TFN membrane fabrication has been limited due to poor dispersion of the nanoparticles in the polyamide (PA) layer of the membrane, and the leaching of the often-hazardous nanoparticles from the TFN membranes.

For various reasons such as their dispersibility in aqueous media, safety, high aspect ratio, and functionality, cellulose nanocrystals (CNCs) are an ideal nanoparticle for inclusion in TFN membranes. Because of their hydrophilicity, CNCs have more commonly been dispersed in the aqueous monomer solution during PA interfacial polymerization. In this thesis, we investigated two different CNC modification routes to improve CNC dispersion within the trimesoyl chloride (TMC)/n-hexane (non-aqueous) monomer solution. In one case, we acetylated the CNCs (ACNCs) using a straightforward, efficient, solvent-free method to achieve a more uniform CNC dispersion in the PA layer. The resulting ACNCs were less hydrophilic, which allowed increased nanoparticle loading and improved dispersion in the PA layer. In an RO desalination process, compared to unmodified CNC-TFN membranes, the NaCl rejection of the ACNC-TFN membranes remained stable (at 98-99%) up to a 0.4 wt% loading, while water permeability increased by up to 40%.

For the second case, we synthesized L-cysteine functionalized CNCs (CysCNCs) and incorporated them into the PA layer for testing in an NF wastewater treatment process. The amine functional groups of L-cysteine covalently bonded with the acyl chloride groups of the TMC monomer. This resulted in improved nanoparticle dispersion but could also have prevented nanoparticle leaching. Moreover, because L-cysteine contains strong chelating groups, their inclusion in the PA layer led to improved heavy metal rejection. A loading of 0.1 wt% CysCNCs in the TFN membranes provided high rejection of both copper and lead ions, 98.1 and 95.2%, respectively. The CysCNCs were also evaluated in an NF desalination process resulting in a 40% increase in water permeability with almost no decline in Na_2SO_4 (97-98%),

$MgCl_2$ and NaCl rejection. The modified CNCs enabled us to overcome the water permeability/selectivity trade-off in CNC-TFN membranes for both RO and NF membrane desalination.

Finally, we developed an experimental protocol to investigate the effect of the adsorption of heavy metal ions (if any) on the performance of thin film composite (TFC) and TFN membranes in NF. We confirmed that adsorption occurred, and the equilibrium capacity of the membranes was reached after 8 – 12 h of the experiment. Despite reaching the equilibrium capacity, the water permeability and heavy metal rejection remained at their highest values. This led to the conclusion that the adsorbed heavy metals altered the membrane surface, thereby improving the performance of both TFC and TFN membranes.

The ability to modify CNCs enables one to achieve a controlled range of hydrophilicity/ hydrophobicity. This allows one to fine-tune CNC compatibility with the TMC/n-hexane non-aqueous monomer solution and enable improved dispersion in the PA layer, eventually leading to improved TFN membrane performance for both RO and NF processes.

Abstrait

L'accès à l'eau potable est l'une des plus grandes préoccupations mondiales. Parce que 97% des ressources mondiales en eau sont de l'eau de mer, le dessalement par procédé membranaire d'osmose inverse (OI) est devenu une technologie vitale pour obtenir de l'eau potable. En même temps, le rejet d'effluents de déchets industriels contenant des ions de métaux lourds dans les ressources en eau disponibles (eau de mer et eau saumâtre) sans prétraitement adéquat est une cause majeure de pollution de l'eau. L'élimination des métaux lourds à l'aide du procédé membranaire de nanofiltration (NF) est une méthodologie de traitement de l'eau reconnue. Les membranes nanocomposites à couches minces (NCM) ont montré une amélioration considérable des performances en utilisant à la fois les processus OI et NF. Cependant, la fabrication de la membrane NCM a été limitée en raison de la mauvaise dispersion des nanoparticules dans la couche de polyamide (PA) de la membrane et de la lixiviation des nanoparticules souvent dangereuses des membranes NCM.

Pour diverses raisons telles que leur dispersibilité dans les milieux aqueux, la sécurité, le rapport d'aspect élevé et la fonctionnalité, les nanocristaux de cellulose (NCC) sont une nanoparticule idéale pour l'inclusion dans les membranes NCM. En raison de leur caractère hydrophile, les NCC ont plus souvent été dispersées dans la solution aqueuse de monomère lors de la polymérisation interfaciale du PA. Dans cette thèse, nous avons étudié deux voies différentes de modification des NCC pour améliorer la dispersion des NCC dans la solution monomère de chlorure de trimésoyle (CTM)/n-hexane (non aqueux). Dans un cas, nous avons acétylé les NCC (NCCA) en utilisant une méthode simple, efficace et sans solvant pour obtenir une dispersion de NCC plus uniforme dans la couche de PA. Les NCCA résultants étaient moins hydrophiles, ce qui a permis d'augmenter la charge de nanoparticules et d'améliorer leur dispersion dans la couche de PA. Dans un processus de dessalement OI, par rapport aux membranes NCC-NCM non modifiées, le rejet de NaCl des membranes NCCA-NCM est resté stable (à 98-99 %) jusqu'à une charge de 0,4 % en poids, tandis que la perméabilité à l'eau a augmenté jusqu'à 40 %.

Pour le deuxième cas, nous avons synthétisé des NCC fonctionnalisés par la L-cystéine (NCC-Cys) et les avons incorporés dans la couche de PA pour les tester dans un procédé de traitement des eaux usées par NF. Les groupes fonctionnels amine de la L-cystéine sont liés de manière covalente avec les groupes chlorure d'acyle du monomère CTM. Cela a permis d'améliorer la dispersion des nanoparticules mais également pourrait avoir empêché la lixiviation des nanoparticules. De plus, comme la L-cystéine contient des groupes chélateurs

puissants, leur inclusion dans la couche de PA a conduit à un meilleur rejet des métaux lourds. Une charge de 0,1% en poids de NCC-Cys dans les membranes NCM a fourni un rejet élevé des ions cuivre et plomb, 98,1 et 95,2%, respectivement. Les NCC-Cys ont également été évalués dans un processus de dessalement NF entraînant une augmentation de 40 % de la perméabilité à l'eau avec presque aucune diminution du rejet de Na_2SO_4 (97-98 %), $MgCl_2$ et NaCl. Les NCC modifiés nous ont permis de surmonter le compromis perméabilité à l'eau/sélectivité des membranes NCC-NCM pour le dessalement des membranes OI et NF.

Enfin, nous avons développé un protocole expérimental pour étudier l'effet de l'adsorption des ions de métaux lourds (le cas échéant) sur les performances des membranes composites à couches minces (CCM) et NCM dans la NF. Nous avons confirmé que l'adsorption s'est produite et que la capacité d'équilibre des membranes a été atteinte après 8 à 12 h d'expérience. Malgré l'atteinte de la capacité d'équilibre, la perméabilité à l'eau et le rejet de métaux lourds sont restés à leurs valeurs les plus élevées. Cela a conduit à la conclusion que les métaux lourds adsorbés altéraient la surface de la membrane, améliorant ainsi les performances des membranes CCM et NCM.

La possibilité de modifier les NCC permet d'obtenir une plage contrôlée d'hydrophilie/hydrophobicité. Cela permet d'affiner la compatibilité des NCC avec la solution de monomère non aqueux CTM/n-hexane et d'améliorer la dispersion dans la couche de PA, ce qui conduit finalement à une amélioration des performances de la membrane NCM pour les processus OI et NF.

Preface

Dedication

In memory of my beloved *Father,*
Though he is no longer with us, his memory continues to inspire and drive me forward.

I dedicate this thesis to my *Mother* and my *Friends* and my *Colleagues* for their support and guidance who helped me to proceed in my education and life.

Statement of Contributions

I hereby declare that I (*Fatemeh Abedi*) am the sole author of this thesis. I performed all the nanoparticle modification and membrane synthesis, characterization experiments, and all the data analysis. AFM and FESEM imaging were done by Dr. Yun Liu from the University of Ottawa.

My thesis supervisors, *Prof. Marc A. Dubé* and *Prof. Boguslaw Kruczek* from the Department of Chemical and Biological Engineering at the University of Ottawa, provided the scientific supervision and advice throughout this project, and editorial comments for the written work.

Acknowledgements

I would like to express my earnest gratitude to *Prof. Marc A. Dubé* and *Prof. Boguslaw Kruczek* for their scientific guidance and support, and their mentorship throughout the duration of my time in the Polymer Reaction Engineering (PRE) Group. I am thankful for the support and friendship of the entire PRE group. I also give thanks to the Technical Support Staff in the Department of Chemical & Biological Engineering at the University of Ottawa.

I am thankful to the Natural Sciences and Engineering Research Council of Canada, to Celluforce Inc., to Solecta Inc., and to the University of Ottawa for their donations and financial support.

I would also like to acknowledge Dr. Daryoush Emadzadeh from the University of Ottawa for his general guidance, assistance, and support throughout the duration of this research.

Table of Contents

Abstract ..... **II**

Preface ..... **VI**

Dedication ..... **VI**

Statement of Contributions ..... **VII**

Acknowledgements ..... **VIII**

Table of Contents ..... **IX**

Table of Figures ..... **XI**

Table of Tables ..... **XV**

Nomenclature ..... **XVI**

1. Introduction **1**

1.1 Thesis objectives **4**

1.2 Challenges **4**

1.3 Thesis outline **4**

1.4 References **5**

2. Background **9**

2.1 Introduction **9**

2.2 Membrane technology **11**

2.3 TFN membranes **14**

2.4 Cellulose nanomaterials: structure and properties **15**

2.5 CNC-TFN membranes **18**

2.6 References **22**

3. Modifying cellulose nanocrystal dispersibility to address the permeability/selectivity trade-off of thin-film nanocomposite reverse osmosis membranes **30**

3.1 Abstract **30**

3.2 Introduction **31**

3.3 Experimental section **33**

3.4 Results and discussion **37**

3.5 Conclusion **52**

3.6 Supporting information **53**

3.7 References **53**

4. Improving nanofiltration performance using modified cellulose nanocrystal based thin film nanocomposite (TFN) membranes **59**

4.1 Abstract **59**

4.2 Introduction **60**

4.3 Experimental section **62**

4.4 Results and discussion **67**

4.5 Conclusion **83**

4.6 References **84**

5. Adsorption of heavy metals on the surface of nanofiltration membranes: "A curse or blessing"? **89**

5.1 Abstract **89**

5.2 Introduction **90**

5.3 Experimental Section **92**

5.4 Results and discussion **95**

5.5 Conclusion **106**

5.6 References **107**

6. General discussion and conclusion **111**

6.1 General discussion **111**

6.2 Future work **116**

6.3 Concluding remarks **118**

6.4 References **118**

Appendix A: Supporting information for chapter 3 ..... **121**

Appendix B: Cellulose Nanocrystal (CNC) Addition in Thin Film Nanocomposite (TFN) Membranes: Which Monomer Solution is Preferred? **125**

B.1 Abstract **125**

B.2 Introduction **126**

B.3 Experimental Section **129**

B.4 Results and discussion **131**

B.6 Conclusion **143**

B.7 References **144**

Appendix C: Laboratory safety considerations **146**

Table of Figures

Figure 2.1: Number of publications in Scopus™ between 2013-2023 for "nanocellulose" or "membrane", excluding review articles. 11
Figure 2.2: Classification of hydraulic pressure-driven membrane processes based on pore size and operating pressure range. [26] 12
Figure 2.3: Solute exclusion mechanisms in TFC membranes for RO and NF membranes. [44] 14
Figure 2.4: Four different methods of TFN membrane synthesis. 15
Figure 2.5: Cellulose and cellulose nanocrystal structure. [55] 17
Figure 3.1: ATR-FTIR spectra of CNC, ACNC2 and ACNC4. 38
Figure 3.2: Solid-state ^{13}C-NMR spectra of CNC, ACNC2 and ACNC4. 39
Figure 3.3: ATR-FTIR spectrum of TFC and TFNs in 0.1wt% of CNC and ACNCs. 41
Figure 3.4: Water contact angle of TFC and TFNs in 0.1 and 0.4 wt% of CNC and ACNCs. 42
Figure 3.5: a) Zeta potential of TFC and 0.1 wt% CNC and ACNCs-TFN membranes in pH range 3.5-9, b) Zeta potential of TFC and TFN membranes in pH = 6.5 for different loadings of CNC and ACNCs. 44
Figure 3.6: Membrane surface images for (a) TFC, (b) CNC-TFN 0.1%, (c) ACNC2-TFN 0.1%, (d) ACNC4-TFN 0.1%, (e) CNC-TFN 0.4%, (f) ACNC2-TFN 0.4% and (g) ACNC4-TFN 0.4% membranes (FESEM = 1; AFM = 2). 46
Figure 3.7: Cross-section FESEM images of TFC, CNC-TFN0.1, ACNC2-TFN0.4 and ACNC4-TFN0.4. 47
Figure 3.8: RO performance of TFC and TFN membranes a) water permeability and salt rejection) vs. CNC, ACNC2 and ACNC4 loading. 50
Figure 3.9: Correlation between water/NaCl selectivity vs. water permeability. Data points without labels are from Table 3.4. [2] 52
Figure 4.1: Schematic of CNC modification with acetyl group or L-cysteine. (CNCs include sulfate half-ester groups, not shown). 63
Figure 4.2: AFM images of freeze-dried CNCs, ACNCs and CysCNCs. 67
Figure 4.3: ATR-FTIR spectra of CNC, ACNC and CysCNC. 68
Figure 4.4: ^{13}C-NMR spectra of CNC, ACNC and CysCNC. 69
Figure 4.5: Water contact angle measurements of CNC, ACNC and CysCNC surfaces. 69
Figure 4.6: ATR-FTIR spectra of TFC and TFN membranes in 0.1 wt% CNCs, ACNCs. 71

Figure 4.7: XPS spectra for a) TFC and 0.1 wt% CNC-TFN, ACNC-TFN and CysCNC-TFN membranes, b) C1s spectrum of CNC-TFN0.1, c) O1s spectrum of ACNC-TFN0.1 and d) N1s spectrum of CysCNC-TFN0.1. 72
Figure 4.8: a) Zeta potential of TFC and 0.1 wt% TFN membranes a. in the 3.5 to 9 pH range, b) in pH = 6.5 for different nanoparticle loadings. 74
Figure 4.9: a) Rejection with different PEG molecular weights, b) Pore size distribution of TFC, CNC-TFN, ACNC-TFN and CysCNC-TFN membranes in 0.1 wt% loadings..... 75
Figure 4.10: FESEM and AFM membrane surface images for TFC, CNC-TFN0.1, ACNC-TFN0.1, and CysCNC-TFN0.1. 76
Figure 4.11: Performance of TFC and TFN membranes for a) Na_2SO_4, b) $MgCl_2$, c) NaCl rejection at different nanoparticle loadings..... 78
Figure 4.12: Performance of TFC and TFN membranes for a) $CuSO_4$ and b) $Pb(NO_3)_2$ rejection at different nanoparticle loadings..... 80
Figure 4.13: Long-term performance test of TFC, CNC-TFN0.1 and CysCNC-TFN0.1 membranes with 200 ppm CuSO4 solution as a feed. 82
Figure 4.14: Long-term performance of TFC and CysCNC0.1 in the presence of BSA (200 ppm) as a cationic foulant in the feed solution. 83
Figure 5.1: The concentration of adsorbed a) Cu and b) Pb by the TFC and TFN membranes at the end of different duration performance tests. 96
Figure 5.2: EDX spectra of TFC and TFN membranes after a 16-hour performance test of Cu^{2+} rejection..... 99
Figure 5.3: The contact angles of membranes at the end of different duration tests with heavy metal ions in the feed solutions. a) Cu^{2+}, b) Pb^2. 101
Figure 5.4: The zeta potential of TFC and TFN membranes at the end of different duration tests a) Cu^{2+} and b) Pb^{2+} rejection..... 102
Figure 5.5: a) Water permeability and b) Cu^{2+} rejection during 16-hour performance tests for TFC, CNC-TFN, ACNC-TFN and CysCNC-TFN membranes..... 103
Figure 5.6: a) Water permeability and b) Pb^{2+} rejection during 16-hour performance tests for TFC, CNC-TFN, ACNC-TFN and CysCNC-TFN membranes..... 103
Figure 6.1: Schematic of CNC acetylation and the CNC- and ACNC-TFN membranes..... 113
Figure 6.2: Schematic of CNC acetylation and the CNC- and ACNC-TFN membranes..... 114
Figure A.1: Schematic of CNC acetylation Procedure. 121
Figure A.2: XRD patterns of CNC, ACNC2 and ACNC4. 122

Figure A.3: XRD patterns ATR-FTIR spectrum of TFC and TFNs in 0.1wt% of CNC and ACNC2 and ACNC4. 122
Figure A.4: The XPS spectra of a) TFC, b) CNC-TFN0.1, c) ACNC2-TFN0.1 and d) ACNC4-TFN0.1. 123
Figure A.5: Long-term performance test of CNC-TFN0.1, ACNC2-TFN0.4 and ACNC4-TFN0.4 membranes 124
Figure B.1: Synthesis of the PA layer in TFC membranes for NF and RO processes. 130
Figure B.2: The effect of nanoparticle loading on the water contact angle of TFN RO (a) and NF (b) membranes based on CNC, ACNC and CysCNC nanoparticle loading. Solid bars refer to the TFN membranes with nanoparticles dispersed in the TMC organic monomer solution. Striped bars refer to the TFN membranes with nanoparticles dispersed in the MPD (a) or PIP (b) aqueous monomer solution 135
Figure B.3: The effect of nanoparticle loading on the zeta potential of TFN RO (a) and NF (b) membranes based on CNC, ACNC and CysCNC nanoparticles. Solid lines refer to the TFN membranes with nanoparticles dispersed in the TMC organic monomer solution. Dashed lines refer to the TFN membranes with nanoparticles dispersed in MPD (a) or PIP (b) aqueous monomer solution. 137
Figure B.4: The effect of nanoparticle loading on water permeability and NaCl rejection for TFN RO membranes based on CNC, ACNC and CysCNC nanoparticles. Solid lines and bars refer to TFN membranes with the nanoparticles dispersed in the TMC organic monomer solution. Dashed lines and striped bars refer to the TFN membranes with the nanoparticles dispersed in the MPD aqueous monomer solution. 140
Figure B.5: The effect of nanoparticle loading on water permeability and Na_2SO_4 rejection of TFN NF membranes based on CNC, ACNC and CysCNC nanoparticles. Solid lines and bars refer to TFN membranes with the nanoparticles dispersed in the TMC organic monomer solution. Dashed lines and striped bars refer to the TFN membranes with the nanoparticles dispersed in MPD aqueous monomer solution. 140
Figure B.6: Effect of nanoparticle addition strategy on TFN RO membrane performance in comparison to the upper-bound line ($A/B=46.74\ A^{-1.72}$).[35] Solid coloured symbols show results for the nanoparticle addition to the organic monomer solution; open coloured and other symbols show results for the nanoparticle addition to the aqueous monomer solution 142
Figure B.7: Effect of nanoparticle addition strategy on TFN NF membrane performance in comparison to the upper-bound line ($A/B=96.65\ A^{-1.62}$).[36] Solid coloured symbols show

results for the nanoparticle addition to the organic monomer solution; open coloured and other symbols show results for the nanoparticle addition to the aqueous monomer solution.....143

Table of Tables

Table 2.1: Cellulose nanomaterial types and characteristics. 17
Table 2.2: CNC-TFN membrane performance for RO process. 19
Table 2.3: CNC-TFN membrane performance for NF process. 20
Table 3.1: Characterization of CNC and ACNCs. 39
Table 3.2: Elemental composition of membranes by the XPS analyses. 44
Table 3.3: Surface properties of TFC and TFN membranes. 46
Table 3.4: Comparison of permeability and water/NaCl selectivity of RO membranes.[1] 51
Table 4.1: Modified CNC formulation. 63
Table 4.2: CNC, ACNC and CysCNC characterization. 70
Table 4.3: Elemental composition of membranes by the XPS analyses. 73
Table 4.4: Surface properties of TFC and TFN membranes. 77
Table 4.5: Comparison of NF membrane performance reported in the literature for CNC-TFN membranes. 81
Table 5.1: Summary of the analysis of Cu^{2+} and Pb^{2+} adsorption on TFC and TFN membranes. 96
Table 5.2: Summary of the water contact angle and zeta potential analysis of TFC and TFN membranes before and after Cu^{2} and Pb^{2+} rejection. 101
Table 5.3: Summary of the water permeability and rejection of TFC and TFN membranes before and after the Cu^{2+} and Pb^{2+} rejection 105
Table B.1. Properties of CNC, ACNC and CysCNC. 132
Table C.1: List of chemicals, manufacturer, hazards and required PPE. 146

Nomenclature

ACNC	Acetylated CNC	**Na_2SO_4**	Sodium sulfate
AFM	Atomic force microscopy	**NF**	Nanofiltration
ATR-FTIR	Attenuated total reflectance-Fourier transform infrared spectroscopy	**NMR**	Nuclear magnetic resonance spectroscopy
		PA	Polyamide
BSA	Bovine serum albumin	**PEG**	Polyethylene glycol
CNC	Cellulose nanocrystal	**$Pb(NO_3)_2$**	Lead (II) nitrate
$CuSO_4$	Copper (II) sulfate	**PIP**	Piperazine
CysCNC	L-Cysteine modified CNC	**ppb**	Part per billion
DDW	Distilled deionized water	**ppm**	Parts per million
DW	Distilled water	**PS**	Poly(sulfone)
DS	Degree of substitution	**PES**	Poly(ether sulfone)
EDX	Energy Dispersive X-Ray Spectroscopy	**RO**	Reverse osmosis
HCl	Hydrochloric acid	**SEM**	Scanning electron microscopy
ICP-MS	Inductively coupled plasma-mass spectrometry	**TEM**	Transmission electron microscopy
$MgCl_2$	Magnesium chloride	**TFN**	Thin film nanocomposite
MPD	m-phenylenediamine	**TMC**	Trimesoyl chloride
NaCl	Sodium chloride	**XRD**	X-Ray diffraction
$MgSO_4$	Magnesium sulfate	**XPS**	X-ray photoelectron spectroscopy
NaOH	Sodium hydroxide	**WHO**	World Health Organization
NaCl	Sodium chloride		

1. Introduction

The shortage and contamination of water resources induced by population increase and industrialization have led to tremendous challenges for global sustainable economic and social development. Given the fact that 97% of global water resources are seawater, desalination has become an important water purification technology. In addition, wastewater discharged from industrial processes continues to contaminate our precious water resources [1,2]. It is no wonder, therefore, that wastewater treatment is also studied extensively.

Among the technologies developed for brackish and seawater desalination, membrane filtration methods are the dominant choice [3]. Of the membrane separation methods, reverse osmosis (RO) and nanofiltration (NF) are the most widely used due to their simplicity, environmental compatibility and relatively low cost [4,5]. In these membrane separation processes, using external hydrostatic pressure, water is passed through a semipermeable membrane while salts and other contaminants are rejected [6]. One of the major contaminants in industrial wastewater are heavy metal ions; they are highly toxic and difficult to decompose or metabolize in biological systems, most notably the human body [7]. Therefore, removing heavy metal ions from contaminated water, which exceeds the allowed concentration limits published by the World Health Organization (WHO) [8], is also essential. Membrane separation, especially NF, is the most popular due to its high rejection of divalent ions and ability to eliminate residual chemical compounds [9,10].

Thin film composite (TFC) membranes are widely utilized in desalination and wastewater purification owing to their high robustness and durability over a broad range of pH and temperatures [11,12]. TFC membranes are typically composed of a polyamide (PA) thin film layer formed onto a porous ultrafiltration support layer (e.g., poly(ether sulfone), poly(sulfone)). The PA selective layer is made via the interfacial polymerization of diamines (aqueous monomer solution) and acid chlorides (organic monomer solution) [13]. Over the past decades, most studies have employed m-phenylenediamine (MPD) or piperazine (PIP) as the aqueous phase monomer to react with trimesoyl chloride (TMC), the organic phase monomer. In fact, the two most successful commercial TFC membranes for RO and NF are fabricated using MPD/TMC and PIP/TMC, respectively [6,14].

Although TFC membranes have undergone significant development, there are still challenges to their optimal performance, including permeability/selectivity trade-offs, fouling, long-term stability, and membrane degradation due to chlorine attack [15,16]. One approach to improve the performance of TFC membranes is incorporating nanoparticles into the PA layer.

This approach yields what are referred to as thin film nanocomposite (TFN) membranes. Some previously tested nanoparticles include carbon-based nanoparticles [17], metal and metal oxide-based nanoparticles [18], halloysite [19], zeolite [20], and most recently, cellulose nanocrystals (CNCs) [9,21]. To our knowledge, there are no applications of TFN membranes at the commercial scale despite their many advantages. One of the most important limitations of TFN membranes pertains to the leaching of nanoparticles from the membrane. Another challenge for the fabrication of TFN membranes is the poor dispersion and agglomeration of the nanoparticles in the PA layer [5,22]. These leaching and dispersion problems result in potential environmental hazards and membrane degradation, leading to performance reduction over time. The leaching problem can potentially be addressed either by anchoring (e.g., covalently bonding) the nanoparticles to the membrane matrix and/or by using safe nanoparticles [23,24].

CNCs are natural rod-shaped, high aspect ratio nanoparticles, which are obtained from the acid hydrolysis of native cellulose (e.g., from wood pulp) [25]. Because cellulose biomass is abundant and CNC production is relatively simple, these nanoparticles are very cost-effective [26]. The biodegradable CNCs have a low environmental impact and are classified as non-toxic. Their nanometer size results in a high specific surface area, and they are amenable to chemical reactions due to the high density of surface hydroxyl (OH) groups [27]. These attributes make CNCs excellent candidate nanoparticles for modifying TFC membranes to improve performance [28].

Despite promising results, such as water permeability enhancement as well as good antifouling properties demonstrated by CNC-TFN membranes via RO or NF processes, these membranes may still suffer from nanoparticle leaching and agglomeration issues [21,29]. Because of the hydrophilic nature of CNCs, most CNC-TFN membranes have been produced by incorporating the CNCs into the aqueous monomer solution (i.e., MPD solution for RO or PIP solution for NF) [21,30,31]. While there are several examples of CNCs dispersed in the aqueous monomer solution for TFN membrane production [32], our laboratory has prepared an innovative TFN membrane by adding the CNCs into the PA layer by dispersing them into the organic TMC/n-hexane solution [33]. Adding hydrophilic nanoparticles into a hydrophobic monomer solution may not appear logical because of the increased chances of nanoparticle agglomeration. However, the fabrication of the PA layer by interfacial polymerization is a sequential process. First, the ultrafiltration (UF) membrane, which will ultimately support the active PA layer, is immersed in an aqueous monomer solution. The excess of the aqueous monomer solution must be removed, which may lead to losing some dispersed nanoparticles.

Only then the organic monomer solution is brought in contact with the support layer saturated with the aqueous monomer solution to initiate the interfacial polymerization. Therefore, the time when nanoparticles must be perfectly dispersed in the hydrophobic monomer solution is much shorter than in the aqueous monomer solution. As a result, the dispersion of hydrophilic nanoparticles in the hydrophobic monomer solution might be justified. This approach led to successful CNC-based TFN membranes with improved antifouling properties and increased water permeability without sacrificing salt rejection in RO process. However, this approach has worked only for relatively small loadings of CNCs (up to 0.1 wt%) [34].

To overcome the limitation of nanoparticles' loading, they may be factionalized to improve their compatibility with the TMC monomer solution. CNCs, because of the abundance of hydroxyl groups, can be modified in various ways. Several CNC surface modification approaches exist to potentially enhance the compatibility of the CNCs with the PA layer leading to anchoring CNCs to the PA layer [35–37]. Surface functionalization of CNCs with acetyl groups via esterification (ACNCs) and with amine groups via amino acid molecules such as L-cysteine (CysCNCs) were the two modification methods investigated in this thesis. Esterification was expected to slightly decrease the hydrophilicity of CNCs, which could improve CNC dispersion in the TMC/n-hexane monomer solution and, consequently, the PA layer [13]. The expected impact of incorporating L-cysteine modified CNCs in the PA layer included: 1- increasing CNC hydrophilicity to improve water permeability, 2- enhancing heavy metal ion rejection due to the thiol (SH) groups of L-cysteine, and 3- covalently bonding the amine (NH_2) groups of L-cysteine to the acyl chloride groups of the TMC monomer, making them less prone to leaching and being anchored in PA strucure. Thus, we hypothesized that CNC modification could improve its dispersibility in the PA layer, thereby allowing an increase in CNC loading, and ultimately improved membrane performance. To verify our hypothesis, we first used acetylated CNCs in RO-TFN membranes for brackish water desalination. Then, we compared the two different modified CNCs (i.e., ACNCs and CysCNCs) into NF-TFN membranes for water desalination and heavy metal rejection.

Size exclusion and electrostatic repulsion (Donnan effect) are the primary mechanisms for rejecting divalent ions using NF-TFC membranes[38]. When TFC or TFN membranes are used for heavy metal separation, in addition to the mechanisms mentioned above, metal ions can be removed by adsorption on the membrane surface; we refer to them as adsorptive membranes [39–43]. The term adsorptive implies the existence of an adsorption capacity, after which the rejection of heavy metals should decrease[44]. There is no consensus on the effect of the adsorbed heavy metals on NF-TFC/TFN membrane performance. Thus, through a novel

experimental protocol, we investigated the adsorption content on the NF-TFC/TFN membrane surfaces and its effect on membrane performance.

1.1 Thesis objectives

The focus of this project was to fabricate TFN membranes based on modified CNCs for RO and NF processes for water purification. We hypothesized that the surface modification of CNCs would facilitate their incorporation into the PA layer by their dispersion in the organic TMC/n-hexane monomer solution. Herein lies one innovative element of this thesis: the use of CNC modification to enhance their compatibility with the organic monomer solution rather than the aqueous monomer solution.

A secondary objective of this project was to explore the effect of modified CNC loading on CNC-TFN membrane performance, including water permeability, salt rejection, fouling and heavy metal rejection. The final objective was to evaluate the performance of TFC and TFN membranes in NF process for removing heavy metals, focusing on the role of heavy metal adsorption on the membrane performance.

1.2 Challenges

Finding a CNC modification approach that can increase the probability of covalent bonding between CNC and PA functional groups was the first challenge to be met in this project. We considered a method that was straightforward, low-cost, energy-efficient, sustainable and non-toxic. Another challenge in this project was the fabrication methodology of the RO and NF membranes. While interfacial polymerization is not a particularly complicated process, the fabrication of thin film nanocomposites is not straightforward and is sensitive to a variety of factors (e.g., nanoparticle loading and homogeneous dispersion of nanoparticle/monomer solutions) [21]. The final challenge was to design a systematic experimental protocol to monitor the adsorption of heavy metal ions by the NF-TFC and -TFN membranes during actual filtration tests.

1.3 Thesis outline

This thesis includes six chapters and is presented in the form of a series of manuscripts submitted for publication in refereed journals, described below.

Chapter 2 provides a background on membrane technology and CNC-TFN membranes.

Chapter 3 was published in the Desalination Journal. The effects of ACNCs on desalination and the long-term performance of RO-TFN membranes was explored. The TFN membranes were produced by embedding different CNC and ACNC loadings into the PA layer by dispersing them in the organic monomer solution.

Chapter 4 was published in the Journal of Membrane Science. CysCNCs and ACNCs were used in the synthesis of TFN-NF membranes by dispersing them in the organic monomer solution of the PA layer. Membrane performance was assessed for desalination, heavy metal rejection, antifouling, and long-term performance.

Chapter 5 was submitted to the Journal of Membrane Science. In this study, we investigated the correlation between heavy metal adsorption (Cu^{2+}, Pb^{2+}) by TFC, CNC-TFN and modified CNC-TFN membranes and their performance.

Finally, Chapter 6 provides a general discussion summarizing the most important findings in this thesis. The discussion concludes by proposing new, more effective approaches to fabricate sustainable membranes. This chapter contains elements of a manuscript submitted to the Canadian Journal of Chemical Engineering.

1.4 References

[1] N. García Doménech, F. Purcell-Milton, Y.K. Gun'ko, Recent progress and future prospects in development of advanced materials for nanofiltration, Materials Today Communications. 23 (2020) 100888. https://doi.org/10.1016/j.mtcomm.2019.100888.

[2] B. Al-Najar, C.D. Peters, H. Albuflasa, N.P. Hankins, Pressure and osmotically driven membrane processes: A review of the benefits and production of nano-enhanced membranes for desalination, Desalination. 479 (2020) 114323. https://doi.org/10.1016/j.desal.2020.114323.

[3] M. Qasim, M. Badrelzaman, N.N. Darwish, N.A. Darwish, N. Hilal, Reverse osmosis desalination: A state-of-the-art review, Desalination. 459 (2019) 59–104. https://doi.org/10.1016/j.desal.2019.02.008.

[4] A. Giwa, N. Akther, V. Dufour, S.W. Hasan, A critical review on recent polymeric and nano-enhanced membranes for reverse osmosis, RSC Adv. 6 (2016) 8134–8163. https://doi.org/10.1039/C5RA17221G.

[5] S. Lin, Energy Efficiency of Desalination: Fundamental Insights from Intuitive Interpretation, Environ. Sci. Technol. (2019) acs.est.9b04788. https://doi.org/10.1021/acs.est.9b04788.

[6] J.M. Gohil, P. Ray, A review on semi-aromatic polyamide TFC membranes prepared by interfacial polymerization: Potential for water treatment and desalination, Separation and Purification Technology. 181 (2017) 159–182. https://doi.org/10.1016/j.seppur.2017.03.020.

[7] S. Bolisetty, M. Peydayesh, R. Mezzenga, Sustainable technologies for water purification from heavy metals: review and analysis, Chem. Soc. Rev. 48 (2019) 463–487. https://doi.org/10.1039/C8CS00493E.

[8] A.E. Burakov, E.V. Galunin, I.V. Burakova, A.E. Kucherova, S. Agarwal, A.G. Tkachev, V.K. Gupta, Adsorption of heavy metals on conventional and nanostructured materials for wastewater treatment purposes: A review, Ecotoxicology and Environmental Safety. 148 (2018) 702–712. https://doi.org/10.1016/j.ecoenv.2017.11.034.
[9] N.A. Khan, S.U. Khan, S. Ahmed, I.H. Farooqi, A. Dhingra, A. Hussain, F. Changani, Applications of Nanotechnology in Water and Wastewater Treatment: A Review, AJW. 16 (2019) 81–86. https://doi.org/10.3233/AJW190051.
[10] O.V. Alekseeva, N.A. Bagrovskaya, A.V. Noskov, Sorption of heavy metal ions by cellulose modified with fullerene, Russ J Appl Chem. 88 (2015) 436–441. https://doi.org/10.1134/S107042721503012X.
[11] A. Al Mayyahi, Important Approaches to Enhance Reverse Osmosis (RO) Thin Film Composite (TFC) Membranes Performance, Membranes. 8 (2018) 68. https://doi.org/10.3390/membranes8030068.
[12] J. Ganesan, M.P. Gandhi, M. Nagendran, B. Li, V. Nair, P. Velayudhaperumal Chellam, Functional Properties of Nanoporous Membranes for the Desalination of Water, in: N. Dasgupta, S. Ranjan, E. Lichtfouse (Eds.), Environmental Nanotechnology Volume 4, Springer International Publishing, Cham, 2020: pp. 131–163. https://doi.org/10.1007/978-3-030-26668-4_4.
[13] J.M. Gohil, R.R. Choudhury, Introduction to Nanostructured and Nano-enhanced Polymeric Membranes: Preparation, Function, and Application for Water Purification, in: Nanoscale Materials in Water Purification, Elsevier, 2019: pp. 25–57. https://doi.org/10.1016/B978-0-12-813926-4.00038-0.
[14] M. Adamczak, G. Kamińska, J. Bohdziewicz, Preparation of Polymer Membranes by In Situ Interfacial Polymerization, International Journal of Polymer Science. 2019 (2019) 1–13. https://doi.org/10.1155/2019/6217924.
[15] N. Abdullah, N. Yusof, W.J. Lau, J. Jaafar, A.F. Ismail, Recent trends of heavy metal removal from water/wastewater by membrane technologies, Journal of Industrial and Engineering Chemistry. 76 (2019) 17–38. https://doi.org/10.1016/j.jiec.2019.03.029.
[16] A.A. Yaqoob, T. Parveen, K. Umar, M.N. Mohamad Ibrahim, Role of Nanomaterials in the Treatment of Wastewater: A Review, Water. 12 (2020) 495. https://doi.org/10.3390/w12020495.
[17] S. Xu, H. Lin, G. Li, J. Wang, Q. Han, F. Liu, Anionic covalent organic framework as an interlayer to fabricate negatively charged polyamide composite nanofiltration membrane featuring ions sieving, Chemical Engineering Journal. 427 (2022) 132009. https://doi.org/10.1016/j.cej.2021.132009.
[18] S. Bandehali, A. Moghadassi, F. Parvizian, Y. Zhang, S.M. Hosseini, J. Shen, New mixed matrix PEI nanofiltration membrane decorated by glycidyl-POSS functionalized graphene oxide nanoplates with enhanced separation and antifouling behaviour: Heavy metal ions removal, Separation and Purification Technology. 242 (2020) 116745. https://doi.org/10.1016/j.seppur.2020.116745.
[19] A. Atashgar, D. Emadzadeh, S. Akbari, B. Kruczek, Incorporation of Functionalized Halloysite Nanotubes (HNTs) into Thin-Film Nanocomposite (TFN) Nanofiltration Membranes for Water Softening, Membranes. 13 (2023) 245. https://doi.org/10.3390/membranes13020245.
[20] S.A. Hamid, S.F. Azha, L. Sellaoui, A. Bonilla-Petriciolet, S. Ismail, Adsorption of copper (II) cation on polysulfone/zeolite blend sheet membrane: Synthesis, characterization, experiments and adsorption modelling, Colloids and Surfaces A: Physicochemical and Engineering Aspects. 601 (2020) 124980. https://doi.org/10.1016/j.colsurfa.2020.124980.

[21] H. Saleem, S.J. Zaidi, Nanoparticles in reverse osmosis membranes for desalination: A state of the art review, Desalination. 475 (2020) 114171. https://doi.org/10.1016/j.desal.2019.114171.
[22] M.R. Esfahani, S.A. Aktij, Z. Dabaghian, M.D. Firouzjaei, A. Rahimpour, J. Eke, I.C. Escobar, M. Abolhassani, L.F. Greenlee, A.R. Esfahani, A. Sadmani, N. Koutahzadeh, Nanocomposite membranes for water separation and purification: Fabrication, modification, and applications, Separation and Purification Technology. 213 (2019) 465–499. https://doi.org/10.1016/j.seppur.2018.12.050.
[23] C. Xu, W. Chen, H. Gao, X. Xie, Y. Chen, Cellulose nanocrystal/silver (CNC/Ag) thin-film nanocomposite nanofiltration membranes with multifunctional properties, Environ. Sci.: Nano. 7 (2020) 803–816. https://doi.org/10.1039/C9EN01367A.
[24] X. Song, B. Gan, S. Qi, H. Guo, C.Y. Tang, Y. Zhou, C. Gao, Intrinsic Nanoscale Structure of Thin Film Composite Polyamide Membranes: Connectivity, Defects, and Structure–Property Correlation, Environ. Sci. Technol. 54 (2020) 3559–3569. https://doi.org/10.1021/acs.est.9b05892.
[25] R.E. Abouzeid, R. Khiari, N. El-Wakil, A. Dufresne, Current State and New Trends in the Use of Cellulose Nanomaterials for Wastewater Treatment, Biomacromolecules. 20 (2019) 573–597. https://doi.org/10.1021/acs.biomac.8b00839.
[26] R. Moeinzadeh, A.G. Jadval Ghadam, W.J. Lau, D. Emadzadeh, Synthesis of nanocomposite membrane incorporated with amino-functionalized nanocrystalline cellulose for refinery wastewater treatment, Carbohydrate Polymers. 225 (2019) 115212. https://doi.org/10.1016/j.carbpol.2019.115212.
[27] N.A. Bagrovskaya, O.V. Alekseeva, O.V. Rozhkova, A.N. Rodionova, S.A. Lilin, Extracting heavy metals with cellulose-containing materials, Prot Met. 44 (2008) 394–396. https://doi.org/10.1134/S0033173208040152.
[28] S. Hokkanen, A. Bhatnagar, M. Sillanpää, A review on modification methods to cellulose-based adsorbents to improve adsorption capacity, Water Research. 91 (2016) 156–173. https://doi.org/10.1016/j.watres.2016.01.008.
[29] L. Bai, H. Wu, J. Ding, A. Ding, X. Zhang, N. Ren, G. Li, H. Liang, Cellulose nanocrystal-blended polyethersulfone membranes for enhanced removal of natural organic matter and alleviation of membrane fouling, Chemical Engineering Journal. 382 (2020) 122919. https://doi.org/10.1016/j.cej.2019.122919.
[30] A.M.A. Abdelsamad, M. Matthias, A.S.G. Khalil, M. Ulbricht, Nanofillers dissolution as a crucial challenge for the performance stability of thin-film nanocomposite desalination membranes, Separation and Purification Technology. 228 (2019) 115767. https://doi.org/10.1016/j.seppur.2019.115767.
[31] W. Li, Z. Yang, W. Liu, Z. Huang, H. Zhang, M. Li, X. Ma, C.Y. Tang, Z. Xu, Polyamide reverse osmosis membranes containing 1D nanochannels for enhanced water purification, Journal of Membrane Science. 618 (2021) 118681. https://doi.org/10.1016/j.memsci.2020.118681.
[32] A. Tshikovhi, S.B. Mishra, A.K. Mishra, Nanocellulose-based composites for the removal of contaminants from wastewater, International Journal of Biological Macromolecules. 152 (2020) 616–632. https://doi.org/10.1016/j.ijbiomac.2020.02.221.
[33] F. Asempour, D. Emadzadeh, T. Matsuura, B. Kruczek, Synthesis and characterization of novel Cellulose Nanocrystals-based Thin Film Nanocomposite membranes for reverse osmosis applications, Desalination. 439 (2018) 179–187. https://doi.org/10.1016/j.desal.2018.04.009.
[34] F. Asempour, D. Emadzadeh, T. Matsuura, B. Kruczek, Synthesis and characterization of novel Cellulose Nanocrystals-based Thin Film Nanocomposite membranes for reverse

osmosis applications, Desalination. 439 (2018) 179–187. https://doi.org/10.1016/j.desal.2018.04.009.
[35] M. Kadhom, B. Deng, Synthesis of high-performance thin film composite (TFC) membranes by controlling the preparation conditions: Technical notes, Journal of Water Process Engineering. 30 (2019) 100542. https://doi.org/10.1016/j.jwpe.2017.12.011.
[36] E. Smith, K. Hendren, J. Haag, E. Foster, S. Martin, Functionalized Cellulose Nanocrystal Nanocomposite Membranes with Controlled Interfacial Transport for Improved Reverse Osmosis Performance, Nanomaterials. 9 (2019) 125. https://doi.org/10.3390/nano9010125.
[37] S.-J. Park, W. Choi, S.-E. Nam, S. Hong, J.S. Lee, J.-H. Lee, Fabrication of polyamide thin film composite reverse osmosis membranes via support-free interfacial polymerization, Journal of Membrane Science. 526 (2017) 52–59. https://doi.org/10.1016/j.memsci.2016.12.027.
[38] B. Al-Najar, C.D. Peters, H. Albuflasa, N.P. Hankins, Pressure and osmotically driven membrane processes: A review of the benefits and production of nano-enhanced membranes for desalination, Desalination. 479 (2020) 114323. https://doi.org/10.1016/j.desal.2020.114323.
[39] A.M. Nasir, P.S. Goh, M.S. Abdullah, B.C. Ng, A.F. Ismail, Adsorptive nanocomposite membranes for heavy metal remediation: Recent progresses and challenges, Chemosphere. 232 (2019) 96–112. https://doi.org/10.1016/j.chemosphere.2019.05.174.
[40] L. Qalyoubi, A. Al-Othman, S. Al-Asheh, Recent progress and challenges on adsorptive membranes for the removal of pollutants from wastewater. Part I: Fundamentals and classification of membranes, Case Studies in Chemical and Environmental Engineering. 3 (2021) 100086. https://doi.org/10.1016/j.cscee.2021.100086.
[41] T.S. Vo, M.M. Hossain, H.M. Jeong, K. Kim, Heavy metal removal applications using adsorptive membranes, Nano Convergence. 7 (2020) 36. https://doi.org/10.1186/s40580-020-00245-4.
[42] S. Hao, Z. Jia, J. Wen, S. Li, W. Peng, R. Huang, X. Xu, Progress in adsorptive membranes for separation – A review, Separation and Purification Technology. 255 (2021) 117772. https://doi.org/10.1016/j.seppur.2020.117772.
[43] J.E. Efome, D. Rana, T. Matsuura, C.Q. Lan, Experiment and modeling for flux and permeate concentration of heavy metal ion in adsorptive membrane filtration using a metal-organic framework incorporated nanofibrous membrane, Chemical Engineering Journal. 352 (2018) 737–744. https://doi.org/10.1016/j.cej.2018.07.077.
[44] S.S. Madaeni, E. Salehi, Adsorption of cations on nanofiltration membrane: Separation mechanism, isotherm confirmation and thermodynamic analysis, Chemical Engineering Journal. 150 (2009) 114–121. https://doi.org/10.1016/j.cej.2008.12.005.

2. Background

2.1 Introduction

Water is vital for sustaining healthy life [1]. About 36% of the world's population lives in water-scarce areas, with over two billion people left with no alternative but to drink contaminated water. Over the years, several technologies have been employed for water purification, such as membrane filtration, chemical precipitation, solvent extraction, ion exchange, coagulation and adsorption [2]. The development of membrane materials for water desalination and wastewater treatment has attracted the attention of numerous researchers due to their high performance, low cost and durability [3].

A membrane is often referred to as a permeable or semipermeable barrier that allows the transport of specific molecules/ions while restricting others [4]. In the case of water purification, the ideal membrane is highly water permeable, selective, resistant to fouling, chlorine resistant, mechanically and chemically stable, easily manufacturable, produced from cheap and abundant materials [5,6]. Based on the driving force for the transport and separation of selected species in water, membranes are categorized as pressure-driven or non-pressure-driven processes [7]. Non-pressure driving forces can be temperature (membrane distillation) or electrical potential (electrodialysis) [8]. Commercial pressure-driven membranes are classified into integrally-skinned asymmetric membranes and thin film composite (TFC) membranes [9].

Although TFC membranes have undergone several property-performance improvements in the past few decades, there are still challenges to further develop TFC membranes [9]. The trade-off between water permeability and selectivity, membrane fouling, and membrane degradation due to chlorination are the current major constraints on TFC membrane performance in water purification [10]. There are many strategies to improve TFC membrane properties, including adding a comonomer, adding a cosolvent, surface modification and nanoparticle incorporation [11]. The most common strategy, in particular since the pioneering work of Jeong et al. [12], is to incorporate nanoparticles (e.g. graphene oxide, carbon nanotubes, metal organic frameworks, zeolites and titanium oxide) into the TFC membranes resulting thin-film nanocomposite (TFN) membranes [13]. The use of nanoparticles has led to changes in membrane surface properties such as hydrophilicity, charge density, roughness and crosslinking density of the polymer matrix, and as a result, enhanced membrane performance. However, the application of TFN membranes at the commercial scale has been limited despite their many advantages. One of the most critical issues with TFN

membranes is the leaching of hazardous nanoparticles from the membrane into the downstream (permeate and retentate), which is of concern in following strict drinking water and environmental safety regulations [14]. Another challenge for TFN membrane fabrication is the nanoparticle aggregation in the polymer matrix, leading to sub-optimal performance. These problems result in forming defects in the membrane structure and causing degradation and poor long-term performance [15].

Cellulose nanocrystals (CNCs) offer a suitable alternative to environmentally hazardous nanomaterials. CNCs are natural rod-shaped, high aspect-ratio nanoparticles obtained from the acid hydrolysis of native cellulose (e.g., from wood pulp)[16]. CNCs only became commercially available in 2012 from CelluForce, Inc., in Quebec, Canada. The company operates the world's largest CNC plant, capable of producing 300 tonnes of CNCs per year [17]. CNCs have been added to Canada's Domestic Substance List, allowing their unrestricted production and sale [18]. The biodegradable CNCs have a low environmental impact and are classified as non-toxic [19]. Also, CNCs have received regulatory clearance for use in the US and Europe as they fall into the least toxic classification in the Globally Harmonized System of Classification and Labelling of Chemicals [20]. Because CNCs are safe nanoparticles, any possible leaching during water purification should not pose health and environmental concerns, although preventing their leaching is still a priority [21]. Abundant cellulose biomass feedstock and relatively simple CNC production makes these nanoparticles cost-effective [22]. The cost of CNC materials ranges from 0.65 to 2.80 US$/g, which is relatively lower than carbon nanotubes (8 to 280 US$/g) [23].

The research interest in CNCs for membrane applications can be surmised from the recent increase in research publications on the subject. Figure 2.1 generated from data at scopus.com, presents the number of publications over the past ten years where the terms "nanocellulose" or "membrane" were included in the title, abstract, or keywords. Moreover, the database yielded 7092 results for "nanocellulose" and 590 for "nanocellulose for membrane applications." A scan of these papers reveals that CNCs have been used mostly in TFC membranes. The first introduction of CNCs into pressure-driven based membranes was presented in 2018 by incorporating CNCs into the PA layer of TFC membranes for the RO process [24]. Since then, more than 50 articles reported on the use of CNCs in pressure-driven processes membranes for water and wastewater purification.

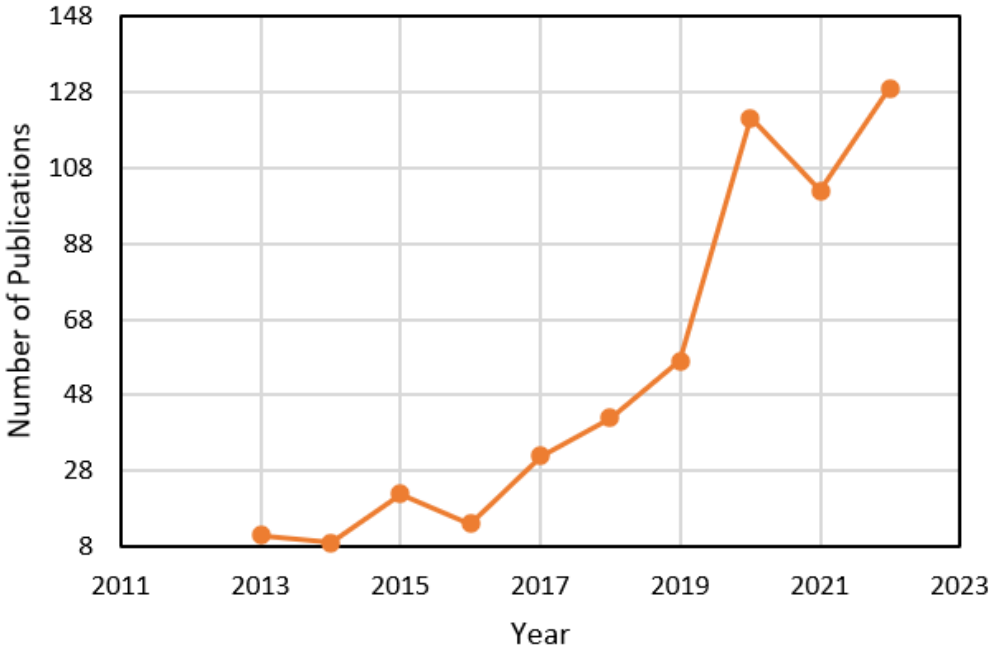

Figure 2.1: Number of publications in Scopus™ between 2013-2023 for "nanocellulose" or "membrane", excluding review articles.

However, to the best of our knowledge, there is a lack of extensive review on the fabrication-performance relationship of CNC-based TFN membranes for pressure-driven processes in water and wastewater treatment. The key challenges and knowledge gaps that limit the practical application of CNCs in TFN nanocomposite membrane synthesis (i.e., how to incorporate CNCs) for water/wastewater treatment processes need to be explored further.

2.2 Membrane technology

The driving force for pressure-driven membranes can be either hydraulic or osmotic pressure [25]. Hydraulic pressure-driven membrane processes are divided into four groups according to the membrane's pore size and operating pressure range: microfiltration (MF): pore size = 0.1–2.0 μm, ultrafiltration (UF): pore size = 2–100 nm, nanofiltration (NF): pore size = 1–10 nm, and reverse osmosis (RO): pore size ≤1 nm (Figure 2.2) [26,27]. Due to the larger pore size of UF and MF membranes than most salt ions (e.g., sodium, chlorine, magnesium, sulfate), they are not commonly used for brackish and seawater desalination [28]. Indeed, UF and MF membranes are considered pre-filtration processes mainly for dye, foulant, bacteria, and viruses [29]. Forward osmosis (FO) is the process in which the driving force is osmotic pressure. Osmosis is defined as a natural process in which water molecules spontaneously move from a low-concentration solution (low osmotic pressure) to a high-concentration solution (high osmotic pressure) across a membrane[20]. The flow of water molecules can be

reversed by an external hydraulic pressure applied to a solution of higher concentration. In such a case, the process occurring is known as reverse osmosis (RO) [30]. Compared to hydraulic pressure-driven membrane processes, FO offers energy consumption savings and lower membrane fouling. However, the internal concentration polarization needs to be minimized for high productivity (i.e., water permeability) [31].

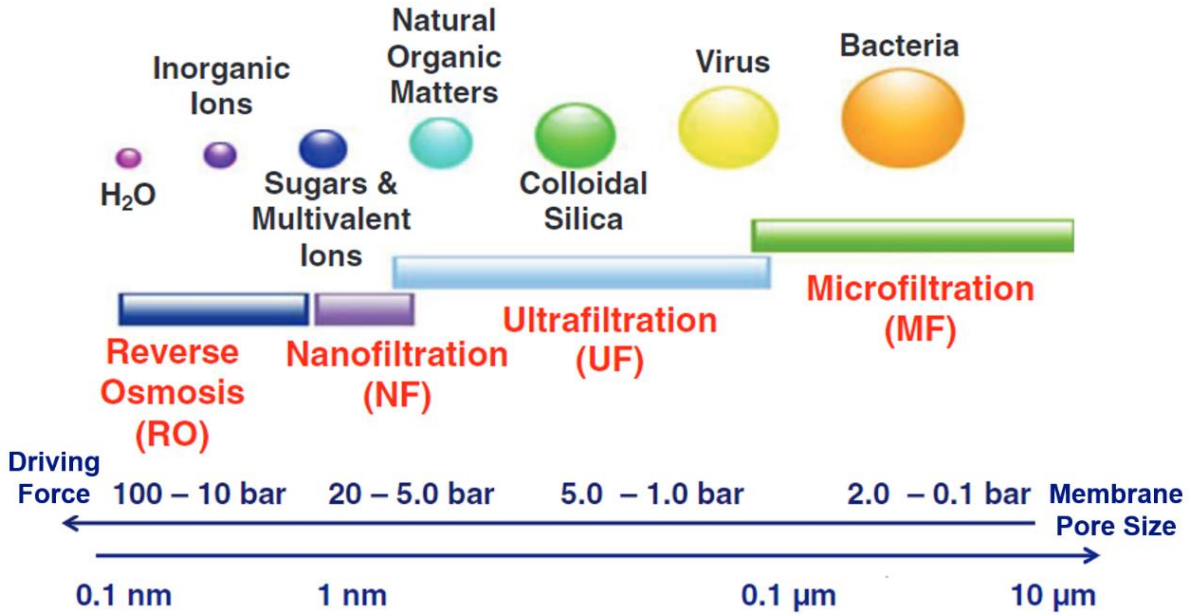

Figure 2.2: Classification of hydraulic pressure-driven membrane processes based on pore size and operating pressure range. [26]

The TFC membrane was first synthesized by Cadotte in 1980 to desalinate seawater via the RO process [32]. TFC membranes are generally comprised of three layers: a selective layer with a thickness of 50-200 nm, an integrally skinned asymmetric porous support, usually a UF or MF membrane (e.g., polysulfone: PS or polyether sulfone: PES) with a thickness less than 40 µm, and a polyester nonwoven fabric (thickness < 120 µm) to provide mechanical strength [33,34]. The dense selective layer, which acts as the barrier regulating solute rejection and water permeability, is typically polyamide (PA). It is formed on top of the support layer using interfacial polymerization. This reactive process brings two monomers together at an interface between two immiscible phases, producing a thin, usually dense, polymer film [35,36]. The interfacial polymerization with m-phenylenediamine (MPD) in the aqueous phase and trimesoyl chloride (TMC) in the organic phase has been used extensively for the fabrication of RO membranes (Figure 2.3) [37]. By replacing the MPD in the aqueous phase with piperazine (PIP), the process is used to produce NF membranes. The interfacial polymerization is highlighted by fast reaction kinetics yielding a PA layer with a tunable structure and reliable

performance at the commercial scale [38]. Because the diffusion of diamine groups controls the reaction, the polymerization continues until the formed thin film becomes a barrier for the diamine to diffuse; hence, the reaction's self-inhibiting nature [39].

The PA-based TFC membrane surfaces usually possess a negative surface charge density over a pH range of 3.5-9.5 [40]. The negative surface charge density arises from the carboxylic acid groups available in the semi-aromatic PA structure due to the unreacted acyl chloride of the TMC monomer [41]. The morphology of the dense PA layer is typically a smooth layer at the interface and a rough and nodular top surface layer with ridges and valleys confirmed by scanning electron microscopy (SEM) and transmission electron microscopy (TEM) images [42]. The PA layer for NF membranes has a less dense structure than for the RO membranes due to lower crosslinking density. The crosslinking density directly impacts the structure of the PA layer and, therefore, the operating pressure. Thus, the denser RO membranes require a higher operating pressure than NF membranes [26]. The rejection in NF-TFC membranes is governed by electrostatic repulsion (Donnan exclusion and dielectric exclusion) and steric exclusion, while for RO-TFC membranes, the solution-diffusion mechanism (steric exclusion) dominates [43]. According to the Donnan exclusion, the negatively charged surface membranes attract cations and repulse anions. The higher the valence, the stronger the attraction/rejection of the ions by the membrane. At the same time, the feed and permeate should maintain electro-neutrality. In other words, although cations are attracted by the negatively charged NF membranes, their transport across the membrane is limited because of the rejection of their corresponding anions (Figure 2.4) [44].

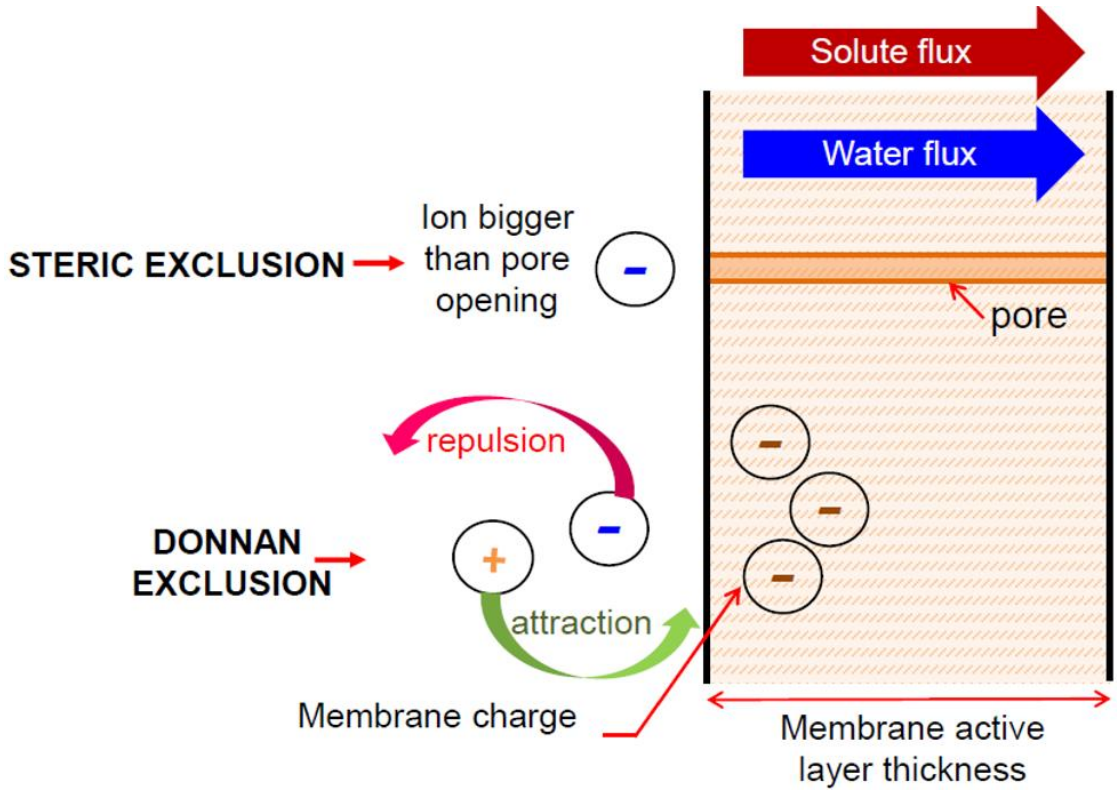

Figure 2.3: Solute exclusion mechanisms in TFC membranes for RO and NF membranes. [44]

2.3 TFN membranes

The incorporation of nanoparticles can tune the membrane structure and physicochemical properties (i.e., hydrophilicity, porosity, surface charge density, crosslinking density, thickness, surface roughness, and chemical and mechanical stability) and introduce unique surface functionalities that could be exploited to affect membrane performance [64]. There is a strong correlation between the fabrication method, surface properties and performance of TFN membranes (Figure 2.5) [45]. Four possible methods for fabricating TFN membranes via PA interfacial polymerization are:

1. Nanoparticles dispersed in the PA layer: For interfacial polymerization of the PA, the nanoparticles can be dispersed in either an aqueous or organic monomer solution [46].

2. Nanoparticles coated on top of the PA layer: Nanoparticles can be deposited directly on the surface of prefabricated TFC membranes using different methods, including self-assembly, coating/deposition, spin coating, vacuum filtration and chemical grafting [1].

3. Nanoparticles dispersed in the support layer: Nanoparticles can be added during the support layer synthesis (e.g., PS and PES) using phase inversion [47].

4. Nanoparticles coated as an interlayer between the PA and support layer [5,48].

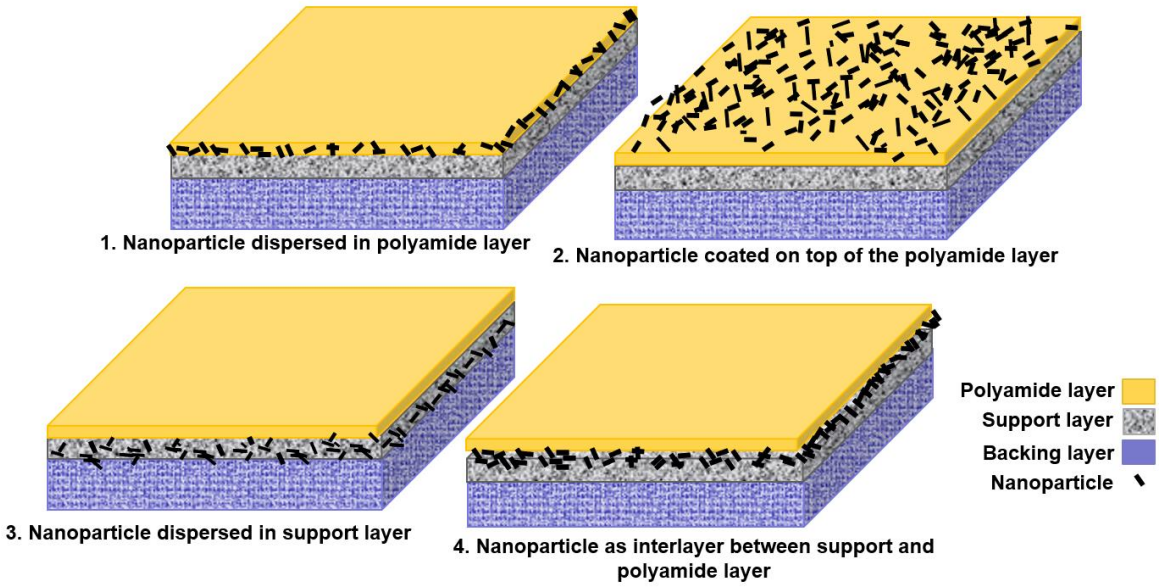

Figure 2.4: Four different methods of TFN membrane synthesis.

The performance of TFN membranes in terms of water permeability and water/salt selectivity for the four fabrication methods for FO/RO and NF processes have been investigated by Wei et al. [32]. Based on 187 pairs of optimal TFN membranes, it was revealed that in TFN membranes prepared by nanoparticle incorporation in the PA active layer, both RO and NF membranes exhibited improvement in water permeability and salt selectivity compared to the other three preparation methods. The nanoparticle participation in the PA formation highly depends on whether they can react with the amine or acyl chloride monomers [8]. In addition, embedding the nanoparticles in the PA layer leads to more noticeable changes in membrane surface properties, including charge density, hydrophilicity, and roughness. The leaching of nanoparticles during long-term performance is always a concern for TFN membranes prepared by nanoparticles as an interlayer. If the support and active layers are connected to the interlayer without sufficient chemical bonding, detachment of PA layers and deterioration of the interlayer could occur [49]. In addition, when nanoparticles are coated on top of the PA layer or as an interlayer, additional steps, or materials such as immobilizing agents are often required during the synthesis of TFN membranes.

2.4 Cellulose nanomaterials: structure and properties

Cellulose nanomaterials are cellulosic materials with at least one dimension in the nano range (diameter or length) [14]. They are extracted from sustainable lignocellulosic biomass (e.g., cellulose, lignin, and hemicellulose) by chemical, mechanical and biological methods.

Cellulose nanomaterials are carbohydrate polymers $(C_6H_{10}O_5)_n$ composed of β-D-glucopyranose repeat units connected by β-1,4 glycosidic linkages composed of three hydroxyl groups, the primary (-OH) at the C-6 position and the secondary (-OH) at C-2 and at C-3 (Figure 2.6) [17].

Depending on the extraction method and source of biomass, cellulose nanomaterials include cellulose nanofibers (CNFs), bacterial nanocellulose (BNC) and CNCs. The process of obtaining CNFs involves applying high shear forces such as grinding, ultrasonication and homogenization, which require high energy consumption [32]. CNFs are comprised of flexible, long, and entangled networks [50]. On the other hand, CNCs with a high degree of crystallinity (80-90%) are produced through the oxidation of cellulosic fibers via hydrolysis under strong acids such as sulfuric acid, phosphoric acid, and hydrochloric acid. During acid hydrolysis, the hydrogen bonds are disrupted, and the amorphous domain is cleaved, finally releasing the nanocrystals [51]. The CNCs' aspect ratio (or length-to-diameter ratio) varies in both length and diameter depending on the source of cellulose and the hydrolysis conditions [52]. Finally, BNC is considered the purest cellulose in the form of nanofibrous networks [53]. BNCs are extracted from aerobic bacteria as an extracellular polysaccharide membrane using a bottom-up approach [11]. The structural characteristics of the different cellulose nanomaterials are provided in Table 2.1.

The application of cellulose nanomaterials in TFC membranes has been mainly focused on CNCs due to their structure compared to CNFs and BNC. CNFs and BNC are entangled 3D networks, making their dispersion more challenging than CNCs. CNF and BNC-based membranes for water purification have been produced as pure paper membranes rather than incorporated into TFC membranes [54].

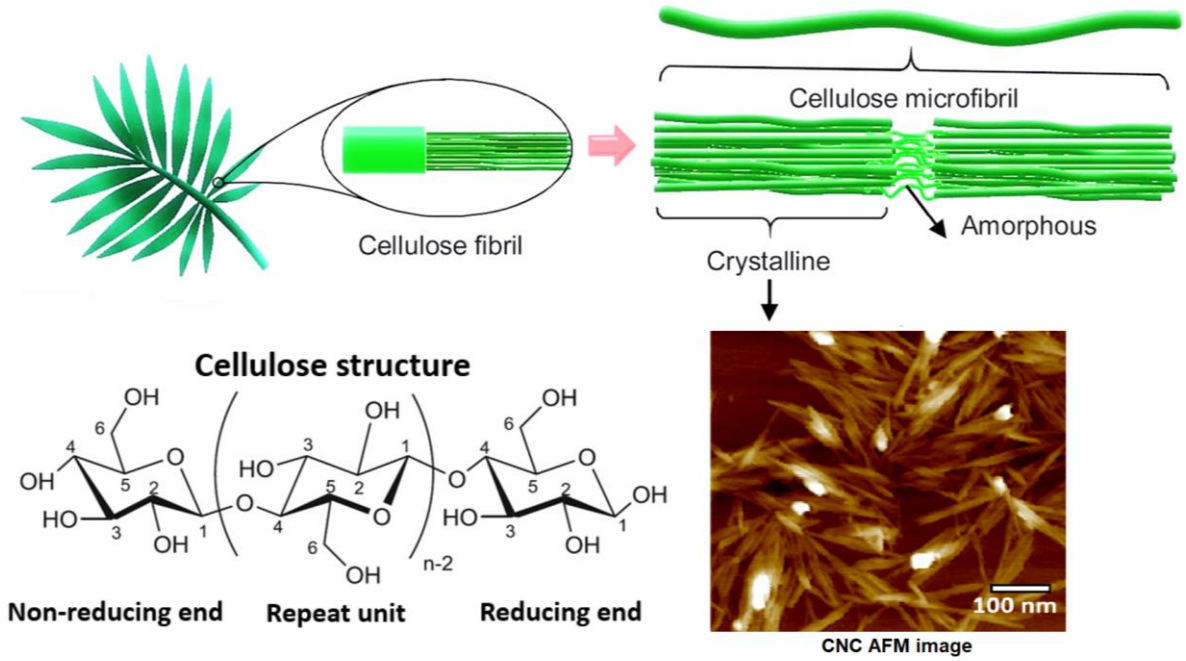

Figure 2.5: Cellulose and cellulose nanocrystal structure. [55]

Table 2.1: Cellulose nanomaterial types and characteristics.

Type	CNFs	BNC	CNCs
Source	Wood, cotton, hemp, etc.	Bacteria	Wood, flax, rice husk, etc.
Extraction process	Mechanical methods, high-shear homogenizer	Aerobic bacteria	Dissolution of amorphous domains- acid hydrolysis of purified cellulosic material
Diameter (nm)	20-50	20-100	5-20
Length (nm)	50-50	300-500	100-300
Size distribution	Poly dispersed	Poly dispersed	Poly dispersed
Structure	Entangled network	3-D network	Rod-shaped particles

The nanometer rod shape of CNCs results in a high specific surface area, and due to the high density of surface hydroxyl (OH) groups, they are amenable to functionalization by, for example, carboxylation, sulfonation, phosphorylation and oxidation, thus contributing to selectivity of CNC-based membranes [56]. The surface hydroxyl groups also make them hydrophilic, which is an advantage for enhancing membrane water permeability [57]. In addition, the membrane surface hydrophilicity improvement is known to be effective in membrane antifouling properties enhancement toward cationic and anionic organic foulants [58]. The negative surface charge density of CNCs also plays a key role in CNC-TFN

membrane surface properties [59]. Even low amounts of CNCs can significantly affect the TFN membrane surface charge density, which is a determining factor for TFN membrane performance [60]. These attributes potentially make CNCs excellent nanoparticles for the performance modification of TFC membranes.

2.5 CNC-TFN membranes

Adding CNCs, which possess no internal pore structure, into TFN membranes generates additional transport routes via nanovoid formation in which the water molecules could pass more quickly to the bulk semi-crosslinked polymer structure [61]. Nevertheless, the strength of the polymer/CNC interactions has a direct influence on the size of these transport routes and, consequently, on the selectivity of the CNC-TFN membranes [62,63].

Tables 2.2 and 2.3 summarize the reported use of CNC-based TFN membranes in RO and NF processes, respectively. The CNC loadings resulting in the highest rejection for different salts and highest water permeability have been reported. The performance of CNC-TFN membranes related to antifouling, chlorine resistance, antimicrobial resistance, heavy metal and dye rejection has also been included. CNC-TFN-based membranes can be synthesized using any of the four methods mentioned earlier. To the best of our knowledge, there is only one report on using CNCs as a coating on top of the PA layer [64], only one report on the dispersion of CNCs in the support layer [43] and two reports on using CNCs as an interlayer (Tables 2.2 and 2.3) [65,66].

Liu et al. [67] investigated the effect of incorporating CNCs, either in the PS support or PA layer (dispersed in an aqueous monomer solution). The CNC addition in the PA led to higher crosslinking density and lower thickness of the active layer resulting higher rejection and water permeability of membranes compared to CNC dispersed in the support layer for the NF process. Jackson et al. [64] coated CNCs on top of the PA layer of TFC membranes using N-ethyl carbodiimide hydrochloride and N-hydroxy succinimide as an immobilizing agent. The chemical immobilization of the CNCs on the membrane surface resulted in increased membrane hydrophilicity, which led to improved water permeability and biofouling resistance in a RO process. Furthermore, Yang et al. [65] prepared CNC-TFN membranes for NF using a two-step method. CNCs were used as an interlayer between the support and PA layer (step 1), and polydopamine was deposited on top of the PA layer (step 2). The CNC interlayer increased the membrane water permeability by almost 200% while only slightly decreasing the solute (Na_2SO_4 and NaCl) rejection due to the poor interaction between the CNC, PA and support

layers. Similarly, CNCs were added as an interlayer in NF-TFN membranes by Wang et al. [68]. The CNC interlayer reduced crosslinking density and led to higher PA layer thickness both of which are not favorable for enhancing desalination. This was attributed to the absorption of the diamine monomer into the support layer and reducing the rate of interfacial polymerization of PA layer. While the three TFN preparation methods used above provided some positive results, the small number of investigations using these methods with CNCs are likely due in part to the success of the fourth method, the addition of CNCs via the monomer solutions.

Table 2.2: CNC-TFN membrane performance for RO process.

Nanoparticle	CNC loading	NaCl Rejection (%)	Water permeability ($L/m^2.h.bar$)	Purpose of CNCs	Ref.
SW30	-	99	1.10	Commercial membrane	[21]
CNC	0.2 wt% in MPD	95	2.60	-	[69]
CNC	0.1 wt% in TMC	97.1	1.8	BSA[a] antifouling	[24]
Tempo-oxidized CNC	0.2 wt% in MPD	97	1.9	-	[70]
Tempo-oxidized CNC	Coated on top of PA	97.8	2.15	E.coli antibacterial, BSA[a] antifouling	[64]

All membranes were tested in low salinity conditions (NaCl concentration in the feed water tank: 2000-3000 ppm, operating pressure: 15-20 bar). BSA: Bovine serum albumin.

Because of the hydrophilic nature of CNCs, most CNC-TFN membranes have been produced by incorporating the CNCs into the aqueous monomer solution (MPD for RO or PIP for NF). For example, Xia et al. [75] prepared CNC-TFN membranes by dispersing phosphorylated CNCs into the aqueous monomer solution. Their NF membranes exhibited enhanced water permeability and Na_2SO_4 rejection by incorporating a relatively small amount of phosphorylated CNCs (0.05 wt%). Further increases in CNC loading led to a deterioration in membrane performance due to CNC aggregation. Smith et al. [63] produced RO-TFNs by dispersing oxidized CNCs into the aqueous MPD monomer solution. The hydrogen bonding between the PA and oxidized CNCs enhanced the surface hydrophilicity of the membrane. This resulted in higher water permeability of oxidized CNC-TFN compared to unmodified CNC-TFN membranes; the NaCl rejection declined with an increase in the oxidized CNC loading beyond 0.2 wt%. To the best of our knowledge, the desalination performance of the CNC-TFNs

membranes for RO and NF processes deteriorated after increasing the CNC loading beyond the amounts reported in Tables 2.2 and 2.3.

Table 2.3: CNC-TFN membrane performance for NF process.

Nanoparticle	CNC loading	Rejection (%)			A[a] ($L/m^2.h.bar$)	Purpose of CNCs	Ref.
		Na_2SO_4	$MgCl_2$	NaCl			
NF90		98.6	50.1	68.6	8.3	Commercial membrane	[65]
NF270		98.1	70.3	37.1	15.2		
CNC	0.01 wt% in PIP	98	27	23	8.7	Dye rejection	[71]
CNC	0.02 wt% in PIP	98	-	21	8.1	Humic acid antifouling	[72]
CNC	0.05 wt% in PIP	98	45	28	10.8	Chlorine resistance	[73]
CNC	0.05 wt% in PIP	93	79	62	3.5	BSA[b] antifouling	[74]
CNC/Ag	0.01 wt% in PIP	99	27	-	12	Humic acid antifouling, E-coli antibacterial	[62]
Carboxylated CNC	0.05 wt% in PIP	98.5	-	35	7.5	-	[43]
Carboxylated CNC	0.05 wt% in support	96.5	-	33	5		
Zwitterionic CNC	0.05 wt% in PIP	98	12	19	8.7	BSA[b] antifouling	[75]
Phosphorylated CNC	0.05 wt% in PIP	95.4	10	5	8.5	Antibiotic rejection	[76]
CNC	Support, PA interlayer	97.7	15.5	6.5	9.2	-	[77]
CNC	Support, PA interlayer	97.2	-	13.4	12	Dye rejection, BSA[b] antifouling	[65]
CNC	Support, PA interlayer/ PDA[c]	98.1	-	13.5	12.4		

All membranes were tested in low salinity conditions (salt concentration in the feed water tank: 1000-2000 ppm, operating pressure: 6-10 bar).
a. A: water permeability of Na_2SO_4 aqueous solution as a feed, b. BSA: Bovine serum albumin, c. PDA: Polydopamine coated on top of the PA layer.

Asempour et al. [78] prepared an innovative CNC-TFN membranes by dispersing CNCs into the organic TMC/n-hexane solution for PA interfacial polymerization. The CNCs significantly enhanced the surface hydrophilicity of the membrane, leading to improved antifouling properties. Moreover, RO desalination experiments with synthetic brackish water led to nearly doubling the water permeability from 1.02 to 1.8 $L/m^2 \cdot h.bar$ without significantly compromising NaCl rejection (97.1%) for a CNC loading of 0.1 wt%. It was found that increasing CNC loading decreased membrane selectivity, which can be attributed to the formation of defects due to the presence of CNC aggregates.

Finding ways to firmly anchor CNCs to the PA layer via easy and practical chemical covalent bonding can increase the TFN membrane lifespan by avoiding defect formation in the PA layer due to a reduction in both CNC aggregation and potentially nanoparticle leaching (limiting factors to the commercialization of TFN membranes) [79].

CNC surface functionalization permits tuning of polymer/nanoparticle interactions to further control TFN membrane performance [45]. To circumvent agglomeration, one would ideally develop a protocol to properly disperse the CNCs in the PA layer. This would suggest modifying the CNCs to make them more dispersible in the organic monomer phase. This allows one to overcome the issues related to the use of CNCs in the aqueous monomer solution. First, rubber rolling step during interfacial polymerization could unintentionally remove nanoparticles together with the excess aqueous amine solution. Thus, one would not have a quantifiable measure of the nanoparticle loading because of the organic nature of the CNCs, which are difficult to detect in a polymer matrix. On the other hand, while inorganic nanoparticles suffer the same fate when dispersed in the aqueous monomer solution, they are at least detectable using methods such as elemental analysis. Also, the remaining nanoparticles could reside in the region between the PA and support layer or at least deep inside the PA layer rather than being exposed to the feed solution during performance operation[45,80,81]. To prevent CNC leaching, one could anchor the CNCs in the PA layer by, for example, covalent bonding with the PA functional groups. Thus, this suggests modifying the CNCs so that they possess the appropriate functional groups to bond with the acyl chlorides of the TMC.

One of the most common surface modifications of CNCs is the esterification of OH groups, which selectively exchanges them with acetyl groups and has been shown to improve CNC dispersion in both aqueous and non-aqueous solvents [82–84]. Acetyl group functionalization makes CNCs less hydrophilic by breaking intermolecular hydrogen bonding and improves their dispersibility in nonpolar organic solvents such as n-hexane. The degree of

substitution of acetyl groups is controllable, which enables varying degrees of hydrophilicity of the modified CNCs [85].

Zwitterionic natural amino acid molecules such as L-arginine and L-cysteine contain multiple amine groups, which can take part in covalent bonding with unreacted acyl chloride groups of PA [86,87]. L-arginine was used by Chen et al as a coating on top of PA layer of RO-TFC membranes [88]. X-ray photoelectron spectroscopy verified the successful covalent attachment of L-arginine and the formation of the zwitterionic membrane surface. The water permeability improved by 39.7%, as well as NaCl rejection increase from 96.42% to 98.08%. Also, modified membranes showed improved fouling-resistance and easy-cleaning properties measured by a three-time cycle filtration test. In addition, a sulphur-complexed strategy to enhance the rejection of heavy metal ions by the coating of L-cysteine on top of the NF-TFC membrane was developed by Zhang et al [86]. Fabricated NF membranes not only showed enhanced desalination performance but also achieved a record rejection of mercury (Hg^{2+}) ions (99.99%). Besides, the sulfur-functionalized NF membranes showed long-term stability without significant loss of mercury rejection, even after six cycles of regeneration.

In another study by Yin et al. [89], Silver (Ag) nanoparticles were grafted on the PA layer of TFC membranes using cysteamine. The Ag nanoparticle leaching from the surfaces of the Ag-grafted membrane was minimal, as tested by both batch and flow-through methods. The results successfully demonstrated that Ag nanoparticles could be grafted on top of PA layer via chemical bonding, leading to enhanced antibacterial and antifouling properties of TFN membranes. It has been reported that surface modification of CNC with L-cysteine can result in a highly efficient biosorbent for mercury ions from aqueous solutions at neutral pH. Also, After three adsorption/desorption cycles, the rejection percentage of mercury could still keep above 70% [90]. The ability of covalent bonding of amino acid molecules with PA functional groups within or on top of the PA layer makes them a promising modifying agent for CNC functionalization. This covalent bonding could lead to a reduction in CNC aggregation and CNC leaching.

2.6 References

[1] G. Abdi, A. Alizadeh, S. Zinadini, G. Moradi, Removal of dye and heavy metal ion using a novel synthetic polyethersulfone nanofiltration membrane modified by magnetic graphene oxide/metformin hybrid, Journal of Membrane Science. 552 (2018) 326–335. https://doi.org/10.1016/j.memsci.2018.02.018.

[2] D. Ankoliya, B. Mehta, H. Raval, Advances in surface modification techniques of reverse osmosis membrane over the years, Separation Science and Technology. 54 (2019) 293–310. https://doi.org/10.1080/01496395.2018.1483404.
[3] S. Bandehali, F. Parvizian, A.R. Moghadassi, S.M. Hosseini, J.N. Shen, Fabrication of thin film-PEI nanofiltration membrane with promoted separation performances: Cr, Pb and Cu ions removal from water, J Polym Res. 27 (2020) 94. https://doi.org/10.1007/s10965-020-02056-x.
[4] A. Al Mayyahi, Important Approaches to Enhance Reverse Osmosis (RO) Thin Film Composite (TFC) Membranes Performance, Membranes. 8 (2018) 68. https://doi.org/10.3390/membranes8030068.
[5] Y. Wen, J. Yuan, X. Ma, S. Wang, Y. Liu, Polymeric nanocomposite membranes for water treatment: a review, Environ Chem Lett. 17 (2019) 1539–1551. https://doi.org/10.1007/s10311-019-00895-9.
[6] S. Bolisetty, M. Peydayesh, R. Mezzenga, Sustainable technologies for water purification from heavy metals: review and analysis, Chem. Soc. Rev. 48 (2019) 463–487. https://doi.org/10.1039/C8CS00493E.
[7] T.-S. Chung, D. Zhao, J. Gao, K. Lu, C. Wan, M. Weber, C. Maletzko, Emerging R&D on membranes and systems for water reuse and desalination, Chinese Journal of Chemical Engineering. 27 (2019) 1578–1585. https://doi.org/10.1016/j.cjche.2019.04.004.
[8] S.S. Madaeni, E. Salehi, A new adsorption–transport and porosity combined model for passage of cations through nanofiltration membrane, Journal of Membrane Science. 333 (2009) 100–109. https://doi.org/10.1016/j.memsci.2009.02.006.
[9] H. Saleem, S.J. Zaidi, Nanoparticles in reverse osmosis membranes for desalination: A state of the art review, Desalination. 475 (2020) 114171. https://doi.org/10.1016/j.desal.2019.114171.
[10] S. Poornima, S. Manikandan, V. Karthik, R. Balachandar, R. Subbaiya, M. Saravanan, N.T. Lan Chi, A. Pugazhendhi, Emerging nanotechnology based advanced techniques for wastewater treatment, Chemosphere. 303 (2022) 135050. https://doi.org/10.1016/j.chemosphere.2022.135050.
[11] C.Y. Tang, Y.-N. Kwon, J.O. Leckie, Effect of membrane chemistry and coating layer on physiochemical properties of thin film composite polyamide RO and NF membranes II. Membrane physiochemical properties and their dependence on polyamide and coating layers, (2009) 15.
[12] H. Wu, B. Tang, P. Wu, Optimizing polyamide thin film composite membrane covalently bonded with modified mesoporous silica nanoparticles, Journal of Membrane Science. 428 (2013) 341–348. https://doi.org/10.1016/j.memsci.2012.10.053.
[13] S.-L. Li, P. Wu, J. Wang, Y. Hu, High-performance zwitterionic TFC polyamide nanofiltration membrane based on a novel triamine precursor, Separation and Purification Technology. 251 (2020) 117380. https://doi.org/10.1016/j.seppur.2020.117380.
[14] N. Abdullah, N. Yusof, W.J. Lau, J. Jaafar, A.F. Ismail, Recent trends of heavy metal removal from water/wastewater by membrane technologies, Journal of Industrial and Engineering Chemistry. 76 (2019) 17–38. https://doi.org/10.1016/j.jiec.2019.03.029.
[15] D. Yadav, S. Karki, P.G. Ingole, Current advances and opportunities in the development of nanofiltration (NF) membranes in the area of wastewater treatment, water desalination, biotechnological and pharmaceutical applications, Journal of Environmental Chemical Engineering. 10 (2022) 108109. https://doi.org/10.1016/j.jece.2022.108109.
[16] R.E. Abouzeid, R. Khiari, N. El-Wakil, A. Dufresne, Current State and New Trends in the Use of Cellulose Nanomaterials for Wastewater Treatment, Biomacromolecules. 20 (2019) 573–597. https://doi.org/10.1021/acs.biomac.8b00839.

[17] R. Das, T. Lindström, P.R. Sharma, K. Chi, B.S. Hsiao, Nanocellulose for Sustainable Water Purification, Chem. Rev. 122 (2022) 8936–9031. https://doi.org/10.1021/acs.chemrev.1c00683.
[18] S. Bandehali, A. Moghadassi, F. Parvizian, Y. Zhang, S.M. Hosseini, J. Shen, New mixed matrix PEI nanofiltration membrane decorated by glycidyl-POSS functionalized graphene oxide nanoplates with enhanced separation and antifouling behaviour: Heavy metal ions removal, Separation and Purification Technology. 242 (2020) 116745. https://doi.org/10.1016/j.seppur.2020.116745.
[19] K. Arola, B. Van der Bruggen, M. Mänttäri, M. Kallioinen, Treatment options for nanofiltration and reverse osmosis concentrates from municipal wastewater treatment: A review, Critical Reviews in Environmental Science and Technology. 49 (2019) 2049–2116. https://doi.org/10.1080/10643389.2019.1594519.
[20] B. Al-Najar, C.D. Peters, H. Albuflasa, N.P. Hankins, Pressure and osmotically driven membrane processes: A review of the benefits and production of nano-enhanced membranes for desalination, Desalination. 479 (2020) 114323. https://doi.org/10.1016/j.desal.2020.114323.
[21] F. Abedi, D. Emadzadeh, M.A. Dubé, B. Kruczek, Modifying cellulose nanocrystal dispersibility to address the permeability/selectivity trade-off of thin-film nanocomposite reverse osmosis membranes, Desalination. 538 (2022) 115900. https://doi.org/10.1016/j.desal.2022.115900.
[22] R. Moeinzadeh, A.G. Jadval Ghadam, W.J. Lau, D. Emadzadeh, Synthesis of nanocomposite membrane incorporated with amino-functionalized nanocrystalline cellulose for refinery wastewater treatment, Carbohydrate Polymers. 225 (2019) 115212. https://doi.org/10.1016/j.carbpol.2019.115212.
[23] A. Bakshi, H. Bustamante, X. Sui, R. Joshi, Structure Dependent Water Transport in Membranes Based on Two-Dimensional Materials, Ind. Eng. Chem. Res. 60 (2021) 10917–10959. https://doi.org/10.1021/acs.iecr.1c01919.
[24] F. Asempour, D. Emadzadeh, T. Matsuura, B. Kruczek, Synthesis and characterization of novel Cellulose Nanocrystals-based Thin Film Nanocomposite membranes for reverse osmosis applications, Desalination. 439 (2018) 179–187. https://doi.org/10.1016/j.desal.2018.04.009.
[25] F. Liu, L. Wang, D. Li, Q. Liu, B. Deng, A review: the effect of the microporous support during interfacial polymerization on the morphology and performances of a thin film composite membrane for liquid purification, RSC Adv. 9 (2019) 35417–35428. https://doi.org/10.1039/C9RA07114H.
[26] N. Abdullah, N. Yusof, W.J. Lau, J. Jaafar, A.F. Ismail, Recent trends of heavy metal removal from water/wastewater by membrane technologies, Journal of Industrial and Engineering Chemistry. 76 (2019) 17–38. https://doi.org/10.1016/j.jiec.2019.03.029.
[27] S.-L. Li, X. Shan, Y. Zhao, Y. Hu, Fabrication of a Novel Nanofiltration Membrane with Enhanced Performance via Interfacial Polymerization through the Incorporation of a New Zwitterionic Diamine Monomer, ACS Appl. Mater. Interfaces. 11 (2019) 42846–42855. https://doi.org/10.1021/acsami.9b15811.
[28] S. Honarparvar, X. Zhang, T. Chen, A. Alborzi, K. Afroz, D. Reible, Frontiers of Membrane Desalination Processes for Brackish Water Treatment: A Review, Membranes. 11 (2021) 246. https://doi.org/10.3390/membranes11040246.
[29] X. Zhao, R. Zhang, Y. Liu, M. He, Y. Su, C. Gao, Z. Jiang, Antifouling membrane surface construction: Chemistry plays a critical role, Journal of Membrane Science. 551 (2018) 145–171. https://doi.org/10.1016/j.memsci.2018.01.039.

[30] Y. Du, B.K. Pramanik, Y. Zhang, L. Dumée, V. Jegatheesan, Recent Advances in the Theory and Application of Nanofiltration: a Review, Curr Pollution Rep. 8 (2022) 51–80. https://doi.org/10.1007/s40726-021-00208-1.
[31] Y.-L. Ji, Q.-F. An, X.-D. Weng, W.-S. Hung, K.-R. Lee, C.-J. Gao, Microstructure and performance of zwitterionic polymeric nanoparticle/polyamide thin-film nanocomposite membranes for salts/organics separation, Journal of Membrane Science. 548 (2018) 559–571. https://doi.org/10.1016/j.memsci.2017.11.057.
[32] J.M. Gohil, P. Ray, A review on semi-aromatic polyamide TFC membranes prepared by interfacial polymerization: Potential for water treatment and desalination, Separation and Purification Technology. 181 (2017) 159–182. https://doi.org/10.1016/j.seppur.2017.03.020.
[33] X. An, Y. Hu, N. Wang, T. Wang, Z. Liu, Breaking the permeability–selectivity trade-off in thin-film composite polyamide membranes with a PEG-b-PSF-b-PEG block copolymer ultrafiltration membrane support through post-annealing treatment, NPG Asia Mater. 11 (2019) 13. https://doi.org/10.1038/s41427-019-0114-1.
[34] M. Asadollahi, D. Bastani, S.A. Musavi, Enhancement of surface properties and performance of reverse osmosis membranes after surface modification: A review, Desalination. 420 (2017) 330–383. https://doi.org/10.1016/j.desal.2017.05.027.
[35] M. Adamczak, G. Kamińska, J. Bohdziewicz, Preparation of Polymer Membranes by In Situ Interfacial Polymerization, International Journal of Polymer Science. 2019 (2019) 1–13. https://doi.org/10.1155/2019/6217924.
[36] B.S. Ooi, J.Y. Sum, J.J. Beh, W.J. Lau, S.O. Lai, Materials and Engineering Design of Interfacial Polymerized Thin Film Composite Nanofiltration Membrane for Industrial Applications, in: Membrane Separation Principles and Applications, Elsevier, 2019: pp. 47–83. https://doi.org/10.1016/B978-0-12-812815-2.00002-8.
[37] V. Freger, Kinetics of Film Formation by Interfacial Polycondensation, Langmuir. 21 (2005) 1884–1894. https://doi.org/10.1021/la048085v.
[38] B.-H. Jeong, E.M.V. Hoek, Y. Yan, A. Subramani, X. Huang, G. Hurwitz, A.K. Ghosh, A. Jawor, Interfacial polymerization of thin film nanocomposites: A new concept for reverse osmosis membranes, Journal of Membrane Science. 294 (2007) 1–7. https://doi.org/10.1016/j.memsci.2007.02.025.
[39] Y. Roy, D.M. Warsinger, J.H. Lienhard, Effect of temperature on ion transport in nanofiltration membranes: Diffusion, convection and electromigration, Desalination. 420 (2017) 241–257. https://doi.org/10.1016/j.desal.2017.07.020.
[40] D. Wang, A critical review of cellulose-based nanomaterials for water purification in industrial processes, Cellulose. 26 (2019) 687–701. https://doi.org/10.1007/s10570-018-2143-2.
[41] A.J. Sayyed, D.V. Pinjari, S.H. Sonawane, B.A. Bhanvase, J. Sheikh, M. Sillanpää, Cellulose-based nanomaterials for water and wastewater treatments: A review, Journal of Environmental Chemical Engineering. 9 (2021) 106626. https://doi.org/10.1016/j.jece.2021.106626.
[42] X. Ma, Z. Yang, Z. Yao, H. Guo, Z. Xu, C.Y. Tang, Tuning roughness features of thin film composite polyamide membranes for simultaneously enhanced permeability, selectivity and anti-fouling performance, Journal of Colloid and Interface Science. 540 (2019) 382–388. https://doi.org/10.1016/j.jcis.2019.01.033.
[43] Y. Liu, L. Bai, X. Zhu, D. Xu, G. Li, H. Liang, M.R. Wiesner, The role of carboxylated cellulose nanocrystals placement in the performance of thin-film composite (TFC) membrane, Journal of Membrane Science. 617 (2021) 118581. https://doi.org/10.1016/j.memsci.2020.118581.

[44] Y. Liu, J.M. Sipe, W. Xu, X. Zhu, L. Bai, D. Xu, G. Li, H. Liang, M.R. Wiesner, Study on the mechanisms for the influence of nanomaterials on the separation performance of nanocomposite membrane from a modeling perspective, Desalination. 532 (2022) 115740. https://doi.org/10.1016/j.desal.2022.115740.
[45] H. Saleem, S.J. Zaidi, Nanoparticles in reverse osmosis membranes for desalination: A state of the art review, Desalination. 475 (2020) 114171. https://doi.org/10.1016/j.desal.2019.114171.
[46] S.Y. Lee, H.J. Kim, R. Patel, S.J. Im, J.H. Kim, B.R. Min, Silver nanoparticles immobilized on thin film composite polyamide membrane: characterization, nanofiltration, antifouling properties, Polym. Adv. Technol. 18 (2007) 562–568. https://doi.org/10.1002/pat.918.
[47] M. Amiri, E. Jafarbeigi, F. Salimi, Fabrication of modified nanofiltration membranes by functionalized cellulose nanocrystals with high anti-fouling capability in removing dye from water and wastewater, Korean J. Chem. Eng. 39 (2022) 616–627. https://doi.org/10.1007/s11814-021-0952-8.
[48] D. Ankoliya, B. Mehta, H. Raval, Advances in surface modification techniques of reverse osmosis membrane over the years, Separation Science and Technology. 54 (2019) 293–310. https://doi.org/10.1080/01496395.2018.1483404.
[49] S.T. Khan, A. Malik, Engineered nanomaterials for water decontamination and purification: From lab to products, Journal of Hazardous Materials. 363 (2019) 295–308. https://doi.org/10.1016/j.jhazmat.2018.09.091.
[50] S. Déon, A. Escoda, P. Fievet, A transport model considering charge adsorption inside pores to describe salts rejection by nanofiltration membranes, Chemical Engineering Science. 66 (2011) 2823–2832. https://doi.org/10.1016/j.ces.2011.03.043.
[51] B. He, H. Peng, Y. Chen, Q. Zhao, High performance polyamide nanofiltration membranes enabled by surface modification of imidazolium ionic liquid, Journal of Membrane Science. 608 (2020) 118202. https://doi.org/10.1016/j.memsci.2020.118202.
[52] M. Liu, C. Yu, Y. Wu, Z. Lü, S. Yu, C. Gao, In situ modification of polyamide reverse osmosis membrane module for improved fouling resistance, Chemical Engineering Research and Design. 141 (2019) 402–412. https://doi.org/10.1016/j.cherd.2018.11.009.
[53] Z. Karim, M. Hakalahti, T. Tammelin, A.P. Mathew, In situ TEMPO surface functionalization of nanocellulose membranes for enhanced adsorption of metal ions from aqueous medium, RSC Adv. 7 (2017) 5232–5241. https://doi.org/10.1039/C6RA25707K.
[54] S.F. Anis, R. Hashaikeh, N. Hilal, Functional materials in desalination: A review, Desalination. 468 (2019) 114077. https://doi.org/10.1016/j.desal.2019.114077.
[55] H. Sari Erkan, N. Bakaraki Turan, G. Onkal Engin, M.S. Bilgili, A review of advantages and challenges of using engineered nanoparticles for waste and wastewater treatments, Int. J. Environ. Sci. Technol. 18 (2021) 3295–3306. https://doi.org/10.1007/s13762-020-03054-8.
[56] M. Bassyouni, M.H. Abdel-Aziz, M.Sh. Zoromba, S.M.S. Abdel-Hamid, E. Drioli, A review of polymeric nanocomposite membranes for water purification, Journal of Industrial and Engineering Chemistry. 73 (2019) 19–46. https://doi.org/10.1016/j.jiec.2019.01.045.
[57] C. Hu, H. Hu, M. Song, J. Tan, G. Huang, J. Zuo, Preparation, characterization, and Cd(II) sorption of/on cysteine-montmorillonite composites synthesized at various pH, Environ Sci Pollut Res. 27 (2020) 10599–10606. https://doi.org/10.1007/s11356-019-07550-4.
[58] C. Gomri, M. Cretin, M. Semsarilar, Recent progress on chemical modification of cellulose nanocrystal (CNC) and its application in nanocomposite films and membranes-A comprehensive review, Carbohydrate Polymers. 294 (2022) 119790. https://doi.org/10.1016/j.carbpol.2022.119790.

[59] A. Kamtsikakis, G. Delepierre, C. Weder, Cellulose nanocrystals as a tunable nanomaterial for pervaporation membranes with asymmetric transport properties, Journal of Membrane Science. 635 (2021) 119473. https://doi.org/10.1016/j.memsci.2021.119473.
[60] H. Zheng, M. Zhu, D. Wang, Y. Zhou, X. Sun, S. Jiang, M. Li, C. Xiao, D. Zhang, L. Zhang, Surface modification of PVDF membrane by CNC/Cu-MOF-74 for enhancing antifouling property, Separation and Purification Technology. 306 (2023) 122599. https://doi.org/10.1016/j.seppur.2022.122599.
[61] R. Das, T. Lindström, P.R. Sharma, K. Chi, B.S. Hsiao, Nanocellulose for Sustainable Water Purification, Chem. Rev. 122 (2022) 8936–9031. https://doi.org/10.1021/acs.chemrev.1c00683.
[62] C. Xu, W. Chen, H. Gao, X. Xie, Y. Chen, Cellulose nanocrystal/silver (CNC/Ag) thin-film nanocomposite nanofiltration membranes with multifunctional properties, Environ. Sci.: Nano. 7 (2020) 803–816. https://doi.org/10.1039/C9EN01367A.
[63] E. Smith, K. Hendren, J. Haag, E. Foster, S. Martin, Functionalized Cellulose Nanocrystal Nanocomposite Membranes with Controlled Interfacial Transport for Improved Reverse Osmosis Performance, Nanomaterials. 9 (2019) 125. https://doi.org/10.3390/nano9010125.
[64] J.C. Jackson, C.H.M. Camargos, V.T. Noronha, A.J. Paula, C.A. Rezende, A.F. Faria, Sustainable Cellulose Nanocrystals for Improved Antimicrobial Properties of Thin Film Composite Membranes, ACS Sustainable Chem. Eng. 9 (2021) 6534–6540. https://doi.org/10.1021/acssuschemeng.1c02389.
[65] L. Bai, J. Ding, H. Wang, N. Ren, G. Li, H. Liang, High-performance nanofiltration membranes with a sandwiched layer and a surface layer for desalination and environmental pollutant removal, Science of The Total Environment. 743 (2020) 140766. https://doi.org/10.1016/j.scitotenv.2020.140766.
[66] J.-J. Wang, H.-C. Yang, M.-B. Wu, X. Zhang, Z.-K. Xu, Nanofiltration membranes with cellulose nanocrystals as an interlayer for unprecedented performance, J. Mater. Chem. A. 5 (2017) 16289–16295. https://doi.org/10.1039/C7TA00501F.
[67] Y. Liu, L. Bai, X. Zhu, D. Xu, G. Li, H. Liang, M.R. Wiesner, The role of carboxylated cellulose nanocrystals placement in the performance of thin-film composite (TFC) membrane, Journal of Membrane Science. 617 (2021) 118581. https://doi.org/10.1016/j.memsci.2020.118581.
[68] W.-H. Yu, Z.-Q. Gan, J.-R. Wang, Y. Zhao, J. Han, L.-F. Fang, X.-Z. Wei, Z.-L. Qiu, B.-K. Zhu, A novel negatively charged nanofiltration membrane with improved and stable rejection of Cr (VI) and phosphate under different pH conditions, Journal of Membrane Science. 639 (2021) 119756. https://doi.org/10.1016/j.memsci.2021.119756.
[69] M. Kadhom, B. Deng, Synthesis of high-performance thin film composite (TFC) membranes by controlling the preparation conditions: Technical notes, Journal of Water Process Engineering. 30 (2019) 100542. https://doi.org/10.1016/j.jwpe.2017.12.011.
[70] E. Smith, K. Hendren, J. Haag, E. Foster, S. Martin, Functionalized Cellulose Nanocrystal Nanocomposite Membranes with Controlled Interfacial Transport for Improved Reverse Osmosis Performance, Nanomaterials. 9 (2019) 125. https://doi.org/10.3390/nano9010125.
[71] L. Bai, Y. Liu, A. Ding, N. Ren, G. Li, H. Liang, Fabrication and characterization of thin-film composite (TFC) nanofiltration membranes incorporated with cellulose nanocrystals (CNCs) for enhanced desalination performance and dye removal, Chemical Engineering Journal. 358 (2019) 1519–1528. https://doi.org/10.1016/j.cej.2018.10.147.
[72] L. Bai, Y. Liu, N. Bossa, A. Ding, N. Ren, G. Li, H. Liang, M.R. Wiesner, Incorporation of Cellulose Nanocrystals (CNCs) into the Polyamide Layer of Thin-Film Composite

(TFC) Nanofiltration Membranes for Enhanced Separation Performance and Antifouling Properties, Environ. Sci. Technol. 52 (2018) 11178–11187. https://doi.org/10.1021/acs.est.8b04102.
[73] S. Huang, M.-B. Wu, C.-Y. Zhu, M.-Q. Ma, J. Yang, J. Wu, Z.-K. Xu, Polyamide Nanofiltration Membranes Incorporated with Cellulose Nanocrystals for Enhanced Water Flux and Chlorine Resistance, ACS Sustainable Chem. Eng. (2019) acssuschemeng.9b01651. https://doi.org/10.1021/acssuschemeng.9b01651.
[74] Y. Rahimi-Kashkouli, M. Rahbari-Sisakht, A. Ghadami Jadval Ghadam, Thin film nanocomposite nanofiltration membrane incorporated with cellulose nanocrystals with superior anti-organic fouling affinity, Environ. Sci.: Water Res. Technol. 6 (2020) 715–723. https://doi.org/10.1039/C9EW00963A.
[75] D. Xia, M. Zhang, C. Tong, Z. Wang, H. Liu, L. Zhu, In-situ incorporating zwitterionic nanocellulose into polyamide nanofiltration membrane towards excellent perm-selectivity and antifouling performances, Desalination. 521 (2022) 115397. https://doi.org/10.1016/j.desal.2021.115397.
[76] Z. Wang, D. Xia, B. Wang, H. Liu, L. Zhu, Highly permeable polyamide nanofiltration membrane incorporated with phosphorylated nanocellulose for enhanced desalination, Journal of Membrane Science. 647 (2022) 120339. https://doi.org/10.1016/j.memsci.2022.120339.
[77] J.-J. Wang, H.-C. Yang, M.-B. Wu, X. Zhang, Z.-K. Xu, Nanofiltration membranes with cellulose nanocrystals as an interlayer for unprecedented performance, J. Mater. Chem. A. 5 (2017) 16289–16295. https://doi.org/10.1039/C7TA00501F.
[78] F. Asempour, D. Emadzadeh, T. Matsuura, B. Kruczek, Synthesis and characterization of novel Cellulose Nanocrystals-based Thin Film Nanocomposite membranes for reverse osmosis applications, Desalination. 439 (2018) 179–187. https://doi.org/10.1016/j.desal.2018.04.009.
[79] L. Xu, B. Shan, C. Gao, J. Xu, Multifunctional thin-film nanocomposite membranes comprising covalent organic nanosheets with high crystallinity for efficient reverse osmosis desalination, Journal of Membrane Science. 593 (2020) 117398. https://doi.org/10.1016/j.memsci.2019.117398.
[80] A.M.A. Abdelsamad, M. Matthias, A.S.G. Khalil, M. Ulbricht, Nanofillers dissolution as a crucial challenge for the performance stability of thin-film nanocomposite desalination membranes, Separation and Purification Technology. 228 (2019) 115767. https://doi.org/10.1016/j.seppur.2019.115767.
[81] W. Li, Z. Yang, W. Liu, Z. Huang, H. Zhang, M. Li, X. Ma, C.Y. Tang, Z. Xu, Polyamide reverse osmosis membranes containing 1D nanochannels for enhanced water purification, Journal of Membrane Science. 618 (2021) 118681. https://doi.org/10.1016/j.memsci.2020.118681.
[82] E. Lizundia, T.-D. Nguyen, J.L. Vilas, W.Y. Hamad, M.J. MacLachlan, Chiroptical, morphological and conducting properties of chiral nematic mesoporous cellulose/polypyrrole composite films, J. Mater. Chem. A. 5 (2017) 19184–19194. https://doi.org/10.1039/C7TA05684B.
[83] A. Biswas, R.L. Shogren, J.L. Willett, Solvent-Free Process to Esterify Polysaccharides †, Biomacromolecules. 6 (2005) 1843–1845. https://doi.org/10.1021/bm0501757.
[84] E. Abraham, D. Kam, Y. Nevo, R. Slattegard, A. Rivkin, S. Lapidot, O. Shoseyov, Highly Modified Cellulose Nanocrystals and Formation of Epoxy-Nanocrystalline Cellulose (CNC) Nanocomposites, ACS Appl. Mater. Interfaces. 8 (2016) 28086–28095. https://doi.org/10.1021/acsami.6b09852.

[85] A. Biswas, J.L. Berfield, B.C. Saha, H.N. Cheng, Conversion of agricultural by-products to methyl cellulose, Industrial Crops and Products. 46 (2013) 297–300. https://doi.org/10.1016/j.indcrop.2013.01.039.
[86] X. Zhang, L. Yan, J. Li, H. Yu, Adsorption of heavy metals by l-cysteine intercalated layered double hydroxide: Kinetic, isothermal and mechanistic studies, Journal of Colloid and Interface Science. 562 (2020) 149–158. https://doi.org/10.1016/j.jcis.2019.12.028.
[87] D. Chen, T. Liu, J. Kang, R. Xu, Y. Cao, M. Xiang, Enhancing the Permeability and Antifouling Properties of Polyamide Composite Reverse Osmosis Membrane by Surface Modification with Zwitterionic Amino Acid L-Arginine, Adv. Mater. Interfaces. 6 (2019) 1900706. https://doi.org/10.1002/admi.201900706.
[88] I. Chen, C. Xu, J. Peng, D. Han, S. Liu, M. Zhai, Novel Functionalized Cellulose Microspheres for Efficient Separation of Lithium Ion and Its Isotopes: Synthesis and Adsorption Performance, Molecules. 24 (2019) 2762. https://doi.org/10.3390/molecules24152762.
[89] J. Yin, Y. Yang, Z. Hu, B. Deng, Attachment of silver nanoparticles (AgNPs) onto thin-film composite (TFC) membranes through covalent bonding to reduce membrane biofouling, Journal of Membrane Science. 441 (2013) 73–82. https://doi.org/10.1016/j.memsci.2013.03.060.
[90] W. Li, B. Ju, S. Zhang, A green L -cysteine modified cellulose nanocrystals biosorbent for adsorption of mercury ions from aqueous solutions, RSC Adv. 9 (2019) 6986–6994. https://doi.org/10.1039/C9RA00048H.

3. Modifying cellulose nanocrystal dispersibility to address the permeability/selectivity trade-off of thin-film nanocomposite reverse osmosis membranes

Fatemeh Abedi, Daryoush Emadzadeh, Marc A. Dubé, Boguslaw Kruczek

The contents of this chapter were published in Desalination, 2023.
(https://doi.org/10.1016/j.desal.2022.115900)

3.1 Abstract

Thin-film nanocomposite reverse osmosis (RO-TFN) membranes with hydrophilic nanoparticles usually face a trade-off between water permeance and salt rejection. In this study, TFN membranes were produced by embedding different loadings of cellulose nanocrystals (CNCs) into the polyamide (PA) active layer by dispersing the CNCs in an organic monomer solution as opposed to the traditional approach where hydrophilic nanoparticles are added to the aqueous monomer solution. To facilitate the addition of the hydrophilic CNCs to the organic monomer solution, the CNCs were acetylated to form ACNCs with different degrees of substitution (DS = 0.7 and 1.7) of the hydroxyl groups. The successful incorporation of the CNCs and ACNCs into RO-TFN membranes was confirmed with ATR-FTIR spectroscopy, surface zeta potential, scanning electron microscopy, atomic force microscopy and water contact angle measurements. The NaCl rejection of ACNC-based TFN membranes remained stable (98-99%) while water permeance increased by 40% in comparison to CNC-TFN membranes. Compared to a reference thin-film composite (TFC) membrane, a two-fold water permeance increase was achieved (2.60 vs. 1.27 L/m^2.h.bar) with a 0.4 wt% loading of ACNC2 in the TFN membrane. The ACNC-TFN membranes were significantly closer to the so-called upper-bound line than the best CNC-TFN membranes and the reference TFC membrane. This study shows the potential of using hydrophilic green nanoparticles in overcoming the permeance-selectivity trade-off of RO-TFN membranes. Hydrophobic functionalization of hydrophilic nanoparticles was demonstrated to be an effective approach in overcoming the limit of CNC nanoparticle incorporation in CNC-TFN membranes.

3.2 Introduction

Greater than 71% of the earth is covered with water, but only less than 1% of this water is available for direct consumption to sustain life [1,2]. Given that 97% of global water resources are seawater, desalination has become a vital water treatment methodology [3,4]. Membrane separation has become increasingly important among the technologies developed for seawater desalination due to its low energy requirements and ease of operation [5,6]. Reverse osmosis (RO) is currently the most effective membrane separation technique for this purpose, used in about 65% of existing water desalination plants [7,8]. Polyamide (PA) thin-film composite (TFC) membranes are the leading membranes used for RO owing to their high robustness and durability [9,10]. They are fabricated via interfacial polymerization of an amine monomer, e.g., m-phenylenediamine (MPD) and an acyl chloride monomer, e.g., trimesoyl chloride (TMC), on a porous support, e.g., polysulfone [11,12].

The two parameters governing RO membrane performance are water permeability and salt rejection, which strongly depend on the membrane's surface properties such as hydrophilicity, charge density, and roughness [13,14]. TFC membranes with greater water permeability can significantly reduce specific energy consumption (by reducing pumping energy), whereas increasing salt rejection improves water permeate quality [15,16]. There are many strategies to improve the properties of the PA layer in RO membranes, including adding a comonomer, adding a cosolvent, PA surface modification and nanoparticle incorporation [17,18]. For example, Xie et al. [19] used a sulfone diamine in place of MPD to prepare TFC membranes. However, the most common strategy, in particular since the pioneering work of Jeong et al. [20], is to incorporate nanoscale additives into the PA layer. The resulting membranes, thin-film nanocomposite (TFN) membranes, provide an excellent pathway to RO membrane performance improvement. One way the nanoparticles can affect the performance of TFN membranes is by modifying the PA network microstructure to create additional pathways for water molecule transport [21,22]. Yin et al. [23] reported how the contributions of hydrophilic vs. hydrophobic and porous vs. nonporous nanoparticles influence RO-TFN membrane performance. Incorporating hydrophilic porous nanosilica, created interior and exterior pathways in the PA structure and led to the highest water permeability compared to other nanoparticles, while salt rejection slightly declined.

Cellulose nanocrystals (CNCs) obtained from the acid hydrolysis of native cellulose (e.g., wood pulp) are nonporous, non-toxic, abundant, and inexpensive nanoparticles [24]. CNCs are of interest as TFC membrane additives due to their unique properties, including rod-shaped, high aspect ratio, and large negative surface charge density [25,26]. The introduction

of hydrophilic CNCs (due to the high density of surface hydroxyl (OH) groups) into the PA layer results in additional transport routes via the formation of external water pathways within the CNC/PA interface [27]. Because CNCs are safe nanoparticles, any possible leaching out during the water purification process should not pose health and environmental concerns [28,29]. In addition, according to the vendor, CelluForce Inc. (Montreal, QC, Canada), CNCs have been added to Canada's Domestic Substance List, which allows their unrestricted production and sale. Also, CNCs have received regulatory clearance for use in the US and Europe as they fall into the least toxic classification in the Globally Harmonized System of Classification and Labelling of Chemicals. If the effectiveness of laboratory-scale CNC-TFN membranes were ideal, their scale-up to an industrial standard would not be restricted by monetary factors.

Most CNC-TFN membranes were produced by incorporating the CNCs into the aqueous MPD monomer solution because of their hydrophilic nature [30–33]. However, some issues are associated with this approach that limits the positive impact of CNCs in improving TFN membrane performance. First, rubber rolling is crucial in removing amine-containing water droplets from the substrate before adding organic monomer solution to prevent undesired micro or macro-voids in the selective layer. This step could unintentionally remove many nanoparticles together with the aqueous amine solution. Besides losing the precious nanoparticles, rubber rolling might also interrupt the orientation or distribution of the nanoparticles in the PA layer. Also, the remaining nanoparticles would reside at the region between the PA layer and substrate or place deep inside the PA layer rather than being exposed to the feed solution [34–36].

Asempour et al. prepared TFN membranes by dispersing CNCs into the TMC/n-hexane solution during interfacial polymerization, for the first time [37]. The results demonstrated a significant water permeability increase with just a slight reduction in salt rejection attributed to aggregation of CNCs in the PA layer, leading to the emergence of defects [38,39]. The question arises as to whether modification of CNCs to become slightly less hydrophilic might improve their dispersibility in the hydrophobic monomer solution, thereby leading to a better dispersion of the nanoparticles in the selective PA layer and, thus, improved membrane solute/water selectivity. To our knowledge, only one study, by Smith et al. [40], reports on the use of modified CNCs in RO-TFN membranes. They used TEMPO-oxidized CNCs in RO-TFN membranes but dispersed them in the aqueous MPD monomer solution. Furthermore, the incorporation of other surface functionalities may permit the tuning of PA/CNC interactions leading to further control over salt rejection and water permeability.

Several surface modification approaches exist to change CNC surface functionality to enhance its dispersibility in the organic monomer solution prior to interfacial polymerization [41–43]. At the same time, it is essential to maintain at least some of the hydrophilic nature of CNCs to ensure PA/CNC interactions in the final membrane responsible for generating additional routes for water transport [27,40]. Strong PA/CNC interactions enhance the CNC miscibility in the PA layer and thus, inhibiting the formation of defects in the PA layer due to CNC aggregation [37,44]. Acetylation, which selectively exchanges hydroxyl with acetyl groups, has been shown to improve CNC dispersibility in organic solvents without significantly changing their morphological integrity [45–47]. The degree of substitution (DS) of acetyl groups can control the hydrophilicity and surface charge density of the CNCs [48]. Tuning the DS to achieve a moderate and controlled CNC hydrophilicity could lead to a more even dispersion of CNCs in the PA layer, thereby overcoming the permeability–selectivity trade-off [16,49,50].

In this study, we tested the hypothesis that tuning the hydrophilicity of CNCs improves their dispersibility in the hydrophobic monomer solution and the brackish water desalination performance of the resulting low-pressure RO membranes. We report on the effect of the degree of substitution of CNC hydroxyl groups with acetyl groups and the loading of modified CNCs on the properties, particularly the RO performance of the resulting TFN membranes. To our knowledge, this is the first time that acetylation has been used for CNC modification, or that of any other nanomaterial, to impact TFN membrane performance.

3.3 Experimental section

3.3.1 Materials

Poly(sulfone) ultrafiltration membranes (PS35) with a molecular weight cut-off of 20 kDa were donated by Solecta, California, USA. The monomers, m-phenylenediamine (MPD, 99% purity), trimesoyl chloride (TMC, >98% purity), and the organic solvent, n-hexane (>99% purity), were purchased from Sigma-Aldrich. The spray-dried powder form of the sulfate sodium salt of CNCs was donated by CelluForce Inc. (Windsor, Quebec). NaCl (laboratory reagent grade) was purchased from Sigma-Aldrich. Ethanol, HCl, KCl, acetic anhydride, iodine, and NaOH were procured from Fisher Scientific. Deionized water was used to make the aqueous MPD solution, and distilled water was used to wash the membranes and prepare the synthetic brackish water feed with NaCl as a solute. All materials were used as received without further purification/ modification except for the modified CNCs, which are described next.

3.3.2 CNC modification

A solvent-free method was used to functionalize the CNCs with acetyl groups. A mixture of 0.57 g CNCs, 9 mL acetic anhydride, and different iodine concentrations as catalyst (0.02 and 0.04 g) was placed in a glass vial equipped with a magnetic stirrer and heated at 100°C for 10 min. The reaction mixture was cooled to room temperature and treated with acetone (0.9 mL) while stirring. The mixture was then washed with 80 mL of a 75% ethanol/deionized water solution. Three washing/centrifugation steps were performed using deionized water until a neutral suspension of ACNCs was obtained. Finally, the ACNCs were re-suspended in deionized water and freeze-dried at -60°C to produce a fine ACNC powder, Figure A.1 (Appendix A).

To investigate the dispersibility of the CNC and ACNC in water and n-hexane, their apparent hydrodynamic particle sizes (Z-average particle size) were characterized via dynamic light scattering (DLS) after probe sonication for three 5-minute intervals at 75% amplitude. We note that CNCs are rod-shaped, and as such, the assumption of a spherical shape inherent in DLS measurements is not valid. Therefore, the measurement should be considered as an apparent or relative measurement of CNC particle sizes.

For quantitative analysis, the degree of substitution (DS) of hydroxyl groups on CNCs with acetyl groups (ACNC2: 0.02 g and ACNC4: 0.04 g iodine as the catalyst) was determined via titration as follows: 5.00 mL NaOH (0.25 mol/L) and 5.00 mL ethanol were added to about 0.1 g ACNC. After 24 h, 10.00 mL HCl (0.25 mol/L) was added to the mixture and titrated using a standard 0.25 mol/L NaOH solution. This procedure was repeated in triplicate, and the percentage of acetyl groups (%AG) was calculated using:

$$\%\mathrm{AG} = \frac{[(V_{b,i}+V_{b,t})c_b - V_a c_a]43}{m_{ac}} 100\% \qquad (3.1)$$

Then, using AG%, the DS was calculated with:

$$\mathrm{DS} = \frac{162\mathrm{AG}\%}{4300\text{-}42\mathrm{AG}\%} \qquad (3.2)$$

where $V_{b,i}$ is NaOH volume, $V_{b,t}$ is NaOH volume spent in titration, c_b is NaOH molarity, V_a is HCl volume, c_a is HCl molarity, 43 is the molecular weight of acetyl group, m_{ac} is the weight of the dried ACNC sample, and 162 is the molecular weight of the anhydrous glucose unit of the CNC chemical structure. In equation 2, 4300 is the molecular weight of the acetyl group multiplied by 100, and 42 is the molecular weight of the acetyl group −1 [47].

3.3.3 Synthesis of TFC and TFN membranes

A PS35 membrane was used as the substrate to synthesize the PA layer by in-situ interfacial polymerization. 0.05% (w/v) TMC and 2% (w/v) MPD solutions were prepared in n-hexane and deionized water, respectively. After 1-2 h of magnetic stirring, specified amounts of CNC, ACNC2 and ACNC4 dried powder (0.05, 0.1, 0.2, or 0.4wt%) were added to the TMC/n-hexane solution and stirred until CNC aggregates were no longer visible (typically, 30-40 min). The mixture was sonicated in an ice bath using a Fisher Scientific 550 sonicator (at 75% amplitude) three times at 5-minute intervals, with 5-minute rest periods. The well-dispersed CNC in TMC/n-hexane solution was used in the interfacial polymerization synthesis of TFN membranes. The process began by pouring 50 mL of MPD solution onto the substrate and waiting for 5 minutes to ensure the MPD solution's penetration into the substrate's pores. Then, the excess MPD solution was drained from the substrate with a Teflon roller. This was followed by pouring 50 mL of the TMC solution (with or without dispersed nanoparticles) on the membrane. After one minute, the excess TMC solution was decanted, and the membrane was rinsed with ~20-50 mL n-hexane, Figure A.2 (Appendix A). Afterwards, the membrane was placed in an oven at 95°C for 10 minutes to dry the excess solvent. Finally, the membrane was carefully washed and stored in deionized water at ambient temperature until it was tested.

3.3.4 Characterization of the nanoparticles and membranes

A Nicolet 6700 FTIR (Thermo Scientific) with a diamond crystal was utilized to obtain the ATR-FTIR spectra of the TFN membranes, CNC, ACNC2 and ACNC4. All scans were recorded at 4 cm^{-1} over a range of wave numbers between 650 and 4000 cm^{-1}. Solid-state ^{13}C-NMR spectra of CNC, ACNC2 and ACNC4 were obtained using a Bruker AVANCE III 400 NMR spectrometer with a single crystal solid-state probe. X-ray diffraction (XRD) (Rigaku Ultima IV Diffractometer) was used to study the crystallinity of the CNC, modified CNCs and TFN membranes. The XRD test was carried out at room temperature with a Bragg-Brentano geometry, using Cu Kα radiation (λ=1.5418 Å). The 2θ range of 4° to 70° was covered with a 0.02° step width and a 3°/min scan speed.

The surface zeta potential measurement of the ACNCs was conducted using a zeta analyzer (Zetasizer PSS0012-22, Malvern Instruments) with a frontal electrophoretic light scattering method. The ACNCs were dispersed in deionized water and probe sonicated before analysis. The Zetasizer was equipped with an adjustable gap cell to measure membrane surface charge. 1 mM of KCl solution was used as the background electrolyte, with its pH adjusted using 0.1 M HCl or 0.1 M NaOH. The sessile water contact angle of the CNC and ACNC dry

powder (pressed into discs) and membrane surfaces were measured using a VCA Optima surface analysis system (AST Products, Inc., Billerica, MA). At least 20 droplets (2 μL) of deionized water in at least seven different locations on each sample were tested at ambient temperature. X-ray Photoelectron Spectroscopy (XPS) elemental surveys were carried out over 1 × 1 mm area of the membranes using an XPS (Kratos Analytical model Axis Ultra DLD spectrometer) machine with monochromated aluminum-K_α Xrays at the power of 150 watts. Membrane morphology was characterized at the top surface and cross-section using field emission scanning electron microscopy (FESEM, Tescan Vega-II XMU) and atomic force microscopy (AFM, Park NX10). The AFM images were obtained using a tapping mode, scanning over 10×10 μm^2 with 512×512 pixel width resolution and an adaptive scan rate of 0.2–2 Hz. The surface topography of the membranes was characterized in terms of the root-mean-square of the height deviations (R_q), the average plane roughness (R_a), the maximum peak-to-valley distance (R_z), and the ratio of the actual surface area for a rough surface to the planar area (r). Accordingly, $r = 1$ indicates a perfectly smooth surface. For each membrane, two samples for AFM analysis were used. Because the apparent contact angle is altered by the surface roughness, solid-liquid interfacial free energy (ΔG_{SL}) was evaluated to characterize the intrinsic surface hydrophilicity of the membranes [32]. The ΔG_{SL} (mJ/m^2) value was calculated from the Young–Dupre equation:

$$\Delta G_{SL} = \gamma_L \left(1 + \frac{\cos\theta}{r}\right) \qquad (3.3)$$

where θ is the average water contact angle and γ_L is the water surface tension (72.8 mJ/m^2 at 25°C), r is the roughness area ratio (i.e., the ratio of actual surface area for a rough surface to the planar area) obtained from AFM topographical images. Accordingly, the minimum value of r for the ideally smooth surface is unity, which maximizes ΔG_{SL} for a given hydrophilicity. As the hydrophilicity of the surface increases, θ decreases (i.e., $\cos\theta$ increases), and the value of ΔG_{SL} increases [51].

3.3.5 Membrane performance

The desalination performance of the membranes was evaluated at typical conditions for low-pressure RO membranes, i.e., using synthetic simplified model brackish water (3000 ppm aqueous NaCl solution) as the feed at a hydraulic pressure of 20 ±1 bar. The membranes were tested in a continuous crossflow system, consisting of three membrane cells arranged in parallel, each with an effective surface area for permeation (A_p) of 17.35 cm^2. The flow rate of feed was maintained at 2.4 ±0.2 L/min to minimize the concentration polarization effect and achieve near-zero recovery conditions [37,52]. The measurements were conducted at 295 ±1

K. Water flux, J_w (L/m^2.h), was calculated by Eq. (3.4) based on the volume of permeate (V_p) collected during a time, t, at steady-state. Salt rejection, R, was evaluated by Equation (3.5), in which C_p and C_f were the feed and permeate concentrations, respectively, measured by conductimetry.

$$J_w = \frac{V_p}{A_p t} \quad (3.4)$$

$$R = (1 - \frac{C_p}{C_f}) \times 100\% \quad (3.5)$$

The membrane water permeability, A (L/m^2.h.bar) and salt permeability, B (L/m^2.h), were calculated using Equations. (3.6) and (3.7)

$$A = \frac{V_p}{A_p t(\Delta P - \Delta \pi)} \quad (3.6)$$

$$B = \frac{1-R}{R} J_w \quad (3.7)$$

where ΔP is the applied hydraulic pressure (bar), and $\Delta\pi$ is the difference of osmotic pressures (bar) between feed and permeate calculated by the van't Hoff equation:

$$\Delta \pi = \Delta C i R T \quad (3.8)$$

in which ΔC is the molar concentration gradient ($\Delta C \approx C_f$), i is the number of ions into which the salt dissociates, R is the ideal gas constant, and T is the absolute temperature. A and B represent membrane permeance rather than membrane permeability. The permeability is thickness-normalized permeance. However, since A and B are traditionally referred to as permeability, we will continue to use the term permeability throughout this paper.

All performance test results are expressed as averaged values from a minimum of four coupons cut from two different synthesized membrane sheets.

3.4 Results and discussion

3.4.1 CNC surface functionalization

In Figure 3.1, the infrared spectra of the ACNCs after washing are shown. The spectra present the evidence of acetylation with three significant ester bond peaks at 1750, 1370 and 1240 cm^{-1}, which belong to carbonyl (C=O), methyl (C-H), and acetyl (C-O) group stretching vibrations, respectively [40,41]. The decreasing O-H stretching vibration at 3300 cm^{-1} for ACNC2 and ACNC4 compared to CNC confirms the substitution of hydroxyl groups with acetyl groups. A lack of peaks in the 1760-1840 cm^{-1} and 1700 cm^{-1} regions confirm that the

ACNCs were free of unreacted acetic anhydride or any acetic acid by-products [45]. The higher acetyl content with increasing iodine catalyst concentration is also demonstrated by the proportionate increase in absorption at the carbonyl (1750 cm^{-1}) and methyl (1370 cm^{-1}) peaks in ACNC4 compared to the ACNC2 spectrum [47]. Esterification was further confirmed via solid-state ^{13}C-NMR spectroscopy (Figure 3.2). The chemical shifts for the unmodified CNC are assigned to C1 (105 ppm), C4 (89 ppm), C2, C3, C5 (72 and 75 ppm), and C6 (65 ppm). The basic cellulose structure was preserved after acetylation, as shown in the spectra of ACNC2 and ACNC4. Moreover, additional peaks at 172 and 21 ppm, reflecting the carbonyl (C=O) and methyl (C-H) groups of acetyl ester, are noted on the ACNC2 and ACNC4 spectra [48,53].

The DS of the ACNCs represents the average number of acetyl groups that replaced the hydroxyl groups in the glucosidic units of the CNC structure; the maximum DS = 3 [49]. After acetylation, the DS, measured by titration, increased from zero to 0.72 for ACNC2 and 1.37 for ACNC4 (Table 3.1). The average water contact angle of CNC and ACNC films ranged from 30.3° for CNC to 58.5° for ACNC2, and 68.6° for ACNC4, indicating the expected decrease in hydrophilicity with DS (Table 3.1, Figure A.3 (Appendix A)).

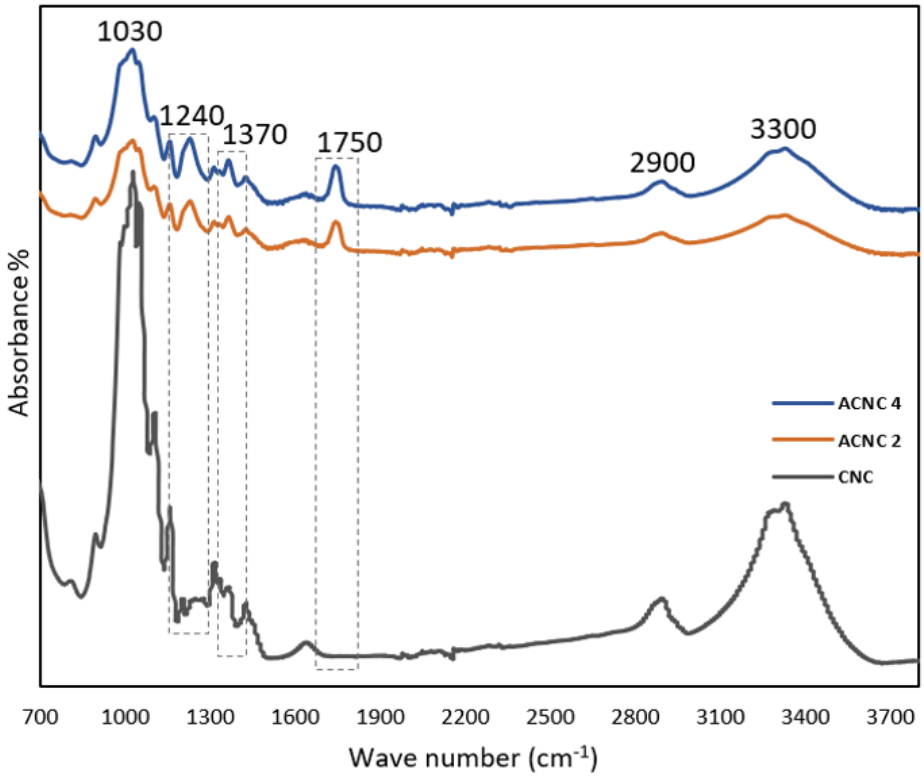

Figure 3.1: ATR-FTIR spectra of CNC, ACNC2 and ACNC4.

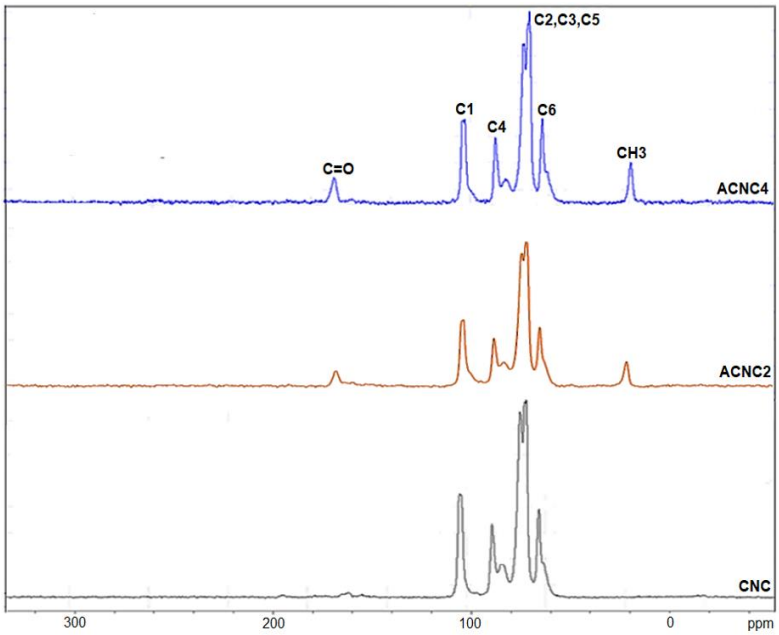

Figure 3.2: Solid-state ^{13}C-NMR spectra of CNC, ACNC2 and ACNC4.

The effect of iodine content on the surface charge density of ACNCs was investigated using zeta potential measurements (Table 3.1). The CNC surface is negatively charged due to the abundance of hydroxyl groups [47,54]. The zeta potential of the CNC, -50.21 mV, increased via acetylation to −39.44 mV for ACNC2 and -35.55 mV for ACNC4; thus, acetylation decreased the negative surface charge density because of neutral methyl group substitution on the CNC surface[53,55]. The apparent particle size of ACNC2 and ACNC4 in n-hexane was 104.3 and 87.8 nm, respectively (Table 3.1), which is significantly smaller than the corresponding particle size of CNC (180.3 nm).

Table 3.1: Characterization of CNC and ACNCs.

Sample	CNC	ACNC 2	ACNC 4
CNC (g)	-	0.57	0.57
I_2 (g)	-	0.02	0.04
Acetic anhydride (g)	-	9.72	9.72
DS	-	0.7 ±0.1	1.3 ±0.1
Contact angle (Degree)	34.3 ±2.3	58.5 ±3.1	68.6 ±1.8
Zeta potential (mV)	-50.2 ±2.1	-39.4 ±1.3	-35.5 ±1.2
Particle size (nm) in n-hexane	180.3 ±3.1	104.3 ±2.4	87.8 ±2.3
Particle size (nm) in water	70.3 ±3.1	82.3 ±1.1	95.8 ±2.4
Crystallinity (%)	94.2 ±2.1	85.4 ±1.6	80.1 ±1.7

Typical PA layer thickness for TFC and TFN membranes ranges from 150 to 200 nm [56]; therefore, the particle size of ACNC2 and ACNC4 was below even the minimum thickness encountered in practice. By acetylating the CNCs, the probability of dispersing them into a nonpolar solvent such as n-hexane increases [28]; thus, the apparent particle sizes (or hydrodynamic radii) of ACNC2 and ACNC4 in n-hexane are smaller than that of CNC. The opposite was true in water, as expected. The acetylation of CNCs is evidently highly tunable and can result in CNCs that are more dispersible in nonpolar solutions without overly compromising their dispersibility in water, as further evidenced by contact angle and particle size measurements (Table 3.1). Slight substitution of hydroxyl groups by neutral acetyl groups helps reduce the probability of inter-hydrogen bonding between OH groups, thus minimizing the aggregation of CNCs.

In addition, The XRD spectra of CNC, ACNC2 and ACNC4 demonstrating the changes in CNC crystallinity degree with no change in the morphology of the CNCs after acetylation are presented in Figure A.4 (Appendix A). The XRD spectra of CNC and ACNC nanoparticles show three peaks at 2θ of approximately 16°, 22° and 34°. ACNCs exhibit a lower degree of crystallinity than CNC due to substituting the hydroxyl groups by the larger acetyl groups, which broke the inter and intramolecular hydrogen bonds of the cellulose structure [47,55]. The crystallinity decreased from 94 ±1.21% for CNC, to 85 ±0.71% for ACNC2, and 80 ±1.52% for ACNC4, consistent with the increasing degree of acetyl group substitution from CNC to ACNC2 to ACNC4.

3.4.2 Membrane surface characterization

The surface functional groups of the TFC and TFN membranes were characterized using ATR-FTIR (Figure 3.3). The three peaks at 1440, 1580, and 1625 cm^{-1} confirm the PA layer's successful formation on top of the PS substrate for both pristine TFC and TFN membranes [37]. The peaks represent the O–H stretching vibration of the carboxylic groups generated by the hydrolysis of acyl chlorides (1440 cm^{-1}), the C–N stretching vibrations and the N–H bending of the secondary amide groups (1580 cm^{-1}), and the C=O stretching vibrations of the N–C=O groups (aromatic amide) (1625 cm^{-1}) [30,57]. For the ACNC-TFN membranes, an additional peak was identified at 1731 cm^{-1}, corresponding to the carbonyl stretching vibrations of the ACNC acetyl groups, indicating successful incorporation of the ACNCs in the membranes [40]. Furthermore, the 1731 cm^{-1} characteristic peak is stronger for the 0.1 wt% ACNC4-TFN than the ACNC2-TFN membrane, consistent with their higher DS. It is noted that even at 0.1 wt% loadings, the nanoparticles are detectable via ATR-FTIR.

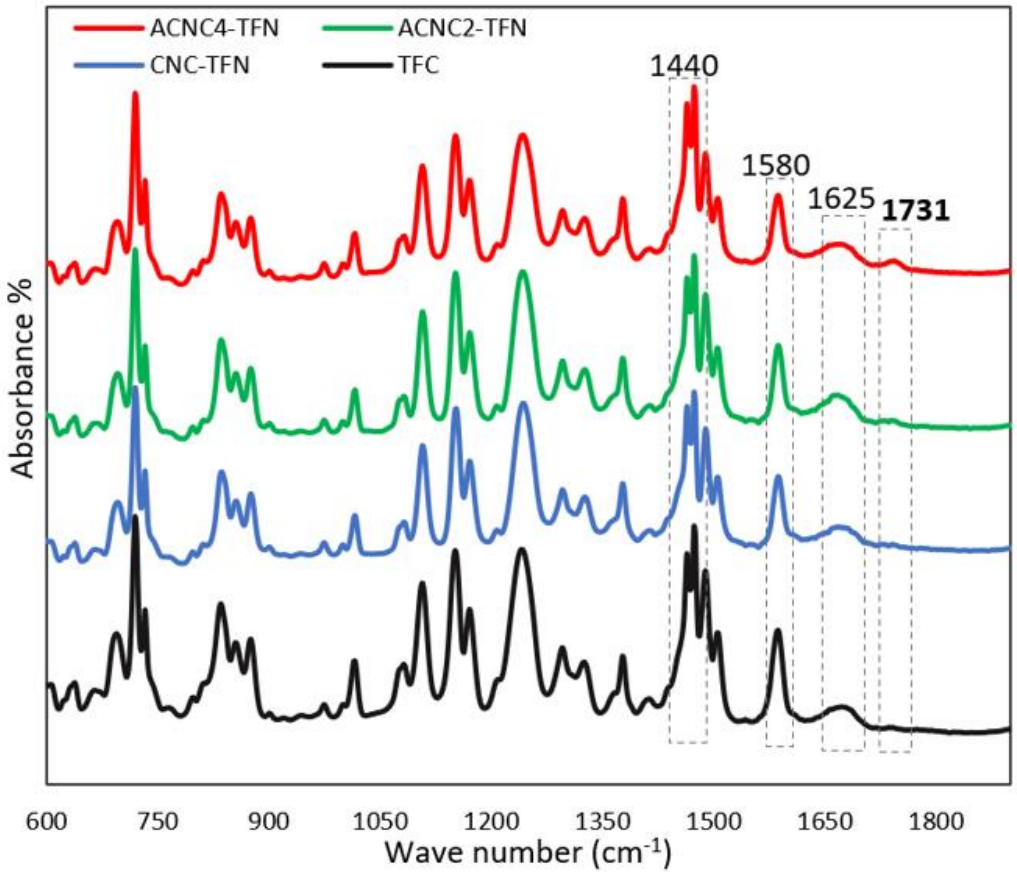

Figure 3.3: ATR-FTIR spectrum of TFC and TFNs in 0.1wt% of CNC and ACNCs.

Figure 3.4 presents the contact angle measurements of the TFC and TFN membrane's surface. In general, the contact angle of TFN membranes is less than that of the reference TFC membrane. The increased hydrophilicity of the TFN membranes can be attributed to the additional hydroxyl groups of the CNCs and ACNCs [58]. The contact angle of the 0.1 wt% TFN membranes increased from 50.1° (CNC-TFNs) to 61.4° (ACNC2-TFN) to 72.3° (ACNC4-TFN), which is consistent with the decreasing hydrophilicity of the CNC to ACNC2 and ACNC4 (Table 3.1). Increasing the CNC loading from 0.1 to 0.4wt% resulted in a contact angle reduction of about 10° for CNC-TFN, whereas for the ACNC2-TFN and ACNC4-TFN membranes, the contact angle increased slightly (i.e., 2-3°). The effect of the DS of ACNCs on the contact angle of the membrane appears stronger than the effect of nanoparticle loading. The ACNC4-TFN0.4 has the most significant decrease in surface hydrophilicity compared to TFC and CNC-TFN0.4 membranes. This indicates reasonable control of membrane surface hydrophilicity by loading acetyl functionalized CNCs. It is important to note that the surface roughness affects the measured contact angle. As a result, solid-liquid interfacial free energy

(ΔG_{SL}), which depends on both the contact angle and surface roughness (Equation 3.3), is a better indicator of the intrinsic surface hydrophilicity than the contact angle [32].

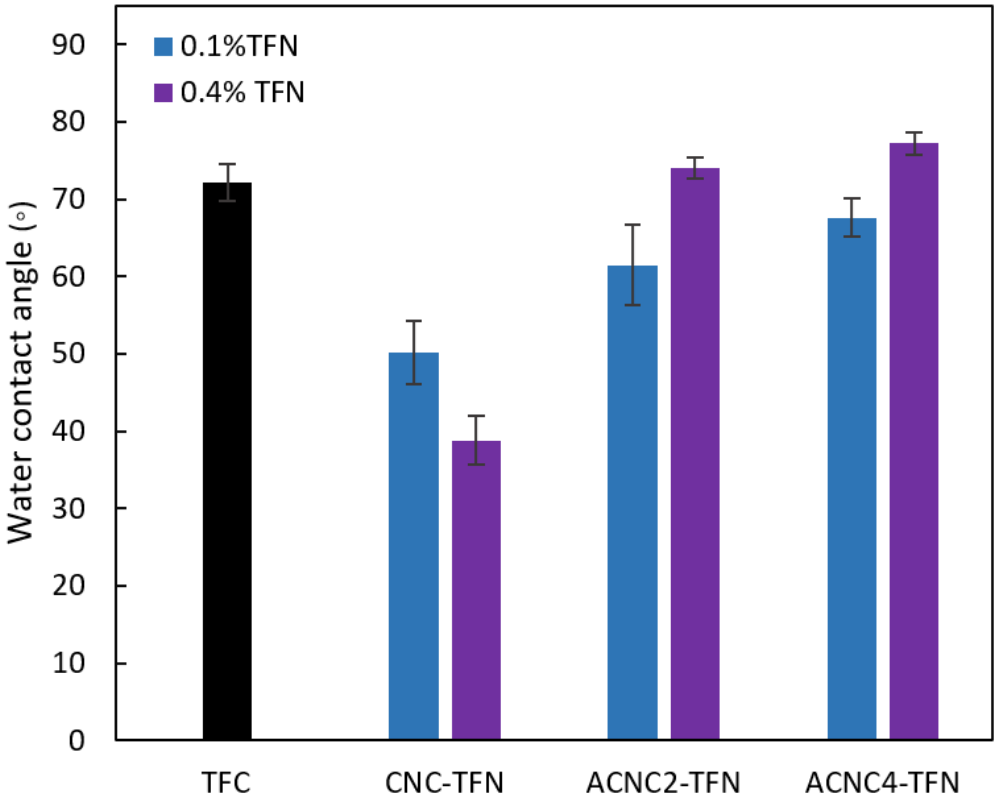

Figure 3.4: Water contact angle of TFC and TFNs in 0.1 and 0.4 wt% of CNC and ACNCs.

Figure 3.5a shows the zeta potential of the membrane surfaces in the pH range 3.5–9. The zeta potential of the membrane surfaces became more negative with an increase in pH. As the nanoparticle loading increased from 0.1 to 0.4 wt%, the zeta potential of TFN membranes decreased to a more negative surface charge density consistent with the contact angle measurements of membranes (Figure 3.5b, Figure 3.4). In the case of ACNC2 and ACNC4-TFNs, this decrease was not as sharp as that for CNC-TFNs due to the lower negative surface charge density of ACNC2 and ACNC4 compared to CNC nanoparticles (Table 3.1). In the TFC membrane, the negative surface charge density arose from the carboxylic acid groups of the unreacted TMC, whereas for the CNC and ACNC-TFN membranes, the contribution to surface charge density was also due to the hydroxyl groups of the nanoparticles [33,59]. The ACNC2-TFN and ACNC4-TFN membranes showed a negative zeta potential below the TFC membranes but higher than that of the CNC-TFN membranes.

The lower absolute value of the membrane surface charge density of ACNC2 and ACNC4-TFN compared to CNC-TFN can be attributed to an increase in the probability of the ACNC nanoparticles interacting with the acyl chloride groups of the TMC monomer (prior to and during interfacial polymerization), which decreases the content of unreacted carboxylic acid groups in the PA layer [27,30]. The zeta potential results confirm that varying the loading of hydrophilic nanoparticles (CNCs) functionalized by acetyl groups regulated the surface charge of the PA-based TFN membranes.

To further investigate the formed PA layer in the TFC and TFN membranes, XPS analysis For CNC-TFN0.1, ACNC2-TFN0.1 and ACNC4-TFN0.1 were performed (Table 3.2, Figure A.4, (Appendix A)). This surface-sensitive method is used to study the elemental composition and chemical binding in the top ~5 nm layer of thin films. It is important to emphasize that the top 5 nm might not represent the entire PA layer. However, in the following discussion, we assume that the composition of the top 5 nm represents the composition of the entire PA layer [57].

During the interfacial polymerization of MPD and TMC monomers, one acyl chloride group of TMC is either reacted with MPD to form a crosslink or with H_2O to form free carboxylic acid [20]. The C/N and O/N ratios of ACNC2-TFN0.1 and ACNC4-TFN0.1 decreased compared to CNC-TFN0.1, suggesting higher degrees of crosslinking for ACNC2 and ACNC4-TFN membranes[44,58]. A smaller C/N or O/N ratios indicate a greater crosslinking network, which would result in the tighter structure of the PA layer and likely smaller pore sizes in the selective layer [59]. It is important to note that XPS is often combined with the MWCO results to elucidate the pore size and pore size distribution in the PA layer [60–62]. Ultimately, the salt rejection data of ACNC-TFN compared to CNC-TFN should indirectly verify if the acetylation of CNCs affects the pore size of the resulting ACNC-TFN membranes.

The presence of ACNCs during interfacial polymerization (dispersed in TMC/n-hexane monomer solution) enhances the sorption of MPD on the interface of two monomer solutions due to the synergistic effect of the hydrophilic interactions and coordination between MPD and ACNCs in comparison to CNCs [60,63]. This greater MPD sorption is consistent with the possible increased crosslinking in the PA layer compared to the TFC and CNC-TFN membranes.

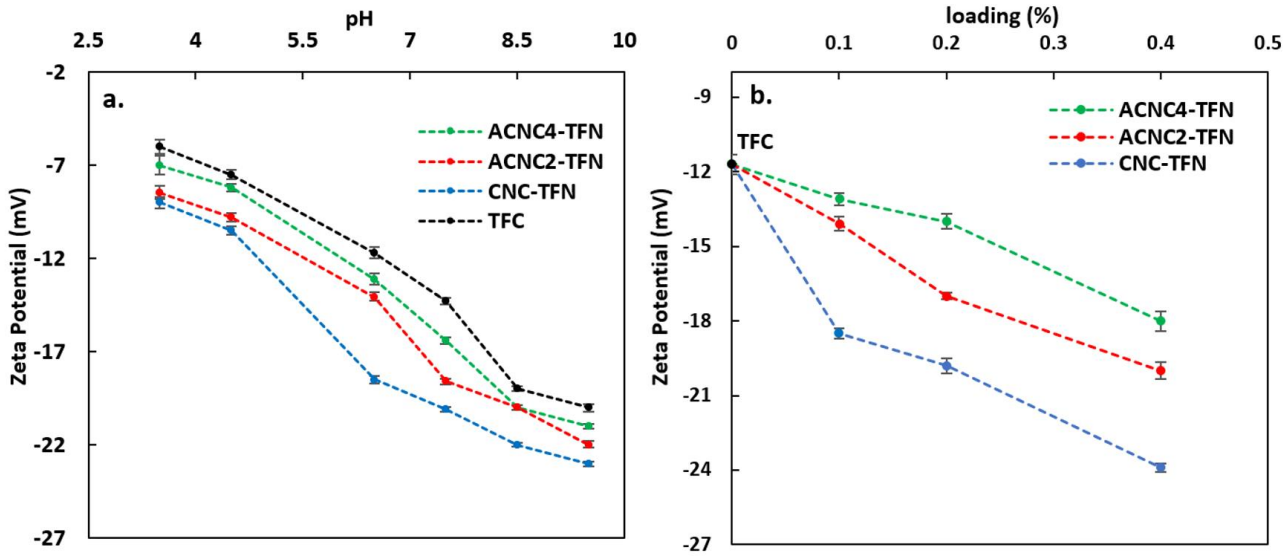

Figure 3.5: a) Zeta potential of TFC and 0.1 wt% CNC and ACNCs-TFN membranes in pH range 3.5-9, b) Zeta potential of TFC and TFN membranes in pH = 6.5 for different loadings of CNC and ACNCs.

In addition, the carboxylic acid group content of the TFN membrane was calculated from XPS spectra. When the CNC or ACNCs are added to the TMC monomer solution, the hydroxyl surface groups of the CNC or ACNCs can also react with the acyl chloride group of TMC, leading to a decrease in carboxylic group content of ACNC2 and ACNC4-TFNs. This carboxylic group content decrease is consistent with a decrease in the absolute value of the zeta potential in the ACNC2 and ACNC4-TFNs compared to CNC-TFN membranes (Figure 3.5a).

Table 3.2: Elemental composition of membranes by the XPS analyses.

Sample	C (%)	O (%)	N (%)	C/N (-)	O/N (-)	COOH content*
TFC	66.56	16.59	9.02	7.38	1.84	3.94
CNC-TFN 0.1	71.71	17.63	9.81	7.30	1.79	3.75
ACNC2-TFN 0.1	75.23	17.46	10.91	6.89	1.60	3.51
ACNC4-TFN 0.1	77.15	17.22	11.33	6.80	1.51	3.38

* The density of carboxyl groups (COOH content) was obtained from O-C=O (Binding energy=288.4 eV) peak area derived from the C1s core level XPS spectra.

The membrane surface morphologies characterized by FESEM and AFM imaging are displayed in Figure 3.6. The FESEM micrographs show typical hybrid nodular and leaf-like morphology for TFC and TFN membrane surfaces [30,40]. The CNC-TFN membranes appear to have a more nodular-like structure, while for ACNC2 and ACNC4-TFNs, the structure was more leaf-like (Figure 3.6 b1-g1). Xu et al. [64] systematically investigated the relationship

between the surface morphology and the performance of TFC membranes. They concluded that compared to smooth, semi-smooth and nodular surface morphologies, the membranes with leaf-like surface morphology were associated with generally higher water permeability and salt rejection. Therefore, qualitatively the surface morphologies of ACNC-TFN compared to CNC-TFN appear to promise a better membrane performance. It is important to note that some researchers also investigate the morphology of the back surface of the PA layer, which provides more insight into the structure of the active layer of TFC and TFN membranes [60–62].

The AFM images exhibited a ridge-and-valley morphology consistent with the SEM images (Figure 3.6 a2-g2). The surfaces of ACNC2-TFN and ACNC4-TFN represent a ridge-and-valley structure with fewer crumples than CNC-TFNs, which may be due to the more uniform distribution of ACNCs within the PA structure. The surface roughness parameters R_q, R_a and R_z and the roughness area ratio (r) are summarized in Table 3.3. As expected, the reference TFC membrane exhibited the lowest R_q, R_a, R_z, and r among all membranes. Introducing nanoparticles in the PA layer increased the surface roughness and the relative surface area of the resulting TFN membranes. The three surface roughness parameters are related to the size of the AFM image features. In contrast, the roughness area ratio relates to the number of features on the membrane surface. Also, r, which affects ΔG_{SL}, does not follow the same trend as R_q, R_a, and R_z. For a given nanoparticle loading, R_q, R_a, and R_z decreased while r increased comparing CNC, ACNC2, and ACNC4-TFNs. On the other hand, when nanoparticle loading increased while the degree of substitution of ACNCs was constant, R_q, R_a, and R_z increased, but r decreased. Considering that large values of R_q, R_a, and R_z with corresponding small values of r indicate aggregation of nanoparticles on the membranes' surface, the results in Table 3.3 suggest that increasing the degree of substitution of ACNCs decreased the tendency of the nanoparticles to aggregate even at higher nanoparticle loadings.

Table 3.3 also summarizes the values of ΔG_{SL}, which measures the intrinsic surface hydrophilicity of the membranes. It is evident that CNC-TFN membranes exhibited the largest ΔG_{SL} because of their low contact angle (θ) (Figure 3.4). Interestingly, although the contact angle of the TFC membrane was the highest in Figure 3.4, the corresponding ΔG_{SL} was not the lowest among all membranes because of its lower r value. For a given loading of nanoparticles, ΔG_{SL} decreases with the increase in the degree of substitution of hydroxyl groups. The effect of nanoparticle loading on ΔG_{SL} is different for the CNC-TFN and ACNC-TFN membranes. More specifically, for CNC-TFN, ΔG_{SL} increases with loading, but the opposite occurs for ACNC-TFN.

Table 3.3: Surface properties of TFC and TFN membranes.

Sample	R_q (nm)	R_a (nm)	R_z (nm)	r (-)	ΔG_{SL} (mJ/m^2)
TFC	34.1 ±2.1	29.2 ±3.1	124.2 ±4.1	1.16	92.7 ±3.1
CNC-TFN 0.1	68.7 ±3.7	49.2 ±5.4	242.7 ±2.4	1.35	107.1 ±4.8
ACNC2-TFN 0.1	54.1 ±1.1	40.4 ±4.1	185.4 ±1.7	1.43	97.1 ±2.1
ACNC4-TFN 0.1	43.2 ±1.9	35.3 ±1.5	146.8 ±3.2	1.5	91.3 ±1.2
CNC-TFN 0.4	75.3 ±4.1	52.9 ±2.6	254.2 ±1.3	1.21	119.7 ±3.4
ACNC2-TFN 0.4	60.6 ±2.5	45.5 ±1.9	220.5 ±2.5	1.39	87.2 ±2.5
ACNC4-TFN 0.4	49.5 ±3.4	41.8 ±2.7	208.3 ±4.9	1.44	84.1 ±1.5

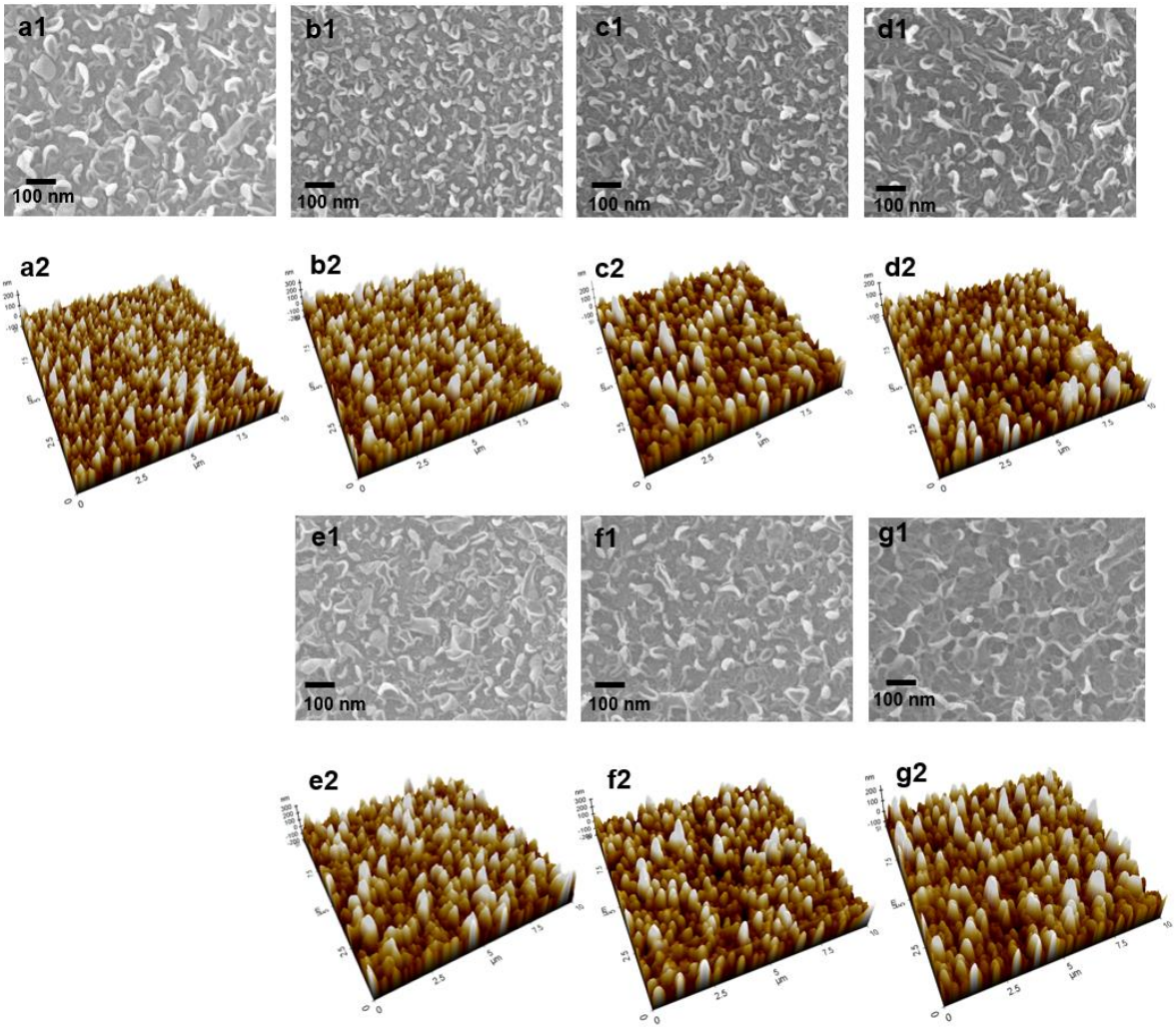

Figure 3.6: Membrane surface images for (a) TFC, (b) CNC-TFN 0.1%, (c) ACNC2-TFN 0.1%, (d) ACNC4-TFN 0.1%, (e) CNC-TFN 0.4%, (f) ACNC2-TFN 0.4% and (g) ACNC4-TFN 0.4% membranes (FESEM = 1; AFM = 2).

Figure 3.7 presents cross-sectional images of TFC, CNC-TFN0.1, ACNC2-TFN0.4 and ACNC4-TFN0.4 membranes obtained using FESEM. The selective PA layer is evident in all images. Moreover, it appears that the thickness of the PA layer decreased in the following order: TFC > CNC-TFN0.1 > ACNC2-TFN0.4 > ACNC4-TFN0.4 A decrease in the thickness of the selective layer might indicate its denser structure.

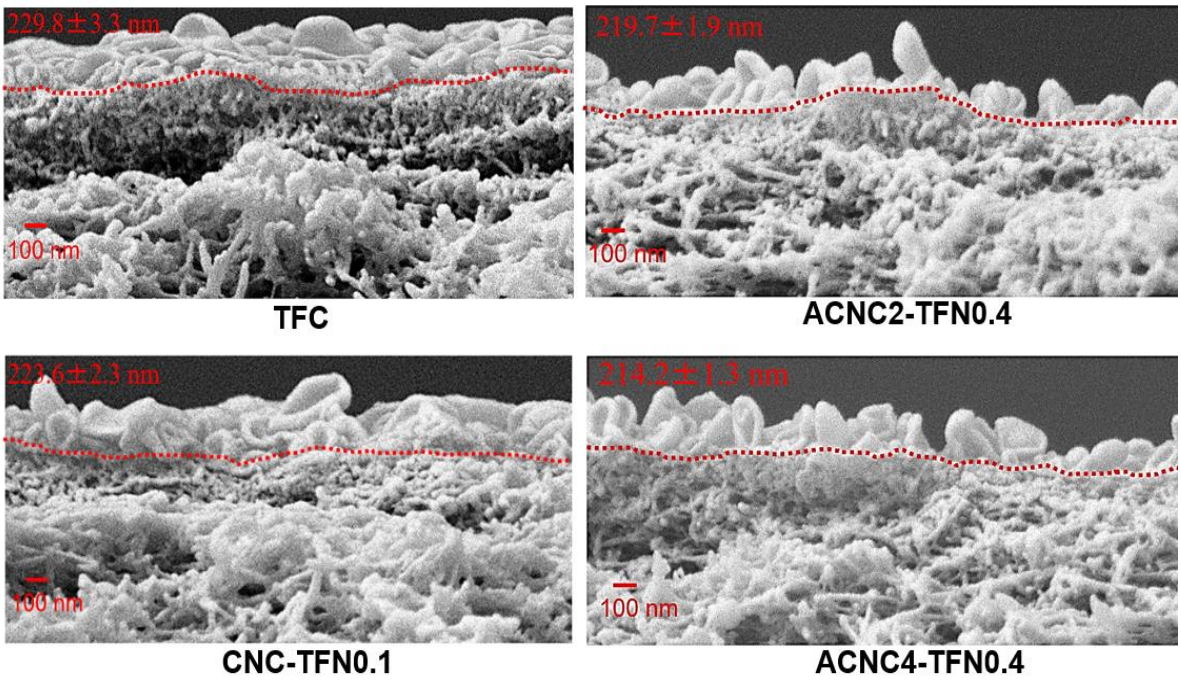

Figure 3.7: Cross-section FESEM images of TFC, CNC-TFN0.1, ACNC2-TFN0.4 and ACNC4-TFN0.4.

3.4.3 Membrane separation performance

Figure 3.8 presents the effect of nanoparticle loading on the water permeability and salt rejection of TFN membranes. The water permeability of all TFN membranes was higher than that of the reference TFC membrane. Although the ACNC-TFN0.2 membranes were less permeable than the ACNC-TFN0.1 membranes, the water permeability of ACNC-TFN membranes generally increased with nanoparticle loading. In particular, the water permeability of ACNC2-TFN0.4 (2.60 ±0.30 L/m^2.h.bar) was more than 100% higher than that of the TFC membrane (1.27 ±0.17 L/ m^2.h.bar). Except for the CNC-TFN membranes, salt rejection of the TFN membranes was similar or higher than that of the reference TFC membranes. The salt rejection of ACNC4-TFN membranes, regardless of nanoparticle loading, was nearly 99% compared to 98% for the reference TFC membrane. In general, the nanoparticle loading improved the performance of ACNC-TFN membranes by either increasing the water

permeability, the salt rejection or both simultaneously. This represents the most desirable effect of nanoparticle loading on TFN membrane performance.

Hydrophilic nonporous nanoparticles such as CNCs and ACNCs lead to the creation of internal voids, increasing the PA layer's free volume. Some researchers consider these internal voids as additional nanochannels at the nanoparticle/PA interface, which in turn could increase the water permeability of the resulting TFN membranes [23,36]. In general, the water permeability increases with surface roughness and hydrophilicity. Yet, the water permeability decreased for CNC-TNF membranes, despite increased surface roughness and surface hydrophilicity (measured by ΔG_{SL}) with the nanoparticle loading. The limited usefulness of unmodified CNCs to improve the performance of the TFN membranes is most likely the result of CNC aggregation at higher loadings. In fact, despite a greater amount of CNCs in the PA layer, there might be less hydrogen bonding between the hydroxyl groups of the CNCs and the PA functional groups. Thus, fewer additional nanochannels could be created at the nanoparticle/PA interface. The presence of CNCs aggregates larger than individual nanoparticles might also lead to some defects in the PA layer [49,65]. It could explain a decrease in salt rejection of CNC-TFN membranes with increased nanoparticle loading. Furthermore, an increase in R_q, R_a and R_z, associated with a decrease in r when nanoparticle loading increases for CNC-TFN membranes (Table 3.3), supports this hypothesis.

The effect of nanoparticle loading on TFN membrane performance changed significantly when the CNCs hydroxyl groups were substituted with acetyl groups. By slightly acetylating CNCs, they became more dispersible in the TMC monomer solution, resulting in greater interactions between the acyl chloride groups of the TMC with the hydroxyl groups of ACNCs. This interaction between TMC and ACNCs, prior to interfacial polymerization, resulted in an improved dispersion of ACNCs within the final PA layer. For ACNC2-TFN0.4 and ACNC4-TFN0.4, the water permeability increased even though the membrane surface hydrophilicity (ΔG_{SL}) and surface roughness (R_q, R_a, R_z) decreased compared to CNC-TFN0.4. The observed increase in the water permeability could arise from a decrease in the thickness of the PA layer (Figure 3.7). Regardless of the type of the nanoparticles and their loading, identical volumes and concentrations of monomer solutions were used to synthesize the PA layer. Suppose a similar mass of PA was formed in every TFC and TFN membrane. Therefore, we hypothesize that a decrease in the thickness of the PA layer could indicate its denser structure. The latter corroborates with the XPS results suggesting the increased crosslinking density in the PA layer with the degree of acetylation of CNCs (Table 3.2). If that is the case, a decrease in the PA layer thickness would not explain the observed increase in the water permeability.

Furthermore, we hypothesize that improvement in the dispersibility of ACNCs might help create more but smaller internal voids in the PA layer of the ACNC-TFN membranes than the CNC-TFN membranes. These tiny internal voids could be considered nanochannels responsible for the observed increase in the water permeability. The proposed hypothesis does not explain the lower water permeability of ACNC-TFN0.2 compared to ACNC-TFN0.1 (Figure 3.8). The observed minimum water permeability of the ACNC-TFN0.2 membranes might arise for the interplay of two effects. On the one hand, as the loading of ACNCs increases, the number of internal voids in the PA layer increases. On the other hand, the surface hydrophilicity (ΔG_{SL}) decreases (Table 3.3).

Rejection values of ACNC2 and ACNC4-TFN membranes remained high (98 – 99%) at all loading levels, unlike that of CNC-TFN membranes. As the ACNCs were more uniformly dispersed than the CNCs, the ACNC surface hydroxyl groups were more available to form intra-hydrogen bonds with PA functional groups rather than inter-hydrogen bonds between hydroxyl groups [20]. The stronger ACNC/PA interactions due to increased hydrogen bonding were consistent with the XPS results suggesting the increased crosslinking density in the PA layer (Table 3.2) and the smaller thickness of the selective layer (Figure 3.7). The zeta potential of ACNC-TFN membranes becomes more negative as the nanoparticle loading increases, which helps maintain high salt rejection of these membranes [67]. Moreover, the acetyl groups being larger than the hydroxyl groups led to an increased steric hindrance to salt transport [40].

The ACNC2-TFN membranes were more permeable but had a lower salt rejection than the ACNC4-TFN membranes. This illustrates the typical trade-off between membrane productivity and membrane selectivity. A question arises: Which of these two membranes exhibits the better RO performance? An objective answer to this question requires comparing membrane performance to the state-of-the-art TFC PA membranes' upper-bound line. The upper-bound line relates the membrane water permeability (A) to the selectivity expressed by the ratio of the water (A) and salt (B) permeabilities (A/B) [2].

Table 3.4 presents the best membranes in each category synthesized in this work in terms of A and A/B. In addition, it includes the performance of other membranes reported in the literature, along with the performance of a commercial RO-SW30 membrane as determined in our testing system. There are hundreds, if not thousands, of RO membranes reported in the literature. The membranes reported in Table 3.4 are low-pressure RO-TFN membranes tested at similar conditions to our membranes. Moreover, these TFN membranes are divided into four groups according to the type of nanoparticles (hydrophilic nonporous, hydrophobic nonporous, hydrophilic porous, and hydrophobic porous).

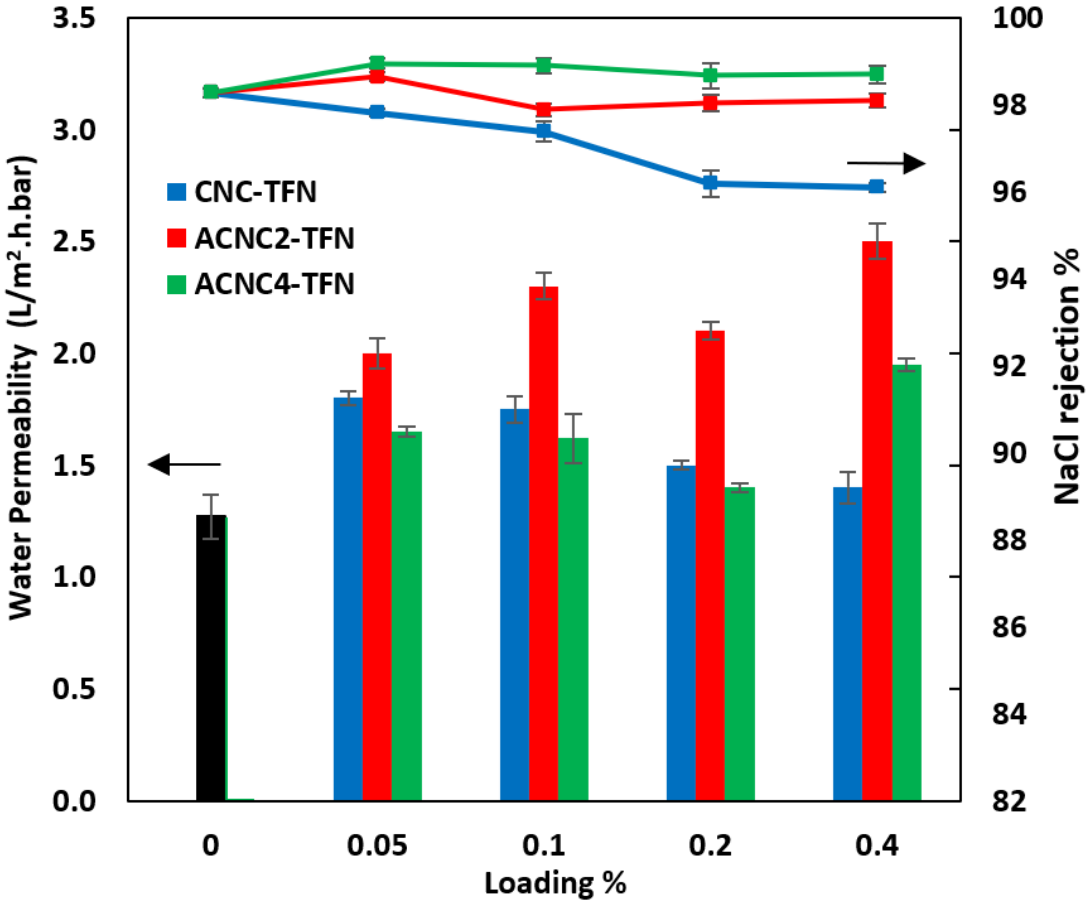

Figure 3.8: RO performance of TFC and TFN membranes a) water permeability and salt rejection) vs. CNC, ACNC2 and ACNC4 loading.

With A = 2.60 ±0.30 L/m².h.bar, the ACNC2-TFN0.4 had the highest water permeability among the membranes in Table 3.4. It is closely followed by TFN based on fluorinated silica (hydrophobic, nonporous) nanoparticles and COOH-HNT (hydrophilic, porous) nanoparticles[23,66]. Considering the selectivity (A/B), not surprisingly, the commercial SW30-RO exhibits the highest value of 4.95 bar^{-1}. The second in this rank is the ACNC4-TFN0.4 membrane with A/B = 3.78.

Figure 3.9 presents the performance data from Table 3.4 compared to the upper-bound line[2]. The ACNC2-TFN0.4 and ACNC4-TFN0.4 membranes are closest to the upper-bound line, which indicates their superiority. Furthermore, between these two membranes, ACNC2-TFN0.4 is closer to the upper bound line than ACNC4-TFN0.4. Representing membrane selectivity by A/B instead of simple R favours the membranes with higher water permeability over those with high salt rejection. This is why the commercial SW30-RO membrane is relatively far from the upper-bound line compared to ACNC2-TFN0.4 and ACNC4-TFN0.4 membranes despite its highest salt rejection among the membranes listed in Table 3.4.

Table 3.4: Comparison of permeability and water/NaCl selectivity of RO membranes.[1]

Sample	Type	Loading (wt%)	A ($L/m^2.h.bar$)	R (%)	A/B (bar^{-1})	Reference
SW30	Commercial	-	1.10	99	4.95	This work
TFC	-	-	1.27	98	2.49	
CNC[a]	Hydrophilic non-porous	0.1	1.8	97.1	1.67	
Tempo-oxidized CNF[b]		0.02	1.88	95.6	1.44	[33]
CNC[c]		0.2	2.60	95	2.60	[68]
Silica[a]		0.1	1.37	98.1	2.50	[23]
ACNC2[a]	Hydrophobic non-porous	0.4	2.60	98	2.56	This work
ACNC4[a]		0.4	1.90	98.7	3.79	
Silica[a]		0.1	1.35	97.2	1.68	[23]
Fluorinated Silica[a]		0.12	2.47	98	3.16	[66]
Copper[c]		-	1.3	95.8	1.1	[69]
COOH-HNT[a]	Hydrophilic porous	0.05	2.4	97.5	1.95	[57]
NH_2-HNT[a]		0.05	1.81	98	2.45	[57]
MCM-41[a]		0.02	2.12	98.5	3.18	[23]
MCM-41[a]	Hydrophobic porous	0.02	1.62	97.4	1.81	[23]
ZIF-8[a]		0.4	1.68	98.8	3.1	[70]

[1] All membranes were tested in low salinity conditions (NaCl salt concentration in the feed water tank: 2000-3000 ppm, operating pressure: 15-20 bar). First two rows are TFC membranes; all others are TFN membranes using the nanoparticle noted.[a] Nanoparticle dispersed in [a] organic solution, [b] aqueous solution, [c] the support layer. ZIF-8: Zeolitic imidazolate framework-8, HNT: Halloysite nanotubes, MCM: Mobil composition of matter No. 41 (Mesoporous silica).

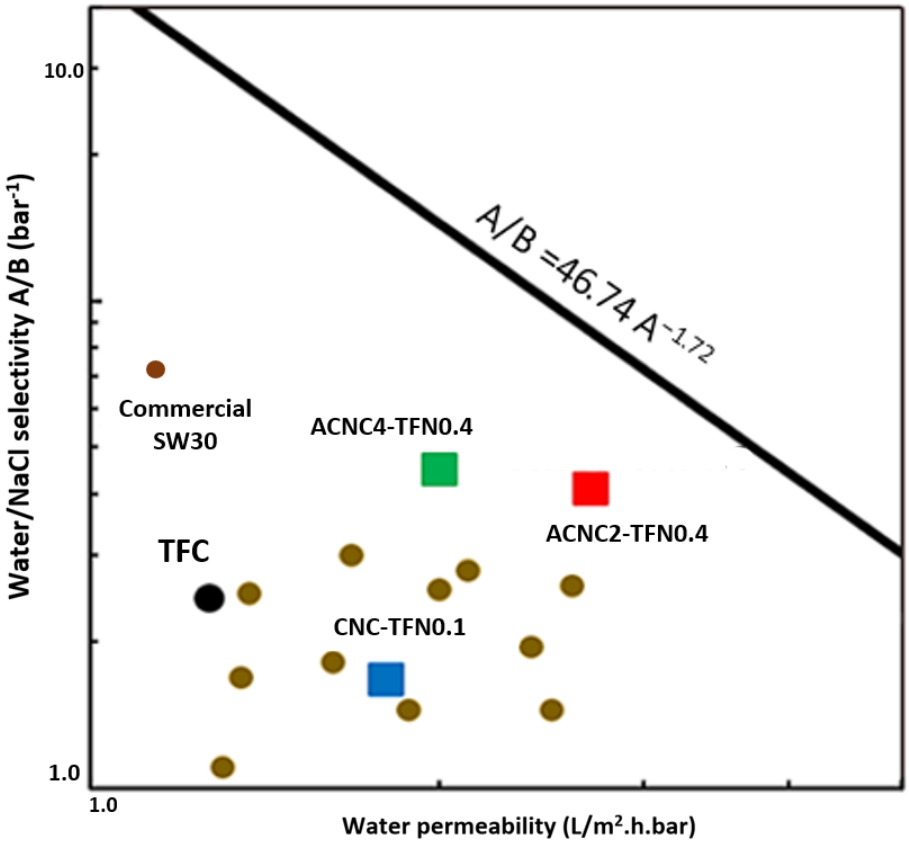

Figure 3.9: Correlation between water/NaCl selectivity vs. water permeability. Data points without labels are from Table 3.4. [2]

3.5 Conclusion

In this study, CNC nanoparticles were modified by substituting surface hydroxyl groups with acetyl groups to decrease the hydrophilicity of the modified nanoparticles, ACNCs. The unmodified and modified CNCs were dispersed in a solution of TMC monomer, which was used to form a polyamide layer by interfacial polymerization with MPD. The acetylation of CNC nanoparticles improved their dispersibility in the TMC monomer solution. The resulting ACNC-based TFN membranes were smoother yet had a higher relative surface than CNC-based TFN membranes, indicating that acetylation of CNCs helped reduce aggregation of nanoparticles in the polyamide layer of TFN membranes. In turn, acetylation of CNCs also helped increase nanoparticle loading in TFN membranes without adversely affecting the RO performance of the resulting TFN membranes. The salt rejection of ACNC-based TFN membranes remained stable (98-99%) and was greater than that of CNC-based TFN membranes at the same nanoparticle loading. The water permeability of ACNC-TFN membranes, up to 2.6 ± 0.3 L/m^2.h.bar, was also up to 40% greater than the water permeability of CNC-TFN membranes. Therefore, hydrophobic functionalization of hydrophilic

nanoparticles improved the resulting TFN membrane's RO performance, pushing them closer to the upper bound line. This work provides an example of how a straightforward nanoparticle functionalization enables one to tailor the properties of TFN membranes to better align with application needs.

3.6 Supporting information

Supporting Information for this Chapter is found in Appendix A.

3.7 References

[1] S.F. Anis, R. Hashaikeh, N. Hilal, Reverse osmosis pretreatment technologies and future trends: A comprehensive review, Desalination. 452 (2019) 159–195. https://doi.org/10.1016/j.desal.2018.11.006.

[2] Y.J. Lim, K. Goh, M. Kurihara, R. Wang, Seawater desalination by reverse osmosis: Current development and future challenges in membrane fabrication – A review, Journal of Membrane Science. 629 (2021) 119292. https://doi.org/10.1016/j.memsci.2021.119292.

[3] R.H. Hailemariam, Y.C. Woo, M.M. Damtie, B.C. Kim, K.-D. Park, J.-S. Choi, Reverse osmosis membrane fabrication and modification technologies and future trends: A review, Advances in Colloid and Interface Science. 276 (2020) 102100. https://doi.org/10.1016/j.cis.2019.102100.

[4] M. Kumar, M.A. Khan, H.A. Arafat, Recent Developments in the Rational Fabrication of Thin Film Nanocomposite Membranes for Water Purification and Desalination, ACS Omega. 5 (2020) 3792–3800. https://doi.org/10.1021/acsomega.9b03975.

[5] H. Sari Erkan, N. Bakaraki Turan, G. Onkal Engin, M.S. Bilgili, A review of advantages and challenges of using engineered nanoparticles for waste and wastewater treatments, Int. J. Environ. Sci. Technol. (2021). https://doi.org/10.1007/s13762-020-03054-8.

[6] L.E. Peng, Z. Yang, L. Long, S. Zhou, H. Guo, C.Y. Tang, A critical review on porous substrates of TFC polyamide membranes: Mechanisms, membrane performances, and future perspectives, Journal of Membrane Science. 641 (2022) 119871. https://doi.org/10.1016/j.memsci.2021.119871.

[7] W. Pronk, A. Ding, E. Morgenroth, N. Derlon, P. Desmond, M. Burkhardt, B. Wu, A.G. Fane, Gravity-driven membrane filtration for water and wastewater treatment: A review, Water Research. 149 (2019) 553–565. https://doi.org/10.1016/j.watres.2018.11.062.

[8] M. Qasim, M. Badrelzaman, N.N. Darwish, N.A. Darwish, N. Hilal, Reverse osmosis desalination: A state-of-the-art review, Desalination. 459 (2019) 59–104. https://doi.org/10.1016/j.desal.2019.02.008.

[9] A. Al Mayyahi, Important Approaches to Enhance Reverse Osmosis (RO) Thin Film Composite (TFC) Membranes Performance, Membranes. 8 (2018) 68. https://doi.org/10.3390/membranes8030068.

[10] M.Q. Seah, W.J. Lau, P.S. Goh, H.-H. Tseng, R.A. Wahab, A.F. Ismail, Progress of Interfacial Polymerization Techniques for Polyamide Thin Film (Nano)Composite Membrane Fabrication: A Comprehensive Review, Polymers. 12 (2020) 2817. https://doi.org/10.3390/polym12122817.

[11] J.M. Gohil, P. Ray, A review on semi-aromatic polyamide TFC membranes prepared by interfacial polymerization: Potential for water treatment and desalination, Separation and

Purification Technology. 181 (2017) 159–182. https://doi.org/10.1016/j.seppur.2017.03.020.
[12] Z.C. Ng, W.J. Lau, T. Matsuura, A.F. Ismail, Thin film nanocomposite RO membranes: Review on fabrication techniques and impacts of nanofiller characteristics on membrane properties, Chemical Engineering Research and Design. 165 (2021) 81–105. https://doi.org/10.1016/j.cherd.2020.10.003.
[13] M. Bassyouni, M.H. Abdel-Aziz, M.Sh. Zoromba, S.M.S. Abdel-Hamid, E. Drioli, A review of polymeric nanocomposite membranes for water purification, Journal of Industrial and Engineering Chemistry. 73 (2019) 19–46. https://doi.org/10.1016/j.jiec.2019.01.045.
[14] P.S. Goh, A.F. Ismail, T. Matsuura, Perspective and Roadmap of Energy-Efficient Desalination Integrated with Nanomaterials, Separation & Purification Reviews. 47 (2018) 124–141. https://doi.org/10.1080/15422119.2017.1335214.
[15] C. Xu, Y. Chen, Understanding water and solute transport in thin film nanocomposite membranes by resistance-in-series theory combined with Monte Carlo simulation, Journal of Membrane Science. 626 (2021) 119106. https://doi.org/10.1016/j.memsci.2021.119106.
[16] Q. Lyu, D.-Y. Kang, S. Hu, L.-C. Lin, Exploiting interior surface functionalization in reverse osmosis desalination membranes to mitigate permeability–selectivity trade-off: Molecular simulations of nanotube-based membranes, Desalination. 491 (2020) 114537. https://doi.org/10.1016/j.desal.2020.114537.
[17] M. Asadollahi, D. Bastani, S.A. Musavi, Enhancement of surface properties and performance of reverse osmosis membranes after surface modification: A review, Desalination. 420 (2017) 330–383. https://doi.org/10.1016/j.desal.2017.05.027.
[18] C.-Y. Chong, W.-J. Lau, N. Yusof, G.-S. Lai, A.F. Ismail, Roles of nanomaterial structure and surface coating on thin film nanocomposite membranes for enhanced desalination, Composites Part B: Engineering. 160 (2019) 471–479. https://doi.org/10.1016/j.compositesb.2018.12.034.
[19] W. Xie, G.M. Geise, B.D. Freeman, H.-S. Lee, G. Byun, J.E. McGrath, Polyamide interfacial composite membranes prepared from m-phenylene diamine, trimesoyl chloride and a new disulfonated diamine, Journal of Membrane Science. 403–404 (2012) 152–161. https://doi.org/10.1016/j.memsci.2012.02.038.
[20] B.-H. Jeong, E.M.V. Hoek, Y. Yan, A. Subramani, X. Huang, G. Hurwitz, A.K. Ghosh, A. Jawor, Interfacial polymerization of thin film nanocomposites: A new concept for reverse osmosis membranes, Journal of Membrane Science. 294 (2007) 1–7. https://doi.org/10.1016/j.memsci.2007.02.025.
[21] S. Zhao, G. Zhang, W. Shen, X. Wang, F. Liu, Design and fabrication of highly selective and permeable polymer membranes, Journal of Applied Physics. 128 (2020) 131102. https://doi.org/10.1063/5.0015975.
[22] R. Dai, H. Guo, C.Y. Tang, M. Chen, J. Li, Z. Wang, Hydrophilic Selective Nanochannels Created by Metal Organic Frameworks in Nanofiltration Membranes Enhance Rejection of Hydrophobic Endocrine-Disrupting Compounds, Environ. Sci. Technol. 53 (2019) 13776–13783. https://doi.org/10.1021/acs.est.9b05343.
[23] J. Yin, Z. Yang, C.Y. Tang, B. Deng, Probing the Contributions of Interior and Exterior Channels of Nanofillers toward the Enhanced Separation Performance of a Thin-Film Nanocomposite Reverse Osmosis Membrane, Environ. Sci. Technol. Lett. 7 (2020) 766–772. https://doi.org/10.1021/acs.estlett.0c00507.
[24] E.J. Foster, R.J. Moon, U.P. Agarwal, M.J. Bortner, J. Bras, S. Camarero-Espinosa, K.J. Chan, M.J.D. Clift, E.D. Cranston, S.J. Eichhorn, D.M. Fox, W.Y. Hamad, L. Heux, B. Jean, M. Korey, W. Nieh, K.J. Ong, M.S. Reid, S. Renneckar, R. Roberts, J.A. Shatkin,

J. Simonsen, K. Stinson-Bagby, N. Wanasekara, J. Youngblood, Current characterization methods for cellulose nanomaterials, Chem. Soc. Rev. 47 (2018) 2609–2679. https://doi.org/10.1039/C6CS00895J.
[25] R.E. Abouzeid, R. Khiari, N. El-Wakil, A. Dufresne, Current State and New Trends in the Use of Cellulose Nanomaterials for Wastewater Treatment, Biomacromolecules. 20 (2019) 573–597. https://doi.org/10.1021/acs.biomac.8b00839.
[26] R. Moeinzadeh, A.G. Jadval Ghadam, W.J. Lau, D. Emadzadeh, Synthesis of nanocomposite membrane incorporated with amino-functionalized nanocrystalline cellulose for refinery wastewater treatment, Carbohydrate Polymers. 225 (2019) 115212. https://doi.org/10.1016/j.carbpol.2019.115212.
[27] L. Bai, Y. Liu, N. Bossa, A. Ding, N. Ren, G. Li, H. Liang, M.R. Wiesner, Incorporation of Cellulose Nanocrystals (CNCs) into the Polyamide Layer of Thin-Film Composite (TFC) Nanofiltration Membranes for Enhanced Separation Performance and Antifouling Properties, Environ. Sci. Technol. 52 (2018) 11178–11187. https://doi.org/10.1021/acs.est.8b04102.
[28] Y. Chu, Y. Sun, W. Wu, H. Xiao, Dispersion Properties of Nanocellulose: A Review, Carbohydrate Polymers. 250 (2020) 116892. https://doi.org/10.1016/j.carbpol.2020.116892.
[29] Y. Liu, H. Liu, Z. Shen, Nanocellulose Based Filtration Membrane in Industrial Waste Water Treatment: A Review, Materials. 14 (2021) 5398. https://doi.org/10.3390/ma14185398.
[30] M. Kadhom, N. Albayati, S. Salih, M. Al-Furaiji, M. Bayati, B. Deng, Role of Cellulose Micro and Nano Crystals in Thin Film and Support Layer of Nanocomposite Membranes for Brackish Water Desalination, Membranes. 9 (2019) 101. https://doi.org/10.3390/membranes9080101.
[31] R. Cruz-Silva, K. Izu, J. Maeda, S. Saito, A. Morelos-Gomez, C. Aguilar, Y. Takizawa, A. Yamanaka, S. Tejiima, K. Fujisawa, K. Takeuchi, T. Hayashi, T. Noguchi, A. Isogai, M. Endo, Nanocomposite desalination membranes made of aromatic polyamide with cellulose nanofibers: synthesis, performance, and water diffusion study, Nanoscale. 12 (2020) 19628–19637. https://doi.org/10.1039/D0NR02915G.
[32] C.H. Park, S. Jeon, S.-H. Park, M.G. Shin, M.S. Park, S.-Y. Lee, J.-H. Lee, Cellulose nanocrystal-assembled reverse osmosis membranes with high rejection performance and excellent antifouling, J. Mater. Chem. A. 7 (2019) 3992–4001. https://doi.org/10.1039/C8TA10932J.
[33] S. Liu, Z.-X. Low, H.M. Hegab, Z. Xie, R. Ou, G. Yang, G.P. Simon, X. Zhang, L. Zhang, H. Wang, Enhancement of desalination performance of thin-film nanocomposite membrane by cellulose nanofibers, Journal of Membrane Science. 592 (2019) 117363. https://doi.org/10.1016/j.memsci.2019.117363.
[34] A.M.A. Abdelsamad, M. Matthias, A.S.G. Khalil, M. Ulbricht, Nanofillers dissolution as a crucial challenge for the performance stability of thin-film nanocomposite desalination membranes, Separation and Purification Technology. 228 (2019) 115767. https://doi.org/10.1016/j.seppur.2019.115767.
[35] H. Saleem, S.J. Zaidi, Nanoparticles in reverse osmosis membranes for desalination: A state of the art review, Desalination. 475 (2020) 114171. https://doi.org/10.1016/j.desal.2019.114171.
[36] W. Li, Z. Yang, W. Liu, Z. Huang, H. Zhang, M. Li, X. Ma, C.Y. Tang, Z. Xu, Polyamide reverse osmosis membranes containing 1D nanochannels for enhanced water purification, Journal of Membrane Science. 618 (2021) 118681. https://doi.org/10.1016/j.memsci.2020.118681.

[37] F. Asempour, D. Emadzadeh, T. Matsuura, B. Kruczek, Synthesis and characterization of novel Cellulose Nanocrystals-based Thin Film Nanocomposite membranes for reverse osmosis applications, Desalination. 439 (2018) 179–187. https://doi.org/10.1016/j.desal.2018.04.009.
[38] Y. Qin, S. Yu, Q. Zhao, G. Kang, H. Yu, Y. Jin, Y. Cao, New insights into tailoring polyamide structure for fabricating highly permeable reverse osmosis membranes, Desalination. 499 (2021) 114840. https://doi.org/10.1016/j.desal.2020.114840.
[39] X. Song, B. Gan, S. Qi, H. Guo, C.Y. Tang, Y. Zhou, C. Gao, Intrinsic Nanoscale Structure of Thin Film Composite Polyamide Membranes: Connectivity, Defects, and Structure–Property Correlation, Environ. Sci. Technol. 54 (2020) 3559–3569. https://doi.org/10.1021/acs.est.9b05892.
[40] E. Smith, K. Hendren, J. Haag, E. Foster, S. Martin, Functionalized Cellulose Nanocrystal Nanocomposite Membranes with Controlled Interfacial Transport for Improved Reverse Osmosis Performance, Nanomaterials. 9 (2019) 125. https://doi.org/10.3390/nano9010125.
[41] E. Abraham, D. Kam, Y. Nevo, R. Slattegard, A. Rivkin, S. Lapidot, O. Shoseyov, Highly Modified Cellulose Nanocrystals and Formation of Epoxy-Nanocrystalline Cellulose (CNC) Nanocomposites, ACS Appl. Mater. Interfaces. 8 (2016) 28086–28095. https://doi.org/10.1021/acsami.6b09852.
[42] H. Liu, M. Zhang, H. Zhao, Y. Jiang, G. Liu, J. Gao, Enhanced dispersibility of metal–organic frameworks (MOFs) in the organic phase *via* surface modification for TFN nanofiltration membrane preparation, RSC Adv. 10 (2020) 4045–4057. https://doi.org/10.1039/C9RA09672H.
[43] J. Tang, Functionalized Cellulose Nanocrystals (CNC) for Advanced Applications, (n.d.) 208.
[44] L. Bai, H. Wu, J. Ding, A. Ding, X. Zhang, N. Ren, G. Li, H. Liang, Cellulose nanocrystal-blended polyethersulfone membranes for enhanced removal of natural organic matter and alleviation of membrane fouling, Chemical Engineering Journal. 382 (2020) 122919. https://doi.org/10.1016/j.cej.2019.122919.
[45] A. Biswas, R.L. Shogren, J.L. Willett, Solvent-Free Process to Esterify Polysaccharides †, Biomacromolecules. 6 (2005) 1843–1845. https://doi.org/10.1021/bm0501757.
[46] D. Viet, S. Beck-Candanedo, D.G. Gray, Dispersion of cellulose nanocrystals in polar organic solvents, Cellulose. 14 (2007) 109–113. https://doi.org/10.1007/s10570-006-9093-9.
[47] J. Xu, Z. Wu, Q. Wu, Y. Kuang, Acetylated cellulose nanocrystals with high-crystallinity obtained by one-step reaction from the traditional acetylation of cellulose, Carbohydrate Polymers. 229 (2020) 115553. https://doi.org/10.1016/j.carbpol.2019.115553.
[48] A. Biswas, J.L. Berfield, B.C. Saha, H.N. Cheng, Conversion of agricultural by-products to methyl cellulose, Industrial Crops and Products. 46 (2013) 297–300. https://doi.org/10.1016/j.indcrop.2013.01.039.
[49] J.D. Moon, B.D. Freeman, C.J. Hawker, R.A. Segalman, Can Self-Assembly Address the Permeability/Selectivity Trade-Offs in Polymer Membranes?, Macromolecules. 53 (2020) 5649–5654. https://doi.org/10.1021/acs.macromol.0c01111.
[50] R. Zhang, J. Tian, S. Gao, B. Van der Bruggen, How to coordinate the trade-off between water permeability and salt rejection in nanofiltration?, J. Mater. Chem. A. 8 (2020) 8831–8847. https://doi.org/10.1039/D0TA02510K.
[51] X. Ma, Z. Yang, Z. Yao, H. Guo, Z. Xu, C.Y. Tang, Tuning roughness features of thin film composite polyamide membranes for simultaneously enhanced permeability, selectivity and anti-fouling performance, Journal of Colloid and Interface Science. 540 (2019) 382–388. https://doi.org/10.1016/j.jcis.2019.01.033.

[52] D. Carter, F.H. Tezel, B. Kruczek, H. Kalipcilar, Investigation and comparison of mixed matrix membranes composed of polyimide matrimid with ZIF – 8, silicalite, and SAPO – 34, Journal of Membrane Science. 544 (2017) 35–46. https://doi.org/10.1016/j.memsci.2017.08.068.
[53] Z. Wu, J. Xu, J. Gong, J. Li, L. Mo, Preparation, characterization and acetylation of cellulose nanocrystal allomorphs, Cellulose. 25 (2018) 4905–4918. https://doi.org/10.1007/s10570-018-1937-6.
[54] N. Olaru, L. Olaru, C. Vasile, P. Ander, Surface modified cellulose obtained by acetylation without solvents of bleached and unbleached kraft pulps, Polimery. 56 (2011) 834–840. https://doi.org/10.14314/polimery.2011.834.
[55] W. Hu, S. Chen, Q. Xu, H. Wang, Solvent-free acetylation of bacterial cellulose under moderate conditions, Carbohydrate Polymers. 83 (2011) 1575–1581. https://doi.org/10.1016/j.carbpol.2010.10.016.
[56] P.S. Goh, A.F. Ismail, Review: is interplay between nanomaterial and membrane technology the way forward for desalination?, J. Chem. Technol. Biotechnol. 90 (2015) 971–980. https://doi.org/10.1002/jctb.4531.
[57] F. Asempour, S. Akbari, D. Bai, D. Emadzadeh, T. Matsuura, B. Kruczek, Improvement of stability and performance of functionalized halloysite nano tubes-based thin film nanocomposite membranes, Journal of Membrane Science. 563 (2018) 470–480. https://doi.org/10.1016/j.memsci.2018.05.070.
[58] L. Bai, Y. Liu, A. Ding, N. Ren, G. Li, H. Liang, Surface coating of UF membranes to improve antifouling properties: A comparison study between cellulose nanocrystals (CNCs) and cellulose nanofibrils (CNFs), Chemosphere. 217 (2019) 76–84. https://doi.org/10.1016/j.chemosphere.2018.10.219.
[59] C. Xu, W. Chen, H. Gao, X. Xie, Y. Chen, Cellulose nanocrystal/silver (CNC/Ag) thin-film nanocomposite nanofiltration membranes with multifunctional properties, Environ. Sci.: Nano. 7 (2020) 803–816. https://doi.org/10.1039/C9EN01367A.
[60] L. Lin, T.M. Weigand, M.W. Farthing, P. Jutaporn, C.T. Miller, O. Coronell, Relative importance of geometrical and intrinsic water transport properties of active layers in the water permeability of polyamide thin-film composite membranes, Journal of Membrane Science. 564 (2018) 935–944. https://doi.org/10.1016/j.memsci.2018.08.002.
[61] M.M. Kłosowski, C.M. McGilvery, Y. Li, P. Abellan, Q. Ramasse, J.T. Cabral, A.G. Livingston, A.E. Porter, Micro-to nano-scale characterisation of polyamide structures of the SW30HR RO membrane using advanced electron microscopy and stain tracers, Journal of Membrane Science. 520 (2016) 465–476. https://doi.org/10.1016/j.memsci.2016.07.063.
[62] H. Yan, X. Miao, J. Xu, G. Pan, Y. Zhang, Y. Shi, M. Guo, Y. Liu, The porous structure of the fully-aromatic polyamide film in reverse osmosis membranes, Journal of Membrane Science. 475 (2015) 504–510. https://doi.org/10.1016/j.memsci.2014.10.052.
[63] L. Lin, R. Lopez, G.Z. Ramon, O. Coronell, Investigating the void structure of the polyamide active layers of thin-film composite membranes, Journal of Membrane Science. 497 (2016) 365–376. https://doi.org/10.1016/j.memsci.2015.09.020.
[64] J. Xu, H. Yan, Y. Zhang, G. Pan, Y. Liu, The morphology of fully-aromatic polyamide separation layer and its relationship with separation performance of TFC membranes, Journal of Membrane Science. 541 (2017) 174–188. https://doi.org/10.1016/j.memsci.2017.06.057.
[65] H. Luo, K. Chang, K. Bahati, G.M. Geise, Engineering Selective Desalination Membranes via Molecular Control of Polymer Functional Groups, Environ. Sci. Technol. Lett. 6 (2019) 462–466. https://doi.org/10.1021/acs.estlett.9b00351.

[66] R. Pang, K. Zhang, Fabrication of hydrophobic fluorinated silica-polyamide thin film nanocomposite reverse osmosis membranes with dramatically improved salt rejection, Journal of Colloid and Interface Science. 510 (2018) 127–132. https://doi.org/10.1016/j.jcis.2017.09.062.
[67] B.-M. Jun, J. Cho, A. Jang, K. Chon, P. Westerhoff, Y. Yoon, H. Rho, Charge characteristics (surface charge vs. zeta potential) of membrane surfaces to assess the salt rejection behavior of nanofiltration membranes, Separation and Purification Technology. 247 (2020) 117026. https://doi.org/10.1016/j.seppur.2020.117026.
[68] M. Kadhom, B. Deng, Synthesis of high-performance thin film composite (TFC) membranes by controlling the preparation conditions: Technical notes, Journal of Water Process Engineering. 30 (2019) 100542. https://doi.org/10.1016/j.jwpe.2017.12.011.
[69] Z. Yang, X. Huang, X. Ma, Z. Zhou, H. Guo, Z. Yao, S.-P. Feng, C.Y. Tang, Fabrication of a novel and green thin-film composite membrane containing nanovoids for water purification, Journal of Membrane Science. 570–571 (2019) 314–321. https://doi.org/10.1016/j.memsci.2018.10.057.
[70] I.H. Aljundi, Desalination characteristics of TFN-RO membrane incorporated with ZIF-8 nanoparticles, Desalination. 420 (2017) 12–20. https://doi.org/10.1016/j.desal.2017.06.020.

4. Improving nanofiltration performance using modified cellulose nanocrystal based thin film nanocomposite (TFN) membranes

Fatemeh Abedi, Marc A. Dubé, Daryoush Emadzadeh, Boguslaw Kruczek

This chapter is a manuscript published in Journal of membrane science, 2023.
https://doi.org/10.1016/j.memsci.2023.121369

4.1 Abstract

Heavy metal ions are one of the principal contaminants in industrial wastewater. Their rejection of nanofiltration processes using thin-film nanocomposite (TFN) membranes is a promising treatment method. L-cysteine functionalized cellulose nanocrystals (CysCNCs) and acetylated CNCs (ACNCs) were synthesized via an iodine-catalyzed method. The successful modification of CNCs was confirmed using ATR-FTIR and ^{13}C-NMR spectroscopy. The modified CNCs were used in the synthesis of TFN membranes. Prior to interfacial polymerization, the CNCs were dispersed into the organic monomer solution (trimesoyl chloride in n-hexane) rather than in the aqueous monomer solution (piperazine), contrary to conventional practice.

Membrane performance was assessed for thin film composite (TFC) and CNC, ACNC and CysCNC-TFN membranes. A simultaneous increase in water permeability/salt and heavy metal rejection of ACNC-TFNs and CysCNC-TFNs was observed. In heavy metal rejection tests, the CysCNC-TFN0.2 membranes exhibited the highest water permeability (16 L/m^2.h.bar) compared to the ACNC-TFN0.1 membranes (14.5 L/m^2.h.bar), the CNC-TFN0.1 membranes (11.5 L/m^2.h.bar), and the TFC membranes (6 L/m^2.h.bar). The heavy metal rejections ranged from 89.2 to 98.4% for the copper ions and 87.0 to 95.2% for the lead ions, in the same order as for the water permeability results. Therefore, the water permeability/selectivity trade-off was overcome. The TFN membrane performance improvements were mainly attributed to both the nanoparticle functionality and their uniform distribution in the polyamide layer via their dispersion in the organic monomer solution. Simultaneous increase observed in water permeability/salt and heavy metal rejection of ACNC-TFNs and CysCNC-TFNs.

4.2 Introduction

Water contamination continues to be a worldwide concern, leading to higher demand for water treatment technologies [1]. Heavy metals are a primary source of severe water contamination in industrial settings. More specifically, nickel (Ni^{2+}), lead (Pb^{2+}), zinc (Zn^{2+}) and copper (Cu^{2+}) are among the most hazardous heavy metal ions in wastewaters and are highly toxic even at low concentrations [2]. Numerous approaches such as adsorption, ion exchange, electrodialysis, and membrane separation have been applied to remove heavy metal ions from wastewater [3]. Membrane technologies, specifically nanofiltration (NF), are preferred in removing heavy metal ions from contaminated water resources because of their low energy consumption and high rejection of multivalent ions [4].

Typically, NF membranes have a thin film composite (TFC) structure composed of a thin polyamide (PA) layer reinforced by a highly permeable polymeric support (e.g., polysulfone) [5]. For NF membranes, the PA layer is synthesized by interfacial polymerization of an aqueous monomer solution (e.g., piperazine (PIP) in water) and an organic monomer solution (e.g., trimesoyl chloride (TMC) in n-hexane) [6]. Although TFC membranes have undergone significant development, there are still challenges to optimal performance, including permeability/selectivity trade-offs, fouling and chlorine resistance [7]. Using additives such as nanomaterials in membrane fabrication, leading to thin film nanocomposite (TFN) membranes, offers the possibility of further performance improvement and overcoming the challenges noted above [8]. The unique structure and surface characteristics of nanomaterials (e.g., high surface area and often, abundant functional groups) also enable their use as adsorbents for heavy metal rejection [9]. The most widely used nanoparticles for heavy metal rejection using NF-TFN membranes include graphene oxide, zeolites, and metal-organic frameworks [10]. However, these nanoparticles are expensive, can easily aggregate (thus limiting their dispersibility), and are susceptible to leaching from the membrane [11].

Cellulose nanocrystals (CNCs) are considered excellent candidates for TFC membrane performance improvement due to their hydrophilic, biodegradable, and non-toxic characteristics [12]. The addition of CNCs into the aqueous monomer solution often limits the positive impact of CNCs in improving TFN membrane performance. For example, Xia et al. [13] prepared CNC-TFN membranes by dispersing hydrophilic phosphorylated CNCs into the aqueous monomer solution. Their NF membranes exhibited enhanced water permeability and Na_2SO_4 rejection by incorporating a relatively small amount of phosphorylated CNCs (0.05 wt%). Further increases in CNC loading led to a deterioration in membrane performance due to CNC aggregation. Although hydrophilic CNCs are more compatible with the aqueous

monomer solution, the initially well-dispersed CNCs may start to aggregate before the interfacial polymerization begins.

Rubber rolling is crucial in removing amine-containing water droplets from the substrate before adding the organic monomer solution to prevent undesired micro- or macro-voids in the selective layer [14]. This step could lead to the unintentional loss of many nanoparticles (i.e., CNCs) during the rejection of the excess aqueous monomer solution. In addition, the remaining unknown nanoparticle loading would reside in the region between the PA layer and the substrate or deep inside the PA layer, rather than being exposed to the feed solution [15]. Our recent work has demonstrated the modification of CNCs via acetylation (ACNCs) to make them less hydrophilic, thereby enabling their dispersion in the organic monomer solution [16]. The improved ACNC dispersibility resulted in overcoming the water permeability-selectivity trade-off even at high loadings of ACNCs (up to 0.4 wt%) in brackish water reverse osmosis desalination. Guzman et al. [17] also confirmed that by dispersing the hydrophilic nanosilica into the organic monomer solution, the water permeability and salt rejection of NF-TFN membranes were higher than dispersing the nanosilica into the aqueous PIP monomer solution at the same loading. They determined that this was because of a more uniform PA layer structure and avoiding the loss of nanosilica during the rubber rolling step.

In this paper, we have used ACNCs to enhance NF-TFN membrane performance and compared their potential with a separate CNC modification using L-cysteine (CysCNCs). CysCNCs could also improve CNC dispersibility in the TMC/n-hexane monomer solution as L-cysteine contains multiple amine (NH_2) groups providing covalent bonding with the acyl chloride groups of the TMC monomer [18]. For this reason, despite increasing the hydrophilicity of the CNCs through L-cysteine modification, covalent bonding should ensure good dispersion in the hydrophobic TMC monomer solution. Some evidence for this was provided by Park et al. [19], who used L-cysteine as an immobilizing agent to coat Ag-SiO_2 on top of the PA layer of TFC-reverse osmosis membranes. The Ag-SiO_2 particles were tightly immobilized, showing long-lasting desalination performance. In addition, CysCNCs have been demonstrated to be effective for heavy metal ion rejection in a batch adsorption system where they exhibited high adsorption capacities for Cu^{2+} and Pb^{2+} due to their large surface area and thiol surface functional groups [20]. An L-cysteine coating on top of the PA layer of TFC-NF membranes was used by Zhang et al. [21]. The resulting L-cysteine coated NF membranes showed a 40% increase in water permeability, a 98% rejection for Na_2SO_4 and a 97% rejection for both Cu^{2+} and Pb^{2+} metal ions. To the best of our knowledge, the use of CNCs in NF-TFN membranes for heavy metal rejection is limited to the work by Hoang et al. [22]. Further

increases in CNC loading (>0.12 wt%.) led to a deterioration in membrane performance ($CuSO_4$ rejection and water permeability) due to aggregation of the CNCs.

The above results highlight the tremendous potential of L-cysteine modified CNCs for use in NF-TFN membranes for water treatment: 1- increasing CNC hydrophilicity should improve water permeability, 2- the thiol (SH) groups of L-cysteine should enhance heavy metal ion capture, and 3- the amine (NH_2) groups of L-cysteine should covalently bond with acyl chloride groups of the TMC monomer and make them less prone to leaching. Thus, we hypothesized that CNC modification with L-cysteine could improve its dispersibility in the PA layer and increase the loading of CNCs into the PA layer. To verify our hypothesis, as noted above, we compared two different CNC modifications that should lead to increased PA/CNC interaction, albeit by different mechanisms. CysCNCs and ACNCs were prepared by functionalizing CNCs with L-cysteine and acetyl groups, respectively, using a straightforward methodology. To our knowledge, ACNCs and CysCNCs (by dispersion into the organic monomer solution) have not been used in NF-TFN membrane applications for desalination and heavy metal ion rejection.

4.3 Experimental section

4.3.1 Materials

Poly(sulfone) ultrafiltration membranes (PS35) with a molecular weight cutoff of 20 kDa were donated by Solecta, California, USA. The monomers, piperazine (PIP, 99% purity), trimesoyl chloride (TMC, >98% purity), and the organic solvent, n-hexane (>99% purity), were purchased from Sigma-Aldrich. The spray-dried powder form of the sulfate sodium salt of CNCs was donated by CelluForce Inc. (Windsor, Quebec). CNC dimensions were 183±88 nm long by 6±2 nm in cross-section, measured by AFM; sulfate half ester content was 249 mmol/kg CNC. Poly(ethylene glycol) (PEG) with different molecular weights (200, 400, 600, and 800 Da), magnesium chloride ($MgCl_2$), sodium sulfate (Na_2SO_4), sodium chloride (NaCl), copper (II) sulfate pentahydrate ($CuSO_4.5H_2O$), and lead (II) nitrate ($Pb(NO_3)_2$) were all laboratory grades and purchased from Sigma-Aldrich. L-cysteine, ethanol, HCl, KCl, NaOH, acetic anhydride and iodine were procured from Fisher Scientific. Distilled deionized water (DDW) was used to make the aqueous PIP solution, and distilled water (DW) was used to wash the membranes and prepare the synthetic water feed solution. All materials were used as received without further purification/modification with the exception of the CNCs.

4.3.2 CNC modification

A solvent-free method was used to functionalize the CNCs with acetyl groups (ACNC) and L-cysteine (CysCNC) (Figure 4.1) [16]. A mixture of CNCs, either acetic anhydride or L-cysteine, and iodine as catalyst was placed in a glass vial equipped with a magnetic stirrer and heated at 100°C for 10 min (Table 4.1). The reaction mixture was cooled to room temperature and treated with acetone (0.9 mL) while stirring. The mixture was washed with 80 mL of a 75% ethanol/DDW v/v solution. Three washing/centrifugation steps were performed using deionized water until a neutral suspension of ACNCs (or CysCNCs) was obtained. Finally, the ACNCs (or CysCNCs) were re-suspended in DDW and freeze-dried at -60°C to produce a fine ACNC (or CysCNC) powder.

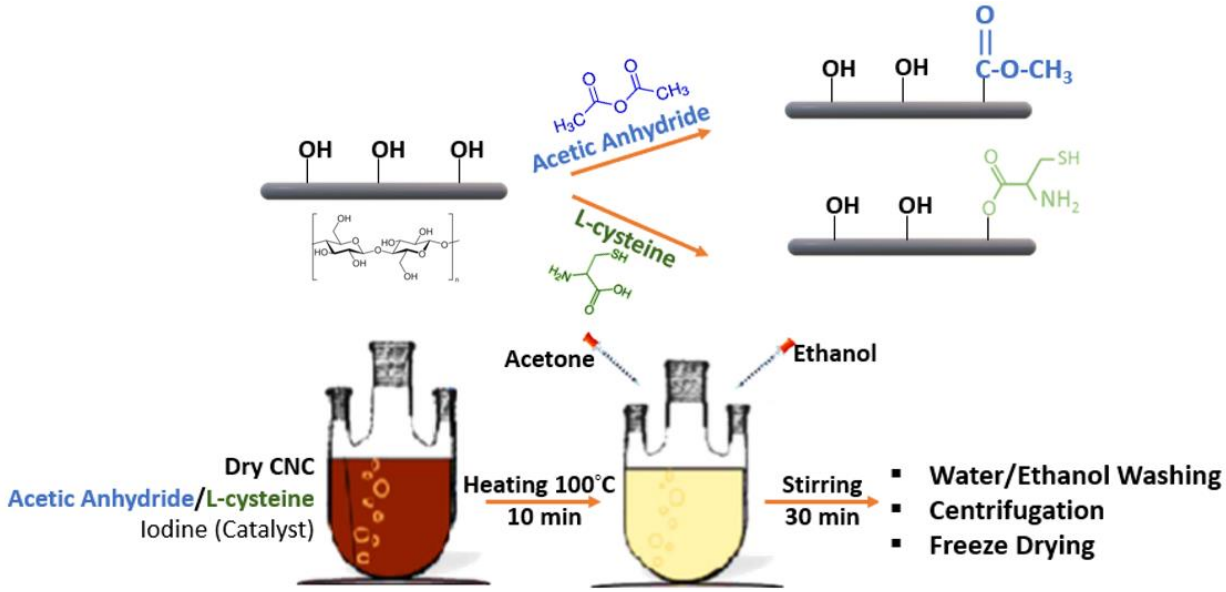

Figure 4.1: Schematic of CNC modification with acetyl group or L-cysteine. (CNCs include sulfate half-ester groups, not shown).

Table 4.1: Modified CNC formulation.

	CNC (g)	L-cysteine (g)	Acetic anhydride (g)	Iodine (g)
ACNC	0.57	-	0.95	0.04
CysCNC	0.57	0.48	-	0.1

4.3.3 Synthesis of TFC and TFN membranes

A PS35 membrane was used as the substrate to synthesize the PA layer by in-situ interfacial polymerization. 0.05% (w/v) TMC and 2% (w/v) PIP solutions were prepared in n-hexane and deionized water, respectively. After 1-2 h of magnetic stirring, specified amounts of unmodified CNC, ACNC or CysCNC dried powder (each at 0.05, 0.1, or 0.2 wt%) were

added to the TMC/n-hexane solution and stirred until CNC aggregates were no longer visible (typically, 30-40 min). The mixture was sonicated in an ice bath using a Fisher Scientific 550 sonicator (at 75% amplitude) three times at 5-minute intervals, with 5-minute rest periods. The process began by pouring 50 mL of PIP solution onto the substrate and waiting 5 minutes to ensure the PIP solution penetrated the substrate pores. Then, the excess PIP solution was drained from the substrate with a Teflon roller. This was followed by pouring 50 mL of the TMC solution (with or without dispersed nanoparticles) onto the membrane. After one minute, the excess TMC solution was decanted, and the membrane was rinsed with ~20-50 mL n-hexane. Afterwards, the membrane was placed in an oven at 95°C for 10 minutes to dry the excess solvent and facilitate crosslinking of the PA structure. Finally, the membrane was carefully washed and stored in DDW at ambient temperature until it was tested.

4.3.4 Characterization of the nanoparticles and membranes

To investigate the dispersibility of the unmodified and modified CNCs in water and n-hexane, their apparent hydrodynamic particle sizes (Z-average particle size) were characterized via dynamic light scattering (DLS) after probe sonication for three 5-minute intervals at 75% amplitude. A Nicolet 6700 FTIR spectrometer (Thermo Scientific) with a diamond crystal was utilized to obtain the ATR-FTIR spectra of the TFN membranes and that of the nanoparticles, i.e., CNC, ACNC and CysCNC. All scans were recorded at 4 cm^{-1} over wave numbers between 650 and 4000 cm^{-1}. Solid-state ^{13}C-NMR spectra of CNC, ACNC and CysCNC were obtained using a Bruker AVANCE III 400 NMR spectrometer with a single crystal solid-state probe. The surface zeta potential measurement of the unmodified and modified CNCs was conducted using a zeta analyzer (Zetasizer PSS0012-22, Malvern Instruments) with a frontal electrophoretic light scattering method. The Zetasizer was equipped with an adjustable gap cell to measure membrane surface charge. 1 mM of KCl solution was used as the background electrolyte, with its pH adjusted using 0.1 M HCl or 0.1 M NaOH. The sessile water contact angle of the CNC, ACNC and CysCNC dry powder (pressed into discs) and membrane surfaces were measured using a VCA Optima surface analysis system (AST Products, Inc., Billerica, MA). At least 20 droplets (2 μL) of deionized water in at least seven different locations on each sample were tested at ambient temperature. Membrane morphology was characterized at the top surface using field emission scanning electron microscopy (FESEM) (Tescan Vega-II XMU) and atomic force microscopy (AFM, Park NX10). The AFM images were obtained in tapping mode, scanning over 10×10 μm^2 of the membrane surface with a 512×512-pixel width resolution and an adaptive scan rate of 0.2–2 Hz. For each membrane, two samples for AFM

analysis were used. In addition, the average size of the unmodified and modified freeze-dried CNC powders was also measured using AFM. To investigate the chemical properties and probable interactions between the nanoparticles and the PA, X-Ray Photoelectron Spectroscopy (XPS) analyses were also conducted. Elemental surveys were carried out over a 1×1 mm^2 area of the membranes using an XPS (Kratos Analytical model Axis Ultra DLD) spectrometer with monochromated aluminum-K_α x-rays at 150 W. The molecular weight cutoff (MWCO) of the TFC and TFN membranes was measured by fitting the rejections of PEG with different molecular weights (200, 400, 600, and 800 Da). The concentration of PEG was measured by UV-Vis spectroscopy (ThermoScientific, USA). The molecular weight with a rejection of 90% was considered as MWCO. The Stokes radius, a (nm) of PEG molecules was calculated from their molecular weight, M_w (Da) (Equation 4.1). Then, the membranes' pore size distribution (PSD) was evaluated (Equation 4.2) [23] .

$$a = 16.73 \times 10^{-3} {M_w}^{0.557} \qquad (4.1)$$

$$\frac{df\ (r_p)}{dr_p} = \frac{1}{r_p ln\sigma_p \sqrt{2\pi}} \exp\left[-\frac{(lnr_p - ln\mu_p)^2}{2(ln\sigma_p)^2}\right] \qquad (4.2)$$

where r_p (nm) is the membrane pore size, μ_p (nm) is the mean effective pore size corresponding to the geometric mean diameter at a rejection of 50%. σ_p is the geometric standard deviation of the membrane, which is equal to the ratio of the Stokes radius at 84.13% to 50% rejection.

The surface topography of the membranes was characterized in terms of the root-mean-square of the height deviations (R_q), the average plane roughness (R_a), the maximum roughness (R_{max}), and the ratio of the actual surface area for a rough surface to the planar area (r). Accordingly, r = 1 indicates a perfectly smooth surface. For each membrane, two samples for AFM analysis were used. Because the apparent contact angle is altered by the surface roughness, the solid-liquid interfacial free energy (ΔG_{SL}) was evaluated to characterize the intrinsic surface hydrophilicity of the membrane. The ΔG_{SL} (mJ/m^2) value was calculated from the Young–Dupre method (Equation 4.3) [16]:

$$\Delta G_{SL} = \gamma_L \left(1 + \frac{cos\,\theta}{r}\right) \qquad (4.3)$$

where θ is the average water contact angle and γ_L is the water surface tension (72.8 mJ/m^2 at 25°C), r is the roughness area ratio (i.e., the ratio of actual surface area for a rough surface to the planar area) obtained from AFM topographical images. Accordingly, the minimum value of r for the ideally smooth surface is unity, which maximizes ΔG_{SL} for a given hydrophilicity.

As the hydrophilicity of the surface increases, θ decreases (i.e., $\cos\theta$ increases), and the value of ΔG_{SL} increases.

4.3.5 Membrane performance

All membrane performance test results are expressed as averaged values from a minimum of four membrane coupons cut from two different synthesized membrane sheets. The NF performance of the membranes was evaluated using a continuous crossflow system consisting of three membrane cells arranged in parallel, each with an effective surface area for permeation (A_p) of 17.35 cm^2. Synthetic brackish water (2000 ppm aqueous salt (NaCl, Na_2SO_4, $MgCl_2$ solutions and 200 ppm aqueous $CuSO_4$ and $Pb(NO_3)_2$) was used as the feed. The flow rate was maintained at 2.4±0.2 L/min to minimize the concentration polarization effect and achieve near-zero recovery [24]. The measurements were conducted at 295±1 K and a hydraulic pressure of 10±1 bar. Water flux, J_w ($L/m^2.h$), was calculated by Equation (4.4) based on the volume of permeate (V_p) collected during a time, t, at steady state. Salt rejection, R, was evaluated by Equation (4.5), in which C_p and C_f were the feed and permeate concentrations, respectively, measured by conductimetry. The concentration of heavy metals was determined using inductively coupled plasma emission mass spectrometry (ICP-MS), and the rejection was calculated using Equation 4.5.

$$J_w = \frac{V_p}{A_p t} \qquad (4.4)$$

$$R = \left(1 - \frac{C_p}{C_f}\right) \times 100\% \qquad (4.5)$$

The membrane water permeability, A ($L/m^2.h.bar$), was calculated using Equation (4.6):

$$A = \frac{J_w}{\Delta P - \Delta\pi} \qquad (4.6)$$

where ΔP is the applied hydraulic pressure (bar), and $\Delta\pi$ is the difference of osmotic pressures (bar) between feed and permeate calculated by the van't Hoff equation:

$$\Delta\pi = \Delta CiRT \qquad (4.7)$$

in which ΔC is the molar concentration gradient ($\Delta C \approx C_f$), I is the number of ions into which the salt dissociates, R is the ideal gas constant (J/mol.K), and T is the absolute temperature, which was maintained at 295±1K during the experiments.

4.4 Results and discussion

4.4.1 CNC modification

The AFM images of CNC, ACNC and CysCNC nanoparticles show their rod-like shape (Figure 4.2). For ACNCs, the average length and diameter were 170±20 and 7±1 nm; for CysCNCs, the average length and diameter were 173±16 and 8±2 nm, respectively, as measured by ImageJ software. In comparison, the unmodified CNCs were measured to have an average length and diameter of 183±88 and 6±2 nm, respectively. Finally, these results confirm that the chemical modification of the CNCs did not significantly affect their morphology.

Figure 4.3 shows the ATR-FTIR spectra of the CNC, ACNC, and CysCNC dried powders. Compared to CNC, the decreasing O-H stretching vibration at 3300 cm^{-1} for ACNC and CysCNC confirms the substitution of hydroxyl groups [25]. The ACNC spectra present evidence of acetylation with three significant ester bond peaks at 1730, 1370 and 1250 cm^{-1}, which relate to carbonyl (C=O), methyl (C-H), and acetyl (C-O) stretching vibrations, respectively. The CysCNC spectra show evidence of L-cysteine functionalization of CNC with two significant peaks at 1540 and 2110 cm^{-1}, which relate to amine (N-H) and thiol (S-H) stretching vibrations, respectively [26,27].

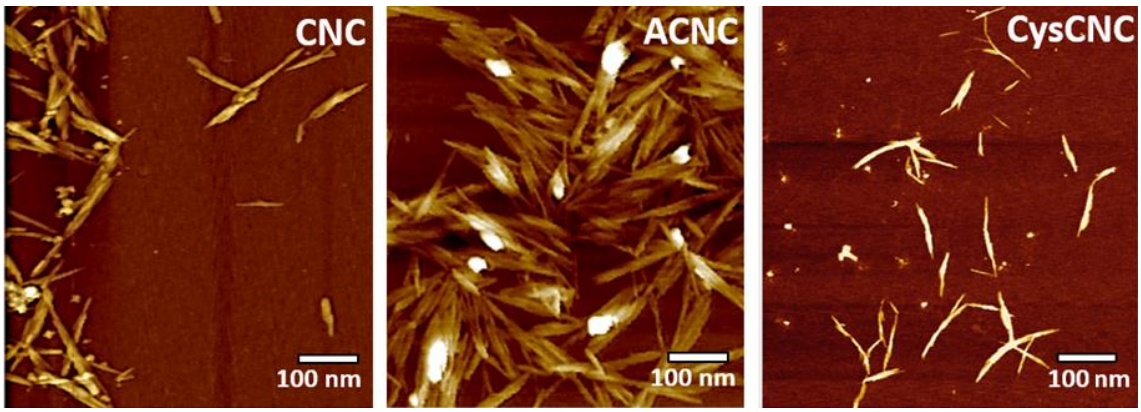

Figure 4.2: AFM images of freeze-dried CNCs, ACNCs and CysCNCs.

CNC modification was further confirmed via solid-state ^{13}C-NMR spectroscopy (Figure 4.4). The chemical shifts for the unmodified CNCs were assigned to C1 (105 ppm), C2, C3 and C5 (72 and 75 ppm), C4 (89 ppm), and C6 (65 ppm) [28]. The basic cellulose structure was preserved after acetylation and L-cysteine functionalization. Additional peaks at 174 and 21 ppm related to the carbonyl (C=O) and methyl (C-H) groups of the acetyl ester are noted on the ACNC spectra [29,30]. L-cysteine functionalized CNC spectra present additional

peaks at 174, 55 and 28 ppm, related to the carbonyl (C=O), amide (C-N) and thiol (C-S) groups of the L-cysteine on the CysCNC spectra [31].

The hydrophilicity of the CNCs and modified CNCs was evaluated by water surface contact angle measurements (Figure 4.5). The average water contact angles of the CNC, ACNC and CysCNC films were 30°, 58.5°, and 24.6°, respectively, indicating the expected decrease in hydrophilicity for ACNC and increase in hydrophilicity for CysCNC compared to that of CNC (Table 4.2). For ACNC, the decreased hydrophilicity was due to the neutral methyl groups (CH_3) of the acetyl groups, while the increased hydrophilicity of the CysCNCs was due to the presence of hydrophilic NH_2 and SH functional groups on the CysCNCs' surface [32].

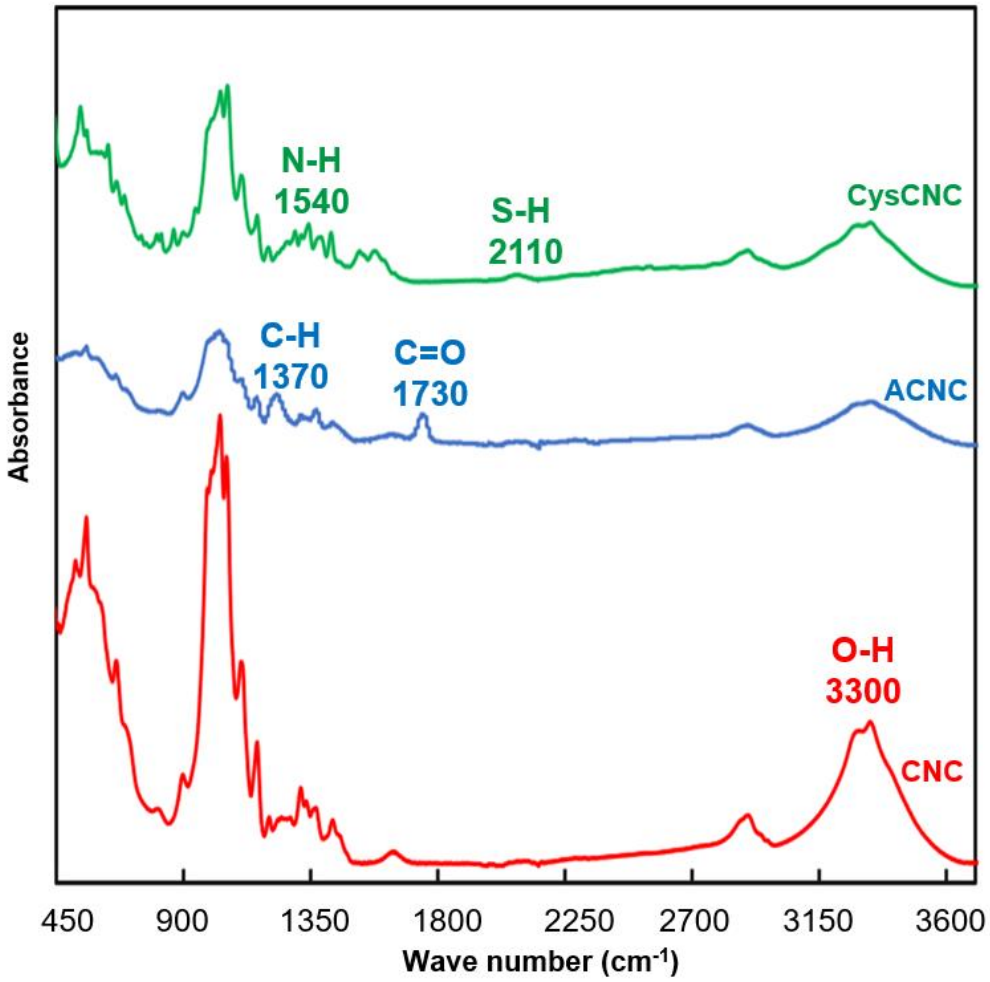

Figure 4.3: ATR-FTIR spectra of CNC, ACNC and CysCNC.

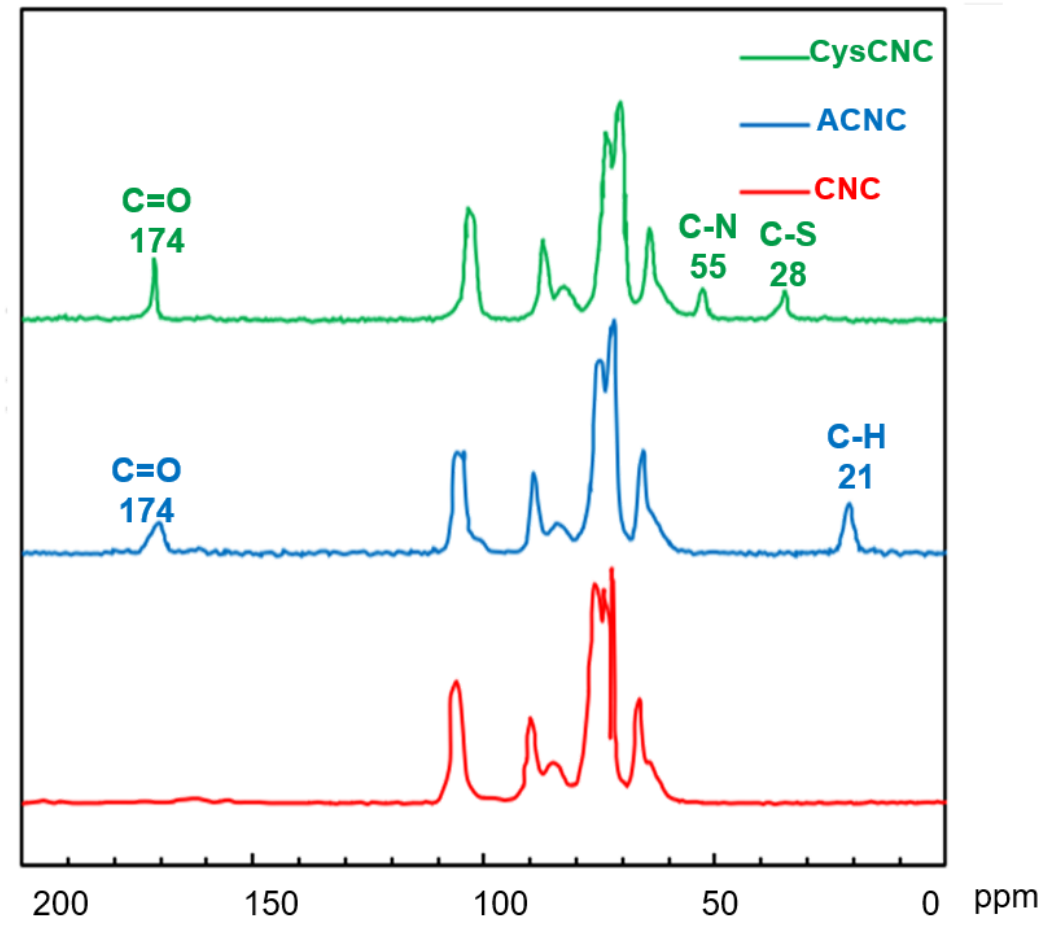

Figure 4.4: ^{13}C-NMR spectra of CNC, ACNC and CysCNC.

Figure 4.5: Water contact angle measurements of CNC, ACNC and CysCNC surfaces.

The surface of unmodified and modified CNCs was also characterized by zeta potential. The unmodified CNC surface was negatively charged due to the relative abundance of hydroxyl groups, (Table 4.2) [33]. The absolute value of the zeta potential (ζ) of the unmodified CNC (-50.2 mV) increased via acetylation and L-cysteine modification to (−39.4) mV for ACNC and (-23.5 mV) for CysCNC, respectively. Interestingly, although CysCNCs have the lowest negative surface charge among the studied nanoparticles, they are the most hydrophilic ones. The acetylation decreased the negative surface charge density because of the presence of neutral methyl groups on the ACNC surface [33], while for the CysCNCs, it was attributed to

the addition of positively charged SH and NH_2 groups of L-cysteine[20]. The apparent particle size of ACNC and CysCNC in n-hexane was 104.3 and 139.8 nm, respectively (Table 4.2), which was significantly smaller than the corresponding particle size of unmodified CNC (180.3 nm). It is important to note that despite being more hydrophilic than CNC, the particle size of CysCNCs in n-hexane is significantly smaller than that of CNC. The lower negative charge density with the addition of steric hindrance (due to the larger L-cysteine functional groups) facilitated the dispersion of hydrophilic CysCNCs into the hydrophobic n-hexane solvent. These two CNC modifications reduced the probability of inter-hydrogen bonding between the OH groups of the CNCs, thus minimizing CNC aggregation in n-hexane solvent. In summary, the acetylation and L-cysteine modification of CNCs resulted in CNCs that were more dispersible in nonpolar solutions without significantly compromising their dispersibility in water.

Table 4.2: CNC, ACNC and CysCNC characterization.

Sample	θ (°)	ζ (mV)	*d* (nm) in n-hexane	*d* (nm) in water
CNC	30.0±2.3	-50.2±2.1	180.3±3.1	70.3±3.1
ACNC	58.5±3.1	-39.4±1.3	104.3±2.4	82.3±1.1
CysCNC	24.6±1.8	-23.5±1.2	139.8±2.3	72.4±1.6

4.4.2 Membrane Surface Characterization

ATR-FTIR analysis was conducted to characterize the surface functional groups of the TFC and TFN membranes (Figure 4.6), suggesting successful interfacial polymerization between the PIP and TMC monomers. The absorption peaks at 1150–1350 cm^{-1}, which existed in the spectra of all the membranes, were attributed to the sulfone groups of the PS support [34]. The characteristic peaks at 1590, 1490, and 1244 cm^{-1} were attributed to the stretching vibrations of the benzene ring, the C-C bond, and the aromatic ether bond, respectively [35]. The peaks appearing at 1670 cm^{-1} were ascribed to C=O stretching vibrations confirming the formation of amide -NHCOO- groups of the PA layer. The peaks at 1445 cm^{-1} were related to the -OH stretching vibrations of the carboxylic groups, which likely were generated by the hydrolysis of the unreacted acyl chlorides of the TMC monomer [36].

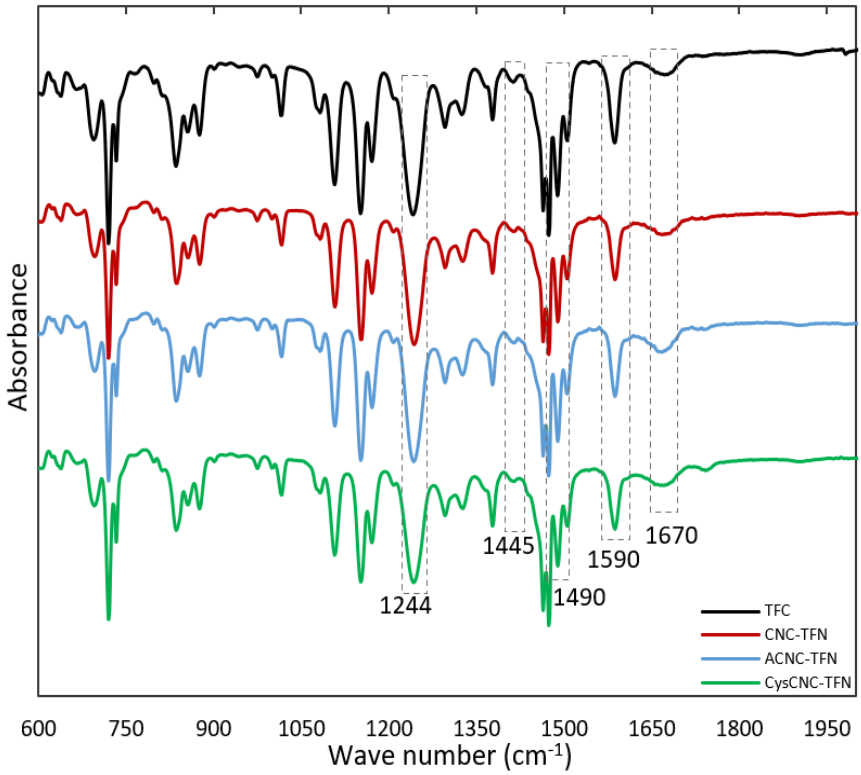

Figure 4.6: ATR-FTIR spectra of TFC and TFN membranes in 0.1 wt% CNCs, ACNCs.

and CysCNCs**.** To further confirm the formation of the PA layer, XPS analyses for TFC and TFN membranes with a loading of 0.1 wt% nanoparticles (CNC-TFN0.1, ACNC-TFN0.1 and CysCNC0.1) were performed (Figure 4.7). The measurement depth of XPS is only a few nanometers, which can reveal the chemical structures of the PA layer regardless of interference from the PS support [37]. The Core level spectra analysis was performed for all membranes and due to comparable results, we showed C1s spectra for CNC-TFN0.1, O1s for ACNC-TFN0.1 and N1s for CysCNC-TFN0.1 membranes.

The peaks at 530.8 eV, 400.2 and 284.8 eV were attributed to the O1s, N1s and C1s binding energies, respectively [38]. The high-resolution C1s, O1s and N1s core-level spectra were deconvoluted; results were similar for all membranes. For CNC-TFN0.1 (deconvoluted C1s core level spectrum), the binding energy peaks at 285.4 eV, 286.9 eV, 288.65 eV and 290.3 were assigned to C-C, C-N, O=C-N and O=C-O, respectively, corresponding to the formation of the -NHCOO- species. The deconvoluted N1s core-level spectrum for ACNC-TFN0.1 showed two peaks at 400.5 and 400.7 eV, which corresponded to the C-N and O=C−N bonds of the amide groups, respectively. The oxygen species at 532.1 and 534.1 eV were assigned to O=C−N and O=C-O, respectively, of the -NHCO- groups in the deconvoluted O1s spectrum

of CysCNC-TFN0.1. In addition, the peak at 533.4 eV was ascribed to the −OH groups of the CNCs, which confirms the presence of CNCs in the PA layer [34].

The C, N, O and carboxylic acid group contents of the TFC and TFN membranes were calculated from the XPS spectra (Table 4.3). The O/N ratios of ACNC-TFN0.1 and CysCNC-TFN0.1 were lower than that of CNC-TFN0.1, suggesting higher degrees of crosslinking for ACNC-TFN0.1 and CysCNC-TFN0.1 [39]. For ACNC-TFN0.1, the hydroxyl groups of ACNCs were more available to form intra-hydrogen bonds with acyl chloride groups rather than inter-hydrogen bonds between hydroxyl groups; this leads to better dispersion of ACNCs in the TMC/n-hexane monomer solution. The dispersion of CysCNCs differs somewhat from ACNCs because the additional NH_2 groups of L-cysteine could also create covalent bonds with the acyl chloride groups of the TMC monomer, thereby improving their dispersion in the TMC/n-hexane monomer solution.

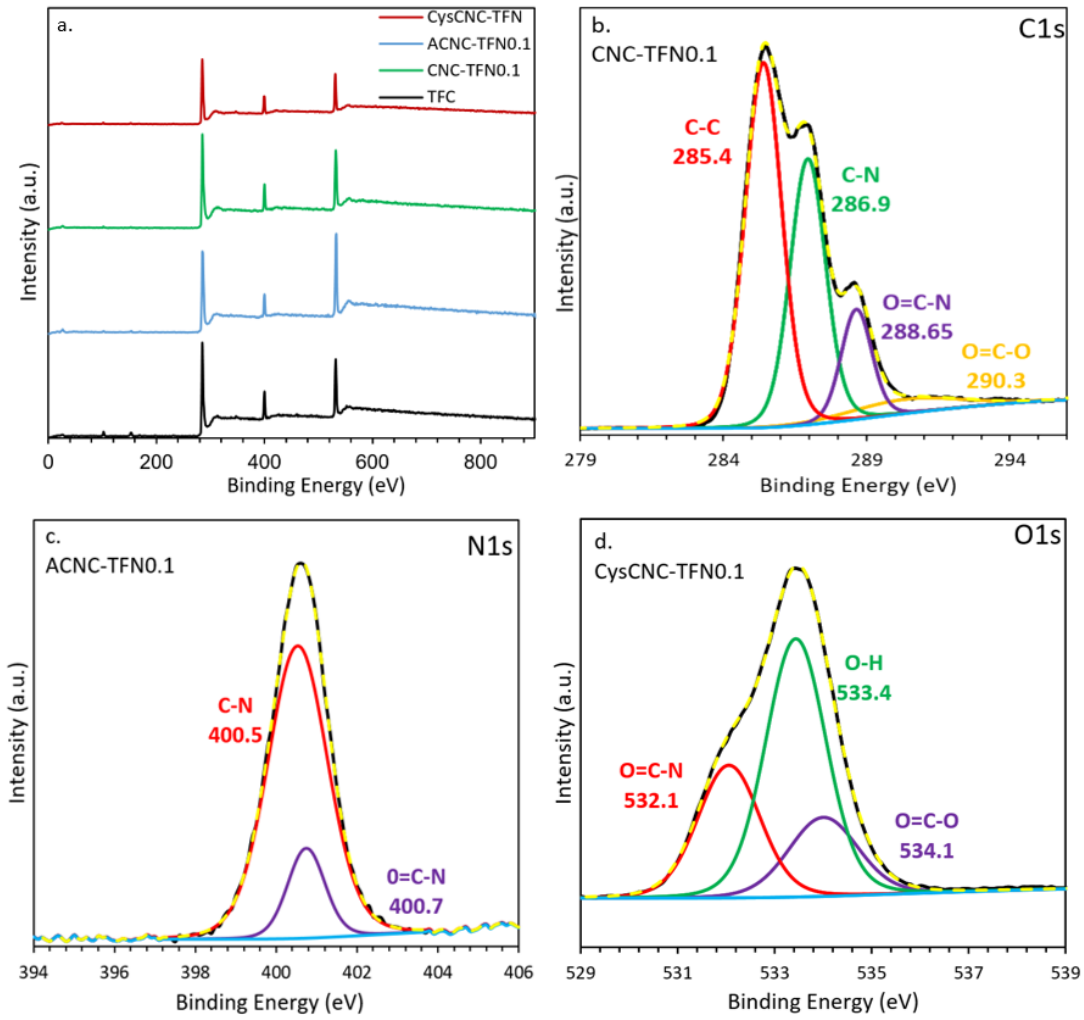

Figure 4.7: XPS spectra for a) TFC and 0.1 wt% CNC-TFN, ACNC-TFN and CysCNC-TFN membranes, b) C1s spectrum of CNC-TFN0.1, c) O1s spectrum of ACNC-TFN0.1 and d) N1s spectrum of CysCNC-TFN0.1.

Table 4.3: Elemental composition of membranes by the XPS analyses.

Membrane	C (%)	O (%)	N (%)	O/N	*COOH content
TFC	69.82	20.11	13.15	1.53	3.91
CNC-TFN0.1	72.41	18.03	12.10	1.49	3.76
ACNC-TFN0.1	76.32	18.14	12.31	1.47	3.41
CysCNC-TFN0.1	78.46	17.42	12.29	1.41	3.26

* The density of carboxyl groups (COOH content) was obtained from the O-C=O (binding energy = 290.3 eV) peak area derived from the C1s core level XPS spectra.

Figure 4.8a shows the zeta potential of the membrane surfaces in the pH range 3.5–9. The zeta potential of the membrane surfaces became more negative with an increase in pH. The zeta potential trends of the CNC-TFN, ACNC-TFN and CysCNC-TFN membranes were consistent with that of the CNC, ACNC and CysCNC nanoparticles (Table 4.3). For the TFC membrane, the negative surface charge density arose from the carboxylic acid groups due to the unreacted acyl chloride of the TMC monomer. An additional contribution to surface charge density for the TFN membranes was due to the functional groups on the nanoparticles [39]. The ACNC-TFN0.1 showed a negative zeta potential below that of the TFC but higher than CNC-TFN0.1. CysCNC-TFN0.1 also showed negative zeta potential but higher than that of the TFC membranes due to positively charged NH_2 and SH groups on the CysCNCs [40]. Furthermore, by increasing the loading of nanoparticles from 0.1 to 0.2 wt%, the surface zeta potential of the CNC-TFN0.2 and ACNC-TFN0.2 membranes became more negative, whereas CysCNC-TFN0.2 showed a lower negative surface charge density (Figure 4.8b). The content of hydroxyl groups of CNC and ACNCs in the PA layer increased with nanoparticle loading, whereas for CysCNC, the content of positive amide and thiol groups increased [41].

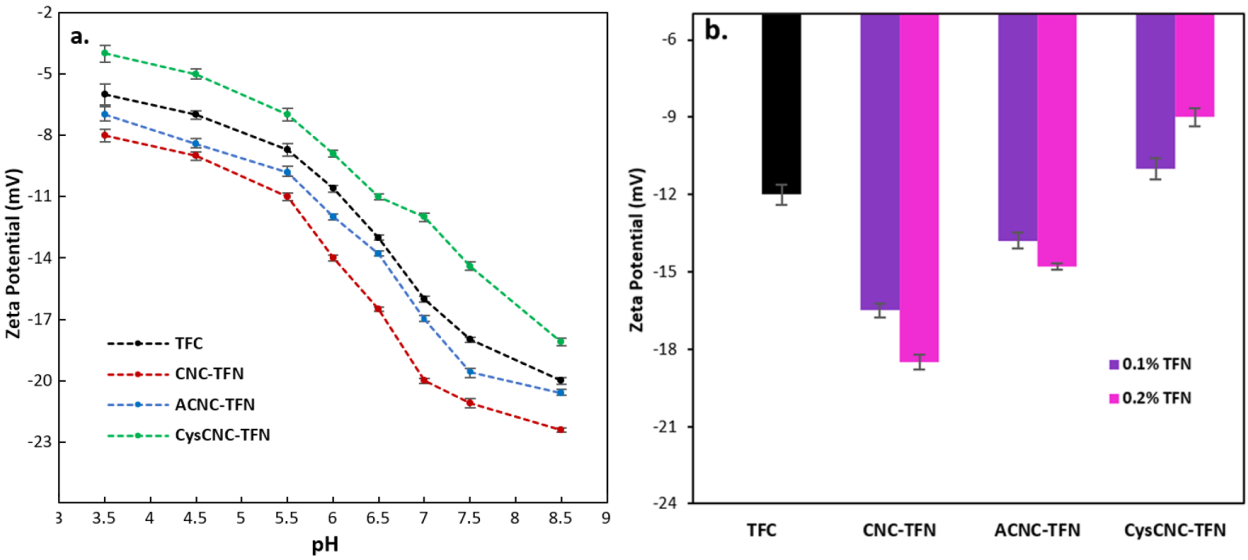

Figure 4.8: a) Zeta potential of TFC and 0.1 wt% TFN membranes a. in the 3.5 to 9 pH range, b) in pH = 6.5 for different nanoparticle loadings.

When the CNCs or modified CNCs were added to the TMC monomer solution, the hydroxyl surface groups of the CNCs or modified CNCs could also react with the acyl chloride groups of the TMC monomer, leading to a lower carboxylic acid group content for CNC-TFN0.1, ACNC-TFN0.1 and CysCNC-TFN0.1 (Table 4.3) [16]. The presence of well-dispersed ACNCs and CysCNCs during interfacial polymerization enhanced the PIP sorption at the interface of the two monomer solutions due to the synergistic effect of the hydrophilic interactions between the PIP and ACNCs (or CysCNCs) [42,43]. This greater PIP sorption led to a higher degree of crosslinking for ACNC-TFN0.1 and CysCNC-TFN0.1 compared to the TFC and CNC-TFN0.1 membranes (Table 4.3).

The MWCO of the TFC membranes (853 Da) decreased to 794, 753, and 691 Da for CNC-TFN0.1, ACNC-TFN0.1, and CysCNC-TFN0.1, respectively (Figure 4.9a). The lowest MWCO (CysCNC-TFN0.2) was likely due to the additional NH_2 groups of the CysCNCs, which provided more reaction sites for the acyl chloride of the TMC monomer to form a PA layer with the highest degree of crosslinking and lowest carboxylic acid group content (Table 4.3) [44]. The ACNC-TFN and CysCNC-TFN membranes exhibited smaller pore sizes and narrower PSD curves than the TFC membranes, which can be related to the dispersibility of the CNCs and modified CNCs in the PA layer.

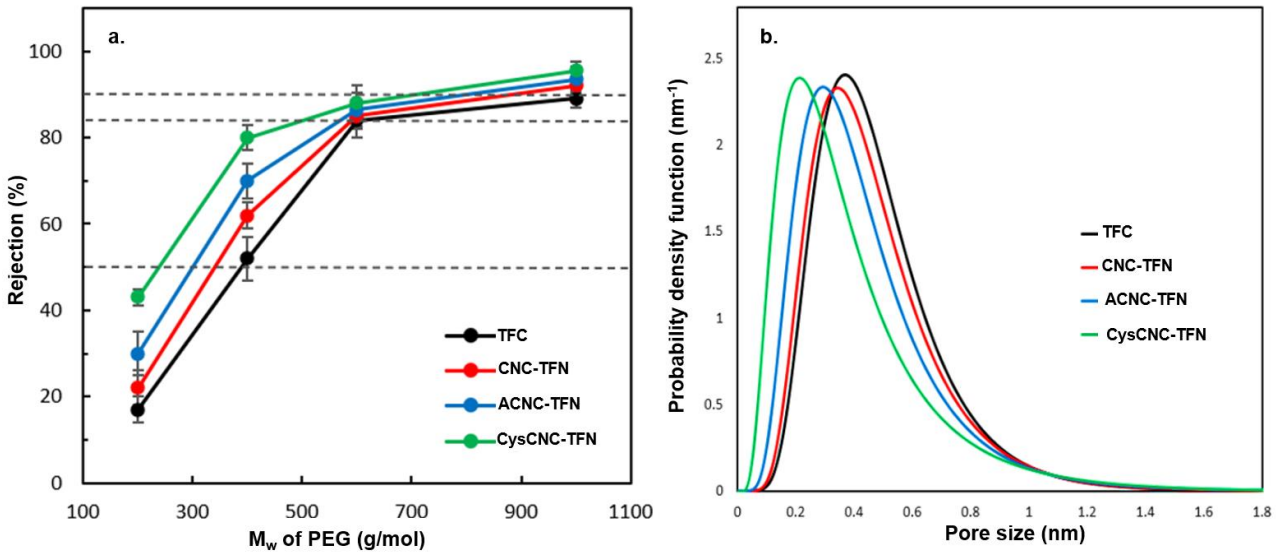

Figure 4.9: a) Rejection with different PEG molecular weights, b) Pore size distribution of TFC, CNC-TFN, ACNC-TFN and CysCNC-TFN membranes in 0.1 wt% loadings.

The membrane surface morphologies characterized by FESEM and AFM imaging, (Figure 4.10). From the FESEM images, the TFC and TFN membranes showed a uniform nodular structure (i.e., rough nodules and spherical globules) consistent with the ridges and valleys in the AFM images [45]. The surface roughness parameters from the AFM imaging, R_q, R_a and R_{max} and the roughness area ratio (r) are summarized in Table 4.4. The three R_q, R_a and R_{max} parameters are related to the size of the AFM image features, and the (r) relates to the number of features on the membrane surface.

The lower surface roughness parameters for the CysCNC-TFN and ACNC-TFN membranes compared to the CNC-TFN membranes is consistent with a more even dispersion of CysCNCs and ACNCs compared to CNCs in the TFN membranes. For CysCNC-TFN membranes, incorporating the hydrophilic CysCNCs in the TMC/n-hexane solution may have accelerated the diffusion of PIP from the aqueous to the organic phase during the interfacial polymerization, resulting in a smoother surface and tighter microstructure (more uniform PA layer). In addition, the immobilization of CysCNC nanoparticles in the PA layer facilitated the uniform dispersion of CysCNCs that could prevent defect formation in the PA layer even at high loadings (0.2 wt%) [46]. These results are consistent with the smaller pore size and narrower PSD, the higher degree of crosslinking, and the lower absolute zeta potential for CysCNC-TFN membranes (Table 4.3, Table 4.4, Figure 4.8a).

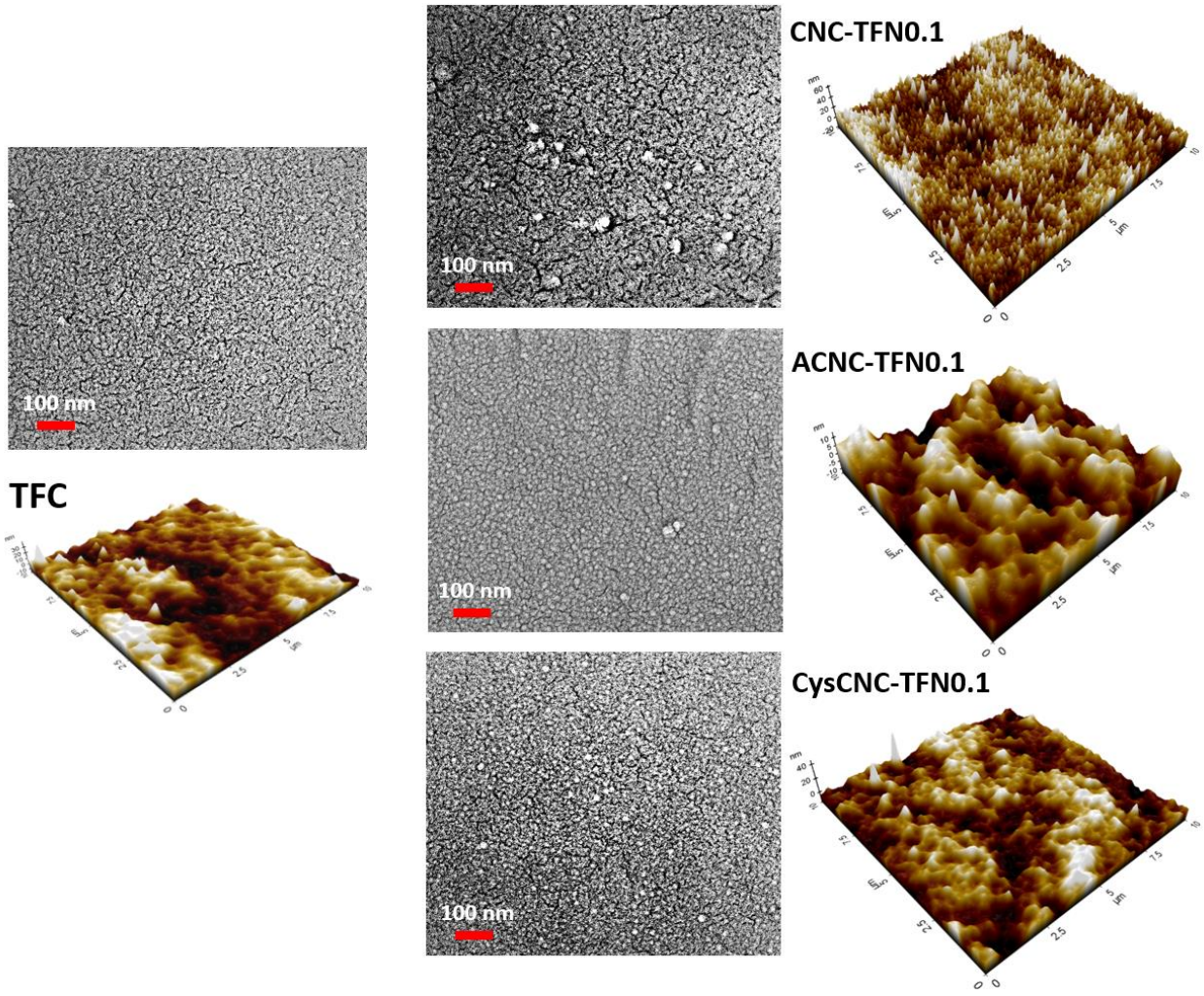

Figure 4.10: FESEM and AFM membrane surface images for TFC, CNC-TFN0.1, ACNC-TFN0.1, and CysCNC-TFN0.1.

The water contact angles and solid-liquid interfacial free energy (ΔG_{SL}) values of the TFC and TFN membrane surfaces are also summarized in Table 4.4. In general, the water contact angles of the TFN membranes were lower than that of the reference TFC, which is attributed to the additional hydrophilic hydroxyl groups of the CNCs, ACNCs and CysCNCs. The contact angle for CNC-TFN0.1 (28.1°) was lower than that for ACNC-TFN0.1 (35.4°) and higher than that for CysCNC-TFN0.1 (24.3°), which is consistent with the contact angle trends of the CNC, ACNC and CysCNC nanoparticle surfaces (Table 4.3). The higher contact angle for ACNC-TFN0.1 was due to substituting hydroxyl groups with less hydrophilic acetyl groups. Because the CysCNCs possess hydrophilic NH_2 and SH groups, the CysCNC-TFN0.2 surface showed the lowest water contact angle compared to all the other TFN membranes [47]. Although the surface of CysCNC-TFN0.2 was more hydrophilic than that of CNC-TFN0.2

from the perspective of their contact angles, because of its higher surface area (highest *r* value), the ΔG_{SL} was lower than for CNC-TFN0.2 as well as for ACNC-TFN0.2.

Table 4.4: Surface properties of TFC and TFN membranes.

	MWCO (Da)	μ_p (nm)	σ_p (-)	R_q (nm)	R_a (nm)	R_{max} (nm)	r (-)	θ (°)	ΔG_{SL} (mJ/m^2)
TFC	854	0.47	1.83	10.2±1.6	8.2±3.2	38.2±4.1	1.24	48.1±2.3	112.1±2.5
CNC-TFN0.1	794	0.42	1.91	18.1±3.1	13.8±2.4	45.5±3.5	1.31	28.4±3.4	121.6±3.1
ACNC-TFN0.1	753	0.38	1.69	14.9±1.4	10.9±4.1	26.3±2.7	1.36	35.7±4.5	116.2±1.8
CysCNC-TFN0.1	691	0.33	1.74	13.8±2.3	9.2±1.9	21.1±4.3	1.5	24.2±1.3	117.1±4.2
CNC-TFN0.2	812	0.44	1.99	23.6±1.1	19.1±1.5	50.5±3.5	1.24	25.3±3.1	125.8±1.4
ACNC-TFN0.2	741	0.36	1.71	18.8±2.4	12.8±4.4	34.3±1.4	1.41	38.5±2.2	113.2±2.2
CysCNC-TFN0.2	682	0.31	1.76	15.2±3.5	10.1±2.1	25.1±2.6	1.53	22.6±1.8	116.7±3.4

4.4.3 Membrane separation performance

The separation performance of the TFC and TFN membranes was evaluated in filtration tests using Na_2SO_4, $MgCl_2$ and NaCl salt solutions (2000 ppm) at a pressure of 10 bar and a pH=6.5 (Figure 4.11). The salt rejection by the TFC and TFN membranes followed the order Na_2SO_4 > $MgCl_2$ > NaCl. The CysCNC-TFN membranes showed the highest rejection for all salts at all loadings, followed by ACNC-TFN and CNC-TFN membranes. While the salt rejections for ACNC-TFN and CysCNC-TFN membranes were comparable to that of the TFC membranes, the CNC-TFN membranes' salt rejection was lower and decreased with nanoparticle loading. For most cases, the ACNC-TFN and CysCNC-TFN membranes salt rejections showed no clear trends with nanoparticle loading. The water permeability results were consistent for each salt solution tested (Figure 4.11). For all CNC-TFN, ACNC-TFN and CysCNC-TFN membranes, the water permeability exceeded that of the TFC membranes. For the CNC-TFN and ACNC-TFN membranes, the maximum water permeability for each salt solution was at 0.1 wt% nanoparticle loading. In contrast, the CysCNC-TFN membranes showed an increasing water permeability with nanoparticle loading to 0.2 wt%.

The water permeability and rejection of $CuSO_4$ and $Pb(NO_3)_2$ are shown in Figure 4.12. The CysCNC-TFN0.2 water permeability (15 L/m^2.h.bar) was 150% higher compared to the

TFC membrane (6 L/m^2.h.bar), 15% higher than ACNC-TFN0.2 (13 L/m^2.h.bar), and 30% higher than CNC-TFN0.1 (11.5 L/m^2.h.bar). These trends point to two main factors affecting the water permeability of TFN membranes: the hydrophilicity of the membrane surface and the morphology of the PA layer, which is determined by the quality of the dispersion of the nanoparticles.

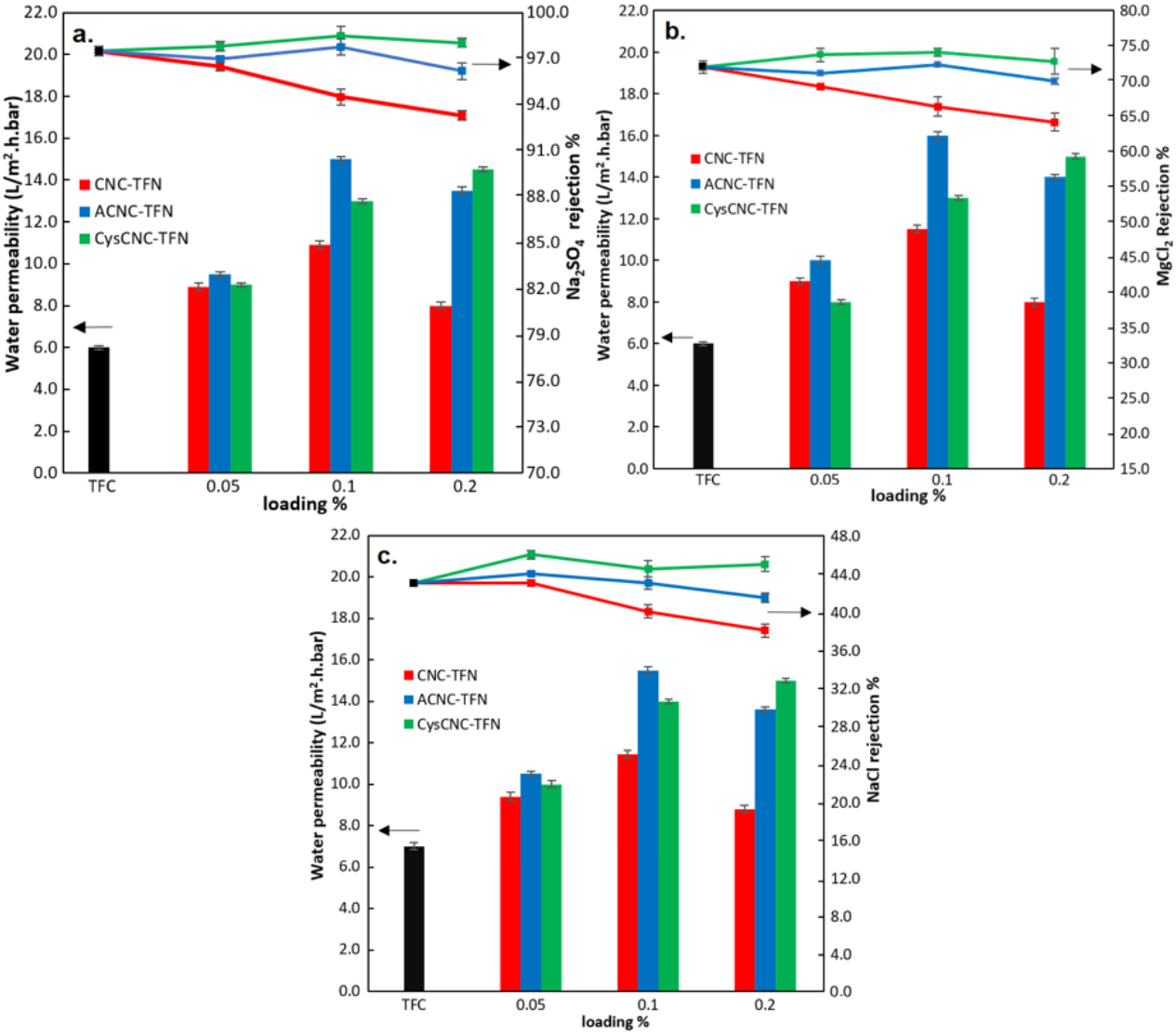

Figure 4.11: Performance of TFC and TFN membranes for a) Na_2SO_4, b) $MgCl_2$, c) NaCl rejection at different nanoparticle loadings.

The rejection of NF membranes is primarily governed by electrostatic repulsion (Donnan effect) and size exclusion [39]. According to the Donnan effect, the negatively charged surface membranes attract cations and repulse anions. The higher the valence, the stronger the attraction/rejection of the ions by the membrane. At the same time, the feed and permeate should maintain electro-neutrality. In other words, although cations are attracted by

the negatively charged NF membranes, their transport across the membrane is limited because of the rejection of their corresponding anions [14]. The results in Figures 4.11 and 4.12 confirm higher rejection of the Na_2SO_4 and $CuSO_4$ salts for a given membrane compared to other salts (i.e., NaCl, $MgCl_2$ and $Pb(NO_3)_2$). The valence of the salt anion is not the only parameter determining rejection by the NF membranes; another factor is the hydrated radius of the salt ions present in the feed solution. For $CuSO_4$, the hydrated radius of Cu^{2+} and SO_4^{2-} are 0.41 nm and 0.37 nm, respectively. This is slightly larger than the hydrated radius of Na^+ (0.35 nm) [36]. Yet, the rejection of Na_2SO_4 and $CuSO_4$ were comparable. For the salts with monovalent anions (Cl^- and NO_3^-), the rejections for a given membrane followed the order: $Pb(NO_3)_2$ > $MgCl_2$ > NaCl. The lowest rejection observed for NaCl salts was because the constituent ions were monovalent and had the smallest hydrated radius. On the other hand, the higher rejection of $Pb(NO_3)_2$ compared to $MgCl_2$ cannot be explained on the basis of the difference in the hydrated radius. The thiol (SH) functional groups of CysCNCs introduced extra sites to enhance the heavy metal rejection through complexation or adsorption [48]. The Cu-S and Pb-S coordinative interactions (chelation effect) can lead to the higher rejection of Cu^{2+} and Pb^{2+} metal cations. It was shown that the bond formation of Cu^{2+} is higher than that of Pb^{2+} [49]. More specifically, as a family of Lewis bases, sulphur-containing species have a highly polarizable donor center that can react strongly with the orbitals of Lewis acids, such as heavy metal ions. Bandehali et al. [50] have also confirmed that due to the chelation ability of thiol groups and hydrophilic amide groups of L-cysteine modified POSS nanoparticles, the NF membranes showed high water permeability, divalent salt and metal ions (Na_2SO_4 and $CuSO_4$) rejection [51].

As previously noted, the CysCNC-TFN membranes showed the highest rejection for a given salt at a given nanoparticle loading. This was despite the fact that CysCNC-TFN membranes had the lowest negative surface charge density compared to CNC-TFN and ACNC-TFN membranes. At the same time, the CysCNC-TFN membranes had the smallest pore size and PSD compared to the other membranes, as well as the highest degree of crosslinking compared to the other TFN membranes. This indicates that the smallest pore size (0.33 nm), narrowest PSD, and a higher degree of crosslinking (tighter structure) of Cys-CNC-TFN compared to other membranes played a more critical role in determining the degree of salt rejection than the surface charge density.

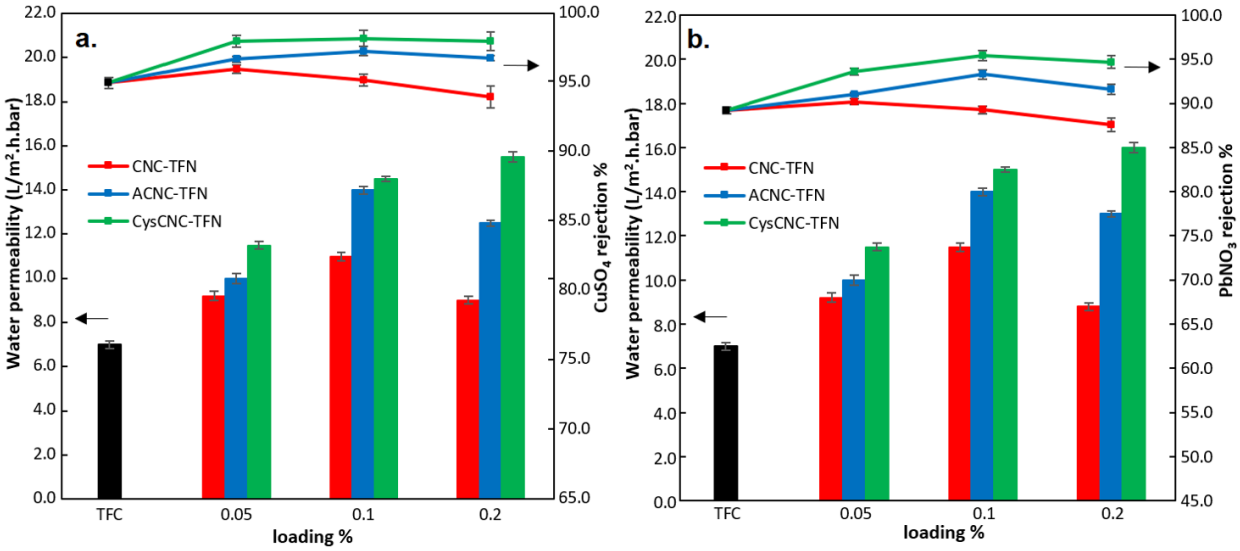

Figure 4.12: Performance of TFC and TFN membranes for a) $CuSO_4$ and b) $Pb(NO_3)_2$ rejection at different nanoparticle loadings.

Table 4.5 compares the nanofiltration performance of CNCs and modified CNCs-based TFN membranes from this work and the literature. Table 4.5 also includes two commercial membranes (NF90 and NF270). CNCs and modified CNCs are incorporated into the TFN membranes for different purposes. For example, to overcome permeability/selectivity performance trade-offs, to improve antifouling and chlorine resistance, etc

In the case of our membranes, the ultimate goal was to evaluate their suitability for heavy metal rejection. However, we also evaluated their nanofiltration performance and stability in long-term tests with and without the feed solution's fouling agent (BSA). Therefore, we included the primary purpose of using CNCs in the references listed in Table 4.5. It is important to emphasize that our membranes are the only ones in Table 4.5 for which CNCs were added to the TMC solution. Comparing our ACNC-TFN and CysCNC-TFN membrane performance with the membranes listed in Table 4.5, we can conclude that ACNC-TFN0.2 and CysCNC-TFN0.2 show excellent water permeability. The CysCNC-TFN0.2 showed the highest water permeability (16 L/m^2 h bar), comparable only to the commercial NF270 membrane but 35% higher than the highest water permeability of the literature TFN membranes. At the same time, their Na_2SO_4 rejection ranging between 98 and 99% was comparable to the best membranes in Table 4.5. All performance data of our membranes reported in Figures 4.11 and 4.12 and Table 4.5 correspond to the regular performance tests. It took 3–4 h for membranes to attain a steady state and to ensure that we ran each experiment for 6–8 h. At the same time, it is possible that nanoparticles could leach out from the membranes in long-term performance tests. Therefore, we investigated the stability of our TFN

membranes (CNC-TFN0.1 and CysCNC-TFN0.1) in 7-day tests using a 200 ppm aqueous $CuSO_4$ solution as a feed. We also performed a similar test with the lab synthesized TFC membrane for reference. The results of these tests are displayed in Figure 4.13.

Table 4.5: Comparison of NF membrane performance reported in the literature for CNC-TFN membranes.

Nanoparticle	CNC loading	Salt Concentration (ppm)	Rejection (%)			A[a] ($L/m^2.h.bar$)	Purpose of CNCs	Ref.
			Na_2SO_4	$MgCl_2$	NaCl			
CNC	0.1 wt% in TMC	2000	94.5	66.1	40.4	10.9	$CuSO_4$ and $Pb(NO_3)_2$ rejection	This work
ACNC	0.2 wt% in TMC		98.1	74.1	44.5	14.8		
CysCNC	0.2 wt% in TMC		98.8	72.3	43.3	15.7		
NF90	-	2000	98.6	50.1	68.6	8.3	Commercial membrane	[34]
NF270	-	2000	98.1	70.3	37.1	15.2		
CNC	0.01 wt% in PIP	2000	98	27	23	8.7	Cationic and anionic dye rejection	[23]
CNC	0.02 wt% in PIP	2000	98	-	21	8.1	Humic acid antifouling	[52]
CNC	0.05 wt% in PIP	1000	98	45	28	10.8	Chlorine resistance	[38]
Carboxylated CNC	0.05 wt% in PIP	2000	98.5	-	35	7.5	-	[39]
CNC	0.05 wt% in PIP	1000	93	79	62	3.5	BSA[b], antifouling	[53]
Zwitterionic CNC	0.05 wt% in PIP	1000	98	12	19	8.7	BSA[b], antifouling	[13]
Phosphorylated CNC	0.05 wt% in PIP	1000	95.4	10	5	8.5	Antibiotic rejection	[35]
CNC/Ag	0.01 wt% in PIP	2000	99	27	-	12	Humic acid antifouling, E-coli antibacterial	[55]

*Na_2SO_4 aqueous solution as a feed. ** BSA: Bovine serum albumin

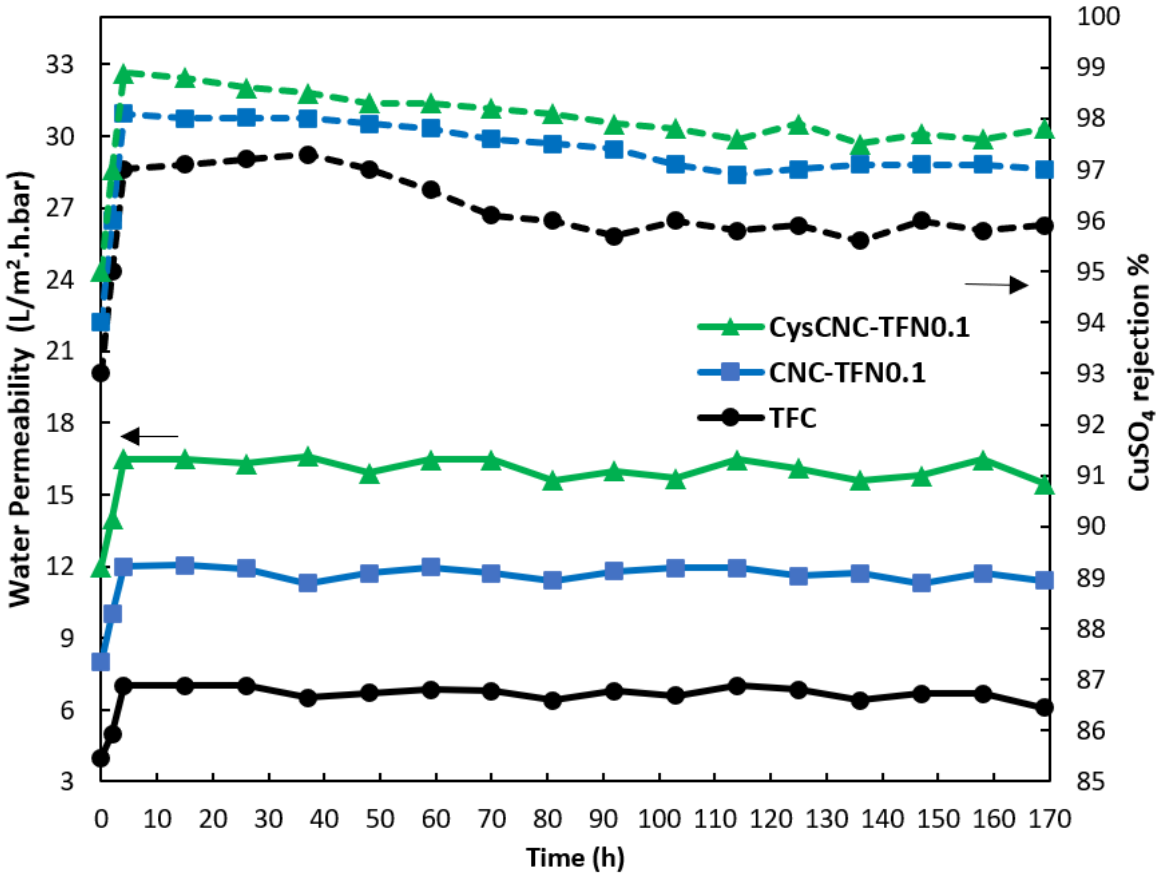

Figure 4.13: Long-term performance test of TFC, CNC-TFN0.1 and CysCNC-TFN0.1 membranes with 200 ppm CuSO4 solution as a feed.

For all membranes in Figure 4.13, including the reference TFC membrane, the water permeability and CuSO4 rejection increase during the first 4 h of the experiment. This behavior is representative of all tests. However, the increase's magnitude and duration varied for different salts and from membrane to membrane in the regular 6–8 h tests. Following the initial increase, the water permeability is generally constant in the first two days, after which it slightly decreases. This decrease in permeability is much smaller than the initial increase. After four days, the water permeability remains practically constant. On the other hand, after the initial increase, the CuSO4 rejection is practically constant during the entire experiment. The performance trend for TFN and TFC membranes in Figure 4.13 are similar, indicating the nanoparticles' stability in TFN membranes. Moreover, it appears that TFN membranes' water permeability experiences a smaller decline between the 2nd and the 4th day of the experiment than the reference TFC membrane.

We also examined the water permeability of the membranes in long-term tests in the presence of a cationic foulant, a 200 ppm BSA solution, as a feed. We used the CysCNC-TFN01 membrane to represent TFN membranes and the TFC membrane as a reference. The

results of these experiments are presented in Figure 4.14. Both membranes experienced the most significant permeability decline in the first 10 h, and the relative decrease for the TFC membrane (14%) is slightly larger than that for the TFN membrane (10%). However, considering that without BSA in the feed, the water permeability increased considerably in the first 4 h (see Figure 4.13), the actual decline because fouling of BSA was considerably larger than what appears in Figure 4.14. After the first 10 h, the water permeability of both membranes continues to decrease, but at a much lower rate. In fact, the decrease in water permeability in the remaining 160 h of experiments is clearly smaller than in the first 10 h.

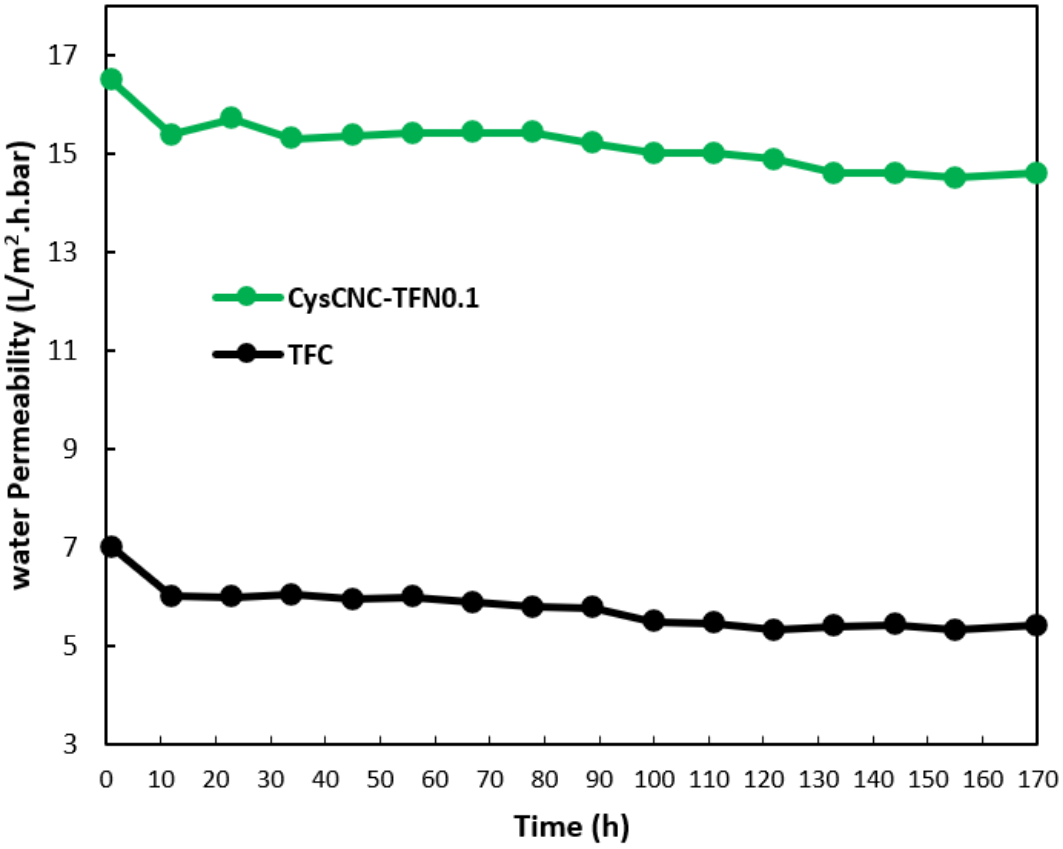

Figure 4.14: Long-term performance of TFC and CysCNC0.1 in the presence of BSA (200 ppm) as a cationic foulant in the feed solution.

4.5 Conclusion

TFN membranes are a promising alternative for the rejection of heavy metals from wastewaters in NF processes. The nanoparticles in the TFN membranes play an important role in membrane performance. As with most nanocomposite materials, their effectiveness is heavily influenced by their aspect ratio, their concentration, their dispersibility and their functionality. CNCs have, by their nature, a high aspect ratio. Their hydrophilicity has led to

their use primarily in aqueous dispersions and this has been demonstrated in the production of TFN membranes by their dispersion in the aqueous monomer phase prior to interfacial polymerization. In this study, CNCs were modified using acetylation (ACNCs) and L-cysteine (CysCNCs) functionalization to improve their dispersibility into the organic monomer solution. The ACNCs' increased dispersibility was due to an increase in their hydrophobicity by virtue of their acetylation. On the other hand, the CysCNCs were better dispersed because of the covalent bonding between the L-cysteine amine groups and the acyl chloride groups on the TMC monomer.

The modified CNC-TFN membranes were compared to CNC-TFN and TFC membranes. In heavy metal rejection tests, the order of water permeability performance was the same as the order of heavy metal rejection, which indicates the overcoming of the water permeability/selectivity trade-off. The best performance was exhibited by the CysCNC-TFN0.2 membranes with a water permeability of 16 $L/m^2.h.bar$ and copper and lead rejections of 98.4 and 95.2%, respectively. The resulting membranes had the highest surface hydrophilicity combined with the smallest pore size and pore size distribution. The key to the superior performance of the CysCNC-TFN membranes was not only their high hydrophilicity but also their functionality, which permitted covalent bonding with the TMC monomer and led to their improved dispersibility in the PA layer. This work provides an example of how a controllable nanoparticle functionalization enables one to tailor the properties of TFN membranes to better align with application needs.

4.6 References

[1] L.E. Peng, Z. Yang, L. Long, S. Zhou, H. Guo, C.Y. Tang, A critical review on porous substrates of TFC polyamide membranes: Mechanisms, membrane performances, and future perspectives, Journal of Membrane Science. 641 (2022) 119871. https://doi.org/10.1016/j.memsci.2021.119871.

[2] S. Bandehali, F. Parvizian, H. Ruan, A. Moghadassi, J. Shen, A. Figoli, A.S. Adeleye, N. Hilal, T. Matsuura, E. Drioli, S.M. Hosseini, A planned review on designing of high-performance nanocomposite nanofiltration membranes for pollutants removal from water, Journal of Industrial and Engineering Chemistry. 101 (2021) 78–125. https://doi.org/10.1016/j.jiec.2021.06.022.

[3] D.J. Johnson, N. Hilal, Nanocomposite nanofiltration membranes: State of play and recent advances, Desalination. 524 (2022) 115480. https://doi.org/10.1016/j.desal.2021.115480.

[4] X. Feng, D. Peng, J. Zhu, Y. Wang, Y. Zhang, Recent advances of loose nanofiltration membranes for dye/salt separation, Separation and Purification Technology. 285 (2022) 120228. https://doi.org/10.1016/j.seppur.2021.120228.

[5] D. Yadav, S. Karki, P.G. Ingole, Current advances and opportunities in the development of nanofiltration (NF) membranes in the area of wastewater treatment, water desalination,

biotechnological and pharmaceutical applications, Journal of Environmental Chemical Engineering. 10 (2022) 108109. https://doi.org/10.1016/j.jece.2022.108109.
[6] H. Sari Erkan, N. Bakaraki Turan, G. Onkal Engin, M.S. Bilgili, A review of advantages and challenges of using engineered nanoparticles for waste and wastewater treatments, Int. J. Environ. Sci. Technol. 18 (2021) 3295–3306. https://doi.org/10.1007/s13762-020-03054-8.
[7] A.A. Yaqoob, T. Parveen, K. Umar, M.N. Mohamad Ibrahim, Role of Nanomaterials in the Treatment of Wastewater: A Review, Water. 12 (2020) 495. https://doi.org/10.3390/w12020495.
[8] V.V. Bhaskar, N.J. Kaleekkal, Next-generation thin-film composite nanofiltration membranes for water remediation: a review, Emergent Mater. (2021). https://doi.org/10.1007/s42247-021-00273-8.
[9] S. Poornima, S. Manikandan, V. Karthik, R. Balachandar, R. Subbaiya, M. Saravanan, N.T. Lan Chi, A. Pugazhendhi, Emerging nanotechnology based advanced techniques for wastewater treatment, Chemosphere. 303 (2022) 135050. https://doi.org/10.1016/j.chemosphere.2022.135050.
[10] N. Abdullah, N. Yusof, W.J. Lau, J. Jaafar, A.F. Ismail, Recent trends of heavy metal removal from water/wastewater by membrane technologies, Journal of Industrial and Engineering Chemistry. 76 (2019) 17–38. https://doi.org/10.1016/j.jiec.2019.03.029.
[11] M.R. Esfahani, S.A. Aktij, Z. Dabaghian, M.D. Firouzjaei, A. Rahimpour, J. Eke, I.C. Escobar, M. Abolhassani, L.F. Greenlee, A.R. Esfahani, A. Sadmani, N. Koutahzadeh, Nanocomposite membranes for water separation and purification: Fabrication, modification, and applications, Separation and Purification Technology. 213 (2019) 465–499. https://doi.org/10.1016/j.seppur.2018.12.050.
[12] C. Gomri, M. Cretin, M. Semsarilar, Recent progress on chemical modification of cellulose nanocrystal (CNC) and its application in nanocomposite films and membranes-A comprehensive review, Carbohydrate Polymers. 294 (2022) 119790. https://doi.org/10.1016/j.carbpol.2022.119790.
[13] D. Xia, M. Zhang, C. Tong, Z. Wang, H. Liu, L. Zhu, In-situ incorporating zwitterionic nanocellulose into polyamide nanofiltration membrane towards excellent perm-selectivity and antifouling performances, Desalination. 521 (2022) 115397. https://doi.org/10.1016/j.desal.2021.115397.
[14] Y. Liu, J.M. Sipe, W. Xu, X. Zhu, L. Bai, D. Xu, G. Li, H. Liang, M.R. Wiesner, Study on the mechanisms for the influence of nanomaterials on the separation performance of nanocomposite membrane from a modeling perspective, Desalination. 532 (2022) 115740. https://doi.org/10.1016/j.desal.2022.115740.
[15] M. Bassyouni, M.H. Abdel-Aziz, M.Sh. Zoromba, S.M.S. Abdel-Hamid, E. Drioli, A review of polymeric nanocomposite membranes for water purification, Journal of Industrial and Engineering Chemistry. 73 (2019) 19–46. https://doi.org/10.1016/j.jiec.2019.01.045.
[16] F. Abedi, D. Emadzadeh, M.A. Dubé, B. Kruczek, Modifying cellulose nanocrystal dispersibility to address the permeability/selectivity trade-off of thin-film nanocomposite reverse osmosis membranes, Desalination. 538 (2022) 115900. https://doi.org/10.1016/j.desal.2022.115900.
[17] M.R. De Guzman, M.B.M.Y. Ang, C.-L. Lai, C.A. Trilles, J.M. Pereira, R.R. Aquino, S.-H. Huang, K.-R. Lee, Choice of Apposite Dispersing Medium for Silica Nanoparticles Leading to Their Effective Embedment in Nanocomposite Nanofiltration Membranes, Ind. Eng. Chem. Res. 58 (2019) 17937–17944. https://doi.org/10.1021/acs.iecr.9b03456.
[18] S. Bandehali, F. Parvizian, A. Moghadassi, J. Shen, S.M. Hosseini, Improvement in separation performance of PEI-based nanofiltration membranes by using L-cysteine

functionalized POSS-TiO2 composite nanoparticles for removal of heavy metal ion, Korean J. Chem. Eng. 37 (2020) 1552–1564. https://doi.org/10.1007/s11814-020-0535-0.
[19] S.-H. Park, Y.-S. Ko, S.-J. Park, J.S. Lee, J. Cho, K.-Y. Baek, I.T. Kim, K. Woo, J.-H. Lee, Immobilization of silver nanoparticle-decorated silica particles on polyamide thin film composite membranes for antibacterial properties, Journal of Membrane Science. 499 (2016) 80–91. https://doi.org/10.1016/j.memsci.2015.09.060.
[20] W. Li, B. Ju, S. Zhang, A green L -cysteine modified cellulose nanocrystals biosorbent for adsorption of mercury ions from aqueous solutions, RSC Adv. 9 (2019) 6986–6994. https://doi.org/10.1039/C9RA00048H.
[21] H.-L. Zhang, H. Cai, Y. Xia, P. Zhang, S.-W. Xiong, J.-G. Gai, An L -cystine/ L -cysteine impregnated nanofiltration membrane with the superior performance of an anchoring heavy metal in wastewater, RSC Adv. 10 (2020) 3438–3449. https://doi.org/10.1039/C9RA09380J.
[22] M.T. Hoang, T.D. Pham, D. Verheyen, M.K. Nguyen, T.T. Pham, J. Zhu, B. Van der Bruggen, Fabrication of thin film nanocomposite nanofiltration membrane incorporated with cellulose nanocrystals for removal of Cu(II) and Pb(II), Chemical Engineering Science. 228 (2020) 115998. https://doi.org/10.1016/j.ces.2020.115998.
[23] L. Bai, Y. Liu, A. Ding, N. Ren, G. Li, H. Liang, Fabrication and characterization of thin-film composite (TFC) nanofiltration membranes incorporated with cellulose nanocrystals (CNCs) for enhanced desalination performance and dye removal, Chemical Engineering Journal. 358 (2019) 1519–1528. https://doi.org/10.1016/j.cej.2018.10.147.
[24] D. Carter, F.H. Tezel, B. Kruczek, H. Kalipcilar, Investigation and comparison of mixed matrix membranes composed of polyimide matrimid with ZIF – 8, silicalite, and SAPO – 34, Journal of Membrane Science. 544 (2017) 35–46. https://doi.org/10.1016/j.memsci.2017.08.068.
[25] Z. Wu, J. Xu, J. Gong, J. Li, L. Mo, Preparation, characterization and acetylation of cellulose nanocrystal allomorphs, Cellulose. 25 (2018) 4905–4918. https://doi.org/10.1007/s10570-018-1937-6.
[26] M. Bansal, B. Ram, G.S. Chauhan, A. Kaushik, l-Cysteine functionalized bagasse cellulose nanofibers for mercury(II) ions adsorption, International Journal of Biological Macromolecules. 112 (2018) 728–736. https://doi.org/10.1016/j.ijbiomac.2018.01.206.
[27] R. Yang, K.B. Aubrecht, H. Ma, R. Wang, R.B. Grubbs, B.S. Hsiao, B. Chu, Thiol-modified cellulose nanofibrous composite membranes for chromium (VI) and lead (II) adsorption, Polymer. 55 (2014) 1167–1176. https://doi.org/10.1016/j.polymer.2014.01.043.
[28] X. Yang, Q. Pan, Y. Ao, J. Du, Z. Dong, M. Zhai, L. Zhao, Facile preparation of L-cysteine–modified cellulose microspheres as a low-cost adsorbent for selective and efficient adsorption of Au(III) from the aqueous solution, Environ Sci Pollut Res. 27 (2020) 38334–38343. https://doi.org/10.1007/s11356-020-09789-8.
[29] M. Taghavi, M.A. Zazouli, Z. Yousefi, B. Akbari-adergani, Kinetic and isotherm modeling of Cd (II) adsorption by l-cysteine functionalized multi-walled carbon nanotubes as adsorbent, Environ Monit Assess. 187 (2015) 682. https://doi.org/10.1007/s10661-015-4911-x.
[30] J.E. Rosen, F.X. Gu, Surface Functionalization of Silica Nanoparticles with Cysteine: A Low-Fouling Zwitterionic Surface, Langmuir. 27 (2011) 10507–10513. https://doi.org/10.1021/la201940r.
[31] J. Shao, Y. Yang, C. Shi, Preparation and adsorption properties for metal ions of chitin modified by L-cysteine, J. Appl. Polym. Sci. 88 (2003) 2575–2579. https://doi.org/10.1002/app.12098.

[32] H.Y. Choi, J.H. Bae, Y. Hasegawa, S. An, I.S. Kim, H. Lee, M. Kim, Thiol-functionalized cellulose nanofiber membranes for the effective adsorption of heavy metal ions in water, Carbohydrate Polymers. 234 (2020) 115881. https://doi.org/10.1016/j.carbpol.2020.115881.
[33] J. Xu, Z. Wu, Q. Wu, Y. Kuang, Acetylated cellulose nanocrystals with high-crystallinity obtained by one-step reaction from the traditional acetylation of cellulose, Carbohydrate Polymers. 229 (2020) 115553. https://doi.org/10.1016/j.carbpol.2019.115553.
[34] L. Bai, J. Ding, H. Wang, N. Ren, G. Li, H. Liang, High-performance nanofiltration membranes with a sandwiched layer and a surface layer for desalination and environmental pollutant removal, Science of The Total Environment. 743 (2020) 140766. https://doi.org/10.1016/j.scitotenv.2020.140766.
[35] Z. Wang, D. Xia, B. Wang, H. Liu, L. Zhu, Highly permeable polyamide nanofiltration membrane incorporated with phosphorylated nanocellulose for enhanced desalination, Journal of Membrane Science. 647 (2022) 120339. https://doi.org/10.1016/j.memsci.2022.120339.
[36] L. Bai, H. Wu, J. Ding, A. Ding, X. Zhang, N. Ren, G. Li, H. Liang, Cellulose nanocrystal-blended polyethersulfone membranes for enhanced removal of natural organic matter and alleviation of membrane fouling, Chemical Engineering Journal. 382 (2020) 122919. https://doi.org/10.1016/j.cej.2019.122919.
[37] S. Liu, Z.-X. Low, H.M. Hegab, Z. Xie, R. Ou, G. Yang, G.P. Simon, X. Zhang, L. Zhang, H. Wang, Enhancement of desalination performance of thin-film nanocomposite membrane by cellulose nanofibers, Journal of Membrane Science. 592 (2019) 117363. https://doi.org/10.1016/j.memsci.2019.117363.
[38] S. Huang, M.-B. Wu, C.-Y. Zhu, M.-Q. Ma, J. Yang, J. Wu, Z.-K. Xu, Polyamide Nanofiltration Membranes Incorporated with Cellulose Nanocrystals for Enhanced Water Flux and Chlorine Resistance, ACS Sustainable Chem. Eng. (2019) acssuschemeng.9b01651. https://doi.org/10.1021/acssuschemeng.9b01651.
[39] Y. Liu, L. Bai, X. Zhu, D. Xu, G. Li, H. Liang, M.R. Wiesner, The role of carboxylated cellulose nanocrystals placement in the performance of thin-film composite (TFC) membrane, Journal of Membrane Science. 617 (2021) 118581. https://doi.org/10.1016/j.memsci.2020.118581.
[40] M. Jonoobi, A. Ashori, V. Siracusa, Characterization and properties of polyethersulfone/ modified cellulose nanocrystals nanocomposite membranes, Polymer Testing. 76 (2019) 333–339. https://doi.org/10.1016/j.polymertesting.2019.03.039.
[41] S. Bandehali, F. Parvizian, A.R. Moghadassi, S.M. Hosseini, J.N. Shen, Fabrication of thin film-PEI nanofiltration membrane with promoted separation performances: Cr, Pb and Cu ions removal from water, J Polym Res. 27 (2020) 94. https://doi.org/10.1007/s10965-020-02056-x.
[42] L. Lin, T.M. Weigand, M.W. Farthing, P. Jutaporn, C.T. Miller, O. Coronell, Relative importance of geometrical and intrinsic water transport properties of active layers in the water permeability of polyamide thin-film composite membranes, Journal of Membrane Science. 564 (2018) 935–944. https://doi.org/10.1016/j.memsci.2018.08.002.
[43] L. Lin, R. Lopez, G.Z. Ramon, O. Coronell, Investigating the void structure of the polyamide active layers of thin-film composite membranes, Journal of Membrane Science. 497 (2016) 365–376. https://doi.org/10.1016/j.memsci.2015.09.020.
[44] P. Daraei, N. Ghaemi, H. Sadeghi Ghari, An ultra-antifouling polyethersulfone membrane embedded with cellulose nanocrystals for improved dye and salt removal from water, Cellulose. 24 (2017) 915–929. https://doi.org/10.1007/s10570-016-1135-3.
[45] L. Yang, X. Liu, X. Zhang, T. Chen, Z. Ye, Md.S. Rahaman, High performance nanocomposite nanofiltration membranes with polydopamine-modified cellulose

nanocrystals for efficient dye/salt separation, Desalination. 521 (2022) 115385. https://doi.org/10.1016/j.desal.2021.115385.
[46] S.Y. Lee, H.J. Kim, R. Patel, S.J. Im, J.H. Kim, B.R. Min, Silver nanoparticles immobilized on thin film composite polyamide membrane: characterization, nanofiltration, antifouling properties, Polym. Adv. Technol. 18 (2007) 562–568. https://doi.org/10.1002/pat.918.
[47] S. Bandehali, A. Moghadassi, F. Parvizian, J. Shen, S.M. Hosseini, Glycidyl POSS-functionalized ZnO nanoparticles incorporated polyether-imide based nanofiltration membranes for heavy metal ions removal from water, Korean J. Chem. Eng. 37 (2020) 263–273. https://doi.org/10.1007/s11814-019-0441-5.
[48] B. Thabo, B.J. Okoli, S.J. Modise, S. Nelana, Rejection Capacity of Nanofiltration Membranes for Nickel, Copper, Silver and Palladium at Various Oxidation States, Membranes. 11 (2021) 653. https://doi.org/10.3390/membranes11090653.
[49] H. Zhou, H. Zhu, F. Xue, H. He, S. Wang, Cellulose-based amphoteric adsorbent for the complete removal of low-level heavy metal ions via a specialization and cooperation mechanism, Chemical Engineering Journal. 385 (2020) 123879. https://doi.org/10.1016/j.cej.2019.123879.
[50] S. Bandehali, F. Parvizian, A. Moghadassi, S.M. Hosseini, High water permeable PEI nanofiltration membrane modified by L-cysteine functionalized POSS nanoparticles with promoted antifouling/separation performance, Separation and Purification Technology. 237 (2020) 116361. https://doi.org/10.1016/j.seppur.2019.116361.
[51] S. Bandehali, A. Moghadassi, F. Parvizian, Y. Zhang, S.M. Hosseini, J. Shen, New mixed matrix PEI nanofiltration membrane decorated by glycidyl-POSS functionalized graphene oxide nanoplates with enhanced separation and antifouling behaviour: Heavy metal ions removal, Separation and Purification Technology. 242 (2020) 116745. https://doi.org/10.1016/j.seppur.2020.116745.
[52] L. Bai, Y. Liu, N. Bossa, A. Ding, N. Ren, G. Li, H. Liang, M.R. Wiesner, Incorporation of Cellulose Nanocrystals (CNCs) into the Polyamide Layer of Thin-Film Composite (TFC) Nanofiltration Membranes for Enhanced Separation Performance and Antifouling Properties, Environ. Sci. Technol. 52 (2018) 11178–11187. https://doi.org/10.1021/acs.est.8b04102.
[53] Y. Rahimi-Kashkouli, M. Rahbari-Sisakht, A. Ghadami Jadval Ghadam, Thin film nanocomposite nanofiltration membrane incorporated with cellulose nanocrystals with superior anti-organic fouling affinity, Environ. Sci.: Water Res. Technol. 6 (2020) 715–723. https://doi.org/10.1039/C9EW00963A.
[54] J.-J. Wang, H.-C. Yang, M.-B. Wu, X. Zhang, Z.-K. Xu, Nanofiltration membranes with cellulose nanocrystals as an interlayer for unprecedented performance, J. Mater. Chem. A. 5 (2017) 16289–16295. https://doi.org/10.1039/C7TA00501F.
[55] C. Xu, W. Chen, H. Gao, X. Xie, Y. Chen, Cellulose nanocrystal/silver (CNC/Ag) thin-film nanocomposite nanofiltration membranes with multifunctional properties, Environ. Sci.: Nano. 7 (2020) 803–816. https://doi.org/10.1039/C9EN01367A.

5. Adsorption of heavy metals on the surface of nanofiltration membranes: "A curse or blessing"?

Fatemeh Abedi, Marc A. Dubé, Boguslaw Kruczek
This chapter is a manuscript is submitted to Journal of membrane science, 2023.

5.1 Abstract

Adsorptive membranes, formed by dispersing adsorbent particles in the polymer matrix of ultrafiltration (UF) membranes, are among a number of promising technologies for removing heavy metal ions from water. They offer much higher water permeability compared to nanofiltration (NF) membranes. However, because of a limited adsorption capacity, adsorptive membranes require frequent regeneration to maintain their selective properties. In contrast, NF membranes rely on size/steric exclusion and electrostatic repulsion. Moreover, by incorporating adsorptive nanoparticles into, for example, the polyamide (PA) layer in thin film nanocomposite (TFN) membranes, NF membranes, in addition to size/steric exclusion and electrostatic repulsion, can also reject heavy metal ions by adsorption. Some TFN-NF membranes for processing feed solutions containing heavy metal ions require regeneration, implying a detrimental effect of heavy metal adsorption on their performance. Still, some do not, which leads to the question stated in the title of this article.

In this study, we examined the role of heavy metal ions (Cu^{2+} and Pb^{2+}) in feed solutions on their rejection and water permeability TFN membranes containing cellulose nanocrystals (CNCs), acetylated CNCs (ACNCs) and CysCNCs in the PA layer. We performed NF experiments of durations ranging from 1 to 16 h. At the end of each experiment, we measured the membranes' heavy metal adsorption, contact angle, and zeta potential and correlated them with time-dependent water permeability and heavy metal rejection. An increase in heavy metal adsorption with time was associated with a desirable simultaneous increase in water permeability and heavy metal rejection. The equilibrium adsorption was reached 8 – 12 hours from the start of the experiments, while membrane performance remained constant. Therefore, membrane regeneration was not only unnecessary but would be undesirable because the adsorbed heavy metals improve membrane performance. In other words, the adsorption of heavy metals on the surface of NF membranes appears to be a "blessing" rather than a "curse."

5.2 Introduction

Our planet's clean water is scarce because only 2.5% of all the water on Earth is suitable for direct human consumption [1]. At the same time, the growing world population, and associated industrialization and agriculture, have dramatically increased the demand for clean water [2]. Industrial wastewaters often contain hazardous heavy metal ions that are highly toxic, even at low concentrations [3]. Therefore, their removal is essential for safely disposing of or reusing industrial wastewater [4]. Nanofiltration (NF) is a promising technology for removing heavy metals because NF membranes show a high rejection of multivalent ions (including heavy metal ions) while allowing a high water flux [5].

Typically, NF membranes are formed by the interfacial polymerization of piperazine (PIP) in an aqueous solution with trimesoyl chloride (TMC) in an organic n-hexane solution on an ultrafiltration membrane support [6]. The final product is a thin film composite (TFC) membrane with an active polyamide (PA) layer that determines the membrane's separation properties [7]. Compared to TFC-reverse osmosis (RO) membranes, in which the PA layer is formed by the interfacial polymerization of m-phenylenediamine (MPD) and TMC, the active layer in NF membranes has a looser structure because of its lower crosslinking density [8]. Consequently, NF membranes are more permeable than TFC-RO membranes [9]. In addition, the surface of a TFC-NF membrane is typically negatively charged due to carboxylic acid groups from the unreacted acyl chloride of the TMC monomer [10]. However, it is also possible to synthesize positively charged TFC-NF membranes by changing monomer(s) and/or their concentrations [11,12].

The solute rejection in TFC-NF membranes is governed by size/steric exclusion and electrostatic repulsion, while the feed and permeate streams should maintain electroneutrality [13]. The higher the valence, the stronger the attraction/rejection of the ions by the membrane [14]. The negative surface charge of TFC-NF membranes is responsible for very different rejections of Na_2SO_4 and $MgCl_2$ (> 90% versus < 50%) [15]. Although both salts are divalent, the anion of the former (SO_4^{-2}) has a greater valency than the latter (Cl^-). The stronger attraction of Mg^{2+} compared to Na^+ by the TFC-NF membrane does not influence the rejection of the respective salts because of the electroneutrality principle [16].

The surface charge of TFC membranes can also be modified by incorporating nanoparticles into the PA layer, which leads to a new category of membranes – thin film nanocomposite (TFN) membranes [17]. For example, Zhao et al. [18] incorporated poly(dopamine) modified multiwall carbon nanotubes into the PA layer, which led to a positively charged TFN-NF membrane. As a result, the rejection of $MgCl_2$ jumped to 91.5%,

whereas the rejection of Na_2SO_4 plunged to 45.2% compared to the TFC control membrane. In a recent paper [19], Atashgar et al. used functionalized halloysite nanotubes with first-generation poly(amidoamine) dendrimers. These positively charged nanoparticles were not sufficient to cause the membrane surface to be positively charged but decreased the negative surface charge of the resulting TFN membrane. As a result, the rejection of $MgCl_2$ increased to 82 - 90%, while the rejection of Na_2SO_4 remained above 95%. The excellent balance between these membranes' rejections of Na_2SO_4 and $MgCl_2$ was attributed to the local positive charge near the nanoparticles, despite the membrane surface remaining negatively charged [19].

The role of nanoparticles in TFN membranes is not limited to adjusting the surface charge density. Some nanoparticles can adsorb heavy metal ions, thus improving their rejection. The membranes whose rejection relies on only solute adsorption are often called "adsorptive membranes." The adsorptive membranes are usually formed using ultrafiltration (UF) or even microfiltration (MF) membranes. Consequently, they offer very high water permeability, but once adsorption capacity is reached, they lose selectivity and must be regenerated[20–24]. There are several excellent review papers on adsorptive membranes and their application in heavy metal removal from wastewater [25–27]. TFN-NF membranes incorporating nanoparticles capable of adsorbing specific solutes, including heavy metal ions, are not called adsorptive membranes. However, they also rely on the adsorption of specific solutes (e.g., heavy metal ions), but they also offer solute rejection by size exclusion. For example, Zhang et al. incorporated phytic acid into the PA layer and reported record-breaking rejections of Pb^{2+} and Cd^{2+} in long-term performance tests. After each membrane regeneration, the performance slightly declined, but even after the sixth cycle, it was very competitive [28]. Similar results for removing heavy metals from water using TFN membranes with different nanoparticles in the PA layer are reported in the literature [29–33]. These membranes were eventually regenerated, even if their long-term performance was relatively stable. Although not explicitly stated, the necessity of membrane regeneration implies a detrimental effect of adsorbed heavy metals on membrane performance. Membrane regeneration is usually accomplished chemically using strong acids or bases. It often leads to decreased water permeability and heavy metal rejection, attributed to chemically-accelerated aging of the treated membranes and/or nanoparticle leaching [34]. Indeed, the performance of TFN-NF membranes slightly declined after each operation-regeneration cycle [29–33].

On the other hand, there are examples of TFC-/TFN-NF membranes used for heavy metal removal from water that showed very stable performance in 3-5 day tests and were not

regenerated [11,12,35]. We have also recently demonstrated the stable performance of TFN membranes incorporating L-cysteine-modified cellulose nanocrystals (CysCNCs) in 7-day tests with either $CuSO_4$ or $Pb(NO_3)_2$ in the feed solution [36]. Therefore, there is no consensus on the effect of the adsorbed heavy metals on membrane performance and hence on the need to regenerate TFC-/TFN-NF membranes after their exposure to heavy metal ions during water filtration tests.

The long-term stability of TFN membranes with heavy metal salts in the feed solution has prompted us to experimentally investigate the role of heavy metal ions on membrane performance. We have thus designed a unique experimental protocol to monitor the adsorption of Cu^{2+} and Pb^{2+} by TFC- and TFN-NF membranes during continuous filtration tests based on their concentration in the feed and permeate streams, but also by the direct measurement of their mass on the membrane at different times. We considered three types of TFN membranes with the same loading of cellulose nanocrystals (CNCs), acetylated CNCs (ACNCs) and CysCNCs, as well as a TFC membrane as a control. Monitoring time-dependent changes in the concentration of heavy metal ions in the feed and permeate streams is easily accomplished by taking the feed and permeate samples at predetermined time intervals. However, the adsorption of heavy metals on the membrane surface can only be determined at the end of the experiment. To that end, we performed membrane filtration experiments of different duration, from 1 to 16 hours. This allowed us to correlate the adsorbed amount of heavy metals on the membrane surface with the water permeability and rejection of heavy metals. To our knowledge, this is the first investigation that reports the correlation between membrane performance and the adsorption of heavy metals and provides insight into the role of heavy metal ions on the separation performance of adsorptive membranes.

5.3 Experimental Section

5.3.1 Materials

Poly(sulfone) ultrafiltration membranes (PS35) with a molecular weight cutoff of 20 kDa were donated by Solecta, California, USA. The monomers, piperazine (PIP, 99% purity), trimesoyl chloride (TMC, >98% purity), and the organic solvent, n-hexane (>99% purity), were purchased from Sigma-Aldrich (Mississauga, Canada). The spray-dried powder form of the sulphate sodium salt of CNCs was donated by CelluForce Inc. (Windsor, Quebec). The CNCs' sulphate half-ester content was 249 mmol/kg CNC. Copper (II) sulphate pentahydrate ($CuSO_4 \cdot 5H_2O$), lead (II) nitrate ($Pb(NO_3)_2$), magnesium sulphate ($MgSO_4$), and bovine serum

albumin (BSA) were all laboratory grades and purchased from Sigma-Aldrich (Mississauga, Canada). HCl, KCl and NaOH were procured from Fisher Scientific (Mississauga, Canada). Distilled deionized water (DDW) was used to make the aqueous PIP solution, and distilled water (DW) was used to wash the membranes and prepare the synthetic water feed solutions. All materials were used as received without further purification/modification except for the CNCs, which were functionalized with acetyl groups (ACNC) and L-cysteine (CysCNC) using a solvent-free method. Details of the functionalization of CNCs are described elsewhere [36,37].

5.3.2 TFC and TFN membrane synthesis

A PS35 membrane was used as the support to synthesize the PA layer by in-situ interfacial polymerization. 0.1 wt% of unmodified CNC, ACNC, or CysCNC dried powder was added to the TMC/n-hexane solution and stirred until the CNC or modified CNC aggregates were no longer visible (typically, 30-40 min). Details of the membrane fabrication are described elsewhere [36]. The membranes were carefully washed and stored in DDW at ambient temperature until they were tested.

5.3.3 Membrane characterization

The zeta potential of the membrane surface was measured using a zeta analyzer (Zetasizer PSS0012-22, Malvern Instruments) with a frontal electrophoretic light scattering method. The Zetasizer was equipped with an adjustable gap cell to measure membrane surface charge. 1 mM of KCl solution was used as the background electrolyte, with its pH adjusted using a 0.1 M HCl or 0.1 M NaOH solution. The sessile water contact angles of the membrane surfaces were measured using a VCA Optima surface analysis system (AST Products, Inc., Billerica, MA). At least 20 droplets (2 μL) of deionized water over at least seven different locations on each sample were tested at ambient temperature. Energy dispersive X-ray (EDX) spectroscopy was employed to identify the chemical elements contained in the membrane. The heavy metal adsorption on the membranes (mg/cm^2) was measured using inductively coupled plasma emission mass spectrometry (ICP-MS, Agilent 7900).

5.3.4 Membrane performance

The NF performance of the membranes was evaluated using a continuous crossflow system consisting of three membrane cells arranged in parallel, each with an effective surface area for permeation (A_p) of 17.35 cm^2. Before the tests with heavy metal salts, the membranes were

pre-compacted with pure water for at least 1 h at 10 ±1 bar and 295 ±1 K. After reaching a steady permeate flux, concentrated solutions of $CuSO_4 \cdot 5H_2O$ and $Pb(NO_3)_2$ were added to the feed tank (14 L) to make the 200 ppm salt solution. The content in the feed tank was mixed for 30 min using a mechanical stirrer before the feed solution was circulated into the membrane cells. The feed flow rate was maintained at 2.4 ± 0.2 L/min to minimize the concentration polarization and achieve near-zero recovery [38]. The measurements were conducted at 295 ± 1 K and a hydraulic pressure of 10 ± 1 bar. The membranes were characterized in terms of water permeability, A (L/m^2.h.bar), and solute rejection, R, where

$$A = \frac{J_w}{\Delta P - \Delta \pi} \tag{5.1}$$

ΔP is the applied hydraulic pressure (bar), and $\Delta \pi$ is the difference in osmotic pressures (bar) between the feed and permeate, which was negligible. The water flux, J_w (L/m^2.h), was calculated based time t required to collect 10 cm^3 of permeate (V_p):

$$J_w = \frac{V_p}{A_p t} \tag{5.2}$$

The solute rejection was calculated from the:

$$R = 1 - \frac{C_p}{C_f} \tag{5.3}$$

C_p and C_f are solute concentrations in the permeate and feed, respectively. For the test with heavy metal salts, C_p and C_f represent the concentrations of the respective heavy metal determined from 10 mL samples using the ICP-MS analysis. The theoretical concentration of Cu^{2+} and Pb^{2+} in the 200 ppm aqueous salt solutions were 50.9 ppm and 125.1 ppm, respectively.

Regular membrane performance tests with heavy metal salts were carried out for 16 hours, and the permeate samples to determine J_w and C_p were collected every hour. Because of the large volume of the feed solution (14 L), C_f remained practically constant during the entire test, very close to the theoretical concentrations of the heavy metals listed above. The reported A and R represent the average value from at least three independent tests using a given membrane type.

One of the critical objectives of this study was to correlate A and R with the amount of heavy metal adsorbed by the membrane. The latter could only be measured after finishing the performance tests. Therefore, in addition to the regular 16-hour tests, we performed shorter experiments of 1, 2, 4, 6, 8, 12 and 14 hours. After the tests, the membranes were dried and analyzed using ICP-MS. The entire permeation area of the membranes, i.e., 17.35 cm^2, was

sent for elemental analysis. In addition, the contact angle and zeta potential of some used membranes were measured. ICP-MS, zeta potential and contact angle measurements were performed using at least three coupons of a given type of membrane tested for a specific time.

5.4 Results and discussion

Detailed TFC, CNC-TFN, ACNC-TFN and CysCNC-TFN membrane characterizations were presented in a recent publication [36]. Below, we summarize the key results from that study. ATR-FTIR analysis confirmed successful PA layer formation in the TFC and TFN membranes. The CysCNC-TFN membrane showed a negative zeta potential; however, it was less negative than the TFC membranes because of the positively charged NH_2 and SH groups in the CysCNCs. The lower absolute zeta potential for CysCNC-TFN coincided with the smaller pore size, narrower pore size distribution, and higher degree of crosslinking compared to the TFC, CNC-TFN and ACNC-TFN membranes. Because of the hydrophilicity of the NH_2 and SH groups in the CysCNCs, the CysCNC-TFN membranes were more hydrophilic than the TFC, CNC-TFN and ACNC-TFN membranes.

5.4.1 Adsorption of heavy metals during the performance tests

The adsorption of heavy metals by the membranes is usually determined in batch experiments. More specifically, a membrane sample is immersed in a known concentration and volume of a heavy metal solution, which is then agitated using a magnetic stirrer, and the heavy metal concentration in the solution is monitored [39]. A similar method is used to study the leaching of nanoparticles in TFN membranes [40]. Alternatively, the adsorption of heavy metals by the membranes can be directly measured by analyzing membrane samples after different exposure times to heavy metal solutions in batch tests [41]. We used the latter approach in the current study, except the membranes were exposed to heavy metal solutions in actual NF performance tests of different durations. To our knowledge, this approach has not been used previously in investigating NF membrane performance in the presence of heavy metals in the feed solution.

Figure 5.1 presents the concentration of Cu (Figure 5.1a) and Pb (Figure 5.1b) on the membranes after different-length performance tests ranging from 1 to 16 hours. In all cases, the concentration of heavy metals on the membranes increased in the first 12 hours. However, the most notable increases occurred during the first 8 hours, and in some cases, the heavy metal concentration remained practically constant afterwards. A constant heavy metal concentration

after 8 or 12 h indicates the equilibrium adsorption point, referred to as the adsorption capacity. Table B.1 summarizes the results shown in Figure 5.1, where we compare Cu and Pb's "initial" and final concentrations for different membranes. The actual initial concentrations were probably nil, but the "initial concentrations" in Table 5.1 represent the average from the first two tests (i.e., at 1 h and 2 h). The final concentrations (i.e., the adsorption capacity) in Table B.1 are the average values of the last three readings (i.e., 12, 14 and 16 h). In addition to the absolute values, we report the percentage increase in the heavy metal concentrations between the "initial" and final values.

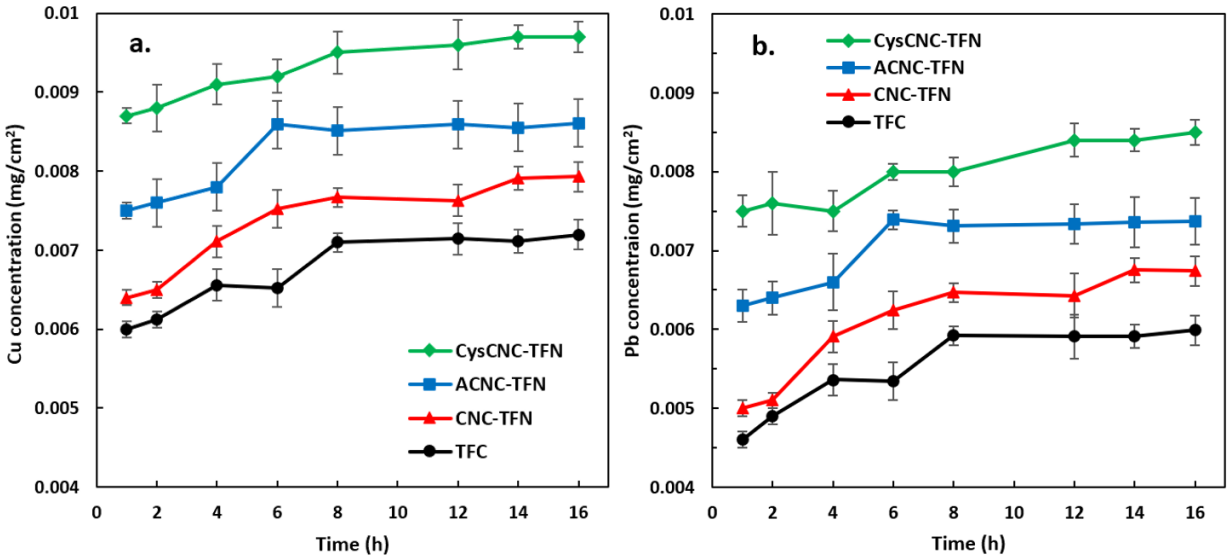

Figure 5.1: The concentration of adsorbed a) Cu and b) Pb by the TFC and TFN membranes at the end of different duration performance tests.

Table 5.1: Summary of the analysis of Cu^{2+} and Pb^{2+} adsorption on TFC and TFN membranes.

Heavy metal concentration (mg/cm²)	**Membrane**			
	TFC	**CNC-TFN**	**ACNC-TFN**	**CysCNC-TFN**
Initial* Cu	0.0061±0.0001	0.0064±0.0003	0.0075±0.0002	0.0086±0.0002
Final** Cu	0.0072±0.0003	0.0079±0.0001	0.0086±0.0002	0.0097±0.0003
*Cu Increase**** (%)	*18*	*23*	*15*	*13*
Initial* Pb	0.0046±0.0001	0.0051±0.0001	0.0062±0.0002	0.0075±0.0003
Final** Pb	0.0059±0.0003	0.0067±0.0002	0.0073±0.0002	0.0085±0.0001
*Pb Increase**** (%)	*28*	*31*	*18*	*13*

*Initial concentration = average after 1- and 2-hour tests
**Final (equilibrium) concentration = average after 12- 14- and 16-hour tests
***Increase = (Final – Initial)/Initial

Considering the adsorption capacities of the membranes for Cu and Pb, regardless of the membrane type, the concentration of adsorbed Cu was greater than that of Pb. The adsorption of heavy metals by the membranes may occur by different mechanisms, for example, complexation and electrostatic interactions [42]. The adsorption of the metal ion depends on its hydrated radius and hydration energy. Generally, the lower the ion's hydrated radius and hydration energy, the higher its adsorption [43]. The hydrated radius and the hydration energy of Cu^{2+} are 4.01 Å and -2099 kJ·mol^{-1}, respectively. The corresponding values for Pb^{+2} are 4.28 Å and -2238 kJ·mol^{-1}, respectively. The differences between the hydrated radius and the hydration energies of Cu^{2+} and Pb^{2+} are consistent with the final concentrations of Cu and Pb on the membranes. The adsorption of the metal ions also depends on the ion's electronegativity. The higher the electronegativity, the higher the adsorption. The electronegativity of Cu^{2+} and Pb^{2+} is 2.20 and 1.91, respectively, or in terms of Pauling units, 1.90 and 1.65, respectively, which is consistent with the higher adsorption capacity of the membranes for Cu compared to Pb [44]. It is important to emphasize that a higher final concentration of Cu compared to Pb on the membranes occurred despite the lower concentration in the feed solution (50.9 ppm versus 125.1 ppm).

For a given ion, the final concentration depends on the membrane type. According to Figure 5.1 and Table 5.1, the adsorption capacity increases in the following order: TFC < CNC-TFN < ACNC-TFN < CysCNC-TFN. The surface charge of all TFC and TFN membranes was negative [36], which explains the adsorption of Cu^{2+} and Pb^{2+} on the membrane surfaces by electrostatic attraction. However, the electrostatic attraction cannot explain the order of the observed adsorption capacities. The higher adsorption capacity of the CNC-TFN membranes compared to the control TFC membranes is due to the high density of negatively charged hydroxyl (–OH) groups on the CNCs, which have the potential to interact with the different heavy metal ions through complexation [42]. However, if the concentration of –OH groups was the determining factor, the adsorption capacity of the CNC-TFN membranes would be greater than that of the ACNC-TFN and CysCNC-TFN membranes, but this was not the case. The divalent Cu^{2+} and Pb^{2+} have a high affinity to oxygen-based groups, where the adsorption may occur due to electron sharing between oxygen atoms in these groups and the heavy metal ions. This is likely why the final adsorption capacity of the ACNC-TFN membranes was greater than that of the CNC-TFN membranes. On the other hand, the highest adsorption capacity of the CysCNC-TFN membranes was probably due to the thiol (-SH) groups in L-cysteine. More

specifically, sulphur-containing groups have a highly polarizable donor center that can react strongly with the orbitals of weak Lewis acids, such as heavy metal ions [39].

Despite the highest adsorption by the CysCNC-TFN membranes, the percentage increases between the initial and the final concentrations of Cu and Pb were the lowest for these membranes. Specifically, for both Cu^{2+} and Pb^{2+}, the percentage increases between the heavy metals' initial and final concentrations increased in the following order: CysCNC-TFN < ACNC-TFN < TFC < CNC-TFN. This order was strongly affected by the "initial" concentration of the heavy metal ions on the membranes. As previously stated, the "initial" concentrations represent the averages from the first two experiments (i.e., 1 and 2 h). Assuming that the actual initial concentration of heavy metals, i.e., before the test, was zero, the combined highest "initial concentration" and the lowest percentage increase in Table B.1 might indicate the fastest adsorption kinetics of heavy metals by the CysCNC-TFN membranes.

5.4.2 The effect of heavy metal adsorption on membrane properties

The ICP-MS analysis of the membranes after different duration performance tests discussed in the previous section provides direct proof that the membranes adsorbed Cu^{2+} and Pb^{2+}. Moreover, this analysis concluded that equilibrium adsorption of heavy metal ions was reached between 8 – 12 hours of exposing the membranes to the feed solutions containing heavy metal ions. To confirm the order of heavy metal adsorption by different membranes, EDX spectroscopic analysis of the membranes after a 16-hour performance test was conducted, i.e., after reaching the equilibrium adsorption capacity. Figure 5.2 summarizes the EDX spectroscopic analysis of the membranes tested with a 200 ppm aqueous solution of $CuSO_4 \cdot 5H_2O$.

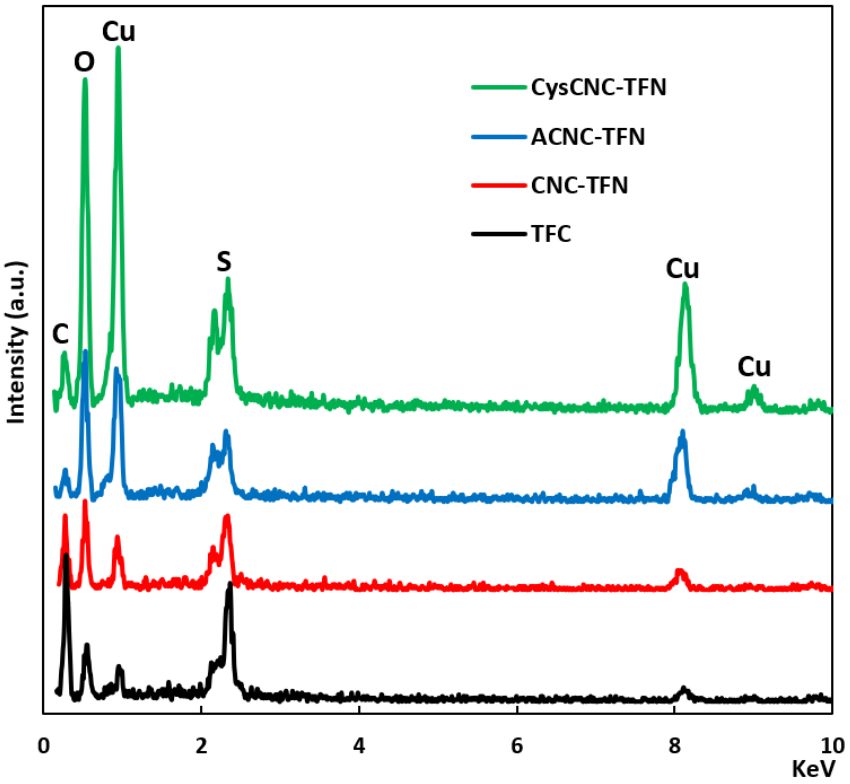

Figure 5.2: EDX spectra of TFC and TFN membranes after a 16-hour performance test of Cu^{2+} rejection.

The Cu peaks appeared at 1.21, 8.03 and 8.90 KeV positions for all membranes [45]. The intensity of the Cu peaks increased in the following order: TFC < CNC-TFN < ACNC-TFN ≈ CysCNC-TFN. This order is similar to that of the adsorption capacities of the membranes, except for the similar intensities of the Cu peaks for ACNC-TFN and CysCNC-TFN membranes. It is important to emphasize that the peak at 2.61 KeV, related to sulphur [46], appeared in all spectra in Figure 5.2. It was most likely due to the sulphur of the polysulfone support. Sulphur was also present in the half-ester sulphate groups of the CNCs. However, given the relatively low loading of nanoparticles in the TFN membranes, the sulphur from the CNCs was unlikely to have contributed significantly to the 2.61 KeV peaks. The same applies to the sulphur from the L-cysteine in the CysCNC-TFN membrane.

We also performed EDX spectroscopic analyses for the membranes after the tests with $Pb(NO_3)_2$ in the feed solution. However, the Pb peak overlapped with the S peak of the membranes, so it was impossible to distinguish the Pb peak from the S peak [47].

The adsorbed heavy metals should change the surface properties of the membranes, such as contact angle and zeta potential. These changes, if any, provide indirect proof of the adsorption of heavy metal ions from the feed solution by the membranes. Therefore, the samples from the membranes tested in different duration experiments were also analyzed using

the contact angle and zeta potential measurements. Figures 5.3 and 5.4 demonstrate the surface contact angle and zeta potential after the different duration experiments. Figures 3a and 4a show these properties after the tests with $CuSO_4 \cdot 5H_2O$ in the feed solution and Figures 5.3b and 5.4b after the tests with $Pb(NO_3)_2$ in the feed solution. The figures include the initial properties of the membrane (i.e., before exposing the membranes to heavy metal ions in the performance tests). Each point in Figures 5.3 and 5.4 represents the average from at least three membrane coupons, and the error bars represent the corresponding two standard deviations. Regardless of the membrane type and heavy metal salt in the feed solution, the contact angle decreased (Figure 5.3) while the zeta potential increased (Figure 5.4) with experiment duration. The changes in zeta potential with time appear to be greater than those in contact angle but not as large as the corresponding changes in the concentration of the adsorbed heavy metals (Figure 5.1). To quantify the above statement, Table 5.2 summarizes the results from Figures 5.3 and 5.4, showing the average values measured for the new (fresh) membranes, the average values after the three most extended tests (12, 14 and 16 h), and the percentage change of the properties relative to the corresponding properties of the new membranes. Selecting the three most extended experiments to calculate the final average values is fully justified by Figures 5.3 and 5.4. The negative percentage change for the contact angles indicates its decrease with experiment duration. However, because the initial values were negative for the zeta potential, the negative percentage change indicates an increase in zeta potential with time.

The most remarkable observation when comparing Figures 5.3 and 5.4 with Figure 5.1 is the similarity of the trends even though the magnitudes of the property changes are different. Also, for a given membrane, the change in the property (contact angle, zeta potential) is greater after the tests with $CuSO_4 \cdot 5H_2O$ than $Pb(NO_3)_2$, which is consistent with a higher adsorption capacity of the respective membranes for Cu^{2+} than Pb^{2+}. This provides solid evidence that the observed changes in the membranes' contact angles and zeta potentials are directly linked to the adsorption of Cu^{2+} and Pb^{2+} by the membranes. In other words, Figures 3 and 4 further prove that heavy metal ions from the respective feed solutions were adsorbed during the performance tests.

Hydrated divalent positive ions, such as Cu^{2+} and Pb^{2+}, when adsorbed on a solid surface, produce strong hydration forces, which result in greater attraction of water molecules and hence increased hydrophilicity [48]. This explains a decrease in contact angle with the exposure time to the feed solution containing heavy metal ions. At the same time, the adsorption of Cu^{2+} and Pb^{2+} explains a decrease in the negativity of the surface zeta potential

of the membranes. However, the orders of the percentage changes of the zeta potentials and contact angles are different and generally do not correspond to the adsorption capacities of the membranes for Cu^{2+} and Pb^{2+}.

Table 5.2: Summary of the water contact angle and zeta potential analysis of TFC and TFN membranes before and after Cu^{2} and Pb^{2+} rejection.

Contact angle (º)	**Membrane**			
	TFC	**CNC-TFN**	**ACNC-TFN**	**CysCNC-TFN**
Fresh*	48.1±2.4	28.3±3.0	35.1±3.2	24.6±3.0
Final** Cu	43.2±3.1	26.1±2.6	33.8±2.8	21.4±3.2
% *Change**** Cu	*-10.2*	*-7.77*	*-3.70*	*-13.0*
Final** Pb	45.1±2.6	26.7±2.8	34.2±3.5	23.5±2.9
% *Change**** (%) Pb	*-6.24*	*-5.65*	*-2.56*	*-4.47*
Zeta potential (mV)	**TFC**	**CNC-TFN**	**ACNC-TFN**	**CysCNC-TFN**
Fresh *	-11.1	-16.5	-14.3	-13.2
Final** Cu	-9.30	-14.8	-10.8	-8.80
% *Change**** Cu	*-16.2*	*-10.3*	*-24.5*	*-33.3*
Final** Pb	-10.5	-15.2	-11.4	-10.2
% *Change**** (%) Pb	*-5.41*	*-7.88*	*-20.3*	*-22.7*

*Fresh = value obtained for the fresh membrane
**Final = average after 12- 14- and 16-hour tests
***Increase = (Final – Fresh)/Fresh

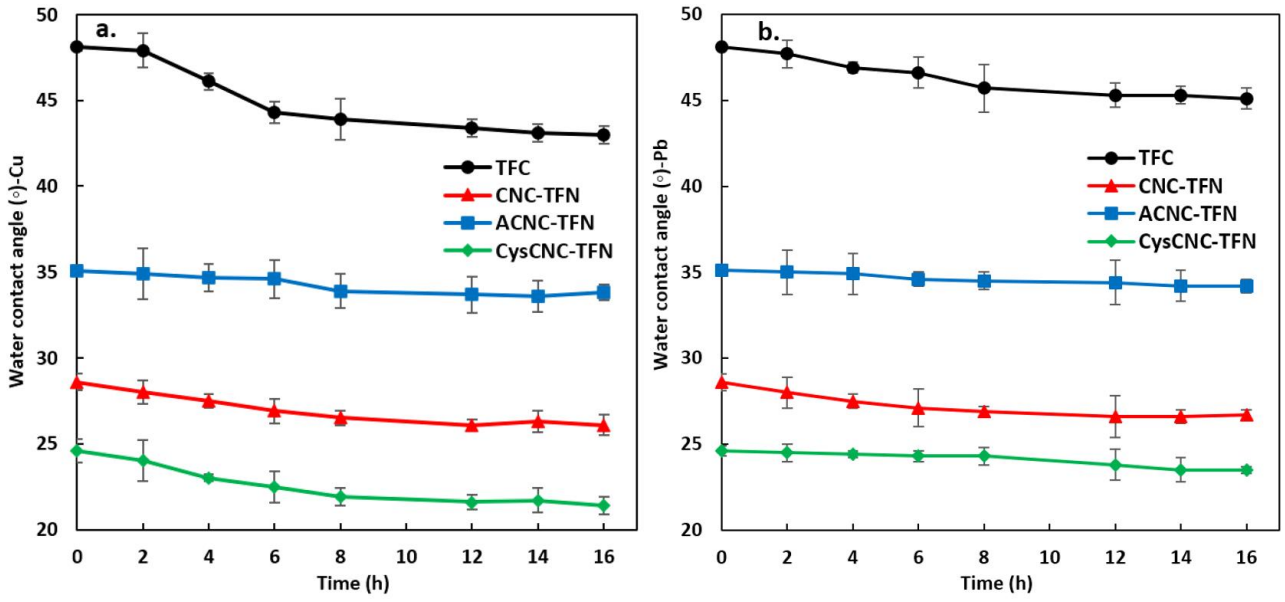

Figure 5.3: The contact angles of membranes at the end of different duration tests with heavy metal ions in the feed solutions. a) Cu^{2+}, b) Pb^{2}.

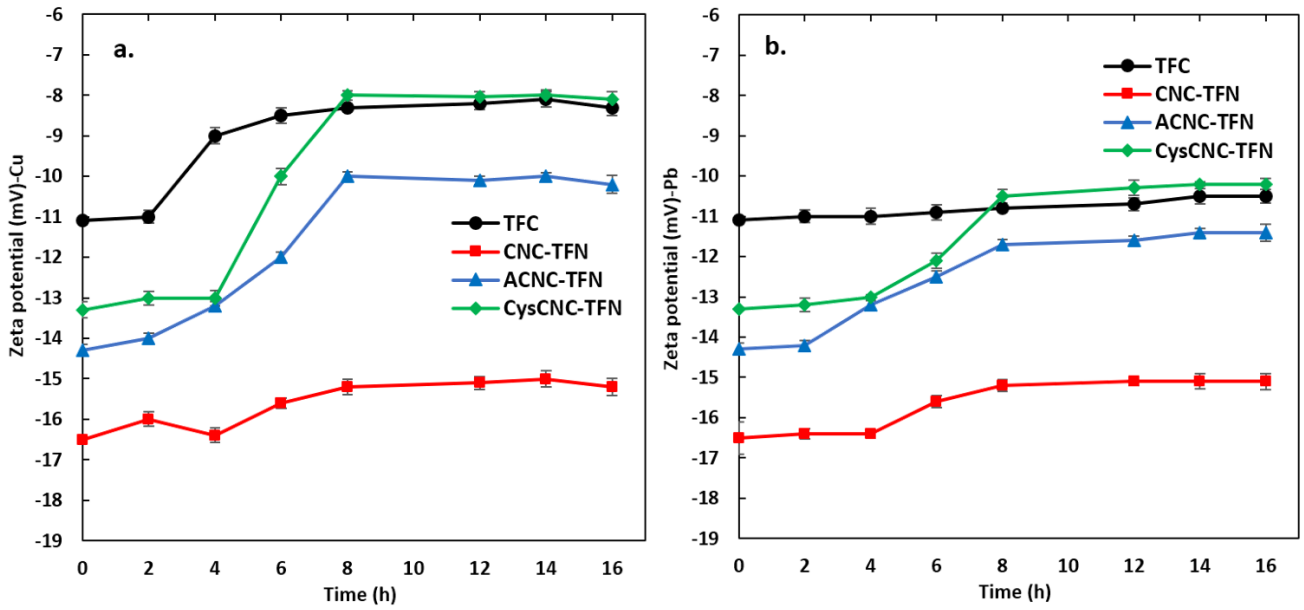

Figure 5.4: The zeta potential of TFC and TFN membranes at the end of different duration tests a) Cu^{2+} and b) Pb^{2+} rejection.

5.4.3 The effect of heavy metal adsorption on membrane performance

We have shown that the membranes adsorb Cu^{2+} and Pb^{2+} from the feed solution during the performance tests and that the membranes' corresponding contact angles and zeta potentials change accordingly. The ultimate question arises, does the adsorption of heavy metals affect membrane performance? Figures 5.5 and 5.6 show the water permeability and heavy metal rejection as a function of time during continuous 16-hour experiments. Figures 5.5a and 5.6a show these properties in the tests with $CuSO_4 \cdot 5H_2O$ in the feed solution and Figures 5.5b and 5.6b in the tests with $Pb(NO_3)_2$ in the feed solution. Each point in Figures 5 and 6 represents the average from at least three independent experiments, and the error bars are the corresponding two standard deviations. Table 5.3 summarizes the results shown in Figures 5.5 and 5.6. The initial water permeabilities and rejections in Table 5.1 represent the first reading after 1 hour from the initiation of the experiment. The final water permeabilities and rejections are the average values of the last 4 hours of the respective experiments. However, as shown in Figures 5.5 and 5.6, the water permeabilities and solute rejections appeared to reach constant values after 4 hours. The final properties were similar, whether based on the last 4 hours (12 – 16 h) or after 4 hours of the experiment (4 – 16 h). In addition, similarly to Tables 5.1 and 5.2, Table 5.3 reports the percentage increase from the initial to the final water permeabilities and solute rejections.

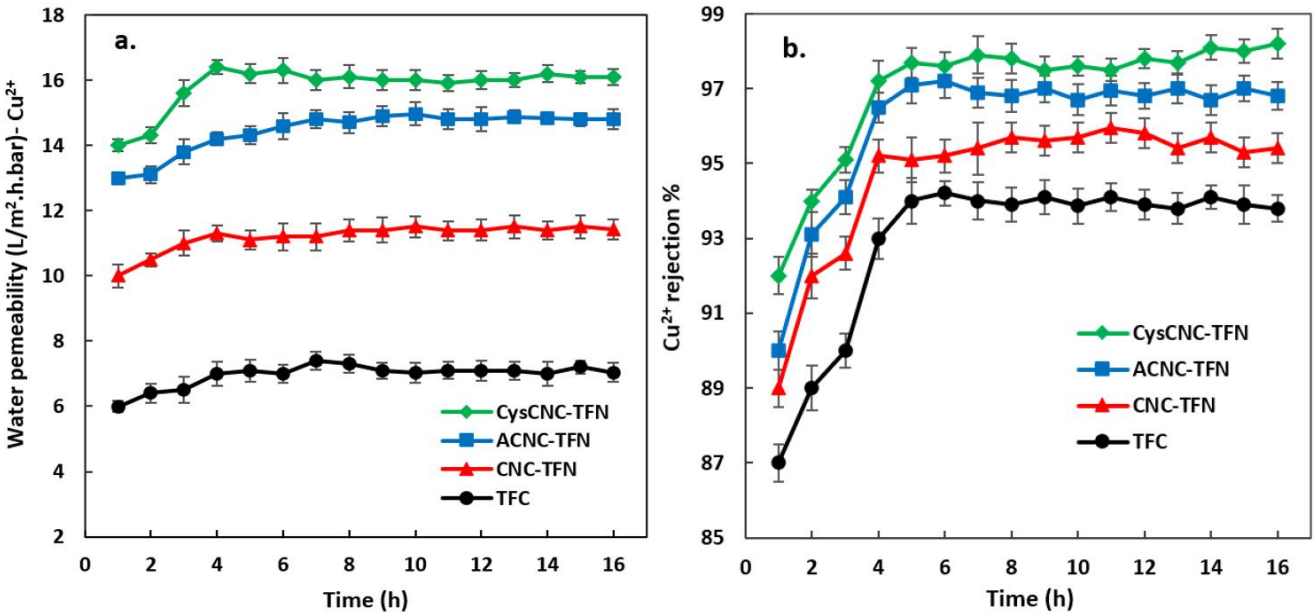

Figure 5.5: a) Water permeability and b) Cu^{2+} rejection during 16-hour performance tests for TFC, CNC-TFN, ACNC-TFN and CysCNC-TFN membranes.

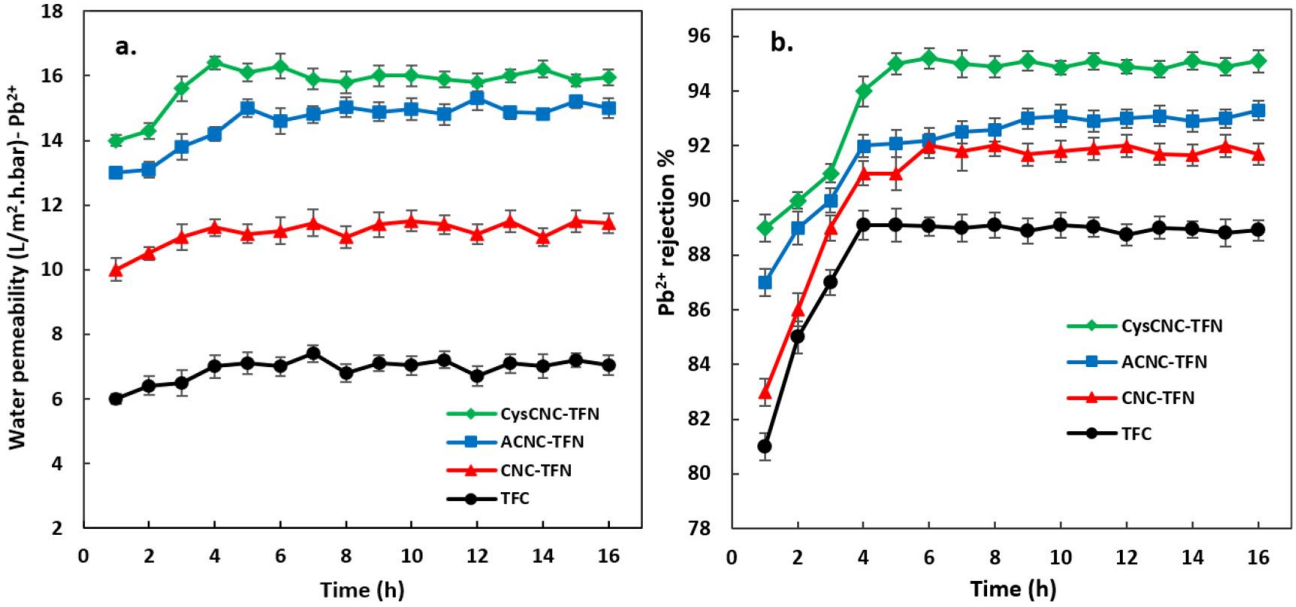

Figure 5.6: a) Water permeability and b) Pb^{2+} rejection during 16-hour performance tests for TFC, CNC-TFN, ACNC-TFN and CysCNC-TFN membranes.

Regardless of the membrane type and the heavy metal salt in the feed solution, the water permeability and solute rejection increased with time and reached a plateau, as indicated above, after 4 hours. The most remarkable result was that despite reaching the equilibrium adsorption capacity, the membranes' water permeability and solute rejection did not decrease but remained constant. It should be emphasized, though, that the stable performance of the membranes was attained faster than the heavy metal adsorption equilibrium and the membranes' final contact

angle and zeta potential. The fact that the water permeability and solute rejection did not decrease after reaching adsorption equilibrium indicates that the adsorption of heavy metals did not contribute directly to solute rejection; it contributed indirectly by changing membrane properties as evidenced by a decrease in the surface contact angle and increase in the zeta potential. In other words, although the membranes in this study, particularly TFNs, can be considered to be adsorptive membranes, their performance, particularly solute rejection, does not rely on the adsorption phenomenon but instead on Donnan potential and size exclusion, which govern the rejection properties of NF membranes.

An increase in solute rejection might appear more significant than an increase in water permeability; however, it is because of the water permeability and the solute rejection scales. Considering the percentage changes in Table 5.3, the increase in water permeability was greater than that in solute rejection. Although the adsorption capacity for Cu^{2+} by the membranes was greater than that for Pb^{2+} (Table 5.1), the type of heavy metal ion in the feed solution did not appear to affect the percentage increase in the water permeability and solute rejection of the membranes. The final water permeabilities of the membranes were also not affected by the heavy metal ion, but the final solute rejections were greater for Cu^{2+} (up to 98%) than for Pb^{2+} (up to 95%). The higher rejections of Cu^{2+} than Pb^{2+} were likely due to the higher valency of SO_4^{2-} compared to NO_3^-. As indicated by the zeta potential measurements, TFC and TFN membranes are negatively charged, which leads to the repulsion of negatively charged ions according to their valency. At the same time, the feed solution should have maintained its electroneutrality.

There is no clear trend between the membrane type and the percentage increase in the water permeability and solute rejection. However, the membrane type strongly affects the order of the final water permeabilities, i.e., TFC < CNC-TFN < ACNC-TFN < CysCNC-TFN. The most permeable CysCNC-TFN membranes had an average final water permeability near 19 $L \cdot m^{-2} \cdot h^{-1} \cdot bar^{-1}$, which was 13% greater than the initial water permeability (i.e., after 1 hour). The adsorption of heavy metals did not change the order of water permeabilities and solute rejections by the membranes. In other words, the initial and final orders of water permeabilities and solute rejections were the same. Moreover, the water permeabilities and solute rejection orders were the same, i.e., TFC < CNC-TFN < ACNC-TFN < CysCNC-TFN. The same order of water permeabilities and solute rejection is desirable as it overcomes the trade-off between membrane productivity and selectivity. Overcoming the trade-off between membrane productivity and selectivity in this study resulted from intelligent modifications of the CNC

nanoparticles, which improved their dispersibility in the TMC monomer solution before the interfacial polymerization with the PIP monomer solution [36].

Table 5.3: Summary of the water permeability and rejection of TFC and TFN membranes before and after the Cu^{2+} and Pb^{2+} rejection.

Water permeability ($L \cdot m^{-2} \cdot h^{-1} \cdot bar^{-1}$)	**Membrane**			
	TFC	**CNC-TFN**	**ACNC-TFN**	**CysCNC-TFN**
Initial* Cu	6.0	10.0	13.0	14.0
Final** Cu	6.8	11.3	14.8	16.0
% *Change**** Cu	*13.3*	*13.0*	*13.9*	*14.3*
Initial* Pb	6.1	10.0	13.0	14.0
Final** Pb	6.5	11.5	15.0	18.8
% *Change**** Pb	*6.6*	*15.0*	*15.4*	*12.9*
Rejection (%)	**TFC**	**CNC-TFN**	**ACNC-TFN**	**CysCNC-TFN**
Initial* Cu	87.0	89.0	90.0	92.0
Final** Cu	94.0	95.0	97.0	98.0
% *Change**** Cu	*8.1*	*6.7*	*7.8*	*6.5*
Initial* Pb	81.0	83.0	87.0	89.0
Final** Pb	88.8	91.6	93.0	95.0
% *Change**** Pb	*9.6*	*10.4*	*6.9*	*6.7*

*Initial = after 1 h
**Final = average from 12-16 h
***Change = (Final – Initial)/Initial

The increases in water permeability and solute rejection were consistent with the corresponding increase in membrane hydrophilicity and increase in zeta potential (the zeta potential becoming less negative), which were attributed to the adsorption of the heavy metal by the membranes. An increase in water permeability could be expected because membrane hydrophilicity is known to enhance water permeability [3]. On the other hand, an increase in solute rejection with increasing the zeta potential, i.e., with zeta potential becoming less negative, might be surprising. On the one hand, the lesser negative surface charge will lead to less repulsion of the negative counter ions and, thus, lower rejection. On the other hand, at a pH of 6, maintained in the feed solution, heavy metals can also form hydroxides (e.g., MOH^+ or $M(OH)_2$ in addition to the basic iconic form (M^{2+})[43]. These metal hydroxides might be sufficiently large to be rejected by the size exclusion principle. Although the overall surface charge density remains negative, the adsorption of heavy metals may lead to local regions with positive surface charges. In these regions, electrostatic repulsion might also contribute to rejecting heavy metal ions and hydroxides [19]. The higher equilibrium adsorption of heavy metal might indicate the presence of more positively charged regions (consistent with the zeta potential being less negative) where the repulsion of positively charged metal ions and

hydroxides may overcompensate a decreased rejection based on the repulsion of negatively charged counterions.

5.5 Conclusion

We have experimentally examined the role of heavy metal ions in a feed solution on their rejection and water permeability of TFC and TFN membranes. We performed NF experiments of different duration ranging from 1 to 16 h. At the end of each experiment, the concentration (i.e. adsorption) of heavy metals (Cu or Pb) on the membrane was determined using ICP-MS analysis. We also measured the contact angle and the zeta potential on the tested membranes. This allowed us to correlate the changes in the concentration of heavy metals on the membranes with their zeta potential and contact angle changes. More importantly, the developed experimental protocol allowed us to correlate time-dependent changes in the water permeability and heavy metal rejection with their adsorption during the actual performance experiments. The membranes used in this study, CNC-TFN, ACNC-TFN and CysCNC-TFN, could be considered adsorptive because of the electrostatic attraction between Cu^{2+} and Pb^{2+} with negatively charged membrane surfaces and electron sharing between different atoms of functional groups of nanoparticles and the heavy metal ions. The control TFC membrane can also be considered adsorptive because of its negative surface charge density.

The equilibrium adsorption of heavy metal ions by the membranes was reached after 8 – 12 hours during continuous performance tests, and the adsorption capacity depended on the metal ion (Cu^{2+} > Pb^{2+}) and the membrane type: TFC < CNC-TFN < ACNC-TFN < CysCNC-TFN. The adsorbed heavy metals decreased the surface contact angle (increased membrane hydrophilicity) and increased zeta potential (zeta potential became less negative). For all membranes, an increase in heavy metal concentration on the membranes was associated with a desirable simultaneous increase in water permeability and heavy metal rejection. The membrane performance remained stable after reaching the adsorption capacity for the heavy metals. This indicates that the adsorption phenomenon did not contribute directly to the rejection of heavy metal ions, and the combination of electrostatic repulsion and size exclusion govern solute rejection by the membranes considered in this study. Consequently, membrane regeneration after reaching the absorption capacity is not necessary. Moreover, it would be undesirable because the adsorbed heavy metals improve the membrane performance. Therefore, the adsorption of heavy metals on the surface of nanofiltration membranes appears to be a "blessing" rather than a "curse".

5.6 References

[1] Z. Samavati, A. Samavati, P.S. Goh, A. Fauzi Ismail, M. Sohaimi Abdullah, A comprehensive review of recent advances in nanofiltration membranes for heavy metal removal from wastewater, Chemical Engineering Research and Design. 189 (2023) 530–571. https://doi.org/10.1016/j.cherd.2022.11.042.

[2] V. Kumar, S.K. Dwivedi, S. Oh, A critical review on lead removal from industrial wastewater: Recent advances and future outlook, Journal of Water Process Engineering. 45 (2022) 102518. https://doi.org/10.1016/j.jwpe.2021.102518.

[3] A.M. Nasir, P.S. Goh, M.S. Abdullah, B.C. Ng, A.F. Ismail, Adsorptive nanocomposite membranes for heavy metal remediation: Recent progresses and challenges, Chemosphere. 232 (2019) 96–112. https://doi.org/10.1016/j.chemosphere.2019.05.174.

[4] D. Yadav, S. Karki, P.G. Ingole, Current advances and opportunities in the development of nanofiltration (NF) membranes in the area of wastewater treatment, water desalination, biotechnological and pharmaceutical applications, Journal of Environmental Chemical Engineering. 10 (2022) 108109. https://doi.org/10.1016/j.jece.2022.108109.

[5] Y. Zhao, T. Tong, X. Wang, S. Lin, E.M. Reid, Y. Chen, Differentiating Solutes with Precise Nanofiltration for Next Generation Environmental Separations: A Review, Environ. Sci. Technol. 55 (2021) 1359–1376. https://doi.org/10.1021/acs.est.0c04593.

[6] R. Castro-Muñoz, L.L. González-Melgoza, O. García-Depraect, Ongoing progress on novel nanocomposite membranes for the separation of heavy metals from contaminated water, Chemosphere. 270 (2021) 129421. https://doi.org/10.1016/j.chemosphere.2020.129421.

[7] L. Qalyoubi, A. Al-Othman, S. Al-Asheh, Recent progress and challenges on adsorptive membranes for the removal of pollutants from wastewater. Part I: Fundamentals and classification of membranes, Case Studies in Chemical and Environmental Engineering. 3 (2021) 100086. https://doi.org/10.1016/j.cscee.2021.100086.

[8] J.M. Gohil, P. Ray, A review on semi-aromatic polyamide TFC membranes prepared by interfacial polymerization: Potential for water treatment and desalination, Separation and Purification Technology. 181 (2017) 159–182. https://doi.org/10.1016/j.seppur.2017.03.020.

[9] F. Abedi, B. Kruczek, M.A. Dubé, Cellulose nanocrystal addition in thin film nanocomposite membranes: Which monomer solution is preferred?, Can J Chem Eng. (2023) cjce.25032. https://doi.org/10.1002/cjce.25032.

[10] S. Tul Muntha, A. Kausar, M. Siddiq, Advances in Polymeric Nanofiltration Membrane: A Review, Polymer-Plastics Technology and Engineering. 56 (2017) 841–856. https://doi.org/10.1080/03602559.2016.1233562.

[11] T. Mu, H.-Z. Zhang, J.-Y. Sun, Z.-L. Xu, Three-channel capillary nanofiltration membrane with quaternary ammonium incorporated for efficient heavy metals removal, Separation and Purification Technology. 248 (2020) 117133. https://doi.org/10.1016/j.seppur.2020.117133.

[12] Z. Wang, X. You, C. Yang, W. Li, Y. Li, Y. Li, J. Shen, R. Zhang, Y. Su, Z. Jiang, Ultrathin polyamide nanofiltration membranes with tunable chargeability for multivalent cation removal, Journal of Membrane Science. 642 (2022) 119971. https://doi.org/10.1016/j.memsci.2021.119971.

[13] M.O. Akharame, O.S. Fatoki, B.O. Opeolu, Regeneration and reuse of polymeric nanocomposites in wastewater remediation: the future of economic water management, Polym. Bull. 76 (2019) 647–681. https://doi.org/10.1007/s00289-018-2403-1.

[14] S. Bason, Y. Kaufman, V. Freger, Analysis of Ion Transport in Nanofiltration Using Phenomenological Coefficients and Structural Characteristics, J. Phys. Chem. B. 114 (2010) 3510–3517. https://doi.org/10.1021/jp911615n.

[15] S. Déon, A. Escoda, P. Fievet, A transport model considering charge adsorption inside pores to describe salts rejection by nanofiltration membranes, Chemical Engineering Science. 66 (2011) 2823–2832. https://doi.org/10.1016/j.ces.2011.03.043.
[16] A.M. Saenz de Jubera, J.H. Herbison, Y. Komaki, M.J. Plewa, J.S. Moore, D.G. Cahill, B.J. Mariñas, Development and Performance Characterization of a Polyamide Nanofiltration Membrane Modified with Covalently Bonded Aramide Dendrimers, Environ. Sci. Technol. (2013) 130711065921008. https://doi.org/10.1021/es400765q.
[17] S. Bandehali, F. Parvizian, H. Ruan, A. Moghadassi, J. Shen, A. Figoli, A.S. Adeleye, N. Hilal, T. Matsuura, E. Drioli, S.M. Hosseini, A planned review on designing of high-performance nanocomposite nanofiltration membranes for pollutants removal from water, Journal of Industrial and Engineering Chemistry. 101 (2021) 78–125. https://doi.org/10.1016/j.jiec.2021.06.022.
[18] F.-Y. Zhao, Y.-L. Ji, X.-D. Weng, Y.-F. Mi, C.-C. Ye, Q.-F. An, C.-J. Gao, High-Flux Positively Charged Nanocomposite Nanofiltration Membranes Filled with Poly(dopamine) Modified Multiwall Carbon Nanotubes, ACS Appl. Mater. Interfaces. 8 (2016) 6693–6700. https://doi.org/10.1021/acsami.6b00394.
[19] A. Atashgar, D. Emadzadeh, S. Akbari, B. Kruczek, Incorporation of Functionalized Halloysite Nanotubes (HNTs) into Thin-Film Nanocomposite (TFN) Nanofiltration Membranes for Water Softening, Membranes. 13 (2023) 245. https://doi.org/10.3390/membranes13020245.
[20] T.S. Vo, M.M. Hossain, H.M. Jeong, K. Kim, Heavy metal removal applications using adsorptive membranes, Nano Convergence. 7 (2020) 36. https://doi.org/10.1186/s40580-020-00245-4.
[21] S. Hao, Z. Jia, J. Wen, S. Li, W. Peng, R. Huang, X. Xu, Progress in adsorptive membranes for separation – A review, Separation and Purification Technology. 255 (2021) 117772. https://doi.org/10.1016/j.seppur.2020.117772.
[22] J.E. Efome, D. Rana, T. Matsuura, C.Q. Lan, Experiment and modeling for flux and permeate concentration of heavy metal ion in adsorptive membrane filtration using a metal-organic framework incorporated nanofibrous membrane, Chemical Engineering Journal. 352 (2018) 737–744. https://doi.org/10.1016/j.cej.2018.07.077.
[23] S.A. Hamid, S.F. Azha, L. Sellaoui, A. Bonilla-Petriciolet, S. Ismail, Adsorption of copper (II) cation on polysulfone/zeolite blend sheet membrane: Synthesis, characterization, experiments and adsorption modelling, Colloids and Surfaces A: Physicochemical and Engineering Aspects. 601 (2020) 124980. https://doi.org/10.1016/j.colsurfa.2020.124980.
[24] S. Poolachira, S. Velmurugan, Efficient removal of lead ions from aqueous solution by graphene oxide modified polyethersulfone adsorptive mixed matrix membrane, Environmental Research. 210 (2022) 112924. https://doi.org/10.1016/j.envres.2022.112924.
[25] S. Mehanathan, J. Jaafar, A.M. Nasir, R.A. Rahman, A.F. Ismail, R.M. Illias, M.H.D. Othman, M. A Rahman, M.R. Bilad, M.N. Naseer, Adsorptive Membrane for Boron Removal: Challenges and Future Prospects, Membranes. 12 (2022) 798. https://doi.org/10.3390/membranes12080798.
[26] R. HMTShirazi, T. Mohammadi, A.A. Asadi, M.A. Tofighy, Electrospun nanofiber affinity membranes for water treatment applications: A review, Journal of Water Process Engineering. 47 (2022) 102795. https://doi.org/10.1016/j.jwpe.2022.102795.
[27] R.J.J. Chia, W.J. Lau, N. Yusof, H. Shokravi, A.F. Ismail, Adsorptive Membranes for Arsenic Removal – Principles, Progress and Challenges, Separation & Purification Reviews. (2022) 1–21. https://doi.org/10.1080/15422119.2022.2114371.

[28] H. Zhang, S. Zhu, J. Yang, A. Ma, W. Chen, Enhanced removal efficiency of heavy metal ions by assembling phytic acid on polyamide nanofiltration membrane, Journal of Membrane Science. 636 (2021) 119591. https://doi.org/10.1016/j.memsci.2021.119591.
[29] M.-Q. Ma, C. Zhang, C.-Y. Zhu, S. Huang, J. Yang, Z.-K. Xu, Nanocomposite membranes embedded with functionalized MoS2 nanosheets for enhanced interfacial compatibility and nanofiltration performance, Journal of Membrane Science. 591 (2019) 117316. https://doi.org/10.1016/j.memsci.2019.117316.
[30] Y. He, Y.P. Tang, D. Ma, T.-S. Chung, UiO-66 incorporated thin-film nanocomposite membranes for efficient selenium and arsenic removal, Journal of Membrane Science. 541 (2017) 262–270. https://doi.org/10.1016/j.memsci.2017.06.061.
[31] H.-L. Zhang, H. Cai, Y. Xia, P. Zhang, S.-W. Xiong, J.-G. Gai, An L -cystine/ L -cysteine impregnated nanofiltration membrane with the superior performance of an anchoring heavy metal in wastewater, RSC Adv. 10 (2020) 3438–3449. https://doi.org/10.1039/C9RA09380J.
[32] S. Kamari, A. Shahbazi, Biocompatible Fe3O4@SiO2-NH2 nanocomposite as a green nanofiller embedded in PES–nanofiltration membrane matrix for salts, heavy metal ion and dye removal: Long–term operation and reusability tests, Chemosphere. 243 (2020) 125282. https://doi.org/10.1016/j.chemosphere.2019.125282.
[33] S. Roy, S. Majumdar, G.C. Sahoo, S. Bhowmick, A.K. Kundu, P. Mondal, Removal of As(V), Cr(VI) and Cu(II) using novel amine functionalized composite nanofiltration membranes fabricated on ceramic tubular substrate, Journal of Hazardous Materials. 399 (2020) 122841. https://doi.org/10.1016/j.jhazmat.2020.122841.
[34] M.O. Akharame, O.S. Fatoki, B.O. Opeolu, Regeneration and reuse of polymeric nanocomposites in wastewater remediation: the future of economic water management, Polym. Bull. 76 (2019) 647–681. https://doi.org/10.1007/s00289-018-2403-1.
[35] J. Tian, H. Chang, S. Gao, R. Zhang, How to fabricate a negatively charged NF membrane for heavy metal removal via the interfacial polymerization between PIP and TMC?, Desalination. 491 (2020) 114499. https://doi.org/10.1016/j.desal.2020.114499.
[36] F. Abedi, M.A. Dubé, D. Emadzadeh, B. Kruczek, Improving nanofiltration performance using modified cellulose nanocrystal-based TFN membranes, Journal of Membrane Science. 670 (2023) 121369. https://doi.org/10.1016/j.memsci.2023.121369.
[37] F. Abedi, D. Emadzadeh, M.A. Dubé, B. Kruczek, Modifying cellulose nanocrystal dispersibility to address the permeability/selectivity trade-off of thin-film nanocomposite reverse osmosis membranes, Desalination. 538 (2022) 115900. https://doi.org/10.1016/j.desal.2022.115900.
[38] D. Carter, L. Rose, T. Awobusuyi, M. Gauthier, F.H. Tezel, B. Kruczek, Characterization of commercial RO membranes for the concentration of ammonia converted to ammonium sulfate from anaerobic digesters, Desalination. 368 (2015) 127–134. https://doi.org/10.1016/j.desal.2015.03.040.
[39] S. Hokkanen, E. Repo, T. Suopajärvi, H. Liimatainen, J. Niinimaa, M. Sillanpää, Adsorption of Ni(II), Cu(II) and Cd(II) from aqueous solutions by amino modified nanostructured microfibrillated cellulose, Cellulose. 21 (2014) 1471–1487. https://doi.org/10.1007/s10570-014-0240-4.
[40] F. Asempour, D. Emadzadeh, T. Matsuura, B. Kruczek, Synthesis and characterization of novel Cellulose Nanocrystals-based Thin Film Nanocomposite membranes for reverse osmosis applications, Desalination. 439 (2018) 179–187. https://doi.org/10.1016/j.desal.2018.04.009.
[41] X. Yang, Q. Pan, Y. Ao, J. Du, Z. Dong, M. Zhai, L. Zhao, Facile preparation of L-cysteine–modified cellulose microspheres as a low-cost adsorbent for selective and

efficient adsorption of Au(III) from the aqueous solution, Environ Sci Pollut Res. 27 (2020) 38334–38343. https://doi.org/10.1007/s11356-020-09789-8.
[42] S.S. Madaeni, E. Salehi, A new adsorption–transport and porosity combined model for passage of cations through nanofiltration membrane, Journal of Membrane Science. 333 (2009) 100–109. https://doi.org/10.1016/j.memsci.2009.02.006.
[43] M. Zhang, S. Hou, Y. Li, Y. Hou, P. Yang, Single evaluation and selection of functional groups containing N or O atoms to heavy metal adsorption: Law of electric neutrality., Chemosphere. 287 (2022) 132207. https://doi.org/10.1016/j.chemosphere.2021.132207.
[44] N.A. Fakhre, B.M. Ibrahim, The use of new chemically modified cellulose for heavy metal ion adsorption, Journal of Hazardous Materials. 343 (2018) 324–331. https://doi.org/10.1016/j.jhazmat.2017.08.043.
[45] A. Waheed, U. Baig, M.A. Ansari, Fabrication of CuO nanoparticles immobilized nanofiltration composite membrane for dye/salt fractionation: Performance and antibiofouling, Journal of Environmental Chemical Engineering. 10 (2022) 106960. https://doi.org/10.1016/j.jece.2021.106960.
[46] S. Bandehali, A. Moghadassi, F. Parvizian, Y. Zhang, S.M. Hosseini, J. Shen, New mixed matrix PEI nanofiltration membrane decorated by glycidyl-POSS functionalized graphene oxide nanoplates with enhanced separation and antifouling behaviour: Heavy metal ions removal, Separation and Purification Technology. 242 (2020) 116745. https://doi.org/10.1016/j.seppur.2020.116745.
[47] S. Bandehali, A. Moghadassi, F. Parvizian, J. Shen, S.M. Hosseini, Glycidyl POSS-functionalized ZnO nanoparticles incorporated polyether-imide based nanofiltration membranes for heavy metal ions removal from water, Korean J. Chem. Eng. 37 (2020) 263–273. https://doi.org/10.1007/s11814-019-0441-5.
[48] S. Xu, H. Lin, G. Li, J. Wang, Q. Han, F. Liu, Anionic covalent organic framework as an interlayer to fabricate negatively charged polyamide composite nanofiltration membrane featuring ions sieving, Chemical Engineering Journal. 427 (2022) 132009. https://doi.org/10.1016/j.cej.2021.132009.

6. General discussion and conclusion

6.1 General discussion

At the global level, potable water is arguably one of the most important commodities for sustainable growth and human survival [1]. Desalination has become an essential water purification technique because approximately 97% of the world's water resources are sea or brackish water [2]. Alternatively, one can treat industrial wastewater, which is usually restricted for use in agricultural and industrial applications [3]. Over the years, several technologies have been employed for water purification, such as membrane filtration, chemical precipitation, solvent extraction, ion exchange, coagulation and adsorption [4]. The development of membrane materials for water desalination and wastewater treatment using pressure-driven processes (i.e., RO and NF) are dominant [5]. Polyamide (PA) thin-film composite (TFC) membranes are the leading membranes used for RO and NF processes owing to their high robustness and durability [6,7]. PA layer is fabricated via interfacial polymerization of an amine monomer, e.g., m-phenylenediamine (MPD) for RO and piperazine (PIP) for NF and an acyl chloride monomer, e.g., trimesoyl chloride (TMC), on a porous support, e.g., polysulfone [8]. Although TFC membranes have undergone significant development, there are still challenges to optimal performance, including permeability/selectivity trade-offs, fouling and chlorine resistance [3]. There are many strategies to improve the properties of the PA layer in RO-TFN and NF-TFC membranes, including adding a comonomer, a cosolvent, PA surface modification and nanoparticle incorporation [9]. Using nanoparticles in membrane fabrication, leading to thin film nanocomposite (TFN) membranes, offers the possibility of performance improvement and overcoming the challenges noted above [10]. However, the aggregation of nanoparticles and the leaching of toxic nanoparticles downstream are two major challenges for TFN membranes' large-scale, commercial applications [11]. In this thesis, these problems were addressed by incorporating cellulose nanocrystals (CNCs) and modified CNCs into RO-TFN and NF-TFN membranes.

CNCs are inherently safe, non-toxic, environmentally friendly, abundant, and low-cost nanoparticles that are easy to disperse in aqueous systems, and this has led to their use in many applications, including water purification [12]. In addition, their hydrophilicity and functionality make them ideal components to enhance the performance of TFN membranes [13]. To the best of our knowledge, in most cases, CNC-TFN membranes are made by dispersing the CNCs or modified CNCs into the aqueous monomer solution rather than the

organic TMC monomer solution prior to interfacial polymerization to fabricate the PA layer [14]. While this approach has demonstrated improvements in membrane performance, issues related to a quantifiable CNC loading and the water permeability-selectivity trade-off led us to explore using CNCs in the organic TMC monomer solution.

Previous work in our laboratory demonstrated the preparation of CNC-TFN membranes by dispersing the CNCs in the organic TMC monomer solution for RO-TFN membranes [15]. The water permeability and salt rejection of CNC-TFN membranes improved up to a CNC loading of 0.1 wt%. However, that loading was shown to be a limiting CNC concentration, likely due to the hydrophilic nature of the CNCs. These results indicated the need to improve CNC dispersion in the organic TMC monomer solution. Thus, we proposed two approaches involving the functionalization of the CNCs: 1- acetylating the CNCs to make them less hydrophilic, and 2- functionalizing the CNCs with L-cysteine to provide covalent bonding between the CNCs and the TMC monomer. These modifications were also expected to address another issue: the leaching of CNCs from the TFN membranes over the long-term performance.

In Chapter 3, we demonstrated the modification of CNCs via acetylation at different degrees of substitution (ACNC2: DS = 0.7 and ACNC4: DS = 1.3) to make them less hydrophilic, thereby enabling their dispersion in the TMC monomer solution. The acetylation was confirmed by FTIR, NMR, and XRD (see Figures. 3.1, 3.2 and A.1). Tuning the DS to achieve a moderate and controlled CNC hydrophilicity led to a more even dispersion of CNCs in the organic monomer solution. The increased dispersibility of the acetylated CNCs (ACNCs) was due to an increase in their hydrophobicity confirmed by water contact angle and surface zeta potential (see Table 3.1). Substitution of surface hydroxyl groups of CNCs by neutral acetyl groups helps reduce the probability of inter-hydrogen bonding between hydroxyl groups, thus minimizing the aggregation of CNCs in non-polar TMC/n-hexane monomer solution as well as the PA layer. The presence of ACNCs during interfacial polymerization (well dispersed in TMC/n-hexane monomer solution) enhanced the sorption of MPD at the interface of the two monomer solutions due to the synergistic effect of the hydrophilic interactions between MPD and ACNCs in comparison to unmodified CNCs. This greater MPD sorption was consistent with an increased PA layer crosslinking density and zeta potential of ACNC-TFN membranes (see Table 3.2). The lower zeta potential of ACNC -TFN compared to CNC-TFN membranes is attributed to an increase in the probability of the ACNC nanoparticles interacting with the acyl chloride groups of the TMC monomer (prior to and during interfacial polymerization), which decreases the content of unreacted carboxylic acid groups in the PA layer, (see Table 3.2). The ACNC-TFN membranes had a smoother surface yet a higher relative surface area

than CNC-TFN membranes based on surface AFM images, indicating that CNC acetylation helped reduce nanoparticle aggregation in the TFN membranes' PA layer (Figure 6.1).

The salt rejection of ACNC-based TFN membranes remained stable (98-99%) and was greater than that of CNC-based TFN membranes at the same nanoparticle loading (see Figure 3.9). Compared to the TFC membrane, a two-fold water permeance increase was achieved (2.60 vs. 1.27 L/m^2.h.bar) with a 0.4 wt% loading of ACNC2 in the TFN membrane. This work provides an example of how hydrophobic functionalization of hydrophilic CNCs is effective in overcoming the limit of CNC nanoparticle incorporation in CNC-TFN membranes. The ACNC-TFN membranes were significantly closer to the so-called upper-bound line than the best CNC-TFN membranes and TFC membranes confirming the overcoming water permeability/selectivity trade-off by ACNC-TFN membranes (see Figure 3.9).

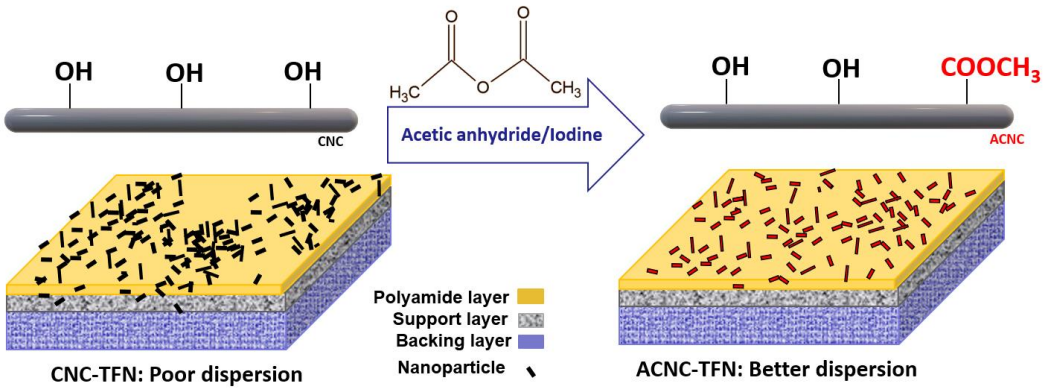

Figure 6.1: Schematic of CNC acetylation and the CNC- and ACNC-TFN membranes.

In Chapter 4, we modified CNCs with L-cysteine (CysCNCs) to improve their dispersibility into the TMC monomer solution of NF-TFN membranes and compared their performance with ACNC-TFN membranes (Figure 6.2). The L-cysteine modification was confirmed by FTIR and NMR (see Figures. 4.2, 4.3). The improved dispersion of the CysCNCs was due to covalent bonding between the L-cysteine amine groups and the acyl chloride groups of the TMC monomer. For CysCNC-TFN membranes, incorporating the well-dispersed hydrophilic CysCNCs in the TMC/n-hexane solution accelerated the diffusion of PIP from the aqueous to the organic phase during the interfacial polymerization of PA, resulting in a smoother surface and tighter microstructure (a more uniform PA layer), (see Figure 4.10). In addition, the immobilization of CysCNC nanoparticles in the PA layer facilitated the uniform dispersion of CysCNCs that could prevent nanoparticle aggregation and defect formation in the PA layer even at high loadings (0.2 wt%). These results are consistent with the smaller pore

size and narrower pore size distribution, the higher degree of crosslinking, and the lower absolute zeta potential for CysCNC-TFN membranes compared to TFC, CNC-TFN, ACNC-TFN membranes (see Table 4.3, Table 4.4, Figure 4.8a).

A simultaneous increase in water permeability and salt and heavy metal rejection of the ACNC-TFNs and CysCNC-TFNs was observed in NF performance compared to CNC-TFN and TFC membranes (see Figure 4.11 and Figure 4.12). The CysCNC-TFN membranes (loading of 0.2 wt%) exhibited the highest water permeability in heavy metal rejection tests. The heavy metal rejections ranged from 89.2 to 98.4% for the copper ions and 87.0 to 95.2% for the lead ions. The order of water permeability performance was the same as that for heavy metal rejection, which indicates that the water permeability-selectivity trade-off was overcome. The key to the superior performance of the CysCNC-TFN membranes was not only their high hydrophilicity but also their functionality, which permitted covalent bonding with the TMC monomer and led to their improved dispersibility in the PA layer. In addition, the thiol (SH) functional groups of CysCNCs introduced extra sites to enhance the heavy metal rejection through complexation or adsorption. The Cu-S and Pb-S coordinative interactions (chelation effect) can lead to the higher rejection of Cu^{2+} and Pb^{2+} metal cations of CysCNC-TFN membranes (Figure 6.2).

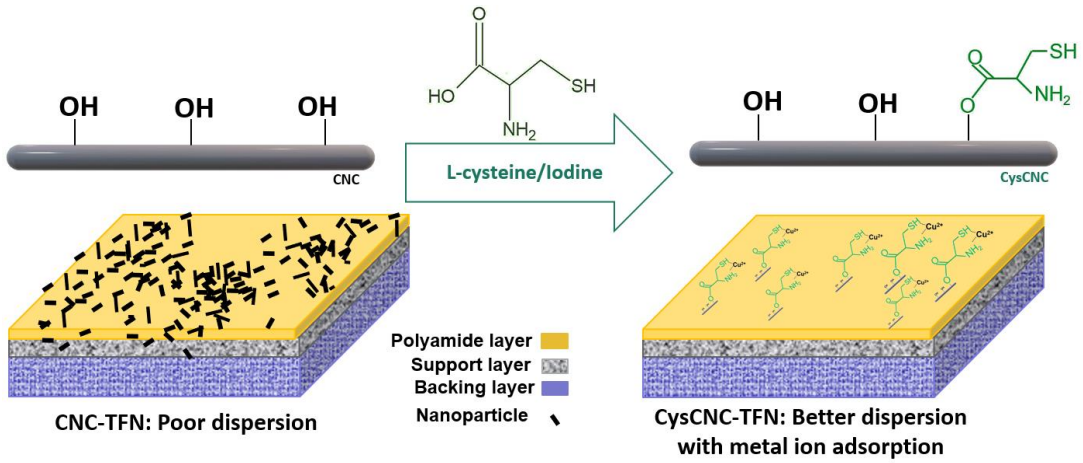

Figure 6.2: Schematic of CNC acetylation and the CNC- and ACNC-TFN membranes.

On the heels of our success with the addition of the modified CNCs into the organic monomer solution, we decided to produce membranes using these same CNCs but by their addition to the aqueous monomer solution for comparison (Figure B.4 and Figure B.5). For the membranes produced via the addition of CNCs to the aqueous monomer solution, the water permeability and salt rejection both increased up to loadings of 0.1 wt% CNC and modified CNC for both RO and NF processes. At CNC loadings beyond 0.1 wt%, both water

permeability and salt rejection decreased. In comparison to the cases where the CNCs and modified CNCs were added to the organic monomer solution, the addition of the CNCs and modified CNCs to the aqueous monomer solution was clearly underperforming. As noted by the simultaneous decline in water permeability and salt rejection, both RO- and NF-TFN membranes prepared by dispersing the CNCs, and even the modified CNCs, into the aqueous monomer solution prior to interfacial polymerization couldn't overcome the permeability-selectivity trade-off. These findings lead us to conclude that the best approach to preparing RO- and NF-TFN membranes with CNCs of any kind is by their addition to the organic monomer solution.

For both CNC and functionalized CNC-based-TFN membranes, we also performed long-term tests for RO and NF processes. The ACNC-TFN membrane's water permeability and NaCl rejection were more stable during the test than CNC-TFN membranes for RO process (see Figure A.5 (Appendix A)). This suggests that the quality of dispersion of the ACNCs in the PA layer led to greater long-term stability. If the nanoparticles were not well-dispersed within the PA layer and did not interact with PA functional groups, they would have been prone to aggregate and leach out during the membrane performance tests leading to decreased membrane performance. In addition, for NF membranes, the stability of TFN membranes was investigated in 7-day tests using a 200-ppm aqueous $CuSO_4$ solution (see Figure 4.13). For all membranes, including the reference TFC membrane, the water permeability and $CuSO_4$ rejection increase during the first 4 h of the experiment. The performance trend for TFN and TFC membranes was similar, indicating the nanoparticles' stability in TFN membranes. The key to the superior performance of the modified CNC-TFN membranes in both RO and NF membranes was not only their high hydrophilicity but also their functionality, which permitted covalent bonding with the TMC monomer and led to their improved dispersibility in the PA layer.

In Chapter 5, we designed a new protocol to investigate the role of the adsorption of heavy metal ions (if any) on TFC and TFN membranes on their water permeability and solute rejection. We investigated the dynamics of adsorption and rejection of heavy metals (Cu^{2+}, Pb^{2+}) by TFC and ACNC- and CysCNC-TFN membranes, (Figure 6.5). We performed NF filtration experiments of different durations from 1 to 16 hours. In addition, we determined the content of heavy metals adsorption on the membranes at the end of different time frames. The results demonstrated that the water permeability reached a constant value after increasing during the first 4 hours of the experiments. The rejection of heavy metals also increased with time, but it took 4 hours to reach a constant value. Interestingly, the amount of heavy metals

adsorbed on the membranes was similar after 8-, 12-, and 16-hour tests. This suggests that the membranes took 4 to 8 hours to reach an equilibrium capacity for heavy metal adsorption. Despite reaching the equilibrium capacity, the water permeability and heavy metal rejection remained at their highest values. We believe that the adsorbed heavy metals from the feed solution improved the performance of both the TFC and TFN membranes. In other words, the adsorbed metal ions on the membrane surface change the surface properties, leading to increased surface hydrophilicity and decreased negative surface zeta potential. In a sense, the metal ion adsorption acts as a pretreatment during the separation process in which the long-term stability of the membranes is enhanced without the need for regeneration cycles.

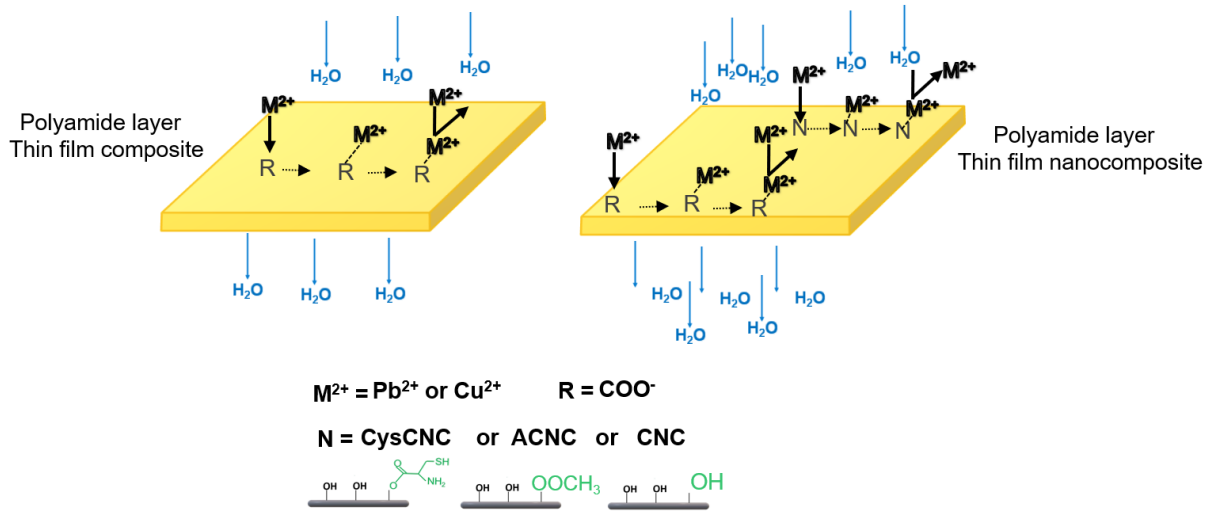

Figure 6.3: Schematic of heavy metal adsorption on TFC and TFN membrane surface.

6.2 Future work

We have developed two CNC modification protocols in which the nanoparticles were functionalized using the same straightforward methodology for both. In future work, we recommend using a sequential modification methodology, and possibly a simultaneous one, where the CNCs are first acetylated and then further functionalized with L-cysteine prior to their incorporation in TFN membranes. This would ensure that the CNCs would be more dispersible in the organic monomer solution (due to acetylation) and able to bond covalently with the organic monomer (via L-cysteine). This should result in an even more significant improvement in membrane performance. In addition, extending the CNC modification methodology to other nanoparticles possessing an abundance of hydroxyl functional groups (e.g., halloysite nanotubes) would be of interest. Eventually, scaling up each modification method to commercial levels would be important.

One area of concern that was pointed to in this thesis was our inability to quantify the amount of CNCs that may have leached from the TFN membranes. Of course, we expected this to not be a problem because of the covalent bonding of the L-cysteine functionalized CNCs to the TMC monomer. One way to quantify this would be to add a tracer element to the CNCs. Silver nanoparticles would be a particularly appropriate choice as they can bind with L-cysteine. Thus, the silver nanoparticles would behave as a tracer in characterization tests of membranes to detect the modified CNCs via elemental analysis. Should leaching be shown to be negligible, the silver nanoparticles would be an interesting addition to the TFN membranes because of their antibacterial properties.

We compared the performance of membranes prepared by dispersing them into the PA layer. The three other preparation methods for TFN membranes should also be explored. For example, CysCNCs can be coated on top of the PA layer. This would be possible because the unreacted amine groups of CysCNCs can covalently bond with the unreacted acyl chlorides of the PA layer, thereby acting as an immobilizing agent.

In this thesis, we demonstrated good laboratory-scale performance of CNC-TFN membranes, but we did not assess their practical application in actual brackish and seawater desalination and wastewater treatment. Therefore, to ensure the potential of the modified CNCs in commercial membrane applications, it would be necessary to test the membranes using actual brackish or seawater for desalination and industrial wastewater. In addition, the modified CNCs we have used have the potential for other applications apart from liquid membrane technology (e.g., gas absorption, adhesives, sensors, drug delivery), and these would bear further investigation.

When preparing TFN membranes, regardless of whether nanoparticles are added to the aqueous or organic monomer solution, the monomer concentrations and their volumes are similar to that of typical TFC membrane formulations. Therefore, aside from the nanoparticle loading, the monomer concentrations and volumes could be optimized. For example, because CNCs can lead to an increased crosslinking density of the PA layer, the concentration of monomers can be adjusted to achieve an optimal crosslinking density to reduce the formation of interfacial defects between the PA matrix and the CNCs.

In recent years, computational chemistry and machine learning methods have been used to model membrane modification and performance. By considering various factors (e.g., nanoparticle size, nanoparticle functional groups, nanoparticle dispersion, and charge density), the performance of the membranes can be predicted.

Finally, we investigated the transport mechanism in the adsorptive NF-TFC and NF-TFN membranes. The results revealed that the metal ions alter the membrane surface properties, which enhances the long-term stability of the membranes. Further tests using actual wastewater would be necessary to provide a more commercially relevant assessment of long-term membrane performance. In addition, further characterization and performance tests can confirm the effect of metal ion adsorption on the TFC and TFN membrane surfaces in the NF process.

6.3 Concluding remarks

The surface modification of CNCs to make them more dispersible in the organic monomer solution enabled the production of TFN membranes with enhanced performance, specifically overcoming permeability-selectivity trade-offs and leading to stable, long-term performance. Thus, CNC surface modification should be focused on improving dispersibility in either the aqueous or organic monomer solution and encouraging covalent bonding with either monomer. It should be noted that good dispersibility of the CNC in the monomer solution does not guarantee similar dispersibility in the final PA layer and that covalent bonding with the monomer provides this guarantee. At the same time, covalent bonding of the nanoparticle with the monomer should prevent their leaching during membrane operation. The success of this approach was demonstrated with L-cysteine-modified CNCs dispersed in the organic monomer.

This work opens new doors to larger-scale production of high-performance TFN membranes for various applications. Acetylated CNCs and L-cysteine-modified CNCs were introduced in this thesis as two types of modified CNC nanoparticles for preparing PA-based TFN membranes. We have discovered that TFN membranes prepared by dispersing modified CNCs in the TMC/n-hexane monomer solution (non-aqueous phase of the interfacial polymerization) lead to enhanced membrane performance in terms of desalination, heavy metal rejection, antifouling, and long-term performance for both RO and NF process. These modified CNC-TFN membranes represent the next generation of TFN membranes.

6.4 References

[1] Z. Samavati, A. Samavati, P.S. Goh, A. Fauzi Ismail, M. Sohaimi Abdullah, A comprehensive review of recent advances in nanofiltration membranes for heavy metal removal from wastewater, Chemical Engineering Research and Design. 189 (2023) 530–571. https://doi.org/10.1016/j.cherd.2022.11.042.

[2] J. Zheng, X. Zhang, G. Li, G. Fei, P. Jin, Y. Liu, C. Wouters, G. Meir, Y. Li, B. Van der Bruggen, Selective removal of heavy metals from saline water by nanofiltration, Desalination. 525 (2022) 115380. https://doi.org/10.1016/j.desal.2021.115380.
[3] V. Kumar, S.K. Dwivedi, S. Oh, A critical review on lead removal from industrial wastewater: Recent advances and future outlook, Journal of Water Process Engineering. 45 (2022) 102518. https://doi.org/10.1016/j.jwpe.2021.102518.
[4] A.M. Nasir, P.S. Goh, M.S. Abdullah, B.C. Ng, A.F. Ismail, Adsorptive nanocomposite membranes for heavy metal remediation: Recent progresses and challenges, Chemosphere. 232 (2019) 96–112. https://doi.org/10.1016/j.chemosphere.2019.05.174.
[5] F. Gholami, A. Asadi, A.A. Zinatizadeh, Efficient heavy metals and salts rejection using a novel modified polysulfone nanofiltration membrane, Appl Water Sci. 12 (2022) 146. https://doi.org/10.1007/s13201-022-01671-x.
[6] A. Al Mayyahi, Important Approaches to Enhance Reverse Osmosis (RO) Thin Film Composite (TFC) Membranes Performance, Membranes. 8 (2018) 68. https://doi.org/10.3390/membranes8030068.
[7] M.Q. Seah, W.J. Lau, P.S. Goh, H.-H. Tseng, R.A. Wahab, A.F. Ismail, Progress of Interfacial Polymerization Techniques for Polyamide Thin Film (Nano)Composite Membrane Fabrication: A Comprehensive Review, Polymers. 12 (2020) 2817. https://doi.org/10.3390/polym12122817.
[8] D.J. Johnson, N. Hilal, Nanocomposite nanofiltration membranes: State of play and recent advances, Desalination. 524 (2022) 115480. https://doi.org/10.1016/j.desal.2021.115480.
[9] R. Castro-Muñoz, L.L. González-Melgoza, O. García-Depraect, Ongoing progress on novel nanocomposite membranes for the separation of heavy metals from contaminated water, Chemosphere. 270 (2021) 129421. https://doi.org/10.1016/j.chemosphere.2020.129421.
[10] S. Hao, Z. Jia, J. Wen, S. Li, W. Peng, R. Huang, X. Xu, Progress in adsorptive membranes for separation – A review, Separation and Purification Technology. 255 (2021) 117772. https://doi.org/10.1016/j.seppur.2020.117772.
[11] H. Saleem, S.J. Zaidi, Nanoparticles in reverse osmosis membranes for desalination: A state of the art review, Desalination. 475 (2020) 114171. https://doi.org/10.1016/j.desal.2019.114171.
[12] C. Gomri, M. Cretin, M. Semsarilar, Recent progress on chemical modification of cellulose nanocrystal (CNC) and its application in nanocomposite films and membranes-A comprehensive review, Carbohydrate Polymers. 294 (2022) 119790. https://doi.org/10.1016/j.carbpol.2022.119790.
[13] L. Yang, X. Liu, X. Zhang, T. Chen, Z. Ye, Md.S. Rahaman, High performance nanocomposite nanofiltration membranes with polydopamine-modified cellulose nanocrystals for efficient dye/salt separation, Desalination. 521 (2022) 115385. https://doi.org/10.1016/j.desal.2021.115385.
[14] F. Abedi, D. Emadzadeh, M.A. Dubé, B. Kruczek, Modifying cellulose nanocrystal dispersibility to address the permeability/selectivity trade-off of thin-film nanocomposite reverse osmosis membranes, Desalination. 538 (2022) 115900. https://doi.org/10.1016/j.desal.2022.115900.
[15] F. Asempour, D. Emadzadeh, T. Matsuura, B. Kruczek, Synthesis and characterization of novel Cellulose Nanocrystals-based Thin Film Nanocomposite membranes for reverse osmosis applications, Desalination. 439 (2018) 179–187. https://doi.org/10.1016/j.desal.2018.04.009.
[16] L. Lin, T.M. Weigand, M.W. Farthing, P. Jutaporn, C.T. Miller, O. Coronell, Relative importance of geometrical and intrinsic water transport properties of active layers in the

water permeability of polyamide thin-film composite membranes, Journal of Membrane Science. 564 (2018) 935–944. https://doi.org/10.1016/j.memsci.2018.08.002.
[17] L. Lin, R. Lopez, G.Z. Ramon, O. Coronell, Investigating the void structure of the polyamide active layers of thin-film composite membranes, Journal of Membrane Science. 497 (2016) 365–376. https://doi.org/10.1016/j.memsci.2015.09.020.

Appendix A: Supporting information for chapter 3

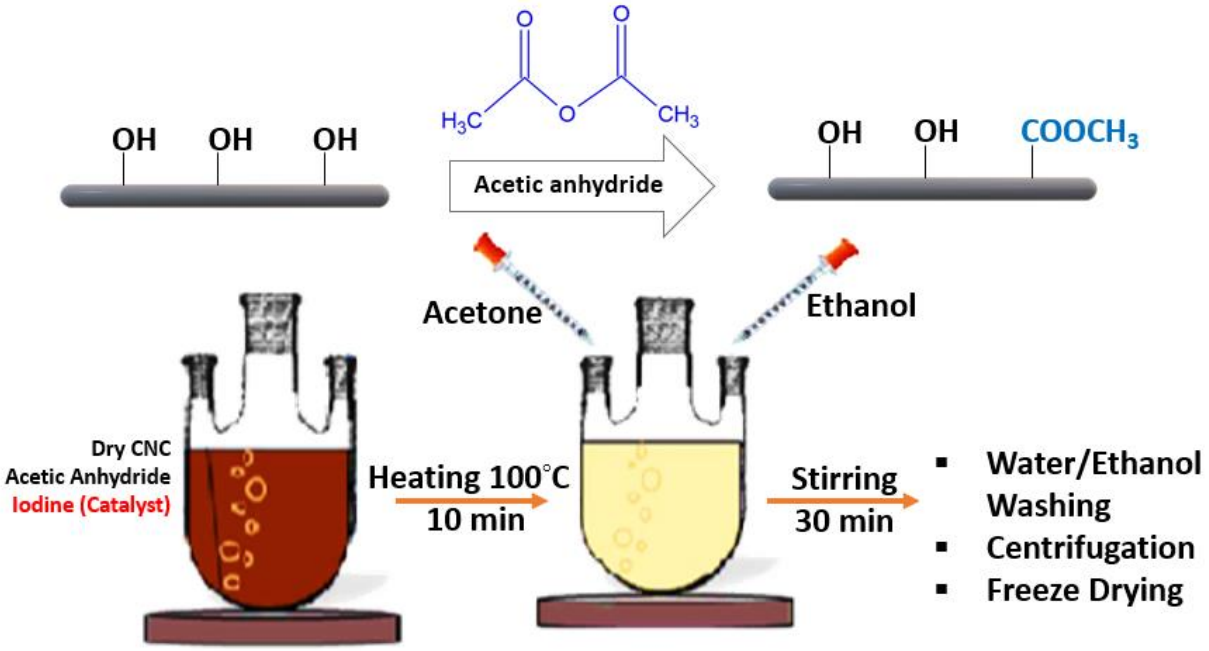

Figure A.1: Schematic of CNC acetylation Procedure.

Figure A.2 displays the result of XRD experiments for CNC and modified CNC nanoparticles. The Segal empirical equation was used to calculate crystallinity (X).

$$X(\%) = \frac{I(16^o) - I(22^o)}{I(22^o)} 100\% \quad \text{(A.1)}$$

where $I(22^o)$ (arbitrary units) represents the peak diffraction intensity corresponding to the crystalline cellulose, and $I(16^o)$ is the peak diffraction intensity corresponding to the amorphous sections [1]. The XRD spectra of TFC, CNC-TFN0.1, ACNC2-TFN0.1 and ACNC4-TFN0.1 are shown in Figure A.3.

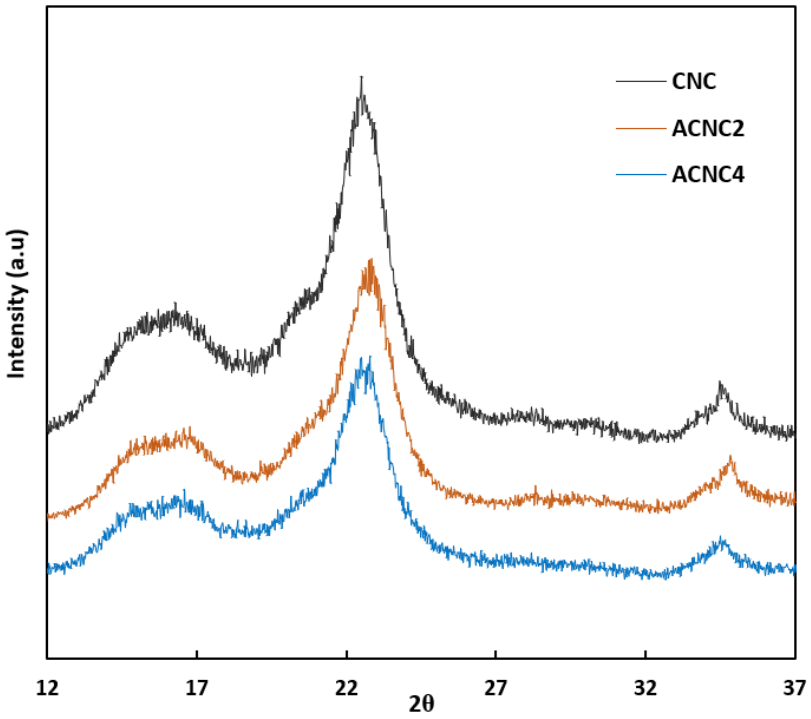

Figure A.2: XRD patterns of CNC, ACNC2 and ACNC4.

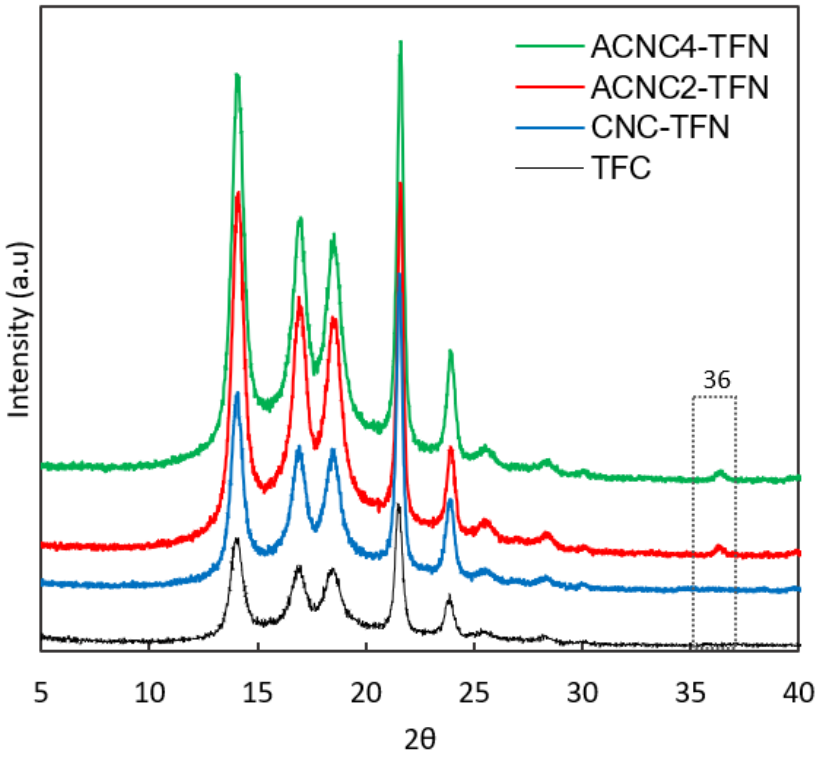

Figure A.3: XRD patterns ATR-FTIR spectrum of TFC and TFNs in 0.1wt% of CNC and ACNC2 and ACNC4.

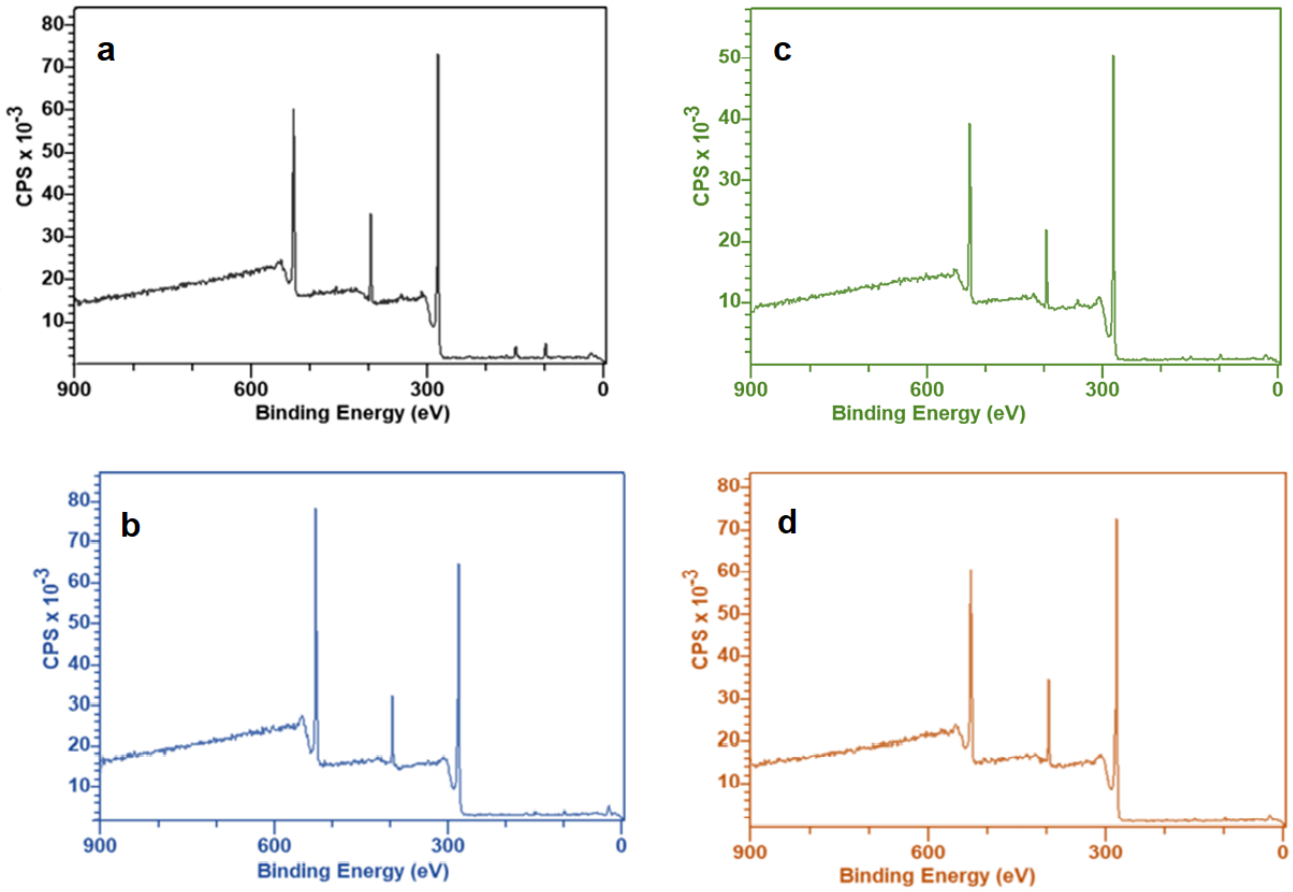

Figure A.4: The XPS spectra of a) TFC, b) CNC-TFN0.1, c) ACNC2-TFN0.1 and d) ACNC4-TFN0.1.

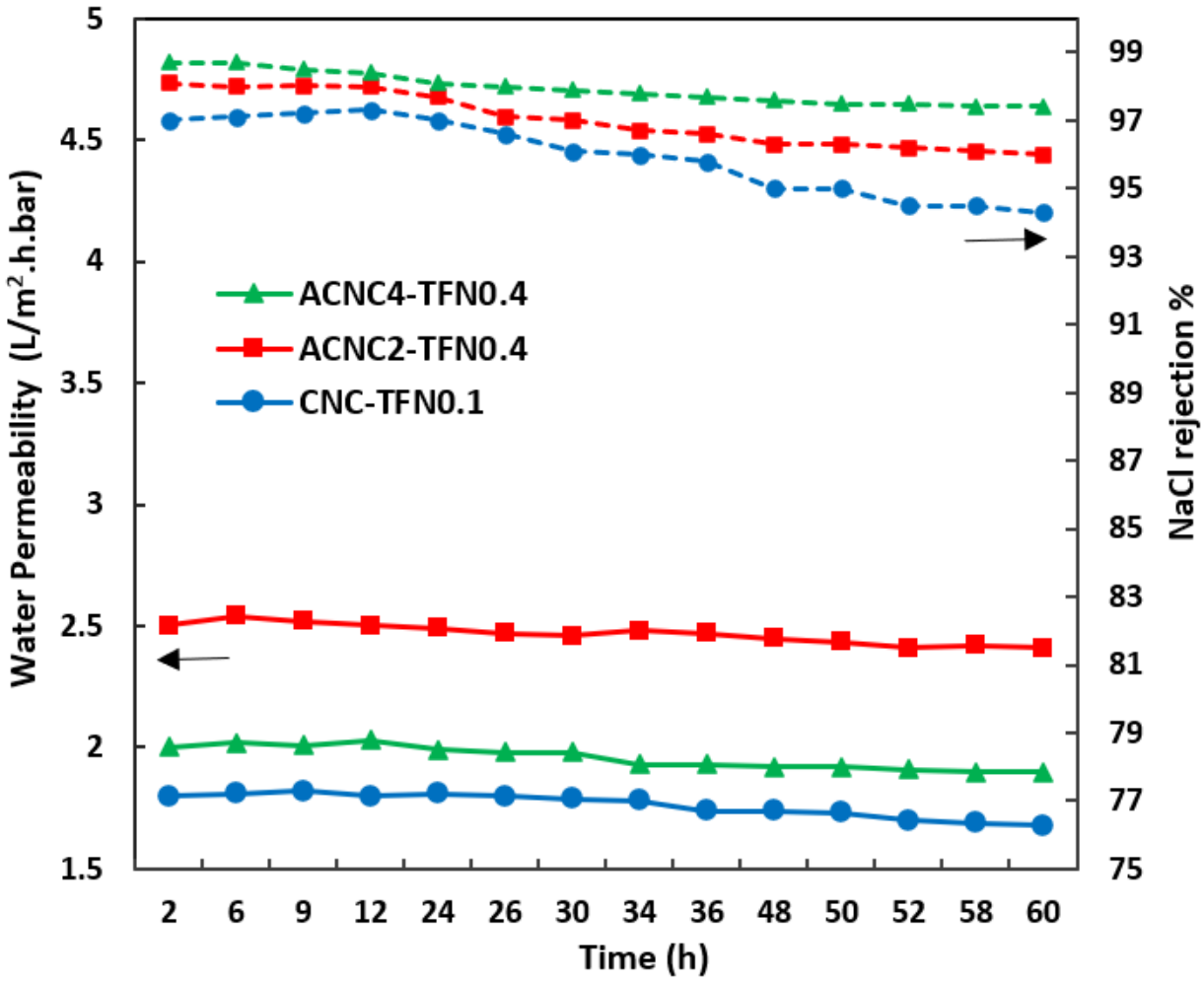

Figure A.5: Long-term performance test of CNC-TFN0.1, ACNC2-TFN0.4 and ACNC4-TFN0.4 membranes.

References

[1] J. Xu, Z. Wu, Q. Wu, Y. Kuang, Acetylated cellulose nanocrystals with high crystallinity obtained by one-step reaction from the traditional acetylation of cellulose, Carbohydrate Polymers. 229 (2020) 115553. https://doi.org/10.1016/j.carbpol.2019.115553.

Appendix B: Cellulose Nanocrystal (CNC) Addition in Thin Film Nanocomposite (TFN) Membranes: Which Monomer Solution is Preferred?

Fatemeh Abedi, Boguslaw Kruczek, Marc A. Dubé

Department of Chemical and Biological Engineering, University of Ottawa, 161 Louis Pasteur, ON, K1N 6N5, Canada.

The contents of this chapter were published in Canadian Journal of Chemical Engineering, 2023.

https://doi.org/10.1002/cjce.25032

B.1 Abstract

Cellulose nanocrystals (CNCs) are biodegradable nanoparticles with a high aspect ratio and abundant surface hydroxyl groups resulting in negatively charged hydrophilic surfaces that make them an ideal candidate to be incorporated in thin-film nanocomposite (TFN) membranes. In this study, we modified the CNCs via acetylation (ACNCs) to reduce their hydrophilicity and via reaction with L-cysteine (CysCNCs) to impart them with functionality that promoted their interaction with the trimesoyl chloride organic monomer used in the preparation of the poly(amide) layer of the TFN membranes. These modifications allowed us to question in which monomer solution the nanoparticles should be dispersed.

Addition of the unmodified CNCs in either the aqueous or organic monomer solution showed little difference in membrane performance. However, the addition of either the ACNCs or the CysCNCs to the organic monomer solution led to a significant increase in membrane performance in reverse osmosis (RO) and nanofiltration (NF) systems compared to their addition to the aqueous monomer solution. In addition, the CysCNCs exhibited performance very near the upper-bound line for RO and NF.

B.2 Introduction

Water is vital for sustaining healthy life[1]. About 36% of the world's population lives in water-scarce areas, with over two billion people left with no alternative but to drink contaminated water. Over the years, several technologies have been employed for water purification, such as membrane separation, chemical precipitation, solvent extraction, ion exchange, coagulation and adsorption[2]. Membrane separation is particularly interesting because of its performance, continuous operation and low operating cost[3]. Therefore, developing membranes for water desalination and wastewater treatment is at the core of membrane separation research.

The thin film composite (TFC) membrane was first synthesized by Cadotte in 1980 to desalinate seawater via the reverse osmosis (RO) process[4]. TFC membranes are generally comprised of three layers: a selective polyamide (PA) layer with a thickness of 50-200 nm, a porous support, usually an ultrafiltration (UF) membrane (e.g., polysulfone or polyether sulfone) with a thickness less than 40 μm, and a polyester nonwoven fabric (thickness < 120 μm)[5,6]. The dense PA layer is the barrier regulating solute rejection and water permeability. The interfacial polymerization with m-phenylenediamine (MPD) in the aqueous solution and trimesoyl chloride (TMC) in the organic solution has been used extensively for the PA layer fabrication of RO TFC membranes[7]. By replacing the MPD in the aqueous solution with piperazine (PIP), the process is used to produce nanofiltration (NF) TFC membranes.

TFC membranes for RO and NF processes have been used in commercial applications for decades. However, challenges still need to be overcome to decrease the cost of RO and NF processes for water reclaiming[8]. These include the trade-off between water permeability and solute rejection, membrane fouling, and resistance to chlorine exposure[9]. The most common strategy to overcome these challenges is to incorporate nanoparticles (e.g., graphene oxide, carbon nanotubes, metal-organic frameworks, zeolites and titanium oxide) into the PA layer, which results in a new category: thin-film nanocomposite (TFN) membranes[10]. The nanoparticles can be used to tune the properties of the PA layer, such as hydrophilicity, porosity, surface charge density, crosslinking density, surface roughness and thickness. In addition, nanoparticles can be used as vehicles to introduce specific functional groups on the membrane surface. However, unlike TFC membranes, the application of TFN membranes at the commercial scale has been limited. One of the most critical issues with TFN membranes is the leaching of nanoparticles from the membrane downstream. As a result, the performance of TFN membranes is not stable. In addition, most currently used nanoparticles are inorganic, and

leaching them into processed water represents a health hazard and violates strict drinking water and environmental safety regulations[11]. Another challenge for TFN membrane fabrication is the nanoparticle aggregation in the polymer matrix, leading to sub-optimal performance because of defect formation in the membrane structure. Also, if nanoparticles aggregate, they will be more prone to leach out from the membrane during its operation[12].

The nanoparticles are incorporated into the PA layer by dispersing them into the aqueous monomer (MPD/PIP) or organic monomer (TMC) solution. Typically, hydrophilic nanoparticles are dispersed in the aqueous monomer solution, while hydrophobic ones are dispersed in the organic monomer solution[13]. In this way, although not explicitly stated, the risk of nanoparticle aggregation prior to interfacial polymerization should, in principle, be minimized. Because most nanoparticles considered for the fabrication of TFN membranes are hydrophilic, they are dispersed in the MPD/PIP monomer solution. However, there are some rare exceptions. For example, Guzman et al.[14] compared the performance of nanosilica-TFN membranes fabricated by dispersing the nanoparticles into the PIP and TMC monomer solutions. Although nanosilica are hydrophilic nanoparticles, the TFN membranes with nanosilica dispersed in the TMC monomer solution performed better than those with the same nanosilica loading in the PIP monomer solution. They attributed this surprising result to the potential loss of nanosilica during the rubber rolling step. This step is necessary to remove the excess aqueous monomer solution from the support layer before pouring the organic monomer solution[4].

As indicated above, the PA layer formation is a sequential process, i.e., the support layer is first saturated with the aqueous monomer solution and only after that with the organic monomer solution. This is because polysulfone or polyether sulfone membranes, generally used as the UF membrane support, are hydrophilic. If the order were changed, the organic hydrophobic monomer solution would not adequately spread on the surface of the UF membrane support, which would compromise the mechanical integrity of the final TFC/TFN membrane[14]. In addition to the potential problem associated with the rubber rolling step to remove the excess aqueous monomer solution (and possibly some nanoparticles). The nanoparticle dispersed in the aqueous monomer solution must resist possible aggregation for much longer than if dispersed in the organic monomer solution. Hydrophilic nanoparticles would naturally aggregate in the hydrophobic environment unless sufficient energy is supplied through magnetic stirring or ultrasonication. In other words, the aggregation of hydrophilic nanoparticles in the hydrophobic/organic monomer solution can be minimized externally until

the hydrophobic/organic monomer solution is spread on the UF membrane support already impregnated with the hydrophilic monomer solution.

Our laboratory has adopted the approach of dispersing hydrophilic nanoparticles, such as cellulose nanocrystals (CNCs)[15], halloysite nanotubes (HNTs) and HNTs functionalized with different generations of poly(amidoamine) dendrimers[16] in the hydrophobic/organic monomer solution. The resulting TFN membranes exhibited significantly better RO performance than the control TFC membrane. However, when the nanoparticle loading increased beyond 0.1 wt%, the TFN membrane performance deteriorated[15,17]. We recently considered the problem of the limited loading of hydrophilic nanoparticles dispersed in the hydrophobic/organic monomer solution by focusing specifically on CNCs. These offer a suitable alternative to hazardous nanomaterials. CNCs are natural, rod-shaped, high aspect-ratio nanoparticles obtained from the acid hydrolysis of native cellulose (e.g., from wood pulp)[18]. These biodegradable CNCs have a low environmental impact and are classified as non-toxic[19]. The surface hydroxyl groups also make them hydrophilic and amenable to functionalization[20].

We considered two different CNC functionalization to increase their loading in the resulting TFN membranes. Because CNCs are very hydrophilic, we modified them via different degrees of acetylation[21]. The resulting acetylated CNCs (ACNCs) were less hydrophilic (water contact angle 58.5^{o} versus 34.3^{o} of CNCs). This allowed fabricating TFN membranes with 0.4 wt% ACNC loadings, which exhibited much better RO performance than unmodified CNC-based TFN membranes with the same nanoparticle loading[21]. We also modified CNCs with L-cysteine (CysCNCs). The resulting CysCNCs were more hydrophilic (water contact angle of 24.6^{o}) than the unmodified CNCs. However, CysCNC nanoparticles formed covalent bonds between the L-cysteine amine and the acyl chloride groups of the TMC monomer[22]. Consequently, even with 0.4 wt% CycCNC loadings, the resulting nanofiltration TFN membranes showed heavy metal rejection, far superior to the corresponding CNC-TFN and control TFC membranes[22].

Based on our experience, we hypothesize that dispersing hydrophilic nanoparticles into the hydrophobic/organic monomer solution is more advantageous than the hydrophilic/aqueous monomer solution, particularly when the hydrophilic nanoparticles can be functionalized to decrease hydrophilicity or to enable covalent bonding with the hydrophobic. However, until now, we have had no empirical proof. Therefore, to validate this hypothesis, we have fabricated CNC-, ACNC-, and CysCNC-based TFN membranes similar to those reported in our recent papers (dispersed in the hydrophobic/organic monomer solution)[23], except for dispersing

these nanoparticles in the hydrophilic monomer (MPD or PIP) solution. We compared the properties of these two types of membranes, including water contact angle, zeta potential, and, most notably, their RO and NF performance. To our knowledge, this is the first comprehensive study attempting to address the question of in which monomer solution hydrophilic nanoparticles should be dispersed when fabricating TFN membranes.

B.3 Experimental Section

B.3.1 Materials

Poly(sulfone) UF membranes (PS35) with a molecular weight cutoff of 20 kDa were donated by Solecta, California, USA. The monomers, m-phenylene diamine (MPD), piperazine (PIP, 99% purity), trimesoyl chloride (TMC, >98% purity), and the organic solvent, n-hexane (>99% purity), were purchased from Sigma-Aldrich (Mississauga, Canada). The spray-dried powder form of the sulphate sodium salt of CNCs was donated by CelluForce Inc. (Windsor, Quebec). The sulphate half-ester content of CNCs was 249 mmol/kg CNC. Sodium sulphate (Na_2SO_4) and sodium chloride (NaCl) were laboratory grades and purchased from Sigma-Aldrich (Mississauga, Canada). HCl, KCl and NaOH were procured from Fisher Scientific (Mississauga, Canada). Distilled deionized water (DDW) was used to make the aqueous MPD or PIP solution, and distilled water (DW) was used to wash the membranes and prepare the synthetic water feed solutions. All materials were used as received without further purification/modification except for the CNCs, which were functionalized with acetyl groups (ACNC) and L-cysteine (CysCNC) using a solvent-free method. Details of the functionalization of CNCs are described elsewhere[21,24].

B.3.2 TFC and TFN membrane synthesis

A PS35 membrane was used as the support to synthesize the PA layer by in-situ interfacial polymerization. Figure B.1 schematically presents the critical steps for fabricating the PA layer for the RO and NF membranes. The only difference between the RO and NF membranes is the hydrophilic monomer: MPD for RO membranes and PIP for NF membranes. The process shown in Figure B.1 leads to a TFC membrane. TFN membranes were prepared by dispersing nanoparticles (CNCs, ACNCs, CysCNCs) in either the aqueous monomer solution (2% (w/v) of MPD or PIP in water) or the organic monomer solution (0.05% (w/v) TMC in n-hexane). Three different loadings of nanoparticles were used: 0.05, 0.1 and 0.2 wt%. A specific amount of nanoparticles (dried powder) was added to the monomer solution and magnetically stirred until nanoparticle aggregates were no longer visible, which typically

required 30-40 min. In addition, the suspensions of nanoparticles in the respective monomer solutions were sonicated before their use to ensure proper dispersion of the nanoparticles. Details of the membrane fabrication protocol are described elsewhere[24]. The membranes were carefully washed and stored in DDW at ambient temperature before use.

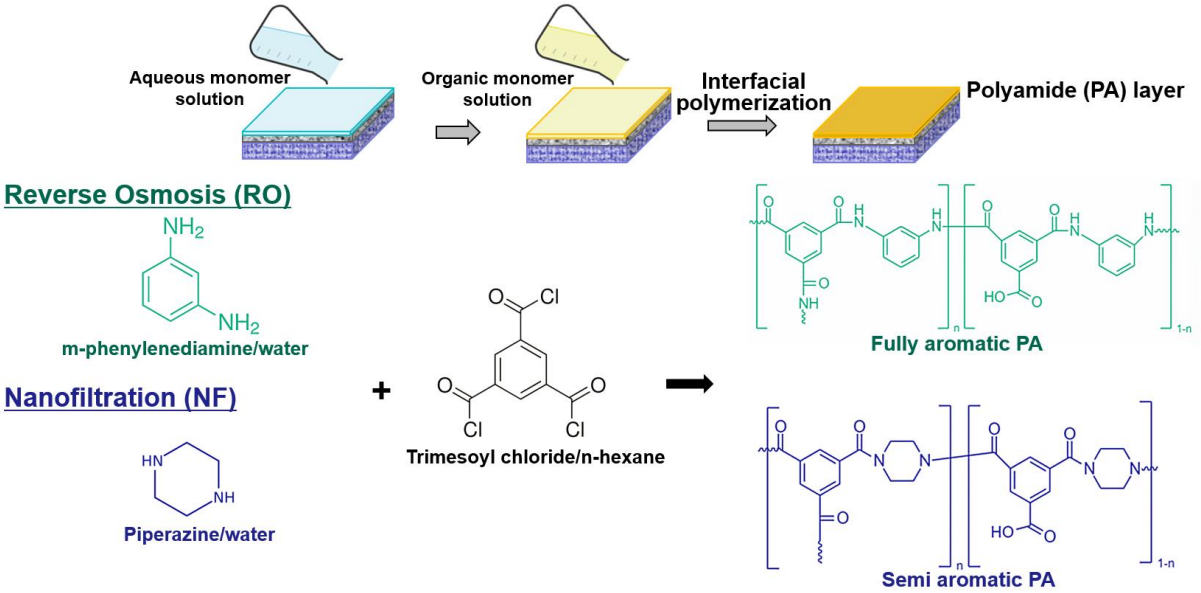

Figure B.1: Synthesis of the PA layer in TFC membranes for NF and RO processes.

B.3.3 Characterization of nanoparticles and membranes

The zeta potential of the nanoparticles and membranes was measured using a zeta analyzer (Zetasizer PSS0012-22, Malvern Instruments) with a frontal electrophoretic light scattering method. The Zetasizer was equipped with an adjustable gap cell to measure membrane surface charge. 1 mM of KCl solution was used as the background electrolyte, with its pH adjusted using a 0.1 M HCl or 0.1 M NaOH solution. The sessile water contact angle of the nanoparticles and membranes was measured using a VCA Optima surface analysis system (AST Products, Inc., Billerica, MA). At least 20 droplets (~2 μL) of deionized water over at least seven different locations on each sample were tested at ambient temperature. The dispersibility of CNCs, ACNCs, and CysCNCs in water and in n-hexane (i.e., the respective solvents for the hydrophilic and hydrophobic monomers) was assessed based on the apparent hydrodynamic particle sizes (Z-average particle size) determined using dynamic light scattering (DLS) after probe sonication for three 5-minute intervals at 75% amplitude.

B.3.4 Membrane performance

The RO and NF performance of the membranes was evaluated using a continuous crossflow system consisting of three membrane cells arranged in parallel, each with an effective surface area for permeation (A_p) of 17.35 cm^2. 2000 ppm aqueous NaCl and Na_2SO_4 solutions were prepared as feeds for RO and NF, respectively. The feed flow rate was maintained at 2.4 ± 0.2 L/min to minimize the concentration polarization and achieve near-zero recovery[25]. The measurements were conducted at 295 ± 1 K and hydraulic pressure of 20±1 bar for RO and 10 ±1 bar for NF.

The membranes were characterized in terms of water permeability (A) and solute rejection (R):

$$\mathrm{A} = \frac{J_w}{\Delta P - \Delta \pi} \tag{B.1}$$

where J_w is the water flux, ΔP is the hydraulic pressure gradient, which was essentially the applied hydraulic pressure, and $\Delta\pi$ is the osmotic pressure gradient.

$$J_w = \frac{V_p}{A_m t} \tag{B.2}$$

where the volume of permeate (V_p) collected during a time, t, at steady-state, and A_m is the membrane area. The osmotic pressure gradient was evaluated from the van't Hoff equation:

$$\Delta\pi = \Delta C i R T \tag{B.3}$$

in which ΔC is the molar concentration gradient ($\Delta C \approx C_f$), i is the number of ions into which the salt dissociates, R is the ideal gas constant, and T is the absolute temperature. Salt rejection was evaluated based on the solute concentration in the feed (C_f) and permeate (C_p) and measured by conductimetry.

$$\mathrm{R} = \left(1 - \frac{C_p}{C_f}\right) \times 100\% \tag{B.4}$$

Membrane performance was also evaluated regarding each membrane's position to the upper-bound line. This required the evaluation of the solute permeability (B):

$$\mathrm{B} = \frac{1-\mathrm{R}}{\mathrm{R}} J_w \tag{B.5}$$

B.4 Results and discussion

B.4.1 Nanoparticle characterization

The successful functionalization of CNCs with acetyl and L-cysteine groups was confirmed by the analyses of the attenuated total reflectance-Fourier Transform infrared (ATR-FTIR) and ^{13}C-NMR spectra. Details of these analyses are discussed elsewhere[21,24]. Based on

the atomic force microscopy images, chemical modification of the CNCs did not significantly affect the morphology of the resulting ACNCs and CysCNCs compared to CNCs. Table B.1 summarizes the properties of unmodified and modified CNCs, including their water contact angle, zeta potential, and particle sizes in water and n-hexane, the solvents for the hydrophobic and hydrophilic monomers, respectively.

Table B.1: Properties of CNC, ACNC and CysCNC.

Properties	**Nanoparticle**		
	CNC	**ACNC**	**CysCNC**
Contact angle (degree)	34.3 ±2.3	58.5 ±3.1	24.6±1.8
Zeta potential (mV)	-50.2 ±2.1	-39.4 ±1.3	-23.5±1.2
Particle size in n-hexane (nm)	180.3 ±3.1	104.3 ±2.4	139.8±2.3
Particle size in water (nm)	70.3 ±3.1	82.3 ±1.1	72.4±1.6

As expected, the contact angle of ACNCs was greater than that of the unmodified CNCs because of the substitution of some of the hydrophilic hydroxyl groups by less hydrophilic acetyl groups. It is important to emphasize that ACNC remains hydrophilic because its water contact angle is significantly smaller than 90^{o}. The hydrophilicity of ACNC is also indicated by its smaller particle size in water (82.3 nm) than in n-hexane (104.3 nm). However, a decrease in the hydrophilicity of ACNCs compared to CNCs is also evident in its larger particle size in water (82.3 vs. 70.3 nm) and its smaller particle size in n-hexane (104.3 vs. 180.3 nm). Partial substitution of the hydroxyl groups by the acetyl groups also resulted in a less negative zeta potential of ACNCs (-39.4 mV) than CNCs (-50.2 mV).

The substitution of hydroxyl groups by L-cysteine groups decreased the water contact angle of the resulting CysCNCs (24.6^{o}) compared to the unmodified CNCs. Also, the particle size of the CysCNCs and CNCs in water are comparable (72.4^{o} vs 70.3^{o}). The CysCNCs had the lowest negative surface charge among the studied nanoparticles, which can be attributed to the addition of the positively charged SH and NH_2 groups of L-cysteine. Interestingly, despite their similar particle sizes in water, the CysCNCs were more compatible with n-hexane than the unmodified CNCs, as indicated by a decrease in the particle size in this solvent from 180.3 to 139.8 nm. The lower negative charge density and steric hindrance resulting from the size of the L-cysteine functional groups are likely responsible for the improved compatibility of this nanoparticle with n-hexane. At the same time, it should be emphasized that ACNCs appear to

be the most compatible with n-hexane among the three types of nanoparticles. In conclusion, the CNC modifications via acetylation and L-cysteine addition made the resulting functionalized nanoparticles more dispersible in n-hexane without significantly compromising their dispersibility in water.

B.4.2 Membrane surface characterization

The successful formation of the PA layer in the TFC and TFN membranes for RO and NF was confirmed by ATR-FTIR and x-ray photoelectron spectroscopy analyses. Details of these analyses are discussed elsewhere[21,24]. Herein, we focus on how the surface properties of the membranes were affected by incorporating CNCs, ACNCs and CysCNCs into the PA layer and, more importantly, if the monomer solution into which the nanoparticles were dispersed affected these properties.

Figure B.2 presents the effect of nanoparticle loading on the water contact angle of the RO (Figure B.2a) and NF (Figure B.2b) membranes. The water contact angle of the NF membranes was significantly lower than that of the RO membranes, which is consistent with the literature. For example, the water contact angle of TFC RO membranes fabricated by interfacial polymerization of MPD and TMC ranges from 65 to 75°[26–28] compared with 45 to 55° for TFC NF membranes fabricated by the interfacial polymerization of PIP and TMC[15,29,30]. The amine groups of MPD are side groups, while the amine groups of PIP are contained in the ring of this monomer. As such, the amine groups of PIP are less accessible to the acyl chloride groups (compared to that of the MPD) of the TMC monomer during interfacial polymerization. As a result, the PA layer of TFC NF membranes has a lower crosslinking degree than that of TFC RO membranes. Another consequence is the higher concentration of unreacted carboxylic acid groups in the PA layer of TFC NF membranes compared to that of TFC RO membranes. Because carboxylic acid groups are hydrophilic, the hydrophilicity of the TFC NF membranes is greater than that of the TFC RO membranes.

The water contact angle of the TFC membranes was greater than that of the respective TFN membranes, regardless of the type of nanoparticle used. In other words, incorporating nanoparticles into the PA layer increased its hydrophilicity, which was not surprising considering the hydrophilic nature of all the nanoparticles used in this study. One would also have expected a lower contact angle (i.e., higher hydrophilicity) for the TFN membranes with higher nanoparticle loading. This was the case for CNC-TFN and CysCNC-TFN membranes but not for the ACNC-TFN membranes. Although ACNC is hydrophilic, it had the highest water contact angle among the nanoparticles considered in this study (Table B.1). An increased

water contact angle with ACNC loading might also indicate some aggregation. Thus, considering the effect of the nanoparticle type for RO and NF membranes, the water contact angle increased in the following order: CysCNC-TFN < CNC-TFN < ACNC-TFN. The TFN membranes hydrophilicity order generally followed the nanoparticles' hydrophilicity order (Table B.1).

The most remarkable finding in Figure B.2 was the higher water contact angle when the nanoparticles were dispersed in the aqueous monomer solution compared to the organic one. A higher water contact angle for a given type of hydrophilic nanoparticle might indicate some nanoparticle aggregation. Both unmodified and modified CNCs contain an abundance of hydroxyl groups. These groups are primarily responsible for the nanoparticles' hydrophilicity. However, the nanoparticles may agglomerate via these hydroxyl groups, reducing their hydrophilicity[31]. It is also possible that when dispersing nanoparticles in the aqueous monomer solution, some nanoparticles were lost during the removal of the excess aqueous monomer solution, thereby reducing the loading of the hydrophilic nanoparticles in the final TFN membranes.

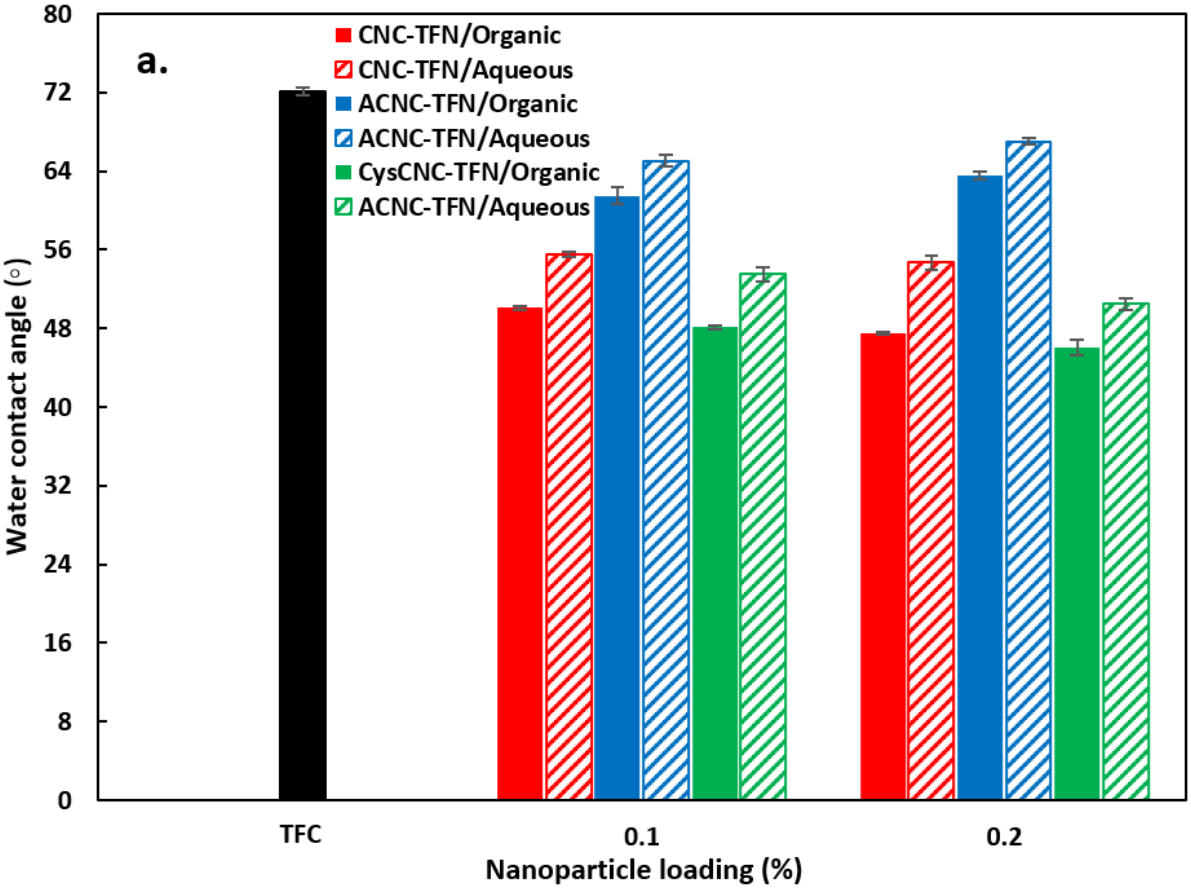

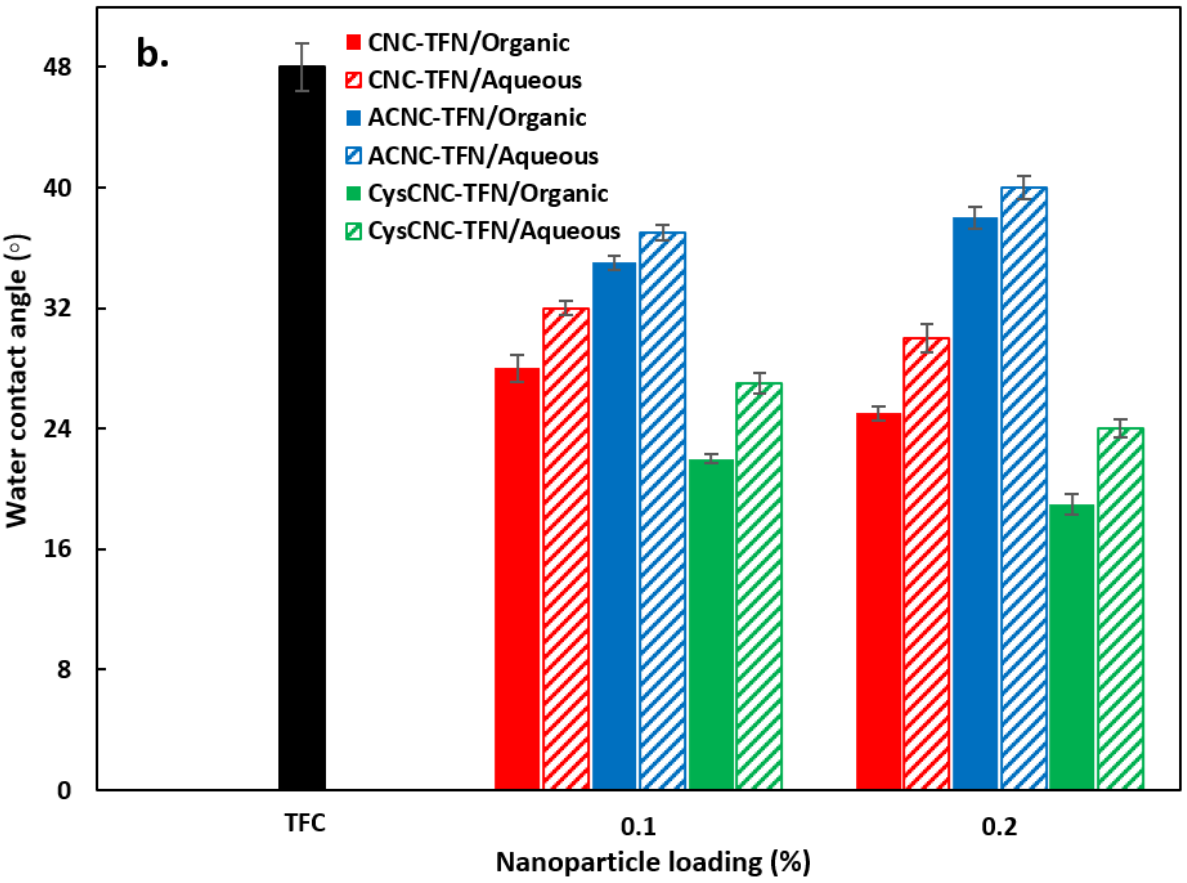

Figure B.1: The effect of nanoparticle loading on the water contact angle of TFN RO (a) and NF (b) membranes based on CNC, ACNC and CysCNC nanoparticle loading. Solid bars refer to the TFN membranes with nanoparticles dispersed in the TMC organic monomer solution. Striped bars refer to the TFN membranes with nanoparticles dispersed in the MPD (a) or PIP (b) aqueous monomer solution.

Figure B.3 presents the effect of nanoparticle loading on the zeta potential of the RO (Figure B.3a) and NF (Figure B.3b) membranes at pH = 6.5. The zeta potential of the TFC RO membranes (-11 mV) is less negative than that of the TFC NF membranes (-14 mV), consistent with the literature[15,26,29,30,32–34]. Although the more negative zeta potential does not necessarily have to correlate with higher membrane surface hydrophilicity, in this case, it does. Furthermore, the higher concentration of unreacted carboxylic acid groups in the PA layer of the TFC NF membranes responsible for their higher hydrophilicity is also responsible for the more negative zeta potential than that of the TFC RO membranes.

The effect of nanoparticle loading on the zeta potential of the membranes appears to be stronger than its effect on the water contact angle (Figure B.2). This effect depends on the type of nanoparticle. For CNC-based TFN membranes, the zeta potential becomes more negative with loading increases from 0.1 to 0.2 wt%. The opposite is true for the CycCNC-based TFN

membranes. The changes in the zeta potential of the TFN membranes compared to the respective control TFC membranes arise from the functional groups of the dispersed nanoparticles. Consequently, an increase in zeta potential with nanoparticle loading for CycCNC-TFN arises from the positively charged SH and NH_2 groups of L-cysteine. It is important to emphasize that although CycCNC-TFN membranes have the least negative surface charge density, they are the most hydrophilic among the TFN membranes considered in this study, which demonstrates that the surface zeta potential does not always correlate with membrane surface hydrophilicity.

For ACNC-TFN membranes, the effect of nanoparticle loading on zeta potential is not apparent. For the RO membranes, the surface charge density of the TFN membranes was more negative than that of the reference TFC membrane and further decreased with ACNC loading. However, for the NF membranes, the surface charge density for the TFN membrane with 0.1 wt% nanoparticle loading was higher than that of the control TFC membrane. Still, a further increase in nanoparticle loading decreased the zeta potential to the level of the control TFC membrane. Despite this unclear effect of nanoparticle loading on the zeta potential for ACNC-TFN membranes, the order of the zeta potential of the TFN membranes corresponds to the order of the zeta potential of the nanoparticles (Table B.1).

Considering the effect of the monomer solution (hydrophilic/aqueous versus hydrophobic/organic) into which the nanoparticles were dispersed on the zeta potential of the resulting TFN membranes, it appears that dispersing nanoparticles in the organic monomer solution had a stronger influence on zeta potential. For a given nanoparticle loading, the zeta potential of the CysCNC-TFN membranes with the nanoparticles dispersed in the TMC monomer solution was less negative than when the nanoparticles were dispersed in MPD (or PIP). For the unmodified CNC-based TFN membranes, the situation was the opposite. It is because, as noted above, the addition of CNCs decreased the zeta potential while the addition of CysCNCs increased the zeta potential of their respective TFN membranes. The results shown in Figure B.3 are consistent with Figure B.2 for the water contact angle. In general, the dispersion of nanoparticles in the organic monomer solution has a greater effect on the resulting membranes' surface properties (i.e., contact angle and zeta potential). As indicated previously, this could be due to the higher probability of aggregation of hydrophilic nanoparticles and/or loss of some nanoparticles prior to the interfacial polymerization. In both cases, the influence of nanoparticles on the surface properties of the resulting TFN membrane would be reduced.

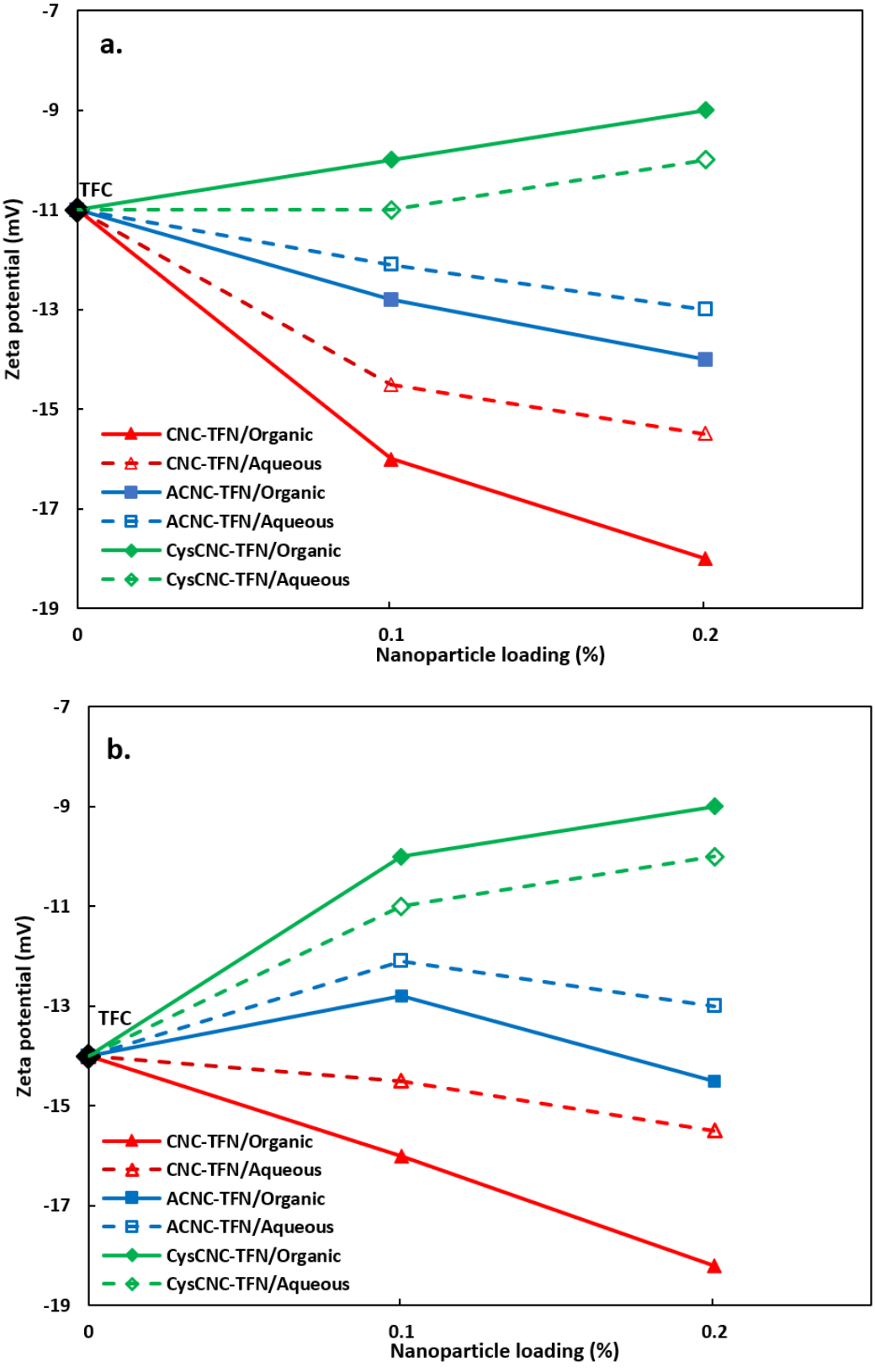

Figure B.2: The effect of nanoparticle loading on the zeta potential of TFN RO (a) and NF (b) membranes based on CNC, ACNC and CysCNC nanoparticles. Solid lines refer to the TFN membranes with nanoparticles dispersed in the TMC organic monomer solution. Dashed lines refer to the TFN membranes with nanoparticles dispersed in MPD (a) or PIP (b) aqueous monomer solution.

B.4.3 Membrane performance

The addition of hydrophilic nanoparticles considered in this study into the hydrophobic/organic monomer solution has a greater effect on the membranes' surface properties than the standard approach of adding the hydrophilic nanoparticles into the hydrophilic/aqueous monomer solution. The ultimate question is if previously discussed differences in the surface properties of the membranes translate to membrane performance.

The membrane performance is shown in two separate figures because of the difference in water permeability of RO and NF membranes and the different solute (NaCl vs Na_2SO_4) in the feed solution. Figure B.4 presents the effect of nanoparticle loading on the water permeability and NaCl rejection of TFN RO membranes prepared by dispersing the nanoparticles in either the aqueous or organic monomer solution. Figure B.5 is similar to Figure B.4, except it shows this effect for TFN NF membranes using a Na_2SO_4 feed solution. The difference in the RO and NF membranes' water permeabilities is due to the respective PA layers' structure. As noted earlier, the former is highly crosslinked because the side amine groups of MPD are more accessible than the ring amine groups of PIP to the acyl chloride groups of the TMC monomer during interfacial polymerization. The higher crosslinking density of the PA layer of the RO membranes leads to its denser structure and lower water permeability than that of the NF membranes. At the same time, RO membranes are highly effective at rejecting monovalent salts such as NaCl. NF membranes can also reject NaCl, but to a much lower level, and they are primarily used to separate multivalent salts from the aqueous feed solution. NaCl and Na_2SO_4 are standard solutes used to characterize the performance of the RO and NF membranes, respectively.

In Figures 4 and 5, the water permeability for the TFN membranes with the nanoparticles dispersed in the organic monomer solution increased with nanoparticle loading up to 0.1 wt%. However, a further increase in loading to 0.2 wt% generally led to decreased water permeability for a given nanoparticle type for both RO and NF membranes. The same trend was observed for the NF TFN membranes with the nanoparticles dispersed in the aqueous monomer solution. However, for the RO TFN membranes with the nanoparticles dispersed in the aqueous monomer solution, although the water permeability of the TFN membranes was higher than that of the control TFC membranes, it decreased with increasing nanoparticle loading.

It is evident in Figures 4 and 5 that the monomer solution into which the nanoparticles are dispersed affects water permeability. More specifically, TFN membranes for which the nanoparticles were dispersed into the organic monomer solution were significantly more

permeable than those with the nanoparticles dispersed in the aqueous monomer solution regardless of the CNC hydrophilicity. One of two possible reasons for the smaller effect of the nanoparticle type and loading on TFN membrane surface properties was a greater amount of nanoparticle aggregation when dispersed in the aqueous monomer solution compared to the organic monomer solution. Aggregation of nanoparticles in the PA layer of TFN membranes could result in membrane defects and, consequently, in a significant increase in water permeability and a dramatic decrease in salt rejection. None of this was seen in Figures 4 and 5. However, this does not mean nanoparticle aggregation does not affect membrane performance and surface properties. It has been reported that before a dramatic increase in membrane permeability and a corresponding decrease in salt rejection is observed, moderate aggregation of nanoparticles may lead to a slight decrease in water permeability[14].

More insight into the effect of the monomer solution into which the nanoparticles are dispersed is revealed by the solute rejections in Figures 4 and 5. The solute rejections of ACNC-TFN and CysCNC-TFN membranes prepared by dispersing the nanoparticles in the organic monomer solution were practically independent of nanoparticle loading, and they oscillated around 98%. On the other hand, solute rejection generally decreased with nanoparticle loading for ACNC-TFN and CysCNC-TFN membranes prepared by dispersing nanoparticles in the aqueous monomer solution. This effect was more pronounced for the NF than for the RO membranes. On the other hand, for the CNC-TFN membranes, as the nanoparticle loading increased, solute rejection decreased regardless of in which monomer solution the CNCs were dispersed. At the same time, for a given CNC loading, solute rejection of the TFN membranes with nanoparticles dispersed in the organic monomer solution was slightly greater than those with the nanoparticles dispersed into the aqueous monomer solution.

The fact that solute rejection by TFN membranes is either independent of nanoparticle loading or slightly decreases in Figures 4 and 5 suggests that nanoparticle aggregation rather than a loss of nanoparticles was a primary cause of the reduced effect of the nanoparticles on the TFN membrane surface properties in which the nanoparticles were dispersed in the aqueous monomer solution. If it were the loss of nanoparticles prior to interfacial polymerization, solute rejection would have approached that of the corresponding control TFC membranes. However, except for the CysCNC-TFN and ACNC-TFN membranes with the nanoparticles dispersed in the organic monomer solution, solute rejection of the other TFN membranes dropped below that of the corresponding TFC membranes.

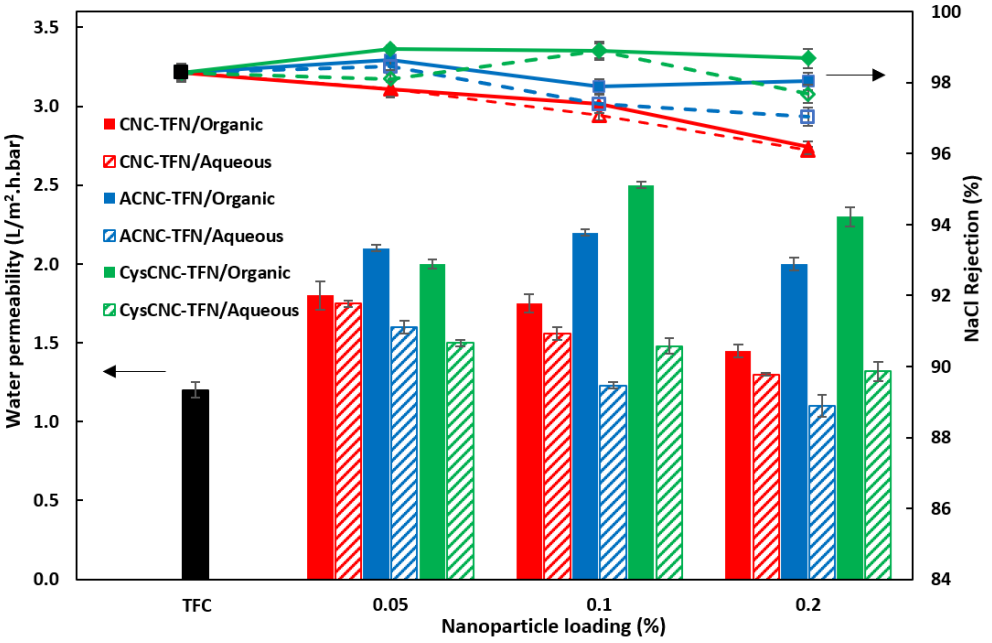

Figure B.3: The effect of nanoparticle loading on water permeability and NaCl rejection for TFN RO membranes based on CNC, ACNC and CysCNC nanoparticles. Solid lines and bars refer to TFN membranes with the nanoparticles dispersed in the TMC organic monomer solution. Dashed lines and striped bars refer to the TFN membranes with the nanoparticles dispersed in the MPD aqueous monomer solution.

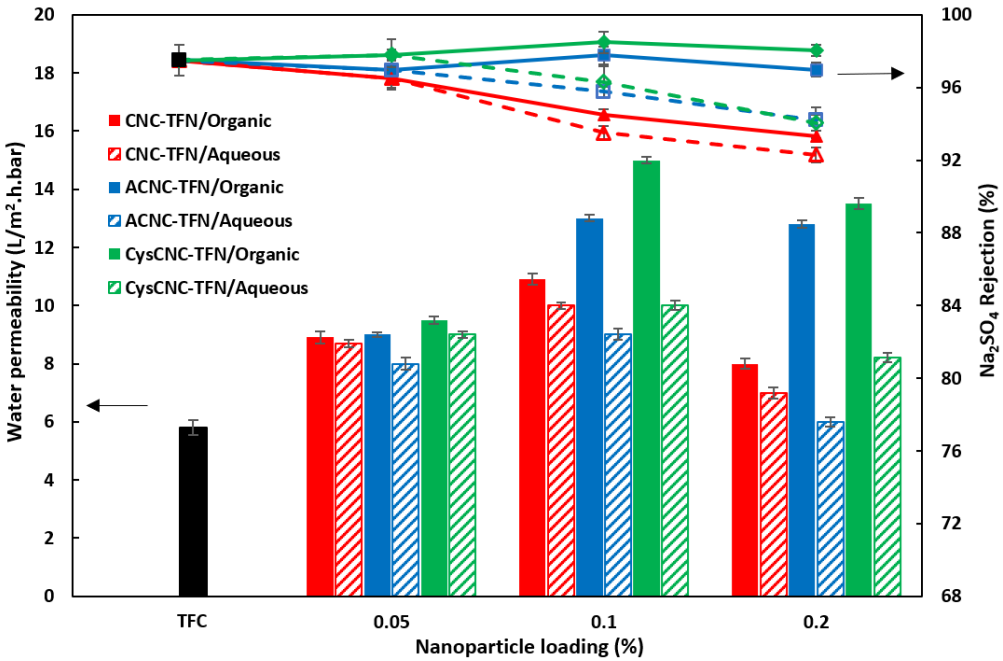

Figure B.4: The effect of nanoparticle loading on water permeability and Na_2SO_4 rejection of TFN NF membranes based on CNC, ACNC and CysCNC nanoparticles. Solid lines and bars refer to TFN membranes with the nanoparticles dispersed in the TMC organic monomer solution. Dashed lines and striped bars refer to the TFN membranes with the nanoparticles dispersed in MPD aqueous monomer solution.

One of the challenges for RO and NF membrane processes is a trade-off between membrane productivity (expressed by water permeability) and selectivity (expressed by the ratio of water and solute permeabilities). Increasing membrane productivity typically leads to a decrease in membrane selectivity and vice-versa. Using the analogy of gas separation membranes, the performance of RO and NF membranes is accessed by their location compared to the so-called upper bound line and the A versus A/B plots, where the water permeability (A) is evaluated using Equation (1) and the solute permeability (B) using Equation (5) based on the water flux and solute rejection. Normally, the combination of A vs A/B places membranes below the upper bound line. The closer the data point to the upper bound line, the better is the membrane performance. The ultimate goal for membrane developers is to fabricate membranes with their performance above the upper bound line.

Figure B.6 presents the performance of the best TFN RO membranes for a given type of nanoparticle and nanoparticle dispersion strategy compared to the respective upper bound line. Figure B.7 is similar to Figure B.6, except that it is constructed for the best TFN NF membranes. For comparison, Figures B.6 and B.7 also include the performance of CNC and modified CNC-based TFN membranes from the literature.

Considering the best CNC-based TFN membrane performances from this study (the closest to the upper bound line), the monomer solution into which the unmodified CNCs were dispersed played an insignificant role. Their respective performance placed the membranes prepared using either strategy very close to each other for both RO (Figure B.6) and NF (Figure B.7) performance. The situation was very different for the ACNC-TFN and CysCNC-TFN membranes. The membranes with nanoparticles dispersed into the organic monomer solution were significantly closer to the respective upper-bound lines than those dispersed in the aqueous monomer solutions. This is because they were both more permeable and selective simultaneously. In other words, the monomer solution into which the nanoparticles were dispersed allowed for overcoming the trade-off between membrane permeability and selectivity. Considering the best ACNC-TFN and CysCNC-TFN membranes, the CysCNC-TFN membranes are closer to the upper bound line for both RO (Figure B.6) and NF (Figure B.7) performance. The excellent RO and NF performance of CysCNC-TFN membranes was probably because of the covalent bonding between the CysCNC amine groups and the TMC monomer before the interfacial polymerization. This allowed the combination of "the best of two worlds," that is, introducing very hydrophilic nanoparticles (which promotes membrane permeability) into the hydrophobic/organic monomer solution without causing excessive nanoparticle aggregation (responsible for maintaining high membrane selectivity).

The lack of the effect of the monomer solution into which the unmodified CNCs were dispersed on membrane performance was likely due to their high hydrophilicity, which suggests their dispersion in the hydrophilic monomer solution and a lack of specific interactions (such as for CysCNCs) between the CNCs and the organic TMC monomer solution.

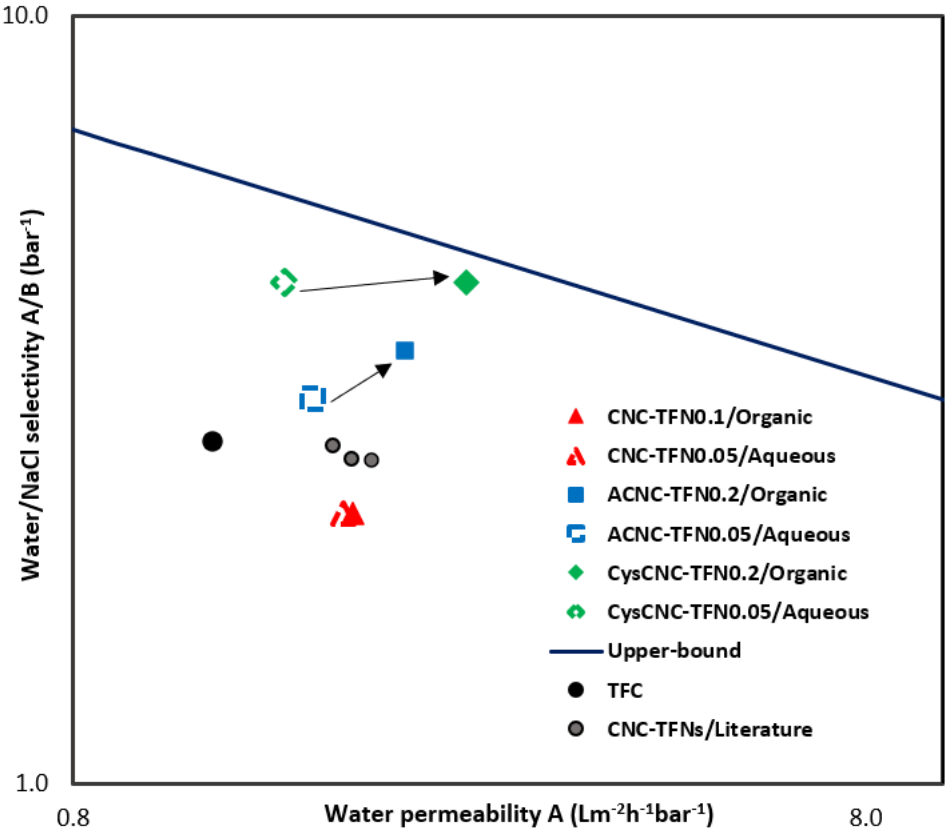

Figure B.5: Effect of nanoparticle addition strategy on TFN RO membrane performance in comparison to the upper-bound line (A/B=46.74 A$^{-1.72}$).[35] Solid coloured symbols show results for the nanoparticle addition to the organic monomer solution; open coloured and other symbols show results for the nanoparticle addition to the aqueous monomer solution.

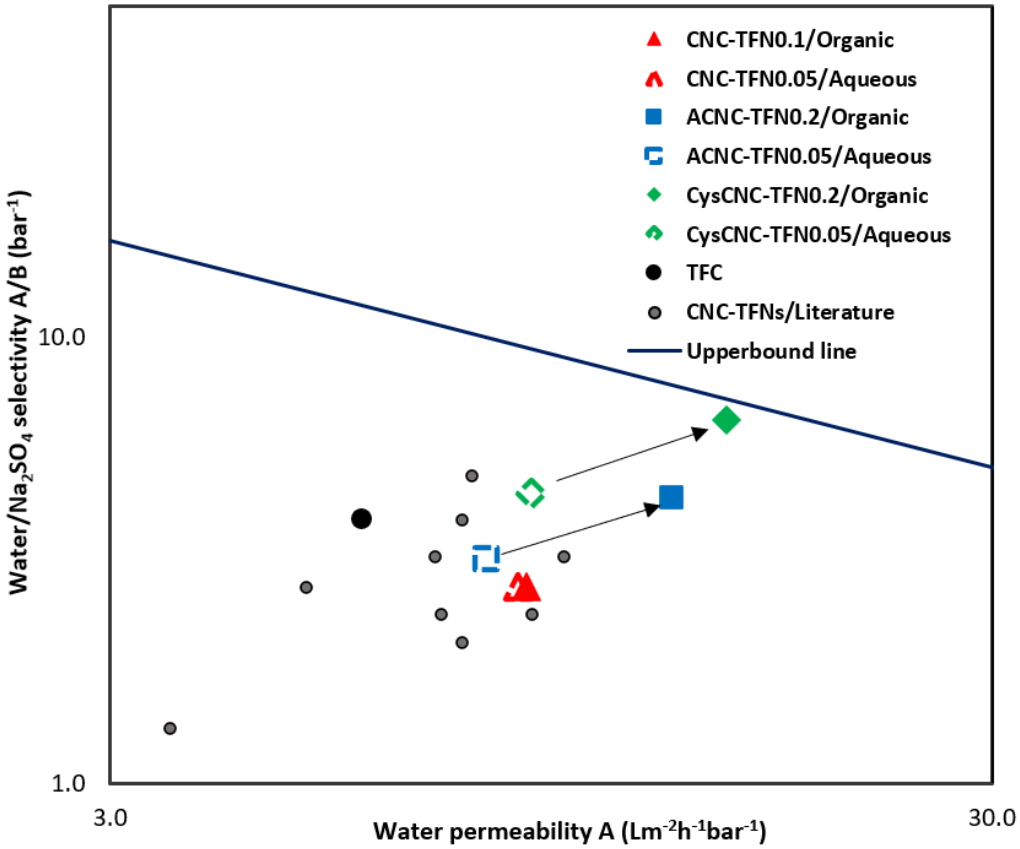

Figure B.6: Effect of nanoparticle addition strategy on TFN NF membrane performance in comparison to the upper-bound line (A/B=96.65 $A^{-1.62}$).[36] Solid coloured symbols show results for the nanoparticle addition to the organic monomer solution; open coloured and other symbols show results for the nanoparticle addition to the aqueous monomer solution.

B.6 Conclusion

In the exciting world of TFN membranes, researchers are only beginning to explore the wealth of available nanoparticles. Many questions on the appropriate fabrication protocols arise in the unique methods used to produce TFN membranes. We have addressed one of these important questions in this study. We asked whether the hydrophilicity of the monomer solution to which the nanoparticles are added should match the nanoparticles' hydrophilicity. To this end, we examined using unmodified CNCs, acetylated CNCs (ACNCs) and L-cysteine modified CNCs (CysCNCs) in both RO and NF membrane systems.

Normal practice dictates that hydrophilic nanoparticles should be dispersed in the hydrophilic/aqueous monomer solution. We have demonstrated herein that the nanoparticle's hydrophilicity is but one part of the story. In the case of the unmodified CNCs used in this study, the monomer solution into which the nanoparticles were dispersed had little effect on

membrane performance. On the other hand, ACNCs and CysCNCs showed remarkably improved performance when dispersed in the organic monomer solution compared to the case where they were dispersed in the aqueous monomer solution. Besides the hydrophilicity of the existing nanoparticle, one can also consider its functionality. The nanoparticle functionality can be exploited to modify its hydrophilicity and promote specific interactions (e.g., covalent bonding) with either of the monomers used in interfacial polymerization. Thus, the functionality of the nanoparticles can also play a significant role in determining the best addition strategy. In any case, rather than following the standard practice without question, we recommend that the dispersion of the nanoparticles into the hydrophobic/organic monomer solution should be considered as an option when optimizing TFN membrane performance.

B.7 References

[1] G. Abdi, A. Alizadeh, S. Zinadini, G. Moradi, *Journal of Membrane Science* **2018**, *552*, 326.
[2] D. Ankoliya, B. Mehta, H. Raval, *Separation Science and Technology* **2019**, *54*, 293.
[3] S. Bandehali, F. Parvizian, A. R. Moghadassi, S. M. Hosseini, J. N. Shen, *J Polym Res* **2020**, *27*, 94.
[4] J. M. Gohil, P. Ray, *Separation and Purification Technology* **2017**, *181*, 159.
[5] X. An, Y. Hu, N. Wang, T. Wang, Z. Liu, *NPG Asia Mater* **2019**, *11*, 13.
[6] M. Asadollahi, D. Bastani, S. A. Musavi, *Desalination* **2017**, *420*, 330.
[7] V. Freger, *Langmuir* **2005**, *21*, 1884.
[8] H. Saleem, S. J. Zaidi, *Desalination* **2020**, *475*, 114171.
[9] S. Poornima, S. Manikandan, V. Karthik, R. Balachandar, R. Subbaiya, M. Saravanan, N. T. Lan Chi, A. Pugazhendhi, *Chemosphere* **2022**, *303*, 135050.
[10] S.-L. Li, P. Wu, J. Wang, Y. Hu, *Separation and Purification Technology* **2020**, *251*, 117380.
[11] N. Abdullah, N. Yusof, W. J. Lau, J. Jaafar, A. F. Ismail, *Journal of Industrial and Engineering Chemistry* **2019**, *76*, 17.
[12] D. Yadav, S. Karki, P. G. Ingole, *Journal of Environmental Chemical Engineering* **2022**, *10*, 108109.
[13] F. Liu, L. Wang, D. Li, Q. Liu, B. Deng, *RSC Adv.* **2019**, *9*, 35417.
[14] M. R. De Guzman, M. B. M. Y. Ang, C.-L. Lai, C. A. Trilles, J. M. Pereira, R. R. Aquino, S.-H. Huang, K.-R. Lee, *Ind. Eng. Chem. Res.* **2019**, *58*, 17937.
[15] M. Amiri, E. Jafarbeigi, F. Salimi, *Korean J. Chem. Eng.* **2022**, *39*, 616.
[16] W.-P. Zhu, J. Gao, S.-P. Sun, S. Zhang, T.-S. Chung, *Journal of Membrane Science* **2015**, *487*, 117.
[17] K. Farokhi, M. Cheraghi, S. Sobhan Ardakani, B. Lorestani, D. Emadzadeh, *International Journal of Environmental Analytical Chemistry* **2021**, 1.
[18] R. E. Abouzeid, R. Khiari, N. El-Wakil, A. Dufresne, *Biomacromolecules* **2019**, *20*, 573.
[19] K. Arola, B. Van der Bruggen, M. Mänttäri, M. Kallioinen, *Critical Reviews in Environmental Science and Technology* **2019**, *49*, 2049.
[20] C. Hu, H. Hu, M. Song, J. Tan, G. Huang, J. Zuo, *Environ Sci Pollut Res* **2020**, *27*, 10599.
[21] F. Abedi, D. Emadzadeh, M. A. Dubé, B. Kruczek, *Desalination* **2022**, *538*, 115900.

[22] S. Y. Lee, H. J. Kim, R. Patel, S. J. Im, J. H. Kim, B. R. Min, *Polym. Adv. Technol.* **2007**, *18*, 562.
[23] M. Bassyouni, M. H. Abdel-Aziz, M. Sh. Zoromba, S. M. S. Abdel-Hamid, E. Drioli, *Journal of Industrial and Engineering Chemistry* **2019**, *73*, 19.
[24] F. Abedi, M. A. Dubé, D. Emadzadeh, B. Kruczek, *Journal of Membrane Science* **2023**, *670*, 121369.
[25] D. Carter, L. Rose, T. Awobusuyi, M. Gauthier, F. H. Tezel, B. Kruczek, *Desalination* **2015**, *368*, 127.
[26] C. Xu, W. Chen, H. Gao, X. Xie, Y. Chen, *Environ. Sci.: Nano* **2020**, *7*, 803.
[27] E. Smith, K. Hendren, J. Haag, E. Foster, S. Martin, *Nanomaterials* **2019**, *9*, 125.
[28] L. Bai, Y. Liu, N. Bossa, A. Ding, N. Ren, G. Li, H. Liang, M. R. Wiesner, *Environ. Sci. Technol.* **2018**, *52*, 11178.
[29] F. Asempour, D. Emadzadeh, T. Matsuura, B. Kruczek, *Desalination* **2018**, *439*, 179.
[30] L. Bai, Y. Liu, A. Ding, N. Ren, G. Li, H. Liang, *Chemical Engineering Journal* **2019**, *358*, 1519.
[31] W.-H. Yu, Z.-Q. Gan, J.-R. Wang, Y. Zhao, J. Han, L.-F. Fang, X.-Z. Wei, Z.-L. Qiu, B.-K. Zhu, *Journal of Membrane Science* **2021**, *639*, 119756.
[32] M. T. Hoang, T. D. Pham, D. Verheyen, M. K. Nguyen, T. T. Pham, J. Zhu, B. Van der Bruggen, *Chemical Engineering Science* **2020**, *228*, 115998.
[33] L. Bai, H. Wu, J. Ding, A. Ding, X. Zhang, N. Ren, G. Li, H. Liang, *Chemical Engineering Journal* **2020**, *382*, 122919.
[34] C. H. Park, S. Jeon, S.-H. Park, M. G. Shin, M. S. Park, S.-Y. Lee, J.-H. Lee, *J. Mater. Chem. A* **2019**, *7*, 3992.
[35] Y. J. Lim, K. Goh, M. Kurihara, R. Wang, *Journal of Membrane Science* **2021**, *629*, 119292.
[36] Z. Yang, L. Long, C. Wu, C. Y. Tang, *ACS EST Eng.* **2022**, *2*, 377.

Appendix C: Laboratory safety considerations

The hazards and required personal protective equipment (PPEs) for all the chemicals used in this project were obtained from the manufacturer's safety data sheets and are summarized in Table B.1. In general, PPEs including respiratory mask, safety goggles, gloves, and lab coat are used during CNC modification and membrane fabrication because of possible contact with monomer vapours during in-situ interfacial polymerization and other hazards.

Table C.1: List of chemicals, manufacturer, hazards and required PPE.

Chemicals	Manufacturing company	Hazards	Personal protective equipment (PPE)
m-phenylenediamine (MPD)	Sigma-Aldrich	May form combustible dust concentrations in air. May cause an allergic skin reaction. Causes serious eye irritation. Toxic if swallowed, in contact with skin or if inhaled.	Tightly fitting safety goggles. Gloves, Complete suit, a full-face respirator
Piperazine (PIP)	Sigma-Aldrich	Flammable solid. Causes severe skin burns and eye damage. May cause an allergic skin reaction or asthma symptoms or breathing difficulties if inhaled.	Tightly fitting safety goggles. Gloves, Complete suit, a full-face respirator
Trimesoyl chloride (TMC)	Sigma-Aldrich	Causes severe skin burns and eye damage.	Protective clothing and gloves, eye protection, and full face respirator
Cellulose nanocrystals (CNCs)	CelluForce	No significant hazard.	Protective clothing and gloves, eye protection
Copper (II) sulfate ($CuSO_4$)	Sigma-Aldrich	Harmful if swallowed. Causes skin irritation and serious eye irritation.	Protective clothing and gloves, eye protection
Lead (II) nitrate ($Pb(NO_3)_2$)	Sigma Aldrich	May intensify fire. Harmful if swallowed or inhaled. Causes serious eye damage. May cause damage to organs through prolonged or repeated exposure. Very toxic to aquatic life with long lasting effects.	Protective clothing and gloves, eye protection
Sodium hydroxide NaCl	Sigma-Aldrich	No significant hazard.	Protective clothing and gloves, eye protection
Magnesium chloride ($MgCl_2$)	Sigma-Aldrich	Causes skin irritation and serious eye irritation. May cause respiratory irritation.	Protective clothing and gloves, eye protection
Sodium (II) sulphate (Na_2SO_4)	Sigma-Aldrich	Hygroscopic. May cause skin, eye, and respiratory tract irritation.	Protective clothing and gloves, eye protection

Bovine serum albumin (BSA)	Fischer Scientific	No significant hazard.	Protective clothing and gloves, eye protection
L-cysteine	Fischer Scientific	Causes skin irritation and serious eye irritation May cause respiratory irritation.	Protective clothing and gloves, eye protection. Avoid breathing dust
Iodine	Sigma-Aldrich	Causes skin and eye irritation. May cause respiratory irritation. Causes damage to organs through prolonged or repeated exposure. Harmful if swallowed, in contact with skin or if inhaled.	Protective clothing and gloves, eye protection, and full face respirator
Hydrochloric acid (HCl)	Sigma-Aldrich	Corrosive material. Causes severe skin burns and eye damage. May cause repertory irritation.	Gloves, eye protection, and full face respirator
Sodium hydroxide (NaOH)	Sigma-Aldrich	Causes severe skin burns and eye damage.	Protective clothing and gloves, eye protection and face protection
Sodium thiosulfate	Sigma-Aldrich	Oxidizing solid. May cause eye, skin, and respiratory irritation.	Protective clothing and gloves, eye protection
Acetic anhydride	Fischer Scientific	Flammable liquid and vapor. Harmful if swallowed. Causes severe skin burns and eye damage. Toxic if inhaled.	Protective clothing and gloves, eye protection
Acetone	Fischer Scientific	Highly flammable liquid and vapor. Causes serious eye irritation. May cause drowsiness.	Protective clothing and gloves, eye protection